Hydrogen bonding in radical copolymerization: A kinetic investigation under industrially relevant conditions

By

JAN ERIK STEFFEN SCHIER

A thesis submitted to the Department of Chemical Engineering

in conformity with the requirements for the

Degree of Doctor of Philosophy

Queen's University

Kingston, Ontario, Canada

May, 2017

Abstract

Radical solution polymerization is a common method to produce a variety of plastics and coatings. Particularly in the automotive industry, large scale semi-batch operations are used to (co)polymerize monomers of the styrenic, acrylate and methacrylate families. To reduce solvent content, traditional non-functional feedstocks have been replaced or augmented with functional monomers like 2-hydroxyethyl methacrylate (HEMA) or 2-hydroxyethyl acrylate (HEA) to produce reactive polymer chains of lowered molar mass. The introduction of such polar and functional reactants affects the radical copolymerization kinetics and introduces solvent dependencies. The goal of this thesis is to identify and characterize these kinetic effects. Using specific kinetic parameters, a comprehensive model will be developed to describe copolymerizations under industrially relevant conditions, while also determining experimental limitations of comonomer incorporation.

Due to the limited availability of reliable kinetic parameters, initial studies focused on the determination of copolymerization parameters involving HEA. The IUPAC recommended pulsed laser polymerization (PLP) technique in combination with size exclusion chromatography (SEC) and nuclear magnetic resonance (NMR) spectroscopy was used to determine propagation rate coefficients and reactivity ratios for HEA with both butyl methacrylate (BMA) and butyl acrylate (BA). Kinetics systematically diverged from classic kinetic behaviour and were solvent dependent. It was proven that hydrogen bonding causes these deviations by comparing HEA copolymerization to that of methoxyethyl acrylate. Simple terminal model predictions or implicit penultimate unit effects were used to represent chain growth kinetic parameters.

Further experimentation was performed to determine the influence of these changing kinetic parameters during production of low molar mass functional HEA copolymers in relevant solvents such as ketones or esters under starved-feed semi-batch operating conditions, similar to those used in industry. H-bonding effects on kinetics were found to be well controlled to HEA contents of maximum 50 wt%. The BMA/HEA copolymerization in ketones is very well represented by a comprehensive

copolymerization model that considers relevant methacrylate and acrylate side reactions and uses the kinetic chain growth parameters measured by the PLP investigations.

Co-Authorship

The bulk of this research in this thesis was conducted independently in the laboratory under the supervision of Dr. Robin A. Hutchinson at Queen's University. The results presented in chapter 3 have been published as two separate papers in a peer-reviewed journal as described later on in this thesis. One of the mentioned papers has been prepared in cooperation with David Cohen-Sacal who has been working as a NSERC summer student in the laboratory.

A third publication, mainly conducted and prepared by Florian Brandl from the Beuermann research group at the Clausthal University of Technology has been accepted for publication, but will not be discussed in detail in this thesis.

Acknowledgments

First and foremost, I would like to thank my supervisor Robin A. Hutchinson for his continued guidance and support over the past 4 years. His expertise, but also his positive attitude made it particular rewarding to immerse in the world of engineering in this new environment (Canada), and I appreciate the opportunity to study abroad and work with researchers from all over the world.

I would like to thank Dr. Mike Grady, Dr. David Nare and coworkers, from Axalta Coating systems, for the opportunity to create this PhD project as part of our longstanding cooperation and the numerous feedback and their preview into work in industry.

Some special thanks go to my hardworking 4th year and summer students Sharmaine, Owen, David and Erica, for lending me their hands in the lab on some of the endeavours.

My thanks go to our collaborations in Germany, namely Florian Brandl, Dr. Sabine Beuermann and my old research group in Paderborn.

To all my friends and colleagues, in and outside our lab-group, thank you for making this journey memorable. Kudos to Calista, Joaquin, Kevin, Flo, Thomas, Sean, Michal, Praf, Joe, Omar, Stu, Kira and many more for those evenings of soccer, chess, bowling, late nights at the lab, the casual pint or just a friendly ear. You know where to find me.

Finally, I am very grateful for my family, especially my parents, who were always supportive but gave me the freedom to develop into the person I am today. To Stephi, my wife, who went with me on this adventure Canada despite the initial transatlantic commute. Thank you, for taking this step together, your love, for being there and the vast experiences we had together, which let me relax and enjoy life when most needed.

Table of Contents

List of Figures

List of Tables

Acronyms and Abbreviations

AA	acrylic acid
BA	butyl acrylate
BL	branching level
BMA `	butyl methacrylate
BuOH	*n*-butanol
BPi	butyl propionate
$CDCl_3$	deuterated chloroform
CSTR	continuous stirred-tank reactor
C_{tr}	transfer to solvent coefficient
D	dead polymer chain
$Đ_M$	dispersity of molar mass distributions, formerly known as polydispersity index, PDI
DMAc	dimethylaceteamide
DMF	N,N-dimethylformamide
DMPA	2,2-dimethoxy-2phenylacetophenone
DMSO-*d6*	deuterated dimethyl sulfoxide (DMSO)
DP	degree of polymerization
EGDA	ethylene glycol diacrylate
EGDMA	ethylene glycol dimethacrylate
ESR	electron spin resonance
f_x	molar fraction of monomer x in monomer or feed solution
F_x	molar fraction of monomer x incorporated into the formed copolymer
f_{ini}	initiator efficiency
FID	flame ionization detector
FT	Fourier transformation
GC	gas chromatography
GMA	glycidyl methacrylate
H-bonding	hydrogen-bonding
HEA	2-hydroxyethyl acrylate
HEMA	2-hydroxyleethyl methacrylate
I	initiator
IPUE	implicit penultimate unite effect
IR	infrared spectroscopy

k_{bb}	backbiting rate coefficient
k_d	initiator decomposition rate coefficient
k_{dp}	depropagation rate coefficient
k_p	propagation rate coefficient
k_s	scission rate coefficient
k_t	termination rate coefficient
k_{tc}	termination by combination rate coefficient
k_{td}	termination by disproportionation rate coefficient
LCST	lower critical solution temperature
LS	light scattering
M	monomer
MA	methyl acrylate
MAA	methacrylic acid
MCR	mid-chain radical
MEA	2-methoxyethyl acrylate
MeOH	methanol
MIAK	methyl isoamyl ketone
MIBK	methyl isobutyl ketone
MM	molar mass
MMA	methyl methacrylate
MMD	molar mass distribution
M_n	number-average molar mass
M_w	weight-average molar mass
NMR	nuclear magnetic resonance spectroscopy
NOE	nuclear Overhauser effect
P	polymer radical
PeOH	*n*-pentanol
Φ	volume fraction
PLP	pulsed laser polymerization
ppm	parts per million
Q	mid-chain radical containing polymer chain
QSSA	quasi steady-state approximation
r	reactivity ratio
ρ	density

RI	refractive index
RP	radical polymerization, formerly known as free radical polymerization FRP
s	implicit penultimate unit effect fitting parameters
SCB	short chain branch
SEC	size exclusion chromatography
SPR	secondary propagating radical
ST	styrene
t_0	reaction time as the inverse to laser frequency
TBPA	*tert*-butyl peroxyacetate
THF	tetrahydrofuran
TM	terminal model
U	unsaturated polymer chain
VAc	vinyl acetate
Vazo-67	1,1'-azobis(cyclohexanecarbonitrile)
X	conversion

Chapter 1 Introduction

Radical Polymerization (RP) is one of the most common and significant methods to produce polymers at a commercial scale.[1] Despite many new developments like controlled radical polymerizations,[2–4] living polymerizations[5] or other catalytically supported approaches[6] RP still competes due to simplicity and high tolerance towards impurities of either organic or aqueous nature.[1] Herein RP is still a major tool in industry as high productivity can be obtained at comparably low cost.[7]

As a wide range of monomers, including ethylenes, (meth)acrylates or styrene derivatives, is amenable to RP,[8] various polymeric products are manufactured for a wide range of applications. One example is the automotive industry, where many acrylic based polymers are used as coating materials.[9] For optimum processing and applications a goal has been set in recent years to obtain fairly low molar mass polymers[10] that include a certain degree of functionality via copolymerization.[11] Functional groups raise the value of the crude product as they allow post-modifications (e.g., crosslinking),[12] whereas lower molar masses decrease the viscosity during the downstream process. This last point is important when handling or applying the coating as a spray, to ensure uniform layer formation on top of the chassis or applicable surface. The reactive functionality is often introduced by hydroxyl containing monomers from which a wide range of post-modifying chemistry is accessible.[13] On the other hand, the total polarity is increased and hydrogen bonding is introduced to the reaction system such that solvent choice can exert a significant effect on reaction (propagation) rates,[14,15] and copolymer composition[16] and microstructure (branching).[17] These solvent effects can be also induced by functional monomers themselves.[18,19] In particular, previous investigations showed that 2-hydroxyethyl acrylate (HEA) undergoes reduced backbiting due to the hydroxyl function.[20] H-bonding effects can be found as well for acrylic (AA) and methacrylic acid (MAA), which show significant solvent effects in, for example, aqueous solution.[21]

To better understand the kinetics of these systems the IUPAC recommended combination of pulsed laser polymerization (PLP) and size exclusion chromatography (SEC)[22,23] is applied, a powerful and unique tool to determine propagation rates (k_p) of systems in bulk or solution. In combination with

nuclear magnetic resonance (NMR) spectroscopy[24] or Fourier transform infrared (FT-IR) spectroscopy,[25] composition investigations are also possible to obtain a classic Mayo-Lewis plot[26] following the terminal model.[8] Based on former investigations it is assumed that the terminal model will not explain all findings. Hence a penultimate approach will likely be necessary to capture the impacts of hydroxyl functionalities and solvent effects.[27] These kinetic investigations provide the starting point for a comprehensive investigation (see Figure 1.1) to adequately determine relevant parameters for an industrially relevant copolymerization model.[28]

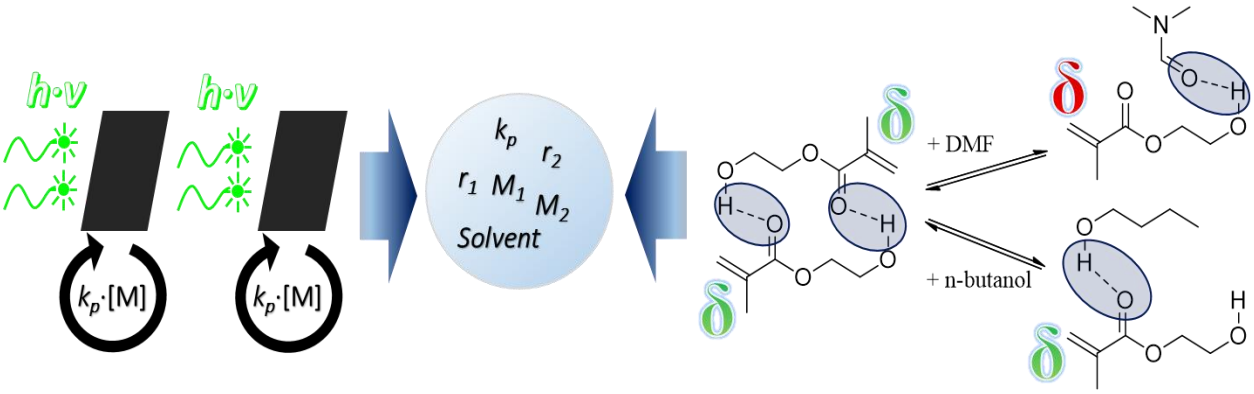

Figure 1.1: Principles of kinetic parameter (center left) estimation and determination through PLP experiments (left), including hydrogen bonding effects with HEMA: bulk system (center right) versus solvent influences of DMF (disrupting effect, top right) and n-butanol (substituting effect, bottom right)[19]

1.1. Thesis Objective

The goal of this study is to enhance the knowledge about H-bonding influences in radical solution polymerization through the investigation of the hydroxyl functional acrylate HEA. Using the IUPAC recommended PLP technique, kinetic chain-growth parameters will be determined in industrially relevant solvents like ketones or esters, as used by our industrial partners Axalta. To fully understand the scope of H-bonding, investigations will be extended to solvents like dimethyl formamide (DMF) and *n*-butanol (BuOH). Using appropriate modelling techniques or representations, kinetic parameters will be

determined and experimentally verified under batch or semi-batch conditions at elevated temperatures. The final goal is the development of a comprehensive copolymerization model that captures all necessary side reactions and H-bonding related effects of functional monomers under reaction conditions similar to those used in industry. Accordingly, practical reaction limitations will be explored related to solubility limits of the more polar monomers. The influence of feedstock quality or impurity levels will be regarded as well.

1.2. Thesis Outline

This thesis is composed based on published peer reviewed articles and unpublished research performed over the last four years. Articles were slightly modified to improve the flow of the presented results.

Chapter 2 provides an overview of the present literature for polymer reaction engineering utilizing RP. Experimental techniques to determine relevant parameters for primary and side reactions are described and critically evaluated based on the systems chemical nature, e.g. H-bonding.

Chapter 3 summarizes the kinetic investigation of reactivity ratios and propagation rate coefficients, using the PLP-SEC or PLP-NMR technique, for methacrylate-acrylate and acrylate-acrylate copolymerizations involving HEA in different solvents, to determine the influence of H-bonding.[19,29] For most results, terminal model predictions or penultimate representations were generated to explain the trends. To better understand the influence of H-bonding, additional experiments involving 2-methoxyethyl acrylate (MEA) were performed.

Chapter 4 delivers the detailed investigation of acrylate only copolymerizations of *n*-butyl acrylate (BA) and HEA in numerous solvents. The investigation allows for the determination of kinetic parameters related to branching, which were then implemented in the respective models. Experimental trends were also compared and analyzed based on the kinetic findings in Chapter 3.

Chapter 5 discusses the semi-batch copolymerization of *n*-butyl methacrylate (BMA) and HEA in industrially relevant solvents under isothermal conditions. The influence of HEA is investigated up to HEA levels of 40 wt%. Using a previously developed terpolymerization model, experimental trends were well represented, demonstrating the utility of the model for industrial application.

Chapter 6 revisits copolymerizations involving HEMA to investigate the previously unresolved presence of high molar mass tails on the polymer molar mass distributions. In addition to demonstrating that esters are a better polar solvent for production of functional copolymers, specialized batch and semi-batch experiments were conducted in the presence of added di(meth)acrylate as an impurity. Using literature kinetic parameters for the BA/HEMA copolymerization, results of isothermal BA/HEMA semi-batch reactions were compared to modelling predictions.

Chapter 7 summarizes the work and suggests further pathways and approaches to improve the understanding of H-bonding in solution copolymerizations.

Chapter 2 Literature Review

2.1. RP Kinetics

To understand mechanisms and explain certain effects in RP it is necessary to start with the basic kinetics of the system. Once the simple steps for homopolymerizations (see Figure 2.1) are understood, it is possible to introduce further reactions which might be necessary for more complex systems, e.g. copolymerizations or solution polymerizations at higher temperatures. To maintain this simplicity the terminal model was introduced. This model assumes that each radical's reactivity is only dependent on the terminal group.

Initiator Decomposition	$I \xrightarrow{k_d} 2f\ I^*$
Chain Initiation	$I^* + M_j \xrightarrow{k_i} P_1^i$
Chain Propagation	$P_n^i + M_j \xrightarrow{k_p} P_{n+1}^i$
Chain Termination	
By Combination	$P_n^i + P_m^i \xrightarrow{k_{tc}} D_{n+m}$
By Disproportionation	$P_n^i + P_m^i \xrightarrow{k_{td}} D_n + D_m$
Chain Transfer	$P_n^i + M_j \xrightarrow{k_{tr}^{mon}} D_n + P_1^i$
To Monomer	$P_n^i + S \xrightarrow{k_{tr}^{sol}} D_n + S^*$
To Solvent or Agent	$S^* + M_j \xrightarrow{k_i^{sol}} P_1^i + S$

Figure 2.1: Nomenclature and elementary reactions of RP: Stars represent primary radicals whereas n and m as subtitles indicate the chain length of a macroradical (*P*) or dead polymer chain (*D*).

Usually reactions are initiated by decomposing (k_d) a thermally labile compound I, such as peroxide-[30] or diazo-[31] containing molecules. As a result of a homogeneous electron pair cleavage, two radicals are formed with an efficiency *f*. Under industrial relevant conditions this factor usually is larger

than 0.5. The following chain initiation (k_i) proceeds by attacking a double bond of monomer M to form P_1. As long as the radical property is maintained, propagation (k_p) by monomer consumption takes place. As radicals can also react with each other, termination can take place by combination (k_{tc}) or disproportionation (k_{td}) to form dead polymer chains D. Alternatively suitable chemical compounds also allow for radical transfer to any compound in the system, such as monomer (k_{tr}^{mon}), solvent or agent (k_{tr}^{sol}).

To keep track of these four elementary reactions, their reaction rates need to be investigated separately; however, overall observable quantities do not provide this information. Especially the total population of radicals P_{tot} is of interest as part of the polymerization rate. It is assumed that rates for radical generation and termination balance out instantaneously under quasi-steady-state conditions (QSSA),[32] so the total concentration can be described as

$$[P_{tot}] = \left(\frac{R_{init}}{k_t}\right)^{0.5} = \left(\frac{2fk_d[I]}{k_{tc}+k_{td}}\right)^{0.5} \tag{2.1}$$

Eqn 2.1 can then be implemented into the polymerization rate (see Eqn 2.2), which shows first-order kinetics with respect to the monomer. This case presents an ideal radical polymerization in batch.

$$R_P = -\frac{d[M]}{dt} = k_p[M]\left(\frac{2fk_d[I]}{k_{tc}+k_{td}}\right)^{0.5} \tag{2.2}$$

Even if radical concentration is known to be constant, k_p the propagation rate coefficient remains as an "unknown" parameter that greatly impacts the total reactivity and heat generation rate, as monomer consumption by chain-initiation or transfer events is assumed to be negligible, due to the high length of macromolecular chains formed in RP (i.e., the long-chain hypothesis). By consideration of termination and transfer reactions, further information about the polymerization system like the degree of polymerization (DP) and polymer molar mass is available, which is shown in Eqn 2.3 for the instantaneous number-average degree of polymerization.

$$DP_n^{inst} = \frac{k_p[M]}{(k_{td}+0.5k_{tc})[P_{tot}]+k_{tr}^{mon}[M]+k_{tr}^{sol}[S]} \tag{2.3}$$

These basic mechanisms and equations can be seen as the starting point for further modelling approaches, extending them, for example, by the method of moments to gain knowledge about the averages of the molar mass distribution which are highly correlated with polymer properties. Other more sophisticated options include the modelling of the complete molar mass distribution[33,34] in comparison to experimental distributions measured by SEC. In the presence of complicating side reactions, further numerical techniques may be necessary for the development of a comprehensive (co)polymerization model. The modelling tool PREDICI® can be used and applied for such approaches, to model industrially relevant batch, semi-batch[28] or CSTR[35] systems, even under consideration of more complex equilibrium reactions, which may occur in the presence of catalysts or under controlled radical polymerization conditions.[36]

2.1.1. Determination of propagation rate coefficients via PLP

Generally polymerization rate coefficients are dependent on pressure and temperature, following a standard Arrhenius dependency.[37,38] Even though early determinations of k_p resulted in quite scattered values,[39] experiments were always performed at low conversions to obtain instantaneous reaction rates. Today the widely accepted and IUPAC recommended technique is Pulsed Laser Polymerization-Size Exclusion Chromatography (PLP-SEC).[19,22,40] Herein the combination of efficient photo polymerization and simple chromatography allows a direct measurement of the propagation rate coefficient k_p not coupled to other rate coefficients.[23] Assuming minimal influences of side reactions, only propagation and termination can take place, while keeping conversions low (< 5%). In detail the reaction is started by a nanosecond burst of UV-light to instantaneously create the radical population. Subsequently propagation and termination take place until the next flash is pulsed. The majority of remaining radicals at that point will be terminated, while a new population is created parallel and again, instantaneously. As mentioned, termination is not complete, such that some radicals survive multiple pulses.[41,42] The success of the PLP experiment is dependent on the ratio of k_p and k_t and the concentration of radicals formed per pulse, as these influence the overall shape of the resultant polymer molar mass distribution (MMD). If radical

concentrations are too low or too high, which is defined as the low or high termination rate limits (LTRL and HTRL), the distribution does not contain the features necessary for estimation of k_p. Thus, preliminary experimentation is required to define the operable conditions for a new system, by varying the photoinitiator concentration, laser beam energy and time between pulses, t_0, the inverse of laser pulse frequency. For unknown systems it is recommended to support these initial investigations by modelling techniques.[43] Once the experimental limits are known, PLP-SEC can also be used to estimate other kinetic issues, such as the mode of termination, even in the presence side reactions.[44]

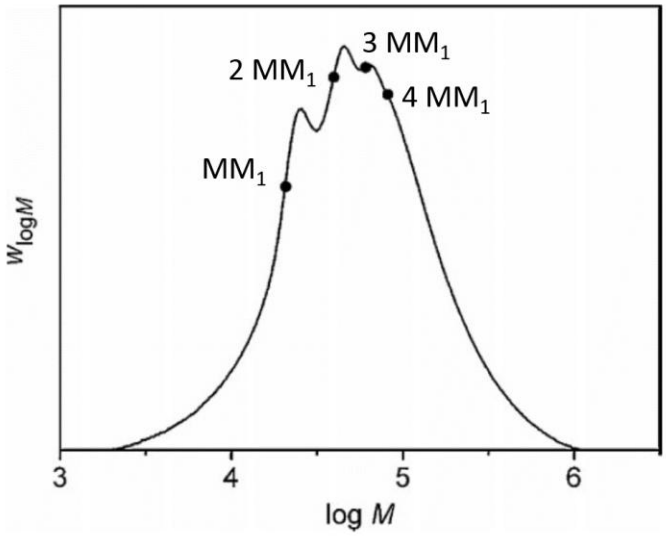

Figure 2.2: Typical MMD obtained by PLP showing multiple inflection points dependent on DP_0 (black points). Adapted with permission from R. Rotzoll, P. Vana, *Macromol. Rapid Commun.* 2009, *30,* 1989-1994.[45] ©Wiley-VCH GmbH&Co. KGaA, Weinheim

Under appropriate experimental conditions, a typical PLP molar mass distribution (MMD) is obtained (see Figure 2.2) that features multiple maxima. It has been shown that the corresponding inflection points are multiples of DP_0, the degree of polymerization that is related to the lifetime of a chain between pulses according to Eqn 2.4:

$$DP_0\, i = \; i\, k_P[M]\, t_0 \tag{2.4}$$

$$with\; i = \mathbb{Z} \geqslant 1$$

Using known relationships between monomer concentration and DP_0 with monomer density ρ and measured molar mass MM_1 to obtain Eqn 2.5:[27]

$$k_p = \frac{MM_1}{\phi_{mon}\,\rho_{mon}\,t_0} \tag{2.5}$$

This equation is not only valid for bulk and solution homopolymerizations, but also copolymerizations. In case of a multi monomer system, k_p represents the composition-averaged rate coefficient k_p^{cop}, presented later, with Φ_{mon} for the volume fraction of both monomers combined in solution.

Whereas only 100 Hz lasers were available until the mid-2000's,[46] instruments are now available to even 500 Hz and 1000 Hz.[47] This technical improvement increases the investigable temperature range especially for fast reacting monomers, like acrylates. Therefore Asua et al.'s benchmark data set from -65 ºC until 20 ºC for butyl acrylate (BA) k_p values obtained at 100 Hz or lower[48] was easily extended up to 70ºC,[47] closer towards commercial applicable temperatures. The reason for the limitation in the case of acrylates is the formation of mid-chain radicals (MCR) by an intramolecular transfer reaction that disrupts the linear relationship between chain length and t_0 during low frequency experiments. Consequently, it is necessary to keep the ratio between propagation and transfer rates always larger than DP_0 (see Eqn 2.6), such that chain length is controlled by propagation in the time intervals between pulses.

$$k_p[M]\,t_0 \;<\; \frac{R_p}{R_{tr}} \tag{2.6}$$

Otherwise MCR may react, despite being less reactive, into scission or backbiting products (see Figure 2.3), to be discussed in more detail later. Experimental evidence for MCRs can be found via electron spin resonance (ESR) experiments, which differentiates between secondary and tertiary radicals,[49] and from the measurement by ^{13}C NMR of quaternary carbons that are formed when monomer adds to the MCR.

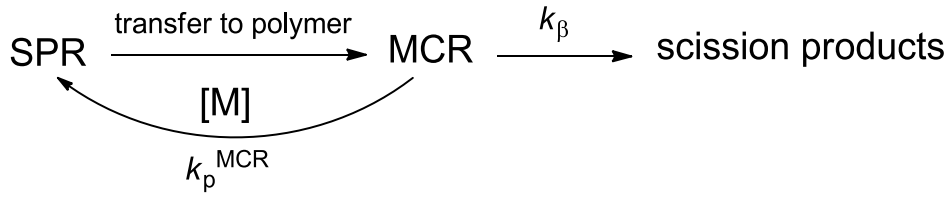

Figure 2.3: MCR formation: an acrylate side reaction[47]

Together with proper SEC detection systems there are almost no boundaries left for the application of PLP-SEC. As absolute molar masses are necessary, investigations can be performed knowing or determining the corresponding Kuhn-Mark-Houwink[50] parameters or refractive index increments (dn/dc).[51] Herein reliable libraries for k_p and reactivity ratios can be created, including the investigation of solvent effects, copolymerization effects or k_p values for newly synthesized monomers.[52,53] One point to remember from the technical point of view might be the increasing importance of temperature control for high frequency PLP setups. As conversions are kept low, reactions heats should also be reasonable. The other factor is the UV-radiation energy, which is naturally absorbed by any compound in the system. Whereas older systems (see Figure 2.4) were able to re-establish set-point temperatures between pulses, higher frequencies can accelerate a temperature overshoot. As t_0 decreases, the magnitude of the heat diffusion times becomes the limiting step. Although the laser market was recently extended by a 1000 Hz setup directly followed by the new record breaking PLP study of *tert*-butyl acrylate,[54] samples synthesized at the higher frequencies should be critically evaluated.

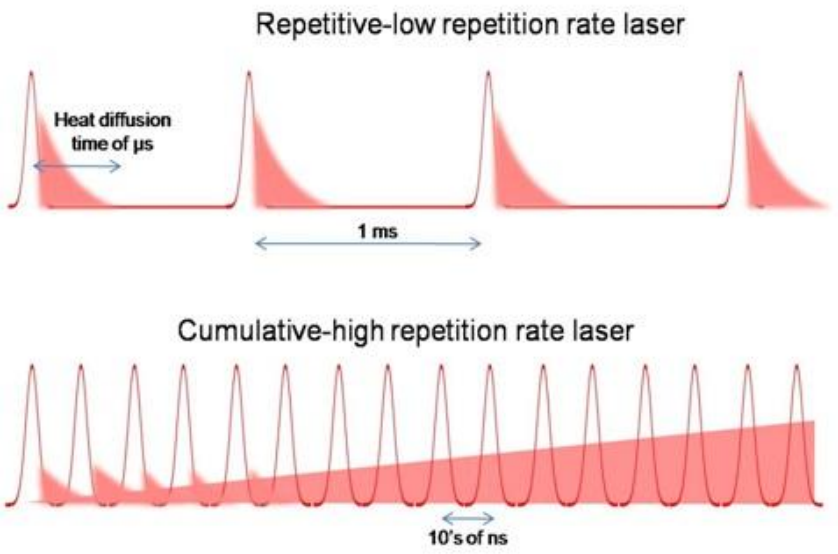

Figure 2.4: Heat accumulation in Laser setups[55]

This becomes evident in regards of a recent model, which describes heat phenomena inside a PLP cell using detailed material and energy balances over a discretized 3D grid representation of the cell volume.[56] Despite the simulated significant increases in the reaction temperature, especially at the center of the cell, the simulation of the full MMD produced demonstrated that the resulting k_p estimates were not significantly affected, although some peak broadening was predicted. The results can be seen as another reminder to maintain low conversions during the PLP experiments, such that reaction temperature in the cell remains at a constant level.

Additionally, a single PLP pulse in combination with near Infrared (SP-PLP-NIR)[57] or the already mentioned ESR (also known as EPR) technique (SP-PLP-EPR)[58–60] allows for the determination of termination coefficient k_t. Whereas k_p is necessary for reliable monomer concentration profiles, the total radical population and DP_n^{inst} are also dependent on k_t according to Eqns 2.1 and 2.3. Similar to the evolution in determining reliable k_p -values, reported results for k_t have uncertainty due to the more complex nature of termination.[61] As a diffusion-controlled rate coefficient, k_t changes throughout the course of reaction with increasing conversion and viscosity besides exhibiting other chain-length dependent behaviour, as observed earlier and now known as the Trommsdorff-Norrish effect.[62,63] As a

starting point to understand these phenomena, the Stokes-Einstein equation[64,65] describes the self diffusion (coefficient D) of a given chain, as originally applied to spherical non-electrolytes.

$$D = \frac{k_B T}{6\pi r \eta} \tag{2.7}$$

With k_B being the Boltzmann constant, the coefficient is further described by the hydrodynamic radius r and the systems viscosity η. Higher viscosities, dependent on conversion, reduce diffusion in the same way as an increased hydrodynamic volume which, for polymer chains, is a factor of DP of the two chains. This explains the chain-length dependency of k_t assuming a quick combination, once the two chains encounter each other in the reaction sphere with the radius r. In case of long-chain macromolecules, structural and geometrical issues become important, considering that the radical is a small part of a much larger (polymer chain) surface. Thus, assuming some entanglement of two approaching macro-radicals, it is necessary to separate the chain-length dependency of k_t itself. Two different regimes are defined, where termination is controlled by either center-of-mass or segmental diffusion.[66] The transition point in between these two regimes of control is defined as the cross-over chain length, i_c, which is usually monomer dependent. Values for i_c range from 100 for MMA[67] to 20 ± 10 for vinyl acetate (Vac),[68] with the value for BA (65 ± 20)[69] intermediate between the two. Although the chain flexibility plays an important role, no predictive correlation is available for now. Finally, in combination with the clear dependency on viscosity, three zones of decreasing termination coefficients should be considered, starting with the two situations described for short-chains, followed by longer chains plus the so-called reaction diffusion, a ceiling diffusion prone to happen for higher conversions and polymer containing systems, such as bulk.[61,70] However, based on monomer-solvent-polymer interactions the evolution of k_t over the course of the reaction can be found to be quite system specific.[66]

2.1.2. Copolymerization: From Terminal to Penultimate

Together with polymerization rate, one key aspect of using multiple monomers (herein A, B as an example) is copolymer composition, which is of significant importance for product application. As mentioned earlier, only terminal radical reactivity generally needs to be taken into account for modeling composition. Hence the two homopolymerizations A*A and B*B will take place besides the crosspropagations A*B and B*A. To describe copolymer composition, Mayo and Lewis introduced reactivity ratios for each monomer, which are given as following:[26]

$$r_1 = \frac{k_{p11}}{k_{p12}};\ r_2 = \frac{k_{p22}}{k_{p21}} \tag{2.8}$$

Knowing these ratios, instantaneous relative copolymer compositions F_i can be predicted from the composition of the monomer mixture.

$$F_1^{inst} = \frac{r_1 f_1^2 + f_1 f_2}{r_1 f_1^2 + 2 f_1 f_2 + r_2 f_2^2} \tag{2.9}$$

$$with\ f_1 = \frac{M_1}{M_1 + M_2}$$

As mentioned in section 1, composition analysis can be performed via various analytical methods, depending on the produced polymer, with r_1 and r_2 values fit after performing a series of low conversion (< 10%) experiments where F_1 is measured as a function of f_1, as shown in Figure 2.5.[71] It has been shown that this description is applicable for a wide range of monomers, including copolymerizations with polar monomers, multiple functionalities and or different kind of radicals, such as acrylates, methacrylates, vinyl esters or styrenes.[11,19,27,29,72–74] While usually solvent choice has no significant effect on the relation between F and f,[75] this generalization tends to be invalid once hydrogen bonding is introduced to the system. In the example shown (see Figure 2.5), acrylamide/methyl methacrylate reactivity ratios (r_1/r_2) vary from (2.43/0.45) in benzene to (0.13/3.59) in DMF, causing a complete inversion in the relative rates of monomer consumption. This result is possible, as benzene is the only solvent in this set of experiments which allows self-associated hydrogen bonding of acrylamide, while not promoting any hydrogen

bonding itself (like alcohols). Similar behaviour is reported for diluted systems of methacrylic acid/ST in a non-interacting solvent.[76]

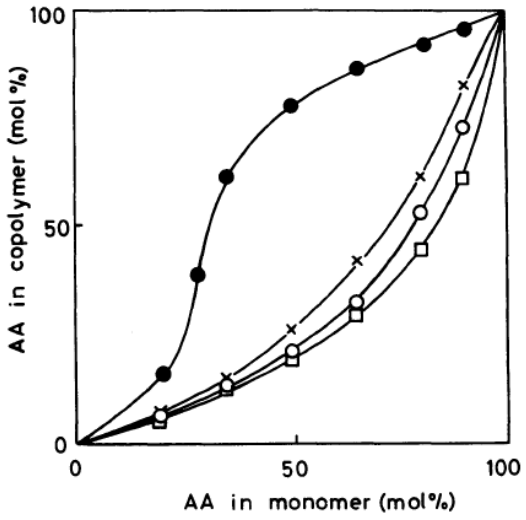

Figure 2.5: Composition data of acrylamide (denoted AA) with methyl methacrylate: solid dots represent benzene values, crosses represent polymerization in benzene/DMF mixture, hollow dots DMF and hollow boxes acetonitrile. Reprinted by permission from Macmillan Publisher Ltd:

Polymer Journal [73], ©1988

Comparable results can also be found for the hydroxyl functional monomers. HEMA, for example, is incorporated into the copolymer more favorably (compared to BMA), whereas this effect can be reduced e.g. again in DMF, which disrupts hydrogen bonding.[11,75]

The terminal model can also be implemented to provide predictions for the copolymer-averaged propagation rate coefficients (k_p^{cop}) using the homo-propagation values k_{11} and k_{22}.[77]

$$k_p^{cop} = \frac{r_1 f_1^2 + 2 f_1 f_2 + r_2 f_2^2}{\left(\frac{r_1 f_1}{k_{11}}\right) + \left(\frac{r_2 f_2}{k_{22}}\right)} \tag{2.10}$$

For some systems, the predictions are in good agreement with experimental values. As soon as more functionality is introduced, such as in solution polymerizations or some styrene copolymerizations, the terminal model no longer provides an accurate representation of reaction rates.[19,27,75]

This problem was already addressed by Merz et al.[78] who proposed that propagation cannot only be dependent on the terminal unit. The reaction focus was extended to the penultimate units, which also influence the radical's reactivity.

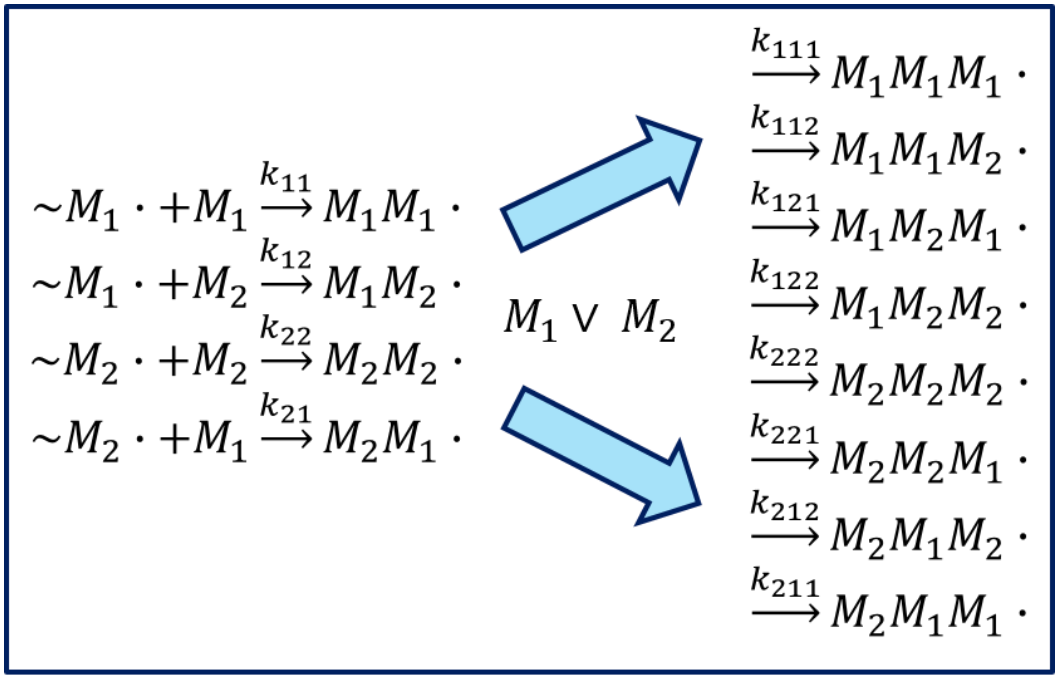

Figure 2.6: Enhancing terminal model propagation kinetics towards the penultimate model; triple indices indicate the two last monomer units on the radical and the reacting monomer

Knowing this, the terminal model predictions can be modified by splitting each former propagation step in two (see Figure 2.6) based on the identity of the penultimate unit. To take this change into account, an additional reactivity factor s_i is introduced, called the radical reactivity ratio, which captures the influence of the penultimate unit for "homo" propagations involving the same monomer.

$$s_1 = \frac{k_{p211}}{k_{p111}}; s_2 = \frac{k_{p122}}{k_{p222}} \tag{2.11}$$

Based on the feed compositions, k_{11} and k_{22} can be now better described with modified expressions:

$$\bar{k}_{11} = \frac{k_{p111}(r_1 f_1 + f_2)}{r_1 f_1 + (\frac{f_2}{s_1})}; \bar{k}_{22} = \frac{k_{p222}(r_2 f_2 + f_1)}{r_2 f_2 + (\frac{f_1}{s_2})} \tag{2.12}$$

Both parameters can then be inserted into equation (7) by directly exchanging with k_{11} and k_{22}.

$$k_p^{cop} = \frac{r_1 f_1^2 + 2 f_1 f_2 + r_2 f_2^2}{\left(r_1 f_1 / \bar{k}_{11}\right) + \left(r_2 f_2 / \bar{k}_{22}\right)} \quad (2.13)$$

While in rare cases monomer reactivity ratios have been proposed to be affected by the penultimate unit, herein it is assumed that the composition is not affected by the penultimate effect (see Eqn 2.12), a treatment known as the Implicit Penultimate Effect (IPUE).[77]

$$r_1 = \frac{k_{p111}}{k_{p112}} = \frac{k_{p211}}{k_{p212}} \quad (2.14)$$

This approximation fits well with experimental results for almost all copolymerization systems. Consequently, composition data (based on relative rates of monomer addition) can be easily described by the terminal model, whereas the IPUE is needed to match reaction rates. Several examples are known, like styrene/HEA[27] and styrene/GMA[51] or functional terpolymers.[79] An example of where the penultimate unit may have a composition effect is reaction with sterically hindered β-pinene, which cannot undergo homopolymerization ($r_1 = 0$) and requires two comonomer units to enable addition of another pinene.[80]

2.1.3. Important side reactions

2.1.3.1. Mid-chain Radicals (MCR)

As mentioned earlier, propagation can be interrupted by the formation of mid-chain radicals by intramolecular chain transfer in which the secondary propagating radical (SPR) can abstract a hydrogen atom from further along the chain, with a favoured abstraction of the hydrogen at position 5 (see Figure 2.7). An important reaction for acrylates,[81] a methacrylate unit at the same position does not provide an available H-atom. Therefore, MCR formation is significantly reduced in high methacrylate containing systems.[82]

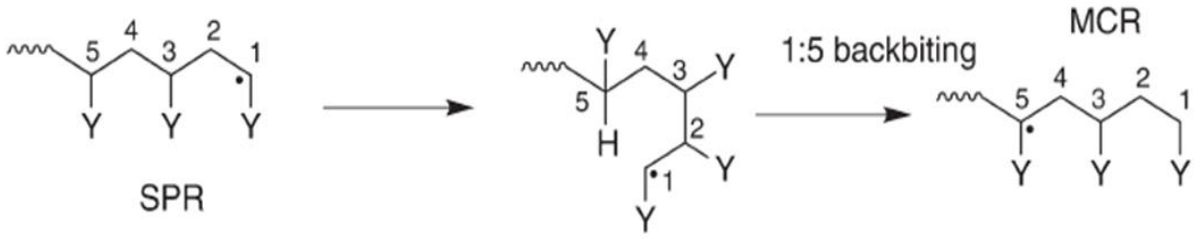

Figure 2.7: Hydrogen abstraction from SPR to MCR. Adapted with permission from M. A. Nasir, F. Heatley, P. A. Lovell, *Macromolecules* 1998, *31,* 2822-2827[81] ©American Chemical Society

Most commonly the MCR will be formed by a 1:5 abstraction, due to the formation of a 6-membered ring, with other but less probable options being 1:3, 1:7 or 1:9 transfers. The corresponding rate for a system including two different monomers 1 and 2 can then be described as:

$$R_{bb} = k_{bb}\,[P^1_{tot}]\,(P_{11}P_{11} + P_{12}P_{21}) \tag{2.15}$$

where P_{xy} represents the probability of a "y" repeat unit following an "x" unit at the copolymer chain end, with "1" indicating the active acrylate species. Once the MCR is formed, it can undergo two major continuing reactions; propagation and β-scission.[41] Due to its tertiary nature, the MCRs are more stable than SPRs, and hence reduces the overall rate of monomer consumption. β-Scission only becomes a noticeable side reaction at higher temperatures. Indications for β-scission are lower molar mass unsaturated macromonomers, which can sometimes be detected in SEC traces,[83] and result in unsaturated terminal double bonds that can also be detected by ^{1}H-NMR.[84] Two different pathways are possible (see Figure 2.8) with the direction influenced in copolymerizations by the type of radicals formed, as a neighbouring methacrylate unit will more likely obtain the radical functionality. In case of continuing propagation from a MCR a short chain branching point is formed. The resulting quaternary carbon can easily be detected in ^{13}C-NMR due to its unique chemical shift around 48 ppm.[85] The extent of branching and scission is very important for the actual polymer properties, as short chain branches may reduce crystallinity and change the rheological properties. Target molar masses might also be missed.[41] An interesting aspect is the actual control of the formation of MCRs. Recent investigations have shown that

branching can be reduced or suppressed by adequate solvent choice[17,20] or suitable chain transfer agents.[86] Especially the first case is interesting for industrial applications, as it is often an easily modified parameter. In particular hydrogen bonding induced by hydroxyl functionalities has a major effect on all backbiting mechanisms and functional monomers may also act in this manner, when present in the system.

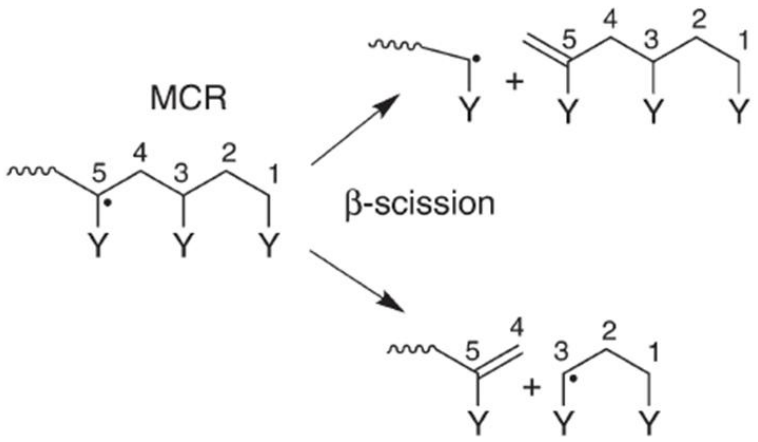

Figure 2.8: Right and left handed β-scission, a high temperature phenomena. Adapted with permission from J. Chiefari, J. Jefferey, R. T. A. Mayadunne, et al., *Macromolecules* 1999, *32*, 7700-7702[87]

2.2. Industrial challenges in solution polymerization

In addition to developing improved knowledge through PLP-SEC kinetic investigation, industry is interested in scaling up processes towards industrial reactors. In the particular case of polymer resins for automotive coatings, high temperature starved feed semi-batch reactions are typically used. The goal is a high polymer content (up to 70 wt%) solution in a volatile organic compound (VOC) as solvent, while maintaining fairly low viscosities by limiting polymer molar masses to attain an easily controllable reaction with stable and constant monomer concentration profiles. The final product will still be sprayable or easy to handle, before mixing with crosslinking agents to form the final coating on the designated

surface. Previously a model for such semi-batch processes was formulated by Hutchinson et al., utilizing a styrene/acrylate/methacrylate system without functional monomers; the model contained all the known mechanisms and side reactions that occur at these higher temperature conditions.[28] The model was tested against lab data run over a wide range of operating conditions similar to those used industrially, and its general form showed to be adequate to represent other methacrylate and acrylate monomer systems for which solvent choice does not influence reaction rates. However, limitations occur for hydrogen bonding containing system, for which solvent alters relative reactivity of monomers as well as polymer branching levels. Additional complications were related to the purity of feed stock materials, such as the presence of small amounts of dimethacrylate impurities, e.g. diethylene glycol dimethacrylates (EGDMA) that are not completely removed from commercial HEMA.[11] It was shown that such impurities led in some cases to a large increase in polymer MMs produced under semi-batch conditions for ST/HEMA and BMA/HEMA, but not BA/HEMA.[11] Further case studies also revealed a solvent dependency of the impurities influence on polymer weight average molar masses, M_w, as shown in Figure 2.9.

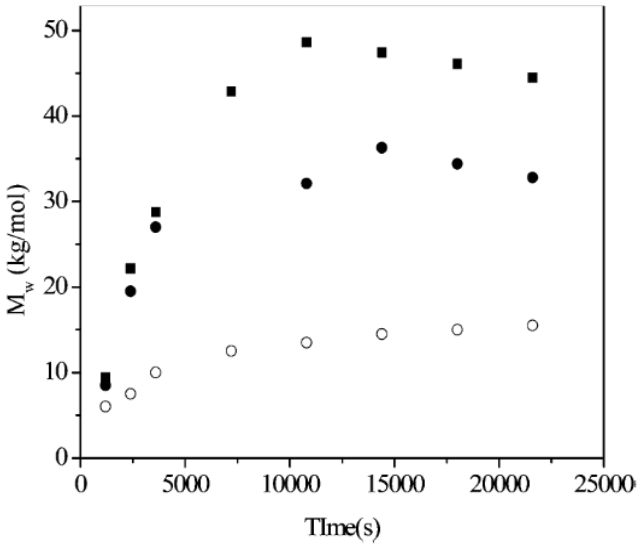

Figure 2.9: BMA homopolymerizations under starved-feed semi-batch conditions (135 ºC): hollow cycles indicate xylene solution; filled cycles indicate xylene solution with 100 ppm EGDMA; squares indicates DMF solution with 100 ppm EGDMA Reprinted with permission from K. Liang, T. R. Rooney, R. A. Hutchinson, *IECR* 2014, *53*, 7296-7304[11] ©2014 American Chemical Society

These anomalies with HEMA, the influence of solvent on relative reactivity and the large influence of EGDMA impurities, were studied only for a limited number of systems. Further work is necessary to generalize the understanding to allow for implementation in the present model. Therefore, it is of interest to investigate and compare the kinetics of the acrylate equivalent HEA. Herein kinetics may vary, as HEA (with its SPR) is significantly more reactive than HEMA, and thus the influence of solvent choice and hydrogen-bonding may be different and needs to be studied (kinetics and semi-batch) in industrially relevant solvents. Commercial HEA is also contaminated with diacrylate impurities, so it is important to know its effect on methacrylate and acrylate polymerization kinetics. Combining the results of this HEA investigation with the previous HEMA studies may also lead to insights as to how to generalize the H-bonding effects in an efficient manner for model implementation.

2.3. Conclusion

As soon as industrially relevant systems are targeted, knowledge of kinetic mechanisms and the corresponding rate coefficients becomes crucial to allow for the development of reliable models to guide process and product improvements. With the introduction of H-bonding containing monomers, even the well-understood mechanisms such as propagation need to be revisited, as additional effects caused by solvent choice, changing the incorporation of functional monomers, may occur. As more and more functional and new (bio renewable) monomers are introduced into commercial products, basic kinetic investigations are of high importance to allow for a good understanding of these complications, with the knowledge then applied to model the systems under industrially-relevant operating conditions.

Chapter 3 Kinetic investigation of hydroxyl containing monomers

The work presented in this chapter was published as *Polym. Chem.* **2016,** *7,* 4567-4574 and *Polym. Chem.* **2017,** *8,* 1943-1952. For the purpose of this thesis their content was combined and modified to provide a logical flow.

3.1. Introduction

The determination and understanding of kinetic parameters of radical copolymerization (RP) is essential for the development of industrially relevant copolymerization models used to reduce cost and waste as well as to improve the process quality. Even small improvements can lead to significant benefits for high-throughput processes. Many investigations have focused on the copolymerization of "classic" non-polar monomers of the methacrylate,[88] acrylate,[48] and styrenic[22] families in bulk or organic media, with no monomer specific solvent effects present on polymerization kinetics,[89,90] with the exception of alcohols. More recently a growing catalogue of kinetic parameters is being developed for functional monomers that are more polar or undergo hydrogen-bonding,[11,21,91–93] generally known as a powerful electrostatic force and the source for DNA self-assembly.[94] However, these studies also show that a certain level of complexity is introduced to RP systems, for example by the introduction of water as a "greener" solvent[95] (for advantages and disadvantages, please refer to source 95) that provides a very polar and dense H-bonding environment that has an immense effect on the RP kinetics of water-soluble monomers.[93,96] Functional monomers are also gaining in importance as a means to introduce reactivity to polymer chains, as part of continued research to develop improved materials and reduce solvent content.[53,92,97] Possible post-modification include crosslinking[12,98] as commonly used for automotive coatings. Accordingly, analysis of these systems must consider kinetic effects not only derived from the nature of monomer but also the solvent, in contrast to the aforementioned classic non-polar systems.

A versatile tool to understand these new functional systems and their propagation chain growth parameters is the IUPAC-recommended pulsed laser polymerization-size exclusion chromatography technique (PLP-SEC).[23] Propagation rate coefficients, k_p, for homo- and co- polymerization can be easily determined with this method, which can also be adapted to study side reactions such as acrylate backbiting and its associated rate coefficients.[54,99,100] Further modifications of the PLP technique also allow for the determination of termination kinetics when combined with additional on-line measurements of monomer or radical concentrations.[59,60]

Some general trends have emerged from these kinetic investigations, with family-like behaviour found for propagating radicals of the same nature; for example, the k_p values of alkyl methacrylates increase roughly by 50% with increasing length of the ester side chain from methyl to dodecyl, although the activation energy remains constant.[88,101] Other factors causing reactivity differences within a particular monomer family include the isometric orientation of side chains (i.e., cyclic structures)[102] and the introduction of functional groups that lead to intermolecular interactions between monomer and solvent or with the polymer chains.[9753] We have been systematically studying the influence of the hydroxyl functionality on polymerization kinetics, generally introduced to systems through addition of 2-hydroxyethyl acrylate (HEA) or 2-hydroxyethyl methacrylate (HEMA) monomers, but also possibly introduced through solvent choice. The interaction between the hydroxyl hydrogen and the carbonyl oxygen of the acrylic ester reduces the electron density at the double bond to increase its reactivity, as detected through infrared spectroscopy;[27,103] thus, the k_p value for HEMA in bulk[104] is found to be higher than that of butyl methacrylate (BMA) by a factor of 2.5. H-bonding, introduced by water as a solvent, also leads to concentration-dependent k_p in aqueous systems,[105] as well as a modified relative reactivity in copolymerization, as has been demonstrated for the most prominent monomer acrylate/methacrylate pairs HEA/HEMA[11,27] and acrylic acid/methacrylic acid (AA/MAA).[2191] While H-bonding is known to lead to the formation of dimers of MAA,[106] it has been shown that monomer dimerization does not correlate with homopropagation k_p values.[21] In an investigation of the solution copolymerization of styrene (ST) and MAA, however, it was hypothesized that interaction between MAA monomer and an incorporated MAA

unit in the polymer backbone can channel MAA towards the propagating radical, leading to an increased incorporation into the copolymer, with the effect on MAA relative reactivity more pronounced under dilute conditions.[76]

In this work, we focus on the copolymerizations of HEA and MEA with acrylic and methacrylic comonomers such as BA and BMA. Experiments were performed in different solvents such as DMF or BuOH, based on findings for HEMA copolymerizations,[11,75] which correlated to the influence of H-bonding and the previously introduced concept (see Chapters 1 and 2) of disruption and substitution. Besides the relevance of HEA as a monomer for our industrial partner, it has a wide range of applications, for example as a component in hydrogels,[107] which can be used for the removal of heavy metals.[108] Furthermore, lower critical solution temperature (LCST) behaviour is exhibited under aqueous conditions, which can be controlled by copolymer composition.[109,110] MEA itself is also an interesting monomer with a variety of applications for its copolymers,[111–113] however it was mainly chosen as a polar HEA analog without the H-bonding capabilities. The direct comparison of both systems is then used to develop a deeper understanding of the origin and magnitude of H-bonding effect on radical copolymerization kinetics.

3.2. Experimental

Monomers HEA (96 % purity, containing 200-650 ppm monomethyl ether hydroquinone as inhibitor), MEA (98 % purity, containing 50-100 ppm monomethyl ether hydroquinone as inhibitor), BMA (99 % purity, containing 10 ppm monomethyl ether hydroquinone as inhibitor), BA (≥ 99% purity, containing 10-60 ppm monomethyl ether hydroquinone as inhibitor) and the photoinitiator 2,2-dimethoxy-2-phenylacetophenone (DMPA, 99% purity) were received from Sigma-Aldrich and used without further purification. The solvents *n*-butanol (BuOH, 99% purity), dimethylformamide (DMF, 99.8 % purity), methyl isobutyl ketone (MIBK, 98.5 % purity), butyl

propionate (BPi, 98% purity) and anhydrous dimethyl sulfoxide d-6 (DMSO-d6, containing 99.9% D) were also used as received from Sigma-Aldrich.

Low conversion pulsed laser photopolymerizations were performed using 5 $mmol \cdot L^{-1}$ DMPA photoinitiator in monomer mixtures, following earlier established procedures.[11,114] All solution polymerizations were prepared using 50 vol% of solvent. Sample mixtures in a quartz cuvette were placed into a temperature-controlled unit and exposed to laser radiation of 351 nm wavelength. A Coherent Excimer Laser Xantos XS (Xe/ F_2 mixture as the reactive gas) was used as the radiation source, creating pulses of 5 ns duration with energy between 1-6 mJ/pulse. Temperatures were controlled to keep variations less than 0.5 °C during pulsing whilst maintaining conversions lower than 5% to maintain PLP structure in the resulting molar mass distributions (MMDs), as well as instantaneous composition conditions. The polymer formed was isolated by evaporating a majority of the supernatant solution under air before precipitation in a suitable ice-cold solvent. BMA homopolymers were precipitated in methanol whereas copolymers were precipitated in a 50/50 mixture of diethyl ether and hexanes. The polymer obtained was then dried under vacuum at 60 °C overnight.

Polymers were dissolved in THF at 3 $g \cdot L^{-1}$ and filtered through 0.2 µm nylon filters for SEC analysis. The SEC setup consists of a Waters 2960 separation module connected to a Waters 410 differential refractometer (DRI) and a Wyatt Instruments Dawn EOS 690 nm laser photometer multi-angle light scattering (LS) detector. The eluent THF was used at flow rates of 0.3 $mL \cdot min^{-1}$ through four Styragel columns maintained at 35 °C. The DRI detector was calibrated by polystyrene standards with narrow dispersities over the range of 870-875000 $g \cdot mol^{-1}$. The LS detector was calibrated with a single polystyrene (PS) standard as a reference. Based on PS-calibration, absolute molar mass distributions from DRI can be obtained via a suitable transformation using the known Mark-Houwink parameters. Results were verified by comparing the output from LS detection which determines absolute molar mass distributions using known

refractive indices (dn/dc values); a necessary routine as the single analysis via Mark-Houwink parameters may not be valid for all copolymerization systems. Table 3.1 provides the necessary parameters for the system examined. It is assumed that copolymerization values can be calculated based on the weight-averaged polymer composition, as shown to be valid in previous studies.[114,27]

Table 3.1: Parameters required for analysis of PLP-SEC results

Monomer	dn/dc ($mL \cdot g^{-1}$)	Mark-Houwink parameters in THF	
		K ($dL \cdot g^{-1}$)	a
HEA[27]	0.066	0.000322	0.602
BMA[115]	0.083	0.000148	0.664
Styrene[115]	0.184	0.000114	0.716

3.3. Results and discussion

3.3.1. Composition analysis of BMA/HEA systems

Copolymer composition is measured in this work by NMR spectroscopy using the side chain peak patterns of BMA and HEA (Figure 3.1). The BMA CH_2 group adjacent to the ester is found at 3.9 ppm, with two CH_2 side chain peaks from HEA at 3.5 ppm and 4.0 ppm surrounding this signal. Additionally, the HEA OH-peak is detected in DMSO-d_6 at 4.7 ppm, giving two reliable possibilities to calculate the HEA content in the copolymer. The OH-peak is assumed to be reliable as no water was detected in the dried polymer samples. The estimates from Eqn 3.1 and 3.2 were in good agreement, with the reported compositions taken as an average.

$$F_{HEA} = \frac{2 \int OH(4.7\ ppm)}{(\int CH_2(3.9\ ppm) + \int CH_2\ (4.0\ ppm))} \quad (3.1.)$$

$$F_{HEA} = \frac{\int CH_2(3.5\ ppm)}{(\int CH_2(3.9\ ppm) + \int CH_2\ (4.0\ ppm))} \quad (3.2.)$$

Given a set of samples over the whole feed composition range, a Mayo-Lewis plot can be established. Reactivity ratios were fit from Eqn 2.9 using non-linear parameter estimation tools in the modelling software PREDICI®. This model for instantaneous copolymer composition, commonly known as the terminal model,[26] has been proven to be valid for a wide range of systems. The BMA/HEA composition data in this study was obtained at 30 °C and 50 °C in bulk and in a variety of solvents with 50 vol%. A few 80 °C samples were checked to ensure that the influence of temperature on r-values is negligible, as also found in other studies.[116,117]

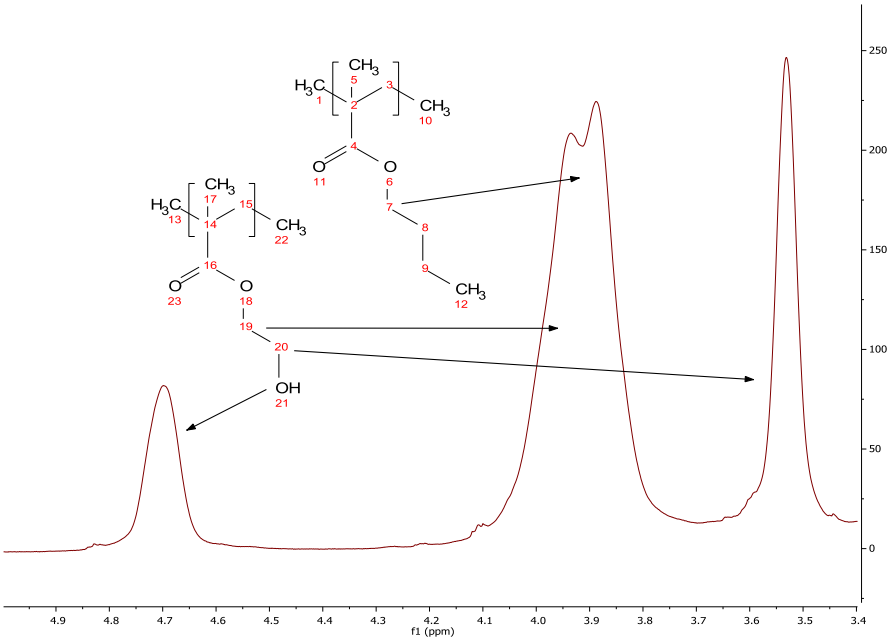

Figure 3.1: Expanded 1H-NMR spectrum showing peak assignments for determination of BMA/HEA copolymer composition in d6-DMSO; sample produced with f_{HEA} = 0.58 in DMF at 50 °C by PLP-SEC.

In the previous investigations with HEMA,[11,75] we found that H-bonding increased the activity of the hydroxyfunctional monomer relative to nonpolar BMA, but that the extent of this influence is affected by solvent choice. There is also an increased relative reactivity of HEA in HEA/BMA bulk copolymerization in comparison to BA in the non-polar BA/BMA system: as shown in Figure 3.2 a), the HEA incorporation is increased over that of BA when copolymerizing

with BMA. A similar influence of H-bonding has been seen before for HEMA copolymerizations[11,114,118] and HEA copolymerized with ST.[27] The best fit reactivity ratios in bulk are r_{HEA} = 0.37 ± 0.09 and r_{BMA} = 0.98 ± 0.13, compared to r_{BA} = 0.40 and r_{BMA} = 2.28 for the BA/BMA system.[119]

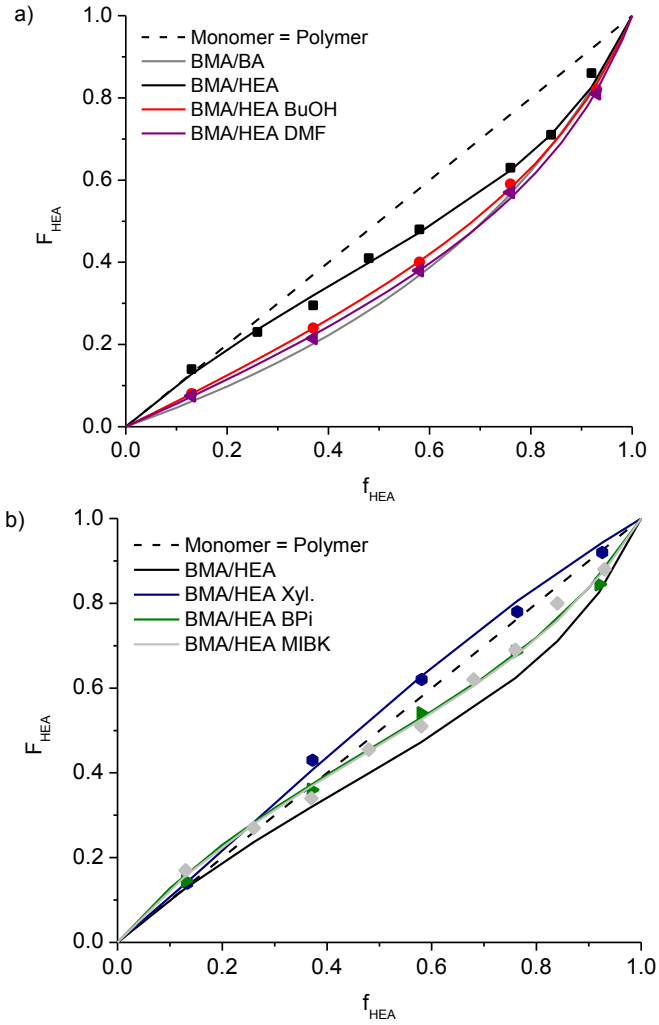

Figure 3.2: Mole fraction hydroxyethyl acrylate (HEA) in HEA/BMA copolymers as a function of HEA composition in the monomer mixture. Experimental results are given as symbols and terminal model fits as lines: a) bulk (black) and solution polymerization in DMF (50 vol%, purple) and BuOH (50 vol%, red), compared to bulk BMA/BA results from literature[119] (dark grey); b) BMA/HEA solution polymerization in MIBK (50 vol%, grey), butyl propionate (50 vol%, green) and xylenes (50 vol%, blue) in comparison to bulk BMA/HEA (black).

To the best of our knowledge, these are the first reported values for this system. Only limited data is available for the related acrylate only BA/HEA system,[120] which also reported increased incorporation rates for HEA into the copolymer, in good agreement with our findings. The significant difference in the r_{BMA} value for HEA compared to BA copolymerization is due to the reduction in electron density, and hence increased reactivity, at the HEA C=C double bond. Note that the r_{BMA} value is very close to unity, with $F_{HEA} \approx f_{HEA}$ for BMA-rich conditions ($f_{HEA} < 0.2$).

We next investigate how this behaviour changes with addition of solvent to the copolymerization system. DMF and BuOH both have a large influence on the relative reactivity in the system: as shown in Figure 3.2 a) these "high interacting" solvents lead to Mayo-Lewis plots that almost reproduce the bulk BA/BMA curve. The two solvents exert this influence by different mechanisms;[11,75,103] whereas both solvents have similar H-bonding acceptor capabilities, BuOH also promotes the BMA reactivity (similar to the increase in k_p as shown in the next section 3.3.2.) relative to HEA by providing hydrogen bonds. In contrast to that DMF, a polar aprotic acceptor that due to its mesomeric structures can be considered as partially charged, only disrupts the HEA-HEA H-bonding and reduces its reactivity relative to the bulk case. As summarized in Table 3.2, both effects result in the increase of the r_{BMA} value.

Table 3.2: Reactivity ratios (with 95% confidence intervals) for BMA/HEA copolymerizations in different solvents (50 vol%), as fit to the data sets plotted in Figure 3.2.

	Bulk	MIBK	BPi	Xyl.	DMF	BuOH
r_{HEA}	0.37 ±0.09	0.49 ±0.09	0.55 ±0.07	1.35 ±0.14	0.31 ±0.08	0.35 ±0.04
r_{BMA}	0.98 ±0.13	0.72 ±0.10	0.80 ±0.09	0.96 ±0.05	1.83 ±0.14	1.66 ±0.06

A series of solvents commonly used in resin production for coatings applications have also been studied. When changing to these lower interacting ketone (MIBK) and ester (BPi) solvents,

HEA is incorporated at slightly higher levels than seen in bulk, as shown in Figure 3.2 b). These results suggest that aliphatic side chains and carbonyl functions interact in a different fashion with the H-bonding mechanism. Whereas the carbonyl function should disrupt H-bonding, its effect is minimized or shielded through the significantly larger non-interacting aliphatic side chains. The logical follow-up can be observed when using xylenes, with no functional group. Accordingly, the reactivity of HEA increases. This trend has been seen before for HEMA copolymerization with styrene in toluene.[75] For HEA copolymerized with BMA, it leads to the unusual result that the acrylate component is incorporated at a greater rate into the copolymer than the methacrylate over the complete HEA composition range in xylenes. There have been several hypothesis put forward to explain the strength of hydrogen bonding in diluted systems such as bootstrap effects or other polar-polar interactions which result in the formation of local concentration gradients, promoting the reactivity of one monomer;[121] however, this explanation is inconsistent with the k_p^{cop} results presented below.

A generalized trend can be seen in the reactivity ratios summarized in Table 3.2, which shows that solvent effects manifest themselves in changing the relative reactivity of monomer addition to the BMA radical for the strongly interacting solvents. The influence of other solvents is seen by small changes in both values that push the system closer towards the diagonal. Similar effects have been observed before for the HEMA systems.[11,75] The effect of xylene remains the only exception, with a strong promotion of HEA incorporation.

3.3.2. Determination and representation of k_p^{cop}

k_p^{cop} was determined over a range of BMA/HEA compositions in bulk and solution following the IUPAC recommended procedure of PLP-SEC. Once SEC curves for the PLP-generated polymer samples were obtained, the first derivative was taken to determine the inflection points used to calculate k_p^{cop} according to Eqn 2.5, with all other parameters known.

Figure 3.3 a) is an example of the MMDs obtained for HEA/BMA samples of two different compositions (10 and 30 vol% HEA in comonomer mixture) prepared in 50 vol% BuOH at 50°C and two different repetition rates. One can see typical PLP structure with the specific shape of several maxima, representing polymer created after *n* laser bursts. The magnitude as well as the positions of the first and second maxima on the first derivative plot vary with frequency; the second maximum is slightly more pronounced at the higher frequencies (here 100 Hz), as a greater fraction of polymer radicals survive the first terminating burst. As shown in Figure 3.3 b), up to four inflection points can be seen under some conditions.

The first peak in the MMD remains the largest maximum, showing that proper frequencies were chosen for the system to obtain high quality results.[88] The positions shift proportionally to the frequency, doubling when frequency is halved from 100 to 50 Hz. (Note that the position of the first inflection point of each 50 Hz sample is roughly at the same position of the second inflection point of the respective 100 Hz sample.) The influence of HEA content on k_p can also be seen in Figure 3, as MMDs shift to higher *M* at increased HEA content. The continuous quality of PLP-SEC traces for the reported data also shows that side reactions such as backbiting can be neglected under these conditions, however should be taken into consideration for acrylate only systems, as reported elsewhere.[54]

The complete set of experimental results (PLP/SEC conditions and resulting MM analysis) are tabulated as Supporting Information (please refer to Table A.3-Table A.8), which also documents the good agreement between inflection point position determined by the two (RI and LS) detectors. Throughout the entire set of data, it was found that the reproducibility of k_p at a given temperature and composition stayed within the expected typical error of roughly 15%;[93] in most cases agreement was within 10%. Values of k_p^{cop} could only be measured to $f_{HEA} = 0.8$, as copolymers with greater HEA fraction are insufficiently soluble in THF for SEC analysis. Similar to as shown in Figure 3.3, the IUPAC consistence criterion for all experiments used to estimate

k_p^{cop} were fulfilled, with all samples having a ratio of two between the first and second inflection points.

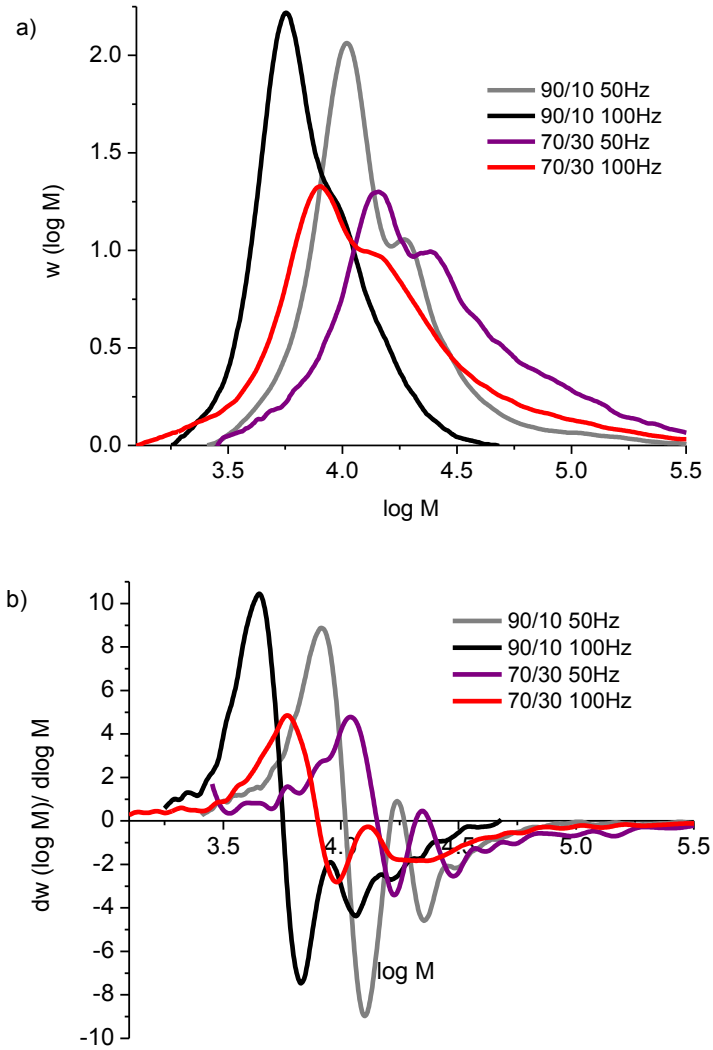

Figure 3.3: Polymer MMDs (a) and corresponding first derivative plots (b) from SEC analysis of PLP-generated BMA/HEA copolymers prepared in BuOH at 50 °C based on monomer volume fraction for BMA/HEA 90/10 at 50 Hz (grey), 100 Hz (black) and BMA/HEA 70/30 at 50 Hz (purple) and 100 Hz (red).

Bulk homopolymerization k_p values are known at 50 °C to be 753 $L \cdot mol^{-1} \cdot s^{-1}$ for BMA[88] and 33000 $L \cdot mol^{-1} \cdot s^{-1}$ for HEA,[27] differing by a factor of over 40. As shown in Figure 3.4, the

k_p^{cop} values determined by PLP-SEC do not dramatically increase from the BMA value with increasing HEA content: with f_{HEA} = 0.77, k_p^{cop} at 50 °C is 3815 L·mol^{-1}·s^{-1}, five times higher than k_{pBMA} and at 80 °C the relative increase is very similar. For a better understanding of this behaviour, a consideration of the radical fractions is helpful. Under the assumption of the terminal model the radical fraction is dependent on crosspropagation rate coefficients and monomer composition.

$$\frac{[P_1]}{[P_2]+[P_1]} = \frac{k_{P_{21}} f_1}{k_{P_{12}} f_2 + k_{P_{21}} f_1} \tag{3.3}$$

where $[P_i]$ is the concentration of chain-end radical i. Setting species 1 as BMA, and with known homopropagation k_p and r-values, it can be calculated that k_{p21} is significantly larger than k_{p12}, favouring the crosspolymerization such that most radicals end in a methacrylate moiety. Thus BMA-HEA behaves as a standard methacrylate acrylate system,[11122] with a dominant fraction of BMA radicals controlling the reaction kinetics.

Figure 3.4 also contains k_p^{cop} values measured in the presence of the non-interacting solvents MIBK, BPi, and xylenes. The data coincide closely with the bulk data over the entire range of composition at both temperatures studied. The slight increase in k_{pBMA} at 80 °C from 1550 L·mol^{-1}·s^{-1} in bulk to 1650 L·mol^{-1}·s^{-1} in ketones and esters and 1700 L·mol^{-1}·s^{-1} in xylenes is consistent with arguments regarding the influence of relative molar volumes of solvent and monomer,[89,123] but is within experimental uncertainty. The negligible solvent effect on k_p^{cop} for this class of solvents is perhaps surprising, given the influence of solvent on copolymer composition (Figure 3.2 b)). The same result (identical k_p^{cop} but varying composition in bulk vs toluene) was also observed for the HEMA/ST system.[75]

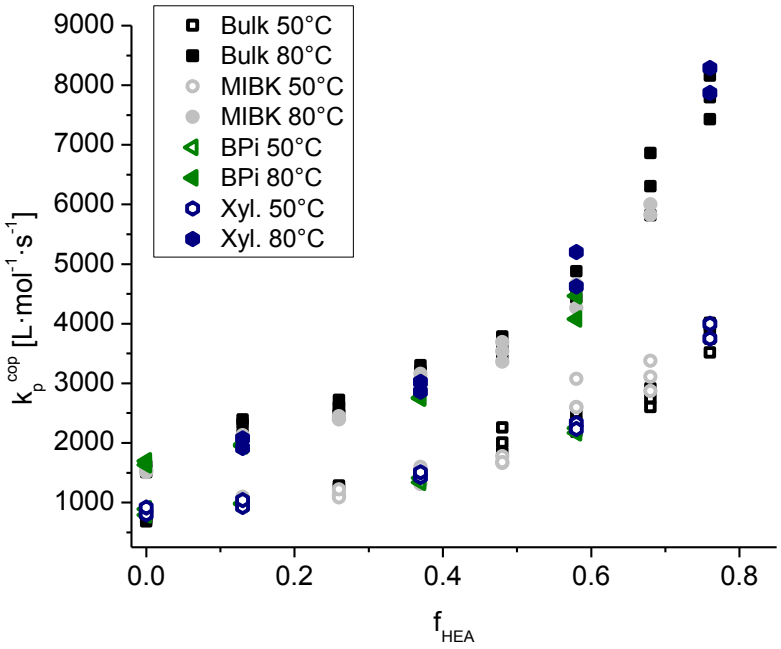

Figure 3.4: k_p^{cop} for BMA/HEA copolymerization as a function of HEA composition (f_{HEA}), as measured by PLP/SEC for bulk (black) and solution polymerization in MIBK (grey), xylenes (blue) and butyl propionate (green) at 50 and 80 °C.

In contrast to the low interacting solvents, BuOH and DMF affect both copolymer composition and k_p^{cop}. Although their influence on the H-bonding mechanism are opposite (BuOH promotes BMA reactivity, DMF decreases HEA reactivity), the resulting k_p^{cop} trends are similar; as shown in Figure 3.5, the k_p^{cop} values are reduced relative to the bulk values for both solvents. This decrease is consistent with the increased values of r_{BMA} (Table 3.2) that lead to an increased BMA incorporation and a higher BMA radical fraction due to the reduced k_{p12} value (Eqn 3.3).

A more detailed examination is necessary to understand why DMF and BuOH have a comparable effect on k_p^{cop}, starting with the homopolymerization of BMA. The value of k_{pBMA} in BuOH is 2200 $L \cdot mol^{-1} \cdot s^{-1}$ at 80 °C, roughly 35% higher than in bulk due to the introduction of H-bonding. Meanwhile DMF has a negligible effect on k_{pBMA}, as no H-bonding is present. As soon as HEA is introduced to the system k_p^{cop} decreases relative to the bulk system for both solvents.

DMF continuously disrupts the H-bonding of HEA so that its reactivity is reduced to that of an alkyl acrylate. However, BuOH continues to promote BMA reactivity, reducing the HEA radical fraction in the system, thus reducing k_p^{cop} relative to bulk. For the latter system, this decrease is counteracted by the positive solvent effect of BuOH on BMA, but as f_{BMA} decreases the net effect is a decreased k_p^{cop} relative to bulk at 80 °C. This influence of BuOH on k_p^{cop} may have some temperature dependency, however, as at 50 °C the k_p^{cop} values remain higher for bulk values even at higher HEA. Similar trends have been reported and attributed to the influence of temperature on H-bonding.[124] At high temperatures it is hypothesized that the increased kinetic energy disrupts more H-bonds than at lower temperatures due to increased molecular movement. Similar effects are also known from polymerizations in high H-bond concentration systems, e.g. aqueous solution.[125] A further approach to explain these results can be found in Figure A.1, which contains room temperature IR measurements that demonstrate the influence of H-bonding on the carbonyl stretching even at low HEA content.

Often the implicit penultimate unit model (IPUE), presented in Eqn 3.4, is required to represent k_p^{cop} data.

$$k_p^{cop} = \frac{r_{BMA} f_{BMA}^2 + 2 f_{BMA} f_{HEA} + r_{HEA} f_{HEA}^2}{\left(\frac{r_{BMA} f_{HEA}}{\bar{k}_{BMA,BMA}}\right) + \left(\frac{r_{HEA} f_{HEA}}{\bar{k}_{HEA,HEA}}\right)} \quad (3.4)$$

$$\bar{k}_{BMA,BMA} = \frac{k_{p_{BMA,BMA,BMA}} (r_{BMA} f_{BMA} + f_{HEA})}{r_{BMA} f_{BMA} + \left(\frac{f_{HEA}}{s_{BMA}}\right)} \; ; \; \bar{k}_{HEA,HEA} = \frac{k_{p_{HEA,HEA,HEA}} (r_{HEA} f_{HEA} + f_{BMA})}{r_{HEA} f_{HEA} + \left(\frac{f_{BMA}}{s_{HEA}}\right)} \quad (3.5)$$

$$with \; s_{BMA} = \frac{k_{p_{HEA,BMA,BMA}}}{k_{p_{BMA,BMA,BMA}}} \; and \; s_{HEA} = \frac{k_{p_{BMA,HEA,HEA}}}{k_{p_{HEA,HEA,HEA}}}$$

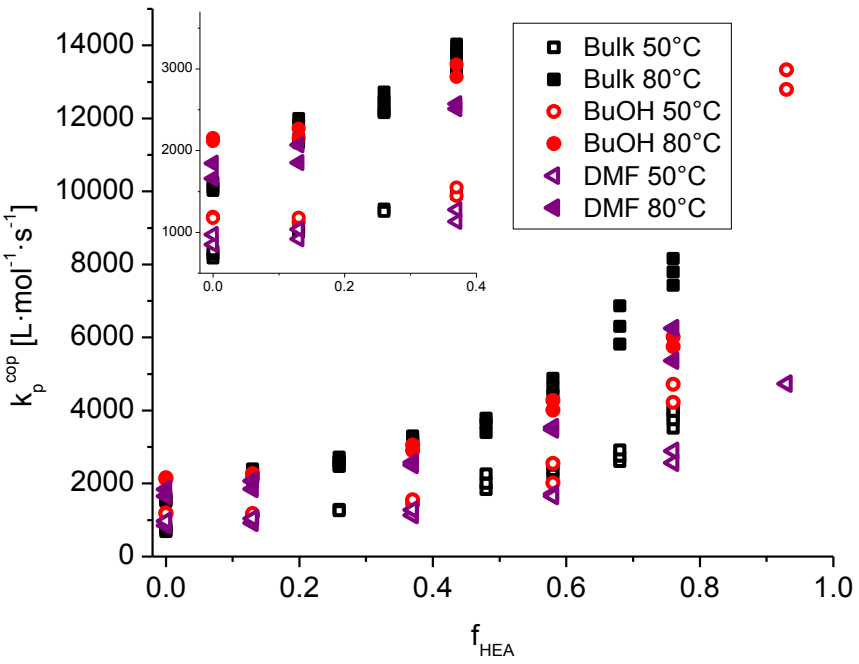

Figure 3.5: k_p^{cop} for BMA/HEA copolymerization as a function of HEA composition (f_{HEA}), as measured by PLP/SEC for bulk (black) and solution polymerization in BuOH (red) and DMF (purple) at 50 and 80°C.

The polymer radical selectivity parameters s_1 and s_2 account for the influence of the penultimate unit next to the propagating radical on monomer addition.[27,75] However, the relative rates of monomer addition are not influenced by the penultimate unit, such that r-values can be fit according to the terminal model. To complete our study, we examine whether the terminal model (Eqn 2.10) is sufficient to represent the k_p^{cop} data, or whether the extra parameters introduced by the IPUE are required to fit the data. Figure 3.6 compares experimental results for the bulk system to the terminal model prediction. As observed for other acrylate/methacrylate[11,126,127] systems and also ST/HEA,[27] the predictions of k_p^{cop} are lower than the experimental data. Then, the IPUE model was fit to the data, again using the non-linear parameter estimation of PREDICI®. While the IPUE can be used to successfully represent the data (see Figure 3.6), there is high uncertainty in the s estimates, especially s_{HEA} which controls the slope of the curve at higher HEA content. However, regardless of temperature the fits still allow for a good representation of experimental

data. More data for HEA-rich systems, including homopolymerizations, is required to reduce the uncertainty in the parameters. As shown in Figure A.2 and Figure A.3, the IPUE is also required to fit the data obtained in BuOH and DMF, as the TM also underpredicts the experimental data.

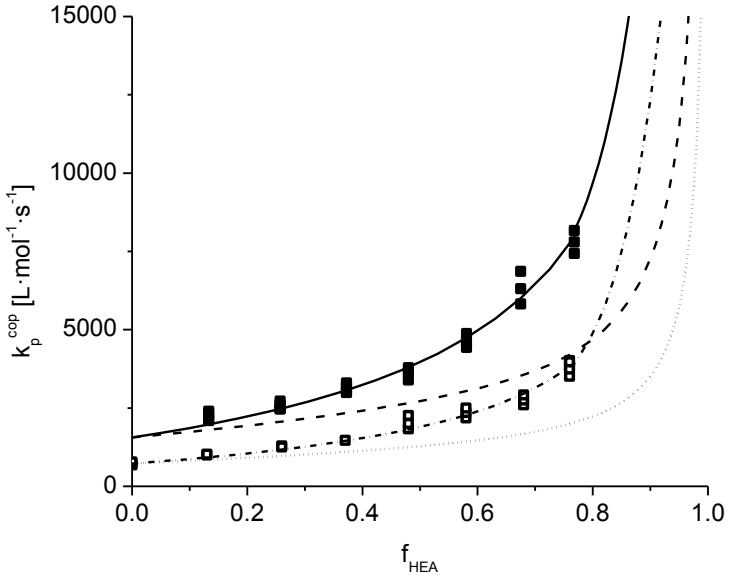

Figure 3.6: Experimental results for k_p^{cop} as a function of f_{HEA} for bulk BMA/HEA copolymerizations at 50 (open symbols) and 80 °C (filled symbols) in comparison to TM predictions (dotted line at 50 °C, dashed line at 80 °C) and IPUE fits (dot-dashed line at 50 °C, solid line at 80 °C) with $s_{BMA} = 3.03 \pm 0.36$ and $s_{HEA} = 1.0 \pm 10$

For the low interacting solvents MIBK, BPi and xylenes it was found experimentally that the variation of k_p^{cop} with HEA content was similar to that of bulk (see Figure 3.4), although composition data indicate a higher incorporation of HEA into the copolymer in these solvents relative to the bulk system (see Figure 3.2 b)). Surprisingly, as shown in Figure 3.7, the TM predictions for these three solvents calculated using the reactivity ratios summarized in Table 2 provide an excellent representation of the experimental data, despite the model's inability to represent the bulk system. The fact that k_p^{cop} is well represented by TM predictions will facilitate the modelling of BMA/HEA copolymerization in these common solvents.

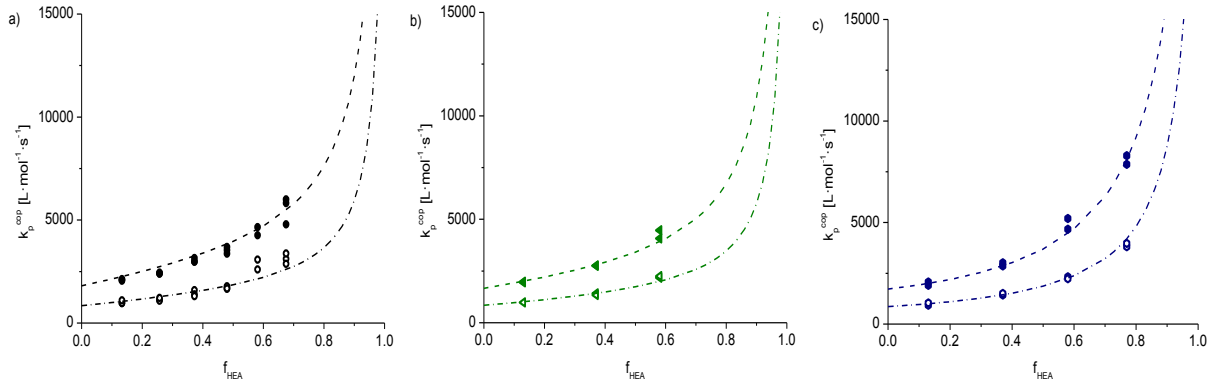

Figure 3.7: Experimental results for k_p^{cop} as a function of f_{HEA} by PLP/SEC for BMA/HEA solution copolymerization at 50 (open symbols) and 80 °C (filled symbols) in MIBK (a), BPi (b) and xylenes (c) in comparison to the TM predictions (lines) calculated using reactivity ratios from Table 3.2

3.3.3. Acrylate only systems

3.3.3.1. BA/HEA copolymerization kinetics

A common starting point for the analysis of copolymerization kinetics is the copolymer composition. For the BA/HEA system ^{1}H-NMR was performed to measure the compositions of copolymer produced via a series of low-conversion PLP experiments performed with known comonomer compositions. The resulting copolymer vs. comonomer composition data were used to estimate the terminal model reactivity ratios fit using the non-linear parameter estimation capabilities of the modelling software PREDICI®, as described in our previous BMA/HEA study.[19] Experiments were performed at 50 ºC covering the complete range of composition for the bulk system, as well as for copolymers produced with 50 vol% monomer in various solvents. Temperature can be assumed to have a negligible effect on copolymer composition, as found in previous studies.[19,117] A 1986 study by Catala et al.[120] found that HEA possessed an increased reactivity in comparison to a non-polar acrylate, similar to what was observed for the corresponding methacrylate relatives in our previous study;[19] no further values for

BA/HEA reactivity ratios could be found. As shown in Figure 3.8, the fraction of HEA incorporated into the copolymer is greater than its fraction in the monomer phase in the bulk system. The preferential incorporation of HEA into the copolymer is also reflected by the best-fit reactivity ratios, r_{BA} = 0.35 ± 0.06 and r_{HEA} = 1.64 ±0.34. These values are, within experimental error, the same as found for the equivalent bulk methacrylate system, BMA/HEMA.[11] This important finding indicates that the influence of monomer induced H-bonding on copolymerization is of similar magnitude for acrylate and methacrylate only systems. However, it is not clear why the HEA (or HEMA) hydroxyl functionality does not also promote the reactivity of the BA (or BMA) in the bulk system; this behaviour may be related to hydrogen bonding between HEMA monomer and units incorporated in the chain, an idea put forth by Noguchi and Kuzuya[76] and currently under further investigation.[128]

The previous methacrylate study also investigated the influence of solvent on the copolymerization parameters, finding that the additional H-bonding introduced through the addition of BuOH equalized the relative reactivity of HEMA and BMA such that the copolymer composition curve shifted to the diagonal.[11] This result was explained by the role of BuOH in establishing H-bonds to both BMA and HEMA monomeric acrylate carbonyl groups. The same behaviour is seen in Figure 3.8 for HEA/BA, with a clear shift to equal reactivity seen when copolymerized in BuOH; the data lie slightly above the diagonal, indicating that a minor preference for HEA incorporation (perhaps caused by marginally stronger H-bonding from HEA than from BuOH) is maintained. The effect of conducting the copolymerization in DMF is similar, with the copolymer composition equal to comonomer composition for BA/HEA (Figure 3.8) as was also found for BMA/HEMA.[11] However, the reason behind the behaviour is quite different, in that DMF disrupts the H-bonding in the system due to its strong H-bonding acceptor properties. Therefore, the two solvent-induced results for BuOH and DMF are identical, but are caused by different effects, namely substitution versus disruption.

In our previous study of HEA/BMA copolymerization, we also examined the influence of less-interacting solvents commonly used in industry, such as ketones and xylenes. These data turned out to be more difficult to interpret; with no functional groups to completely disrupt or induce H-bonding, the

relative incorporation of HEA into the copolymer was found to be even greater than for the bulk system.[19] As presented in Figure 3.8 and summarized in Table 3.3, use of the non-interacting solvents MIBK and xylenes leads to copolymer composition curves that are similar to that of the bulk BA/HEA system: i.e., still with significantly increased HEA incorporation over BA, as also found by Catala et al. in 2-methoxyethanol.[120] Thus, the effects of non-interacting solvents are of different magnitude for HEA copolymerized with BA (HEA compositions in xylenes/MIBK similar in bulk) than with BMA (HEA incorporation enhanced in xylenes/MIBK compared to bulk), although both systems maintain the preferential incorporation of HEA. Further discussion is deferred until after presentation of the accompanying k_p^{cop} data and the comparison between HEA and MEA copolymerization systems.

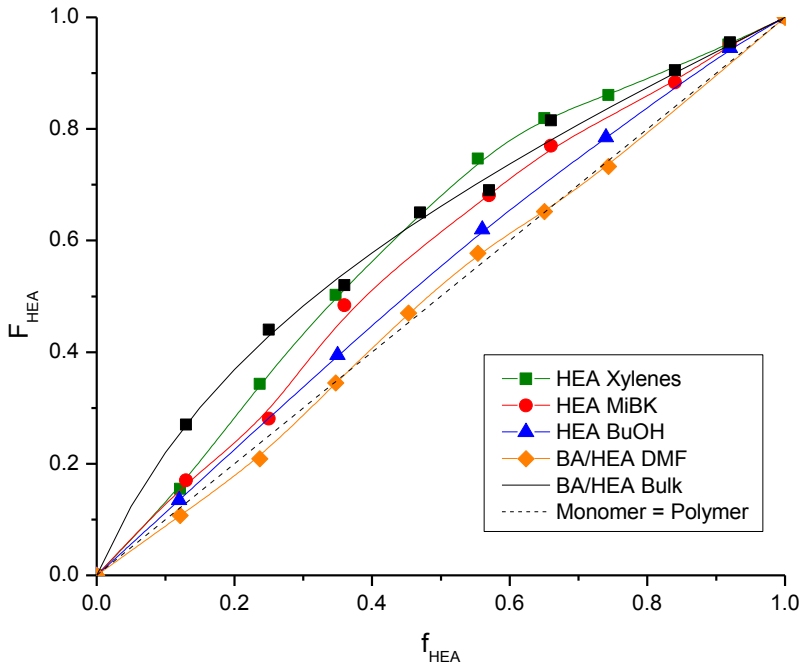

Figure 3.8: Mole fraction of HEA incorporated into copolymer (F_{HEA}) as a function of HEA molar fraction in the monomer mixture (f_{HEA}) measured experimentally (points) and respective terminal model data fits (lines) for BA/HEA copolymerization in bulk (black), xylenes (green), MIBK (red), BuOH (blue) and DMF (orange). Solution experiments conducted with 50 vol% solvent. Best-fit reactivity ratios summarized in Table 3.3.

To complement the copolymer composition data, the PLP-SEC technique has been used to determine how the copolymer-averaged propagation rate coefficient, k_p^{cop}, varies with HEA content in bulk as well as in solution. Unfortunately, the analysis was limited by the solubility of the formed copolymers in THF, found to be $F_{HEA} \approx 0.6$ for the particular MM of PLP-generated acrylates. Results for the HEA/BA study are presented for the 50 ºC experiments, with additional data exhibiting the same trends at 30 ºC included as Figure A.4. The PLP-structured MMDs contain at least two inflection points clearly located on the first-derivative plots,[23,40] as shown in Figure 3.9 for copolymer produced from pulsing a 70/30 v/v BA/HEA mixture in 50 vol% DMF and an 80/20 BA/HEA mixture in 50 vol% xylenes, each at two different repetition rates. The value of k_p^{cop} is again calculated from the position of the first inflection point according to Eqn 2.5. Pulse repetition rates for acrylate only-recipes were kept at a minimum of 400 Hz for bulk and 300 Hz for solution polymerizations to keep the MM in an easily measurable range, while also suppressing the influence of backbiting on the study of chain-end propagation kinetics.[54,129]As seen in Figure 3.9, the MMDs and positions of the first inflection points shift to higher MM values as the repetition rate is decreased, with the corresponding k_p^{cop} values showing good consistency within 10%.

The complete set of results are tabulated as Table A.12 - Table A.16, with the k_p^{cop} values plotted as a function of HEA mol fraction in Figure 3.10. The BA homopolymer value from our studies, 26 500 $L \cdot mol^{-1} \cdot s^{-1}$, is in excellent agreement with the predicted value of 27 500 $L \cdot mol^{-1} \cdot s^{-1}$ from the Arrhenius relation fit to the benchmark data set for bulk BA.[38] Starting with that value, a continuous increase in k_p^{cop} is observed with increasing HEA content in the BA/HEA mixture (Figure 3.10 a)), as expected from the influence of hydroxyl functionality on propagation kinetics.[40,130] A strong influence of H-bonding is seen even at low HEA monomer content, with the addition of 13 mol% HEA increasing k_p^{cop} by 17% above the bulk BA value.

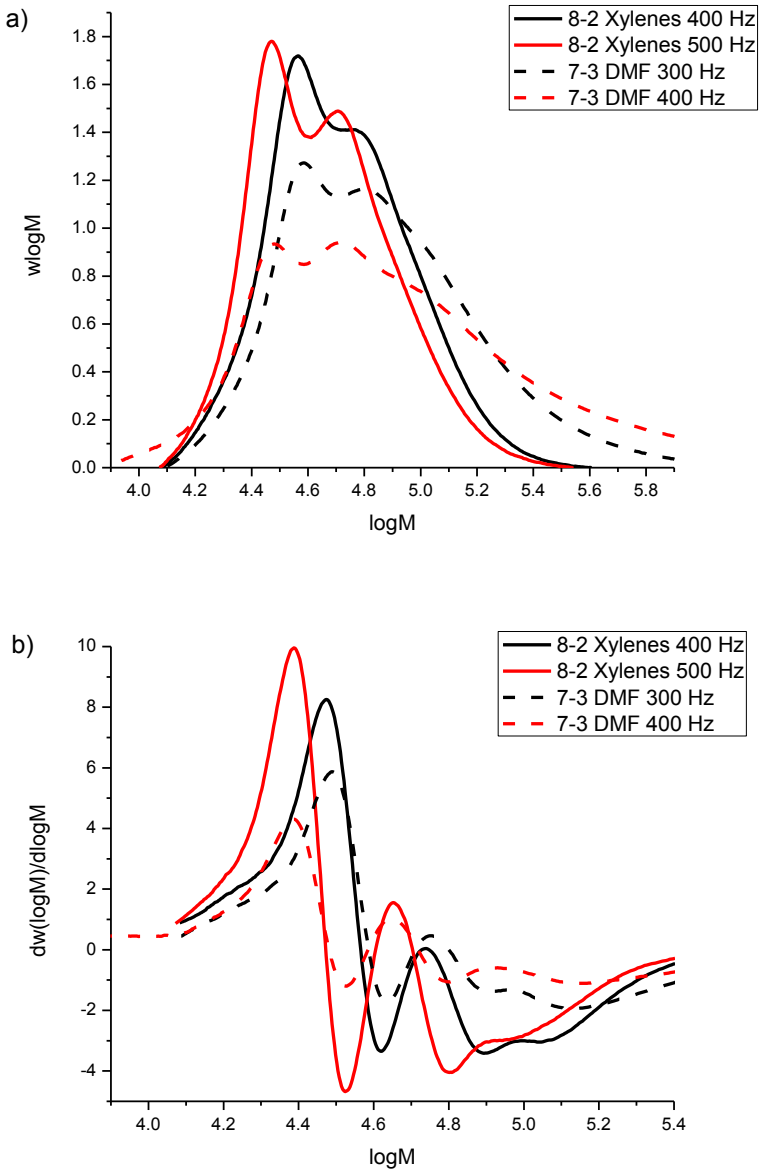

Figure 3.9: a) Molar mass distributions of PLP generated copolymer samples generated at 50 °C from comonomer mixtures of 20/80 BA/HEA (v/v) in xylenes at 400 Hz (—) and 500 Hz (—), and of 30/70 BA/HEA (v/v) in DMF at 300 Hz (--) and 400 Hz (--); b) First derivative plots of respective distributions

The increase continues in a linear fashion to f_{HEA} = 0.5, and then levels out for the last measured composition at 60 mol% HEA. The value of 41 000 L·mol^{-1}·s^{-1} at f_{HEA} = 0.5, however, is higher than the previously published HEA homopropagation value of 33 000 L·mol^{-1}·s^{-1} at 50 °C.[27] This surprising result

suggests that the HEA homopropagation kinetics should be reinvestigated: while k_p^{HEMA} [104] was measured to be more than twice the value of k_p^{BMA}, [115] the literature value of k_p^{HEA} is only 20% higher than the BA value.

The reason for the increase in k_p^{cop} with HEA content is hypothesized to be a combination of increased polarity and H-bonding, both effects increasing the reactivity through the decreased electron density at the double bond.[103] The results obtained in BuOH support this hypothesis, as the k_p^{cop} data are, within experimental uncertainty, the same as the bulk results at intermediate HEA levels (Figure 3.10 a)). At lower HEA levels (including BA homopolymerization), the k_p^{cop} values measured in BuOH are higher than those in bulk due to the higher concentration of H-bonding species present. It is hypothesized that interactions with BuOH disrupt the HEA-HEA hydrogen bonding, increasing k_p^{cop} through interactions with carbonyl groups of both BA and HEA monomer units. This interpretation is supported by the composition data (Figure 3.8), as the reactivity ratios for both monomers are close to unity in BuOH. The copolymerization of HEA and HEMA was found to follow a typical acrylate/methacrylate behaviour,[131] consistent with the idea that the H-bonding equally influenced the reactivity of both monomers. The postulated substitution and disruption mechanism is confirmed by the PLP-SEC experiments performed in DMF, also shown in Figure 3.10 a). The value of k_p^{cop} only slightly increases from the BA value with increasing HEA content, as the DMF decreases HEA reactivity by disruption of the H-bonding, a behaviour previously detected for 2-hydroxypropyl methacrylate in THF.[89] The increased polarity of HEA compared to BA still causes a slight increase in k_p^{cop} with increasing HEA content, a result mirrored by the MEA system described in the next section.

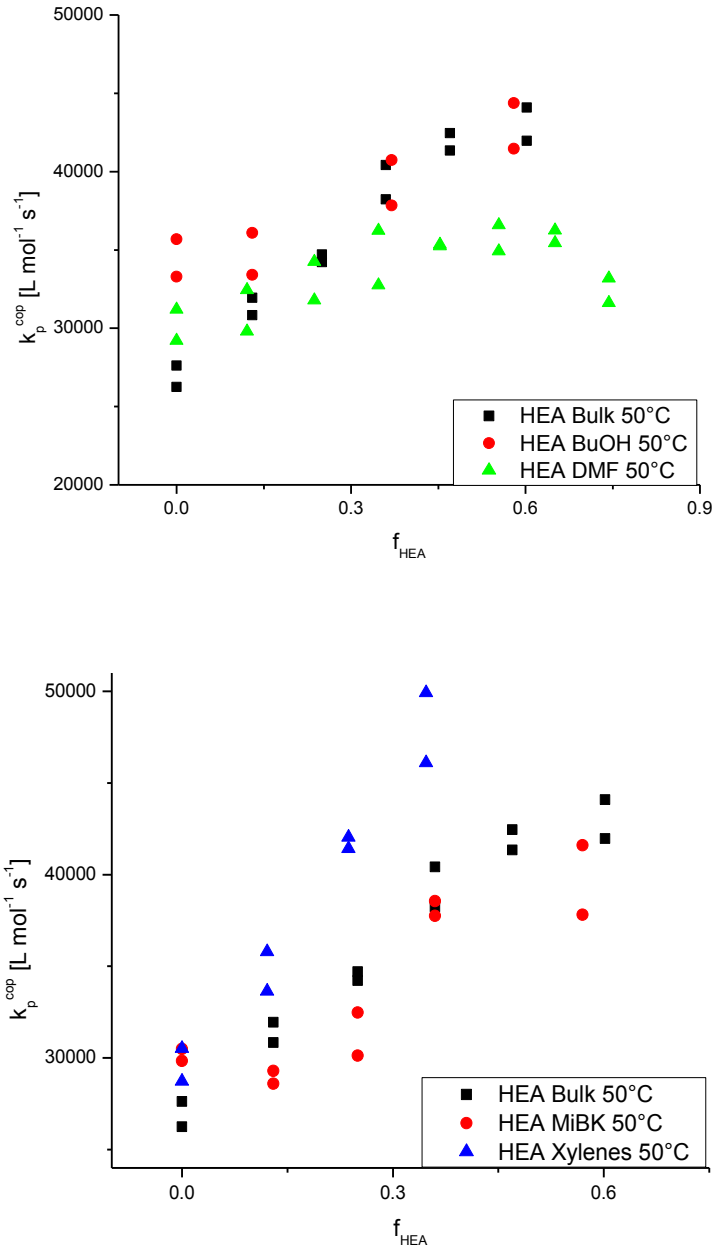

Figure 3.10: a) Evolution of k_p^{cop} for BA/HEA as a function of HEA monomer mole fraction at 50 °C in (a) bulk (black), BuOH (red) and DMF (green), and (b) in bulk (black), MIBK (red) and xylenes (blue).

The influence of the non-interacting solvents xylenes and MIBK on BA/HEA k_p^{cop} have also been compared to bulk behaviour, as shown in Figure 3.10 b). While the incorporation of HEA into the copolymer in MIBK is slightly reduced compared to the bulk system (see Figure 3.8 and Table 3.3), the

evolution of k_p^{cop} in MIBK is quite similar to that in bulk, with the values in MIBK perhaps slightly lower. A similar result was obtained in our previous BMA/HEA study.[19] Since the influence of MIBK as a solvent on propagation kinetics is negligible for both copolymer systems, it can be concluded that the carbonyl function of the solvent is minimally interfering with the extent of HEA H-bonding.

Finally, we consider the results obtained in the non-polar xylenes. Although the copolymer composition produced in xylenes does not deviate greatly from the bulk system (Figure 3.8), it is seen in Figure 3.10 b) that the k_p^{cop} values increase with increasing HEA content in the comonomer mixture at a greater rate than seen in bulk, reaching a value of 48 000 $L \cdot mol^{-1} \cdot s^{-1}$at $f_{HEA} = 0.35$, 20% higher than the corresponding value measured for bulk BA/HEA. Experiments at higher HEA compositions were performed but the polymer could not be analyzed by SEC analysis in THF, as the solutions could not be quantitatively filtered through 0.2 μm nylon filters. The reason behind the higher k_p^{cop} for BA/HEA in xylenes is unclear, as a similar increase (relative to bulk behaviour) was not seen for BMA/HEA.[19] As hypothesized by Noguchi and Kuzuya,[76] perhaps the association between free polar monomer and recently polymerized units near the radical chain end leads to increased incorporation of the polar monomer, especially under diluted conditions in non-polar solvents, and thus the observed increase in k_p^{cop} in the acrylate only system. In contrast, k_p^{cop} in the methacrylate/acrylate system is largely controlled by the methacrylate (BMA) radical and thus is less affected by the H-bonding of the system.

3.3.3.2. BA/MEA Copolymerization Kinetics

A study of the copolymerization kinetics of BA/MEA has also been conducted to determine whether the effects of HEA on copolymerization kinetics can be attributed to increased reactivity caused by H-bonding or is simply a result of the increased polarity of the monomer relative to BA. The procedures and experimental conditions used for the BA/HEA study are repeated, but replacing the hydroxy functionality of HEA with the methoxy group of MEA. Copolymer composition was analyzed again through ^{1}H-NMR over the full range of feed compositions to determine system reactivity ratios.

Therefore, the ratio of the signals arising from the distinct monomer ester side chains was taken. Figure 3.11 shows the spectrum of poly(MEA), and a copolymer of BA and MEA (poly(BA-co-MEA)). The CH_2 group adjacent to the ester group creates a signal at 4.20 ppm in poly(MEA), whereas the same group in poly(BA) produces a peak at 4.05 ppm. The deshielding effect introduced by the methoxy group in MEA creates a resonance of the adjacent CH_2 and CH_3 groups at 3.57 ppm and 3.36 ppm, respectively. In contrast, the butyl chain in poly(BA) produces multiplets at lower chemical shifts, notably the triplet at 0.95 ppm arising from the terminal CH_3 group. Integrating these resolved peaks allows for calculation of relative monomer composition following Eqn 3.6:

$$F_{MEA} = \frac{\int CH_2(3.57\ ppm)}{\int CH_2(4.20\ ppm) + \int CH_2(4.05\ ppm)} \tag{3.6}$$

The results were verified with the triplet at 0.95 ppm to determine the BA (or BMA) content using Eqn 3.7:

$$F_{BA/BMA} = \frac{\frac{2}{3}\int CH_3(0.95\ ppm)}{\int CH_2(4.20\ ppm) + \int CH_2(4.05\ ppm)} \tag{3.7}$$

The calculations were in good agreement, and the reported composition is the average of the two values.

The sharp peak at 3.94 ppm stems from monomethyl ether hydroquinone inhibitor, while the peak at 3.23 ppm is attributed to DMPA photoinitiator residue. The region spanning form 1.4-2.5 ppm contains the resonance from protons in the polymer backbone. Monomers configured with *meso* tacticity give rise to the peaks centred at 1.95 ppm and 1.52 ppm, whereas those in a *racemo* arrangement produce the peak at 1.69 ppm.[132] Note that no residual monomer peaks are found after isolation.

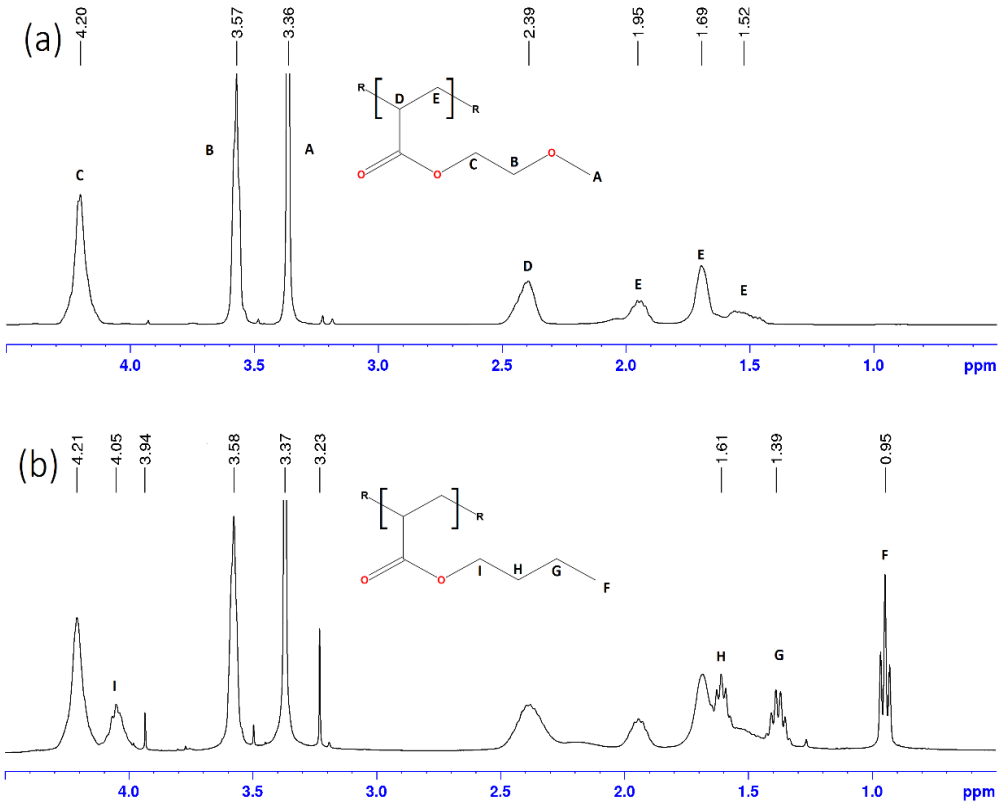

Figure 3.11: ^{1}H NMR assigning peaks to their respective protons (a) of poly(MEA) in $CDCl_3$ and (b) poly(BA-co-MEA) in $CDCl_3$ from a bulk mixture of 30 vol% BA (balance MEA) at 50 ºC

Copolymerization experiments were conducted in bulk and in BuOH and DMF solution, as these solvents had the most influence on HEA reactivity. As shown in Figure 3.12, the copolymer composition measured for all three systems was identical and lay along the diagonal (F_{MEA}=f_{MEA}), indicating that the relative reactivity of MEA and BA are identical (r_1=r_2=1) independent of solvent choice. Comparing this finding to the HEA/BA results (Figure 3.8; with HEA/BA bulk results also shown in Figure 3.12), it can be concluded that it is the hydroxyl function rather than the increased polarity that increases the relative reactivity of HEA. Despite its polar nature, MEA does not interact differently than BA upon the addition of a polar solvent such as BuOH. Indeed, MEA can be seen as a classic comonomer, with reactivity similar to any other alkyl acrylate: thus, for an acrylate-acrylate copolymerization r_1=r_2=1, independent of solvent choice.

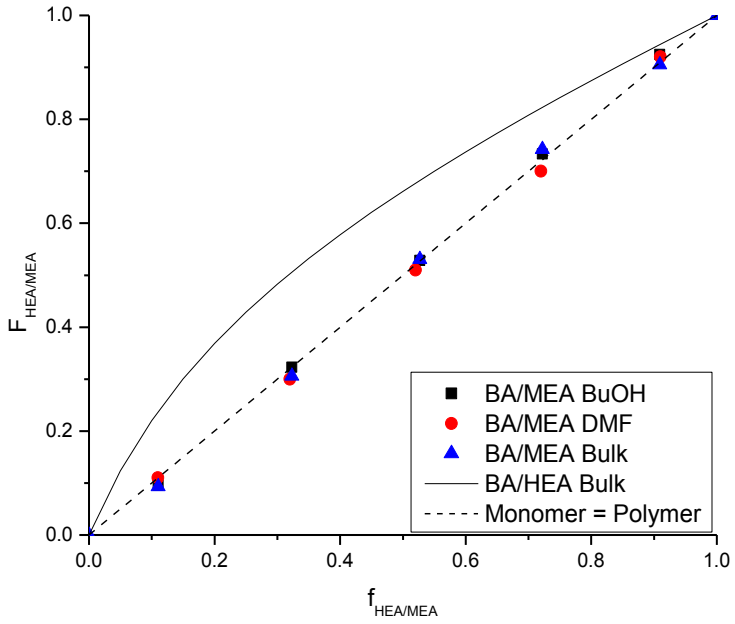

Figure 3.12: Mole fraction of MEA or HEA incorporated into copolymer as a function of the mole fraction in the monomer mixture. Mayo-Lewis plot for BA/HEA copolymerization in bulk (—) and copolymer composition data for BA/HEA copolymerization in DMF (red) and BA/MEA copolymerization in bulk (blue) and BuOH (black).

Table 3.3: Reactivity ratios acquired by fit of the terminal model to copolymer composition obtained by radical copolymerization of BA with HEA and MEA

	HEA Bulk	**HEA Xyl.**	**HEA MIBK**	**HEA DMF**	**HEA BuOH**	**MEA bulk, BuOH and DMF**
$\mathbf{r_{HEA/MEA}}$	1.64 ± 0.34	3.25 ± 0.37	1.87 ± 0.68	1	1.32 ± 0.96	1
$\mathbf{r_{BA}}$	0.35 ± 0.06	0.93 ± 0.07	0.85 ± 0.19	1	0.88 ± 0.44	1

To complete the study, k_p^{cop} values of BA with MEA were determined at 30 and 50 ºC using the PLP-SEC method. As well as providing a comparison to the BA/HEA system, the data are examined to determine for effects induced by the heteroatom in the side chain of MEA compared to BA, as the

propagation kinetics of MEA have not yet been studied. As shown in Figure 3.13, the presence of the methoxy group leads to an increased k_p value, 30% higher than the value for BA at 50 °C (35 000 L mol^{-1} s^{-1} in comparison to 26 500 L·mol^{-1}·s^{-1}), with a similar increase observed at 30 °C. While this relative increase is higher than the 10% higher value reported for ethoxyethyl methacrylate in comparison to BMA,[133] similar effects have been found for nitrogen containing monomers, and were attributed to a change in polarity and electron density.[129] Another useful comparison is glycidyl methacrylate (GMA) vs butyl methacrylate, as the O-atom containing glycidyl group is similar in size to MEA. At 50 °C the value of 1200 L·mol^{-1}·s^{-1} for GMA[134] was found to be significantly higher, by 60%, than that of BMA (750 L·mol^{-1}·s^{-1}).[1] The larger increase for GMA vs BMA compared to MEA vs BA may be related to the cyclic glycidyl group, as other methacrylates with cyclic groups exhibited similar behaviour.[102]

As shown in Figure 3.13, the value of k_p^{cop} increases linearly with increasing MEA content between the two homopolymerization values, both at 30 °C and 50 °C. This result is perhaps expected for a system with reactivity ratios of unity, and can be well-represented by the terminal model. This simple behaviour can be contrasted with the BA/HEA system (Figure 3.10), for which a significantly higher increase in k_p^{cop} is observed compared to the BA homopolymerization end point due to the H-bonding introduced with HEA as a comonomer. H-bonding effects can also be introduced to the BA/MEA system through the addition of BuOH as solvent. At both temperatures, the entire k_p^{cop} curve, including the two homopolymer endpoints, shifts higher by ~30 %. Previous investigations have reported an increase of similar magnitude for the homopropagation kinetics of MMA in alcohols compared to bulk[124,130] and, as reactivity ratios in BuOH remain at unity for the BA/MEA system, a consistent increase of similar magnitude is observed over the complete composition range. Again, a contrast can be made with the more complex behaviour observed for BA/HEA copolymerized in BuOH (Figure 3.10) for which the k_p^{cop} values converge to the bulk values as HEA fraction increases; as there is no monomer related H-bonding

effect in the BA/MEA system, the hydroxyl group of BuOH interacts with both monomers to the same extent.

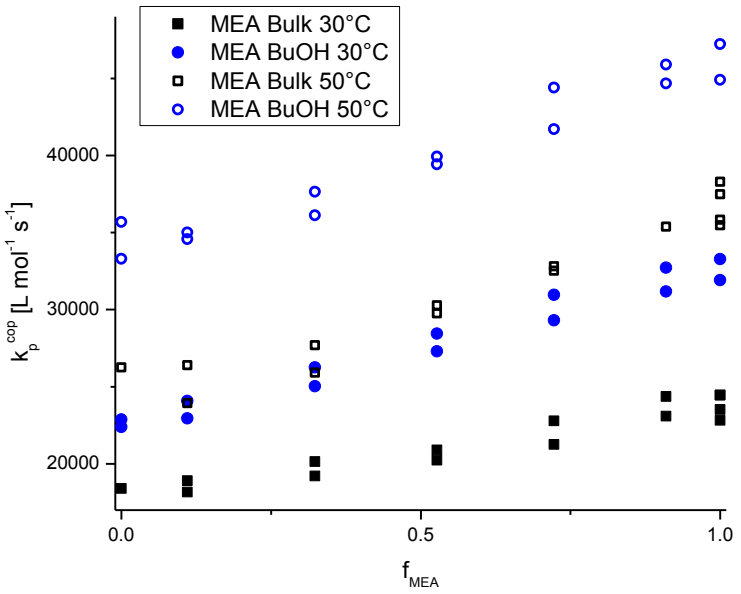

Figure 3.13: Evolution of k_p^{cop} as a function of MEA monomer mole fraction (f_{MEA}) for BA/MEA in bulk (black) and BuOH (blue) at 30 (filled symbols) and 50 °C (hollow symbols)

3.3.4. BMA/MEA Copolymerization

To complete the investigation of the effects that substituting MEA for HEA has on copolymerization kinetics, we have conducted a series of experiments with BMA/MEA to compare to our previous BMA/HEA study.[19] Based on the comparison of BA/MEA with BA/HEA, it is expected that the increased polarity of MEA should not affect its copolymerization kinetics with BMA; i.e., that BMA/MEA behaviour should be similar to that of BMA/BA rather than BMA/HEA. The relation between copolymer and comonomer composition for these two limiting cases is plotted as curves in Figure 3.14. When BMA was copolymerized with HEA, the net effect of both DMF (which disrupts HEA H-bonding) and BuOH (which induces H-bonding to BMA) was to decrease the HEA incorporation into the copolymer, which was found to be almost equal in comparison to the classical BMA/BA case. With

MEA replacing HEA as comonomer, it is seen that all three data sets – bulk, solution polymerization in DMF, and solution polymerization in BuOH – cannot be distinguished from each other within experimental error. As well as demonstrating no solvent effects, the copolymer compositions are found to be similar to the BMA/BA, rather than the BMA/HEA (with its increased acrylate incorporation) bulk system. Thus, when copolymerized with both BA and with BMA, the polar functionality of MEA exerts no influence on copolymer composition in bulk or solution, in stark contrast to HEA.

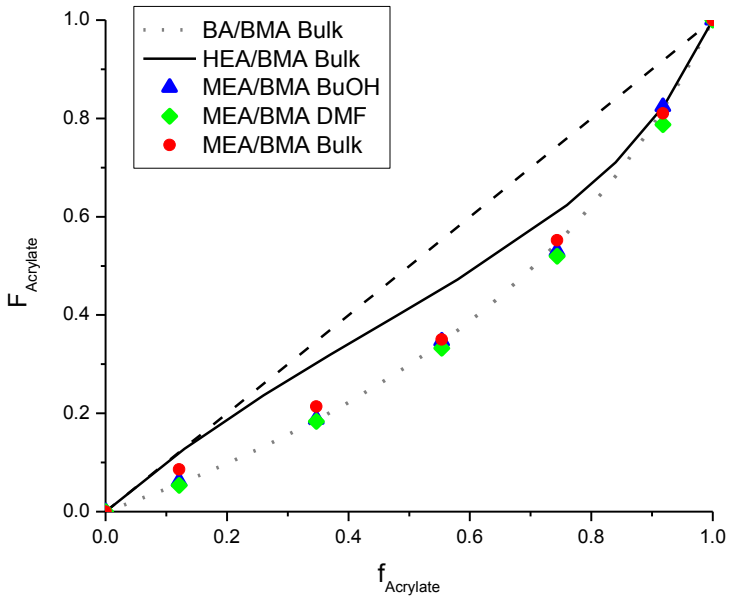

Figure 3.14: Mole fraction of acrylate comonomer incorporated into copolymer as a function of the mole fraction in the monomer mixture. Mayo-Lewis curves for BMA/HEA[19] (—)and BMA/BA[119] (dotted) taken from literature compared to experimental data (points) for BMA/MEA in bulk (red), in 50 v% BuOH (blue), and 50 vol% DMF (green).

We have also used the PLP-SEC technique to examine how solvent choice affects propagation kinetics when MEA is copolymerized with BMA. As shown in Figure 3.15, the values of k_p^{cop} at 50 °C are reduced relative to the bulk HEA/BMA[19] system due to the absence of H-bonding capabilities in MEA. (The plot is truncated at an acrylate content of 75 mol%, due to the order of magnitude increase observed in k_p at high acrylate content but is fully shown in Figure A.5.) Without any H-bonding in the

system, the addition of DMF to BMA/MEA has very little effect on the averaged rate coefficient. However, the addition of BuOH as solvent promotes both the reactivity of BMA and MEA, such that the k_p^{cop} curve is increased throughout the composition range. Again, these effects are similar to those found for the BA/MEA system, and are in sharp contrast to the previously reported influence of solvent on BMA/HEA k_p^{cop} values.[19] Experiments performed at 80 °C, in the supplementary information (see Figure A.5), show identical trends.

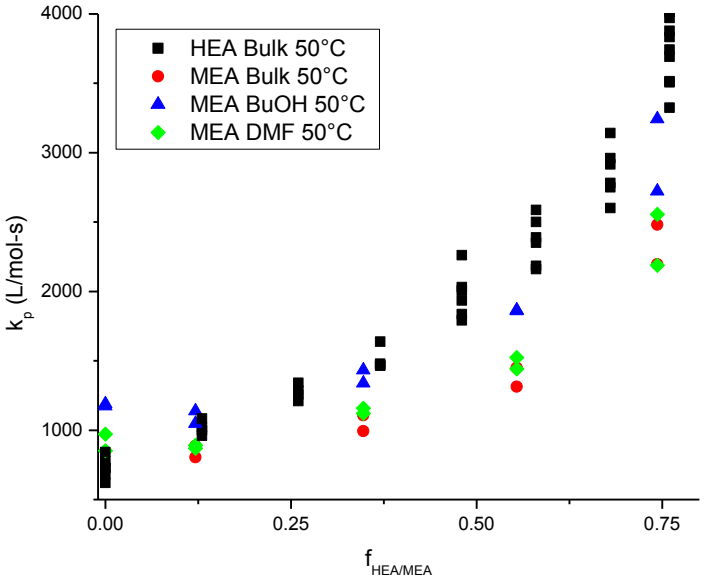

Figure 3.15: Evolution of k_p^{cop} as a function of acrylate monomer mole fraction for BMA/MEA in bulk (red), BuOH (blue) and DMF (green) in comparison to previously published data for BMA/HEA in bulk[19] (black)

With copolymer composition well-represented by the terminal model, it is interesting to consider whether the best-fit reactivity ratios can also adequately describe the composition-averaged propagation rate coefficient for BMA copolymerized with HEA and MEA, or whether the extra parameters contained in the implicit penultimate unit effect (IPUE) model are required. The terminal model, described by Eqn 2.9, provides a prediction of k_p^{cop} using only the reactivity ratios fit from the composition data and the two

homopropagation rate coefficients ($k_{11}=k_{p1}$ and $k_{11}=k_{p2}$). The IPUE model can be used if the terminal model does not adequately represent the data, introducing radical reactivity ratios (s_1 and s_2) that capture the influence that the chain-end penultimate unit exerts on reactivity according to Eqns 2.12 and 2.13.[19]

The *s* values are usually estimated from fitting the variation in k_p^{cop} vs. monomer composition data. However, as the data set from this study is rather limited, we instead have used the values obtained from a previous study of MMA/BA, with $s_{BA}=0.43$ and $s_{BMA}=1.98$,[127] to determine if the behaviour of BMA/MEA is typical of the classical methacrylate/acrylate system. As shown in Figure 3.16 a), while the terminal model does not provide a fit to the experimental data, the penultimate model predictions are quite reasonable. The same general conclusions can be made even for the BMA/HEA data taken from our previous study:[19] the terminal model underpredicts k_p^{cop} significantly, while the penultimate model prediction using MMA/BA radical reactivity values is greatly improved (Figure 3.16 b)). Using the BMA/HEA k_p^{cop} data set to estimate *s* values through least-squares fitting further improves the data representation, perhaps capturing the extra complexity introduced by the H-bonding in the system. Nonetheless, the results of Figure 3.16 b) suggest that using a single pair of radical reactivity ratios is a reasonable approach to representing k_p^{cop} data for methacrylate/acrylate systems, especially in the absence of H-bonding. With this generalization, the task of describing the complete propagation behaviour for a new system is limited to the measurement of homopropagation k_p values by PLP-SEC, and the determination of monomer reactivity ratios from copolymer composition data.

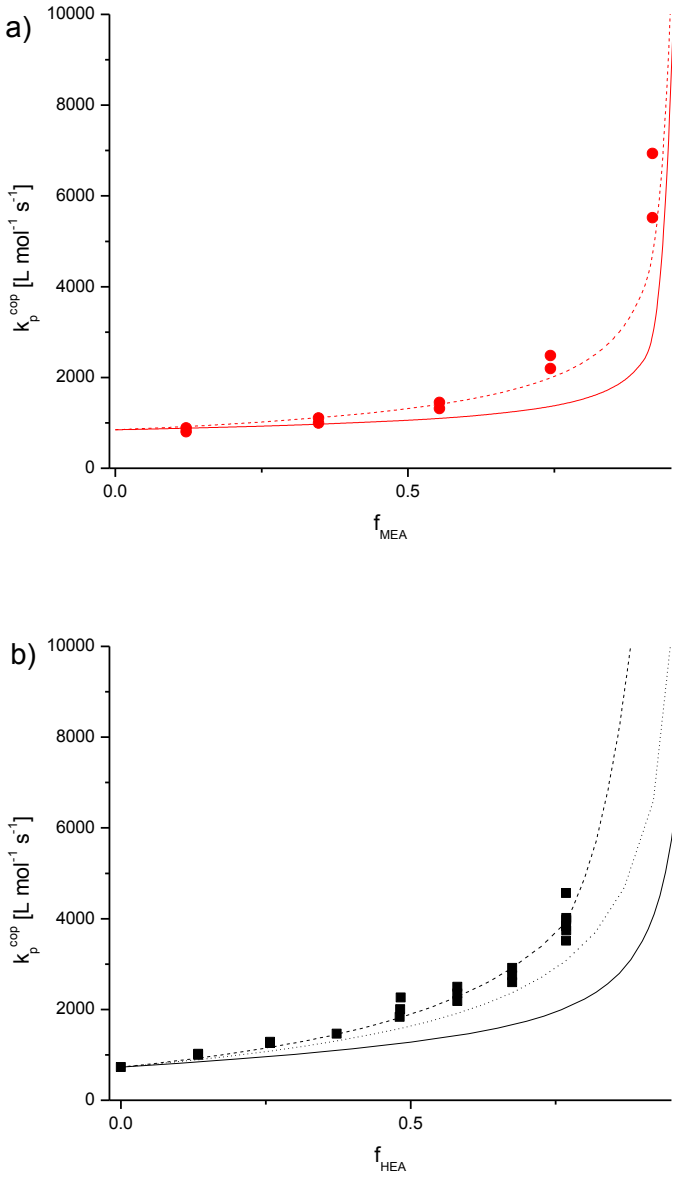

Figure 3.16: Terminal model (—) and IPUE (--) model predictions of k_p^{cop} for BMA copolymerized with (a) MEA and (b) HEA in bulk at 50 °C. IPUE curves for MEA are calculated using *s* values taken from literature, with $s_{methacrylate}$ = 1.98 and $s_{acrylate}$ = 0.43.[127] The BMA/HEA data is taken from a previous study, as is the line calculated with the best-fit IPUE parameters s_{BMA} = 3.03 and s_{HEA} = 1.0[19] (dashed line) together with an IPUE fit using the aforementioned s-values (dotted line)

3.4. Conclusions and Outlook

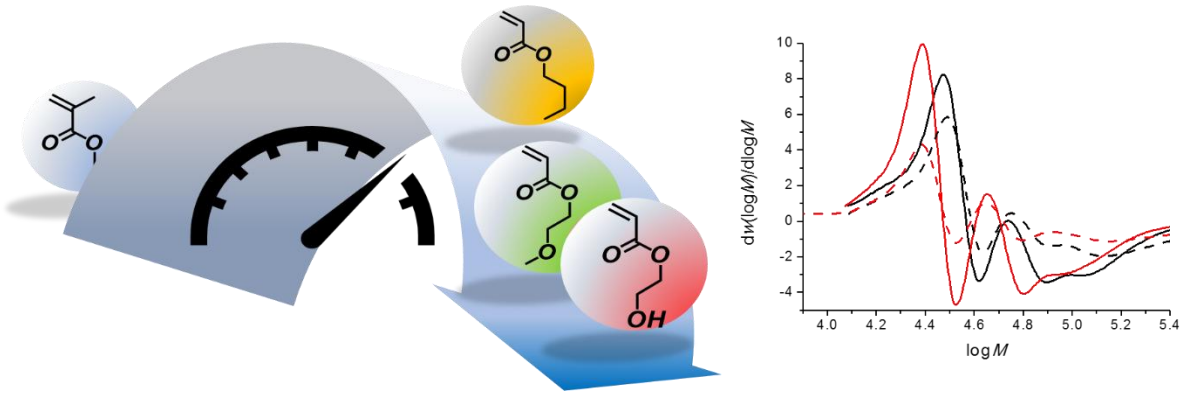

Figure 3.17: Reaction coefficients visualized in perspective; for BMA vs. BA vs. MEA vs. HEA[29]

The copolymerization behaviour of HEA with both BMA and BA is compared to that of MEA (as shown in Figure 3.17), which has been studied using the PLP-SEC technique for the first time. The k_p value for MEA homopropagation is higher than that of BA by 30%, a result attributed to the heteroatom in the side chain. However, the analysis of both copolymer composition and k_p^{cop} data using the PLP-SEC technique showed no increase in MEA incorporation or solvent dependency compared to a "standard" acrylate monomer such as BA. Thus, the acrylate-acrylate copolymerization of BA/MEA is well described by the terminal model with reactivity ratios of unity in both bulk and solution, and an increase in k_p^{cop} found in BuOH due to H-bonding effects induced over the complete composition range. The polymerization behaviour is well understood and well-modeled using both monomer and radical reactivity ratios determined in previous studies of acrylate/methacrylate systems.

In contrast, both copolymer composition and k_p^{cop} are affected by solvent choice for the copolymerization of HEA with both BA and BMA due to the H-bonding induced by the HEA hydroxyl function. In a bulk system, the level of HEA incorporated into the copolymer as well as k_p^{cop} (in case of the acrylate only system) is significantly enhanced compared to that of an alkyl acrylate. Addition of BuOH, which introduces H-bonding in substitution to that of HEA, or DMF, which disrupts H-bonding, brings copolymer composition back to that seen for BA (or MEA) copolymerization. However, the k_p^{cop} curves for BA/HEA in BuOH solution remain complex due to the competing H-bonding between BuOH

and HEA. It was found that the investigated BMA/HEA system was less influenced by solvent choice than BA/HEA, likely due to the controlling influence of the methacrylate monomer on radical fractions in the methacrylate/acrylate system. Work continues to generalize the representation of how the copolymerization behaviour of HEA, but also HEMA and other hydroxyl containing monomers, is influenced by hydrogen bonding. Further experimentation should be put forth for the HEA homopropagation in varying organic solvents. However, special care needs to be taken, based on preliminary experiences described in the last section of Appendix A (see Figure A.6).

Chapter 4 Butyl acrylate (BA) – 2-hydroxylethyl acrylate copolymerization: Side reactions and other kinetic considerations

4.1. Introduction

As highlighted in Chapters 1 and 2, the increased reactivity of secondary acrylate radicals leads to important side reactions that impact polymerization rate as well as polymer MM and structure. Accordingly, with an increased value in k_p and k_t these manifold options include backbiting, or transfer in general. Depending on the application, these side reactions can be beneficial or undesirable. Their influence, for example, is significantly reduced under controlled radical polymerization conditions,[135,136] explained by the short transient lifetime of propagating radicals due to the capping and de-capping in most CRP reactions.[137] However, CRP conditions are costlier, ergo less feasible, for many industrial applications. The rate coefficient for backbiting, k_{bb}, is of particular importance as it results in the formation of MCRs which then can further react by termination, propagation or scission. The rate of polymerization is affected likewise, as the rate of monomer addition to MCRs (k_p^{MCR}) is much slower than that to chain-end radicals (k_p),[54] leading to the definition of an averaged coefficient k_p^{AV} as described in the following equation.[138]

$$k_p^{AV} = \frac{k_p}{1+\frac{k_{bb}}{k_p^{MCR}[M]}} \tag{4.1}$$

Under the assumption, that the majority of MCR forms a branching point,[6] (valid due to the faster rate of reaction k_p^{MCR}·[M] versus scission and termination rates), a simplified expression relating k_{bb} to branching level can be derived, as described in Eqn 4.2. As k_p has been reliably measured by PLP-SEC,[48] and [M] is easily monitored by multiple on-[139,140] and offline[141,142] techniques, k_{bb} can estimated provided that the branching level (BL, the fractional quantity of acrylate units that have undergone branching) is accessible through quantitative ^{13}C-NMR measurements.[81]

$$BL = \frac{k_{bb}}{k_p[M]+k_{bb}} \tag{4.2}$$

This relationship has been used to estimate k_{bb} from batch polymerizations of BA in xylenes up to high conversion (90 %) between 50 and 70 °C,[138] with the resulting values combined with k_{bb} estimates from other techniques to yield the Arrhenius parameters ($A = 7.4 \cdot 10^7$ s^{-1} and $E_a = 32.7$ $kJ \cdot mol^{-1}$); these values were applied by the Hutchinson group to model semi-batch co- and terpolymerizations with BA[28] under similar conditions as examined in this work. The value of 5200 s^{-1} calculated at 138 °C is higher than the value of 3000 s^{-1} estimated in an earlier study based entirely on semi-batch results,[9] indicating perhaps the sensitivity of the k_{bb} estimates between different modus operandi, as the monomer concentration profiles clearly differ. Hence, the error introduced by the assumptions made for Eqn. 4.2 is also dependent on the type of reaction, such as batch or semi-batch. To show the scatter in different data sets a more recent study covering temperatures from 60-140 °C proposed that a the activation energy should increase to 52.3 $kJ \cdot mol^{-1}$.[143] However, this value, based on ^{13}C-NMR measurements, is significantly higher than estimates from other kinetic techniques applied, such as SP-PLP-EPR[144] and also the PLP-SEC study of Nikitin et al,[100] which should be more reliable.

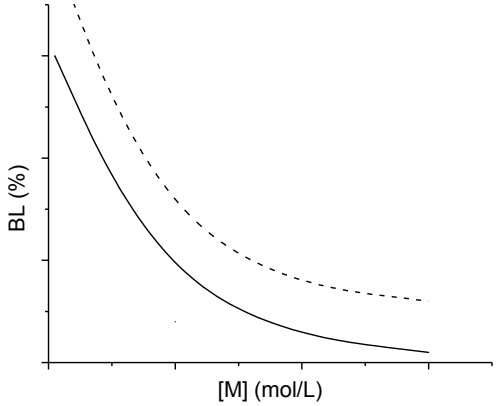

Figure 4.1: Branching level vs. monomer concentration at different temperature T1(-) and T2 (--) with T1 < T2

The above discussion shows that there is still some uncertainty about branching levels in BA, and data for other acrylate systems is scarce. In regards of the development towards more functional, hydrogen bonding bearing monomers (or solvents), this issue gains even more importance due to the

demonstrated reduction of backbiting and branching points in such systems.[17] Despite special care and adjustment for instrumentational error of the NMR technique, one should note that certain trends, especially at branching levels around and lower than 1% per acrylate unit, can be affected by baseline noise or other effects in this advanced but certainly more complex technique.[145]

These considerations (not limited to branching) are especially of importance under operating conditions with elevated temperatures and reduced or low monomer levels[138] such as starved-fed or CSTR[146] reactions. The principle is qualitatively explained in Figure 4.1, accordingly with Eqn 4.2 and the higher activation energy of k_{bb} in comparison to k_p.[144] Through the presence of branching points from monomer addition to MCRs (which create short-chain branches) or the incorporation of scission-derived macromonomers (which create long-chain branches), a range of random comb-like polymer structures or networks can be created, possibly affecting the viscoelastic properties of the polymer.[147] While short chain branches do not greatly affect the viscosity, long chain branching points have a significant impact on such physical and application properties.[148,149]

With the introduction of HEA and the associated solvent effects, the possible influence of H-bonding on acrylate backbiting and related reactions needs to be examined. Consequently, this chapter will focus on the determination and update of these parameters by investigating such side reaction under batch and semi-batch conditions to enhance the current and previously published knowledge.[17,20] Additional conclusions regarding PLP-derived reactivity ratios and industrially relevant operating conditions will be drawn, pushing the limit in terms of maximum HEA incorporation.

4.2. Experimental

4.2.1. Materials

Butyl acrylate (≥99 %, Sigma), methyl acrylate (99 %, Sigma), 2-hydroxylethyl acrylate (96 %, Sigma), deuterated dimethyl sulfoxide, deuterated toluene, 2,2-azobis(2-methylbutyronitrile) (Vazo-67, +99%, DuPont), *tert*-butyl peracetate (50 wt% in mineral spirits, Sigma), dimethylformamide (99 %,

Sigma), n-butanol (≥99.4 %, Sigma), n-pentanol (≥99 %, Sigma), toluene (≥99.5 %, Sigma), xylenes (>99%. Fisher Scientific), 5-methyl-2-hexanone (99 %, Sigma), 2-heptanone (99 %, Sigma) and butyl propionate (99 %, Sigma) were used as received without any further purification.

4.2.2. Batch reaction

Batch reactions were performed in a 25 mL Schlenk tube under isothermal conditions. Initial monomer to solvent ratios were kept at a level of 25 v% monomer to achieve suitable molar masses and branching levels. Vazo-67 was used as an initiator with an initial concentration of 10 $mmol \cdot L^{-1}$ based on total liquid reactor content of 5 mL. In preparation of the reaction, monomer/solvent mixtures were purged thoroughly with nitrogen for at least 15 min, with the subsequent reaction conducted under inert gas conditions at atmospheric pressure for 30 min at 80 °C under constant stirring. The polymerization was then quenched by cooling the tube in liquid nitrogen and the addition of a few drops of a MEHQ ($2\ g \cdot L^{-1}$) solution. A small amount of the reaction mixture was analyzed via GC immediately after the end of reaction. Further purification and isolation of the polymer was done by precipitation in a suitable antisolvent, with liquid nitrogen as the cooling agent, such as $MeOH/H_2O$ (3 to 1 ratio) for BA and MA polymers or diethyl ether for HEA polymers. The crude polymer was then separated from the solution through filtration before drying under vacuum at 60 °C overnight. Only low MM fractions are assumed to be lost, which are most likely beneath the lower calibration limit of the used SEC. The exothermic nature of the reaction did not influence reaction conditions, as reaction temperatures did not exceed values higher than 82 °C. No gas formation or boiling was observed for MA polymerized under these conditions, despite the boiling point of MA of 80 °C, due to the presence of the solvent.

4.2.3. Semi-batch reaction

Reactions were conducted in a 0.6 L LabMax reactor system, with automatic stirring, temperature control, a reflux system and metered reagent mass flow control, at 138 °C, the boiling point of xylenes. Solvents include ketones, esters, DMF and pentanol (PeOH). 129 g of solvent were charged to the reactor, heated to reaction temperature under nitrogen inert gas atmosphere. The feed reservoir was charged with 239 g of monomer solution (at various compositions for the case of comonomer systems) before adding 2 mol% of *tert*-butyl peracetate (TBPO) relative to the monomer content, as reported elsewhere.[142] The reaction mixture was then fed over 6 h into the reactor to reach a final polymer content of 65 wt% in solution, assuming 100 % monomer conversion. 10 samples of 2-3 mL were taken over the course of the reaction. The final samples usually contained more than 10 mL solution to assure proper ^{13}C NMR analysis of the polymer isolated. All samples were immediately quenched through the addition of MEHQ inhibitor (2 g/L) and stored in the freezer. For residual monomer concentrations, a small fraction was then taken to be analyzed via GC, before residual solvent was removed through air stripping and evaporation under vacuum at 60 °C.

4.2.4. Size Exclusion Chromatography (SEC)

Polymers were dissolved in THF at 3-6 $g \cdot L^{-1}$ and filtered through 0.2 μm nylon filters for SEC analysis. The SEC setup consists of a Waters 2960 separation module connected to a Waters 410 differential refractometer (DRI) and a Wyatt Instruments Dawn EOS 690 nm laser photometer multi-angle light-scattering (LS) detector. The eluent THF was used at a flow rate of 0.3 $mL \cdot min^{-1}$ through 4 Styragel coloums maintained at 35 °C. The DRI detector was calibrated by polystyrene standards with narrow dispersities over the range of 870-875000 $g \cdot mol^{-1}$. The LS detector was calibrated with a single polystyrene (PS) standard as a reference. Based on PS-calibration, absolute molar mass distributions from DRI can be obtained via a suitable transformation using the known Mark-Houwink parameters. Results were verified by comparing the output from LS detection which determines absolute molar mass

distributions using known refractive indices (dn/dc values); a necessary routine as the single analysis via Mark-Houwink parameters may not be valid for all copolymerization systems. Table 4.1 provides the necessary parameters for the system examined. It is assumed that copolymerization values can be calculated based on the weight-averaged polymer composition, as shown to be valid in previous studies.[27,114]

Table 4.1: Parameters required for analysis of PLP-SEC results

Monomer	dn/dc ($mL \cdot g^{-1}$)	Mark-Houwink parameters in THF	
		K ($dL \cdot g^{-1}$)	a
HEA[27]	0.066	0.000322	0.602
BA[150]	0.064	0.000122	0.700
MA[151]	0.048	0.000195	0.660
Styrene[115]	0.184	0.000114	0.716

4.2.5. Gas Chromatography (GC)

GC-samples were analyzed using a Varian CP-3800 GC setup. The system combines a CP-8410 autosampler, a CP-117 isothermal split/splitless injector (with a 9:1 split), a 30M chrompack capillary column (CP-Sil 8 CB), an oven and a flame ionization detector (FID) for quantitative analysis of residual compounds. The separation is based on the different boiling points of the compounds using a fine-tuned temperature profile. Due to the high boiling points above 200 °C of hydroxyl containing monomers, it is recommended to set the injector cell temperature to 275 °C for quantitative evaporation. Accordingly, the separation was optimized with a starting temperature of 100 °C (and a final bake out at 275 °C) for the column oven to avoid line broadening of hydroxyl containing monomers on the stationary phase. Hydroxyl containing monomers elute earlier than their hydrophobic counterparts, despite their higher

boiling points. To identify monomers and properly separate them (based on retention time), a calibration was developed with samples of known concentration to construct a plot of integrated peak area versus monomer concentration. All calibration curves with given concentrations and final linear regressions are shown in Figure B.1. Samples of unknown concentration were prepared by diluting 0.02 – 0.06 g in roughly 10 g of acetone. Absolute masses increased inversely proportional with expected monomer concentrations, as monomer levels are expected to be lower at the end of both, batch and semi-batch reactions.

4.2.6. NMR-spectroscopy

NMR samples were prepared by dissolving dried polymer (free of monomer) in a suitable NMR-solvent at concentrations around 2 wt% for ^{1}H-NMR and significantly higher concentrations of 10-30 wt% for ^{13}C-NMR to allow for a quantitative detection of the naturally less abundant ^{13}C-nuclei. Nonpolar homopolymers were commonly analyzed in CDl_3 whereas hydroxyl functional copolymers were analyzed in DMSO-d6. Two different spectrometers were used at 400 or 500 MHz, both models being a Bruker Avance. ^{1}H-NMR spectra were recorded at standard conditions with 3.17 s acquisition time, 1 s relaxation delay, 6μs dead time and 48.4 μs dwell time. The quantitative ^{13}C-NMR was acquired under inverse gated WALTZ16 conditions to suppress Nuclear Overhauser related effects (NOE) with a sufficient main delay time of 10 s per scan as reported elsewhere.[137,152] A sufficient signal to noise ratio was achieved after 3000 scans, with sampling times generally adjusted to allow for more than 4000 scans.

4.3. Results and Discussion

4.3.1. Small-scale batch experiments

Small-scale batch experiments were performed keeping conversions (about 80% in a 30 min reaction as determined by offline GC analysis) in a comparable range, as the monomer concentration has a significant effect on the branching level. Results are summarized in Table 4.2 for various

acrylate/solvent combinations. As initial monomer concentration for each acrylate was kept constant (with 75 v% solvent), and final conversions are similar, the resulting BL measured allows a direct comparison of how solvent choice affects k_{bb}/k_p.

Table 4.2: Final conversions, polymer molar masses and branching levels measured poly(acrylate) produced via small-scale batch polymerizations conducted at 80 C with 75 v% solvent (30 min reaction time, 0.085 mol·L^{-1} Vazo-67)

Monomer	Solvent	$[M]_{ini}$ [mol·L^{-1}]	Conversion [%]	M_n/M_w [g·mol^{-1}]	Branching Level** [% per acrylate unit]
MA	Xylenes	2.60	85.7	10400/19300	3.6
MA	Toluene	2.60	81.3	10500/20600	2.7
MA	n-Butanol	2.60	86.3	27400/61300	1.6
BA	Xylenes	1.65	80.7	21100/41100	3.1
BA	Toluene	1.65	75.9	17100/39500	3.0
BA	n-Butanol	1.65	84.2	36800/87700	2.4
HEA	DMF	2.25	84.8	n.a.	1.8
HEA	n-Butanol	2.25	90.0	n.a	1.2
BA/HEA*	Xylenes	1.90	Phase separation/ precipitation		1.2
BA/HEA*	MIBK	1.90	occurred before 30 min;		1.8
			$F_{HEA} >> f_{HEA}$ at conv. ≈ 50%		

*BA/HEA copolymerizations were performed at a 50/50, volume based, monomer ratio

** 13C-NMR techniques are only reliable above branching levels of 1% per acrylate unit and are associated with a ±0.5 error bar

When comparing the results for MA in xylenes and toluene it can be seen that conversions of 80-85% are reached for both systems, and that the polymer molar masses are also very similar, reinforcing the argument of negligible solvent dependence on radical polymerization parameters for common non-functional acrylates with constant monomer to solvent volume ratios.[40,90] It is somewhat surprising that

there is a noticeable difference in branching levels, measured at 3.6 % in xylenes to 2.7 % in toluene. Whereas this difference is more pronounced in MA, values those measured for poly(BA) produced in the same solvents, resulted in indistinguishable levels of 3.0 and 3.1% branching. However, this difference was not further pursued. The expected family-type behaviour is seen for MA and BA, as with BA the change from xylenes to toluene also had no effect on conversions, branching levels or polymer average molar masses. Because of density and molar mass changes from one monomer to another, the initial concentration changes from MA to BA, and it is known that k_p^{BA} is 30 % greater than k_p^{MA} at 80 °C.[38] Given these minor differences, it is somewhat surprising that the absolute molar masses of poly(BA) are almost double that of the poly(MA) systems.

The family behaviour between BA and MA is also seen when examining the polymerization of both monomers in BuOH. As known from PLP-SEC studies, the presence of alcohols significantly increases k_p[19,153] while also decreasing k_{bb}[17,20] As seen in Table 4.2, this leads to slightly higher conversions (~5%) for the reactions in BuOH compared to those in toluene and xylenes. It also leads to significantly lower BLs measured in BuOH (1.8 and 2.4% for MA and BA, respectively) than in the other solvents. Furthermore, the results agree respecting polymer molar masses (see Eqn 2.3 for DP^{inst}), which are significantly higher for the reactions in BuOH. These results, in agreement with previous investigations, provide proof that H-bonding effectively inhibits the H-abstraction process, reducing the branching levels. Whereas the interactions of the alcohol with polymer chains are of the same nature as with the monomer, as can be seen in IR-spectra,[154] their effect is different. The coordinated solvent molecules probably sterically hinder chain-end movement, such that the 1:5 backbiting mechanism, which is highly related to polymer backbone flexibility, is less probable and chain growth is favoured. Generally speaking, solubility parameters become significantly more important as they are in comparison to propagation kinetics, which can be seen by notable changes in the solvent interaction parameter χ of the same polymer in xylenes or toluene.[155] With both effects taken into account, the increase to almost double the respective molar masses is reasonable. These arguments do not consider the effects of reduced termination or transfer on polymer MMs; reflecting on chain-length dependent kinetic termination

coefficients,[59,61] the longer polymer chains will lead to a decrease in k_t further increasing rate and polymer molar masses.

To enhance this knowledge about solvent induced H-bonding effects, experiments were also carried out with HEA, in butanol and DMF. As poly(HEA) is only sparingly THF-soluble, only conversion and branching data are available. Conversions were found to be similar or slightly higher than those of MA and BA in BuOH, 90 % in BuOH and ≈85 % in DMF (which disrupts H-bonding). The stronger conclusion can be made based on the branching level, which was found to be as low as 1.2 % for poly(HEA) synthesized in BuOH. These values are 30-50 % lower compared to poly(MA) and poly(BA) in BuOH, and decreased even further relative to the alkyl acrylates in xylenes/toluene, showing that H-bonding induced by both solvent and monomer with polymer chains reduce this significant acrylate side reaction. However, the results in DMF need to be further examined, as a previous set of PLP experiments of HEA in DMF[20] suggested that branching levels would increase back to the values found for alkyl acrylates by disrupting the H-bonding. However, the 1.8 % BL is still significantly lower. While DMF is definitely able to disrupt HEA H-bonding (please refer to IR-measurements in Figure A.1), it does not necessarily have the same effect on other solvation effects and polymer chain flexibility. A possible explanation is that the polarity of DMF also interacts and stiffens polymer chains and reduces branching. If so, further insights may lay in χ and its correlation with Hansen solubility parameters[156] or Kamlet-Taft solvatochromic parameters.[103]

The need for semi-batch investigations is demonstrated by the last two experiments summarized in Table 4.2, for BA/HEA copolymerizations in xylenes and MIBK. Despite the high solvent content, both reactions underwent phase separation (precipitation of polymer) after roughly 15 min, with the heterogeneity occurring in xylenes a few minutes earlier. Thus, it is more difficult to evaluate the branching results, which are of the same level as observed for HEA homopolymerization. However, as monomer conversions are likely lower at the point of precipitation, it suggests that the branching rates (relative to propagation) are higher than for HEA homopolymerization. As expected from the PLP-determined reactivity ratios, HEA is preferentially incorporated into the copolymer,[29] which contributes to

the insolubility of the copolymer as the monomer concentration is depleted. Similar phenomena were observed in small-scale PLP experiments, and demonstrated by the insolubility of samples with high F_{HEA} in THF for SEC analysis. To obtain better control in these industrially relevant solvents, the next section presents results for semi-batch copolymerization with increased HEA contents and smaller target polymer molar masses.

4.3.2. Semi-batch reactions with varying HEA contents in high and low interacting solvents

In addition to the preliminary batch study, semi-batch experiments were performed under conditions commonly used in industry, to achieve two major goals. Firstly, the suitability of ester and ketone solvents for HEA copolymerization was tested; despite their increased polarity and the relatively low molar masses of copolymers synthesized in semi-batch, some solubility limitations are expected due to the repulsion between aliphatic solvent side chains and the polar hydroxyl groups of the copolymers. Secondly, DMF and PeOH are used as semi-batch solvents to further investigate the effects of H-bonding on relative comonomer reactivity and backbiting in substituting and disrupting solvents.

4.3.2.1. Acrylate-only copolyermizations of BA and HEA in industrially relevant solvents

The establishment of a versatile library of reaction conditions is very useful to determine limitations and experimental boundaries. Due to its more polar nature (in comparison to xylenes), BPi was chosen as a solvent, expecting good solubility properties for a wide range of HEA compositions. Semi-batch reactions were conducted under the typical conditions of 138 °C and a six-hour feeding period to achieve a final polymer content of 65 wt%, with varying ratios of HEA to BA. As shown in Figure 4.2 experiments could be performed up to HEA levels of 50 wt% with no phase separation or precipitation

observed under reaction conditions. During the initial transient period (up to two hours) for the reaction with 50 wt% HEA, the mixture was observed to become slightly cloudy for a short period before turning transparent for the rest of the reaction, indicating that this was at the edge of solubility limits with some samples precipitating during the post-reaction cooling process. However, the formation of further polymer stabilizes the solution to be stable even at room temperature. To keep homogenous solution polymerization conditions experiments with higher HEA content were not conducted. An examination of the free monomer levels determined via GC (Figure 4.2, top) leads to two initial observations. Up to a HEA content of 25 wt%, the concentration of total free monomer ([BA] + [HEA]) remains roughly constant, decreasing from an initial level of ~0.2 mol·L^{-1}. In contrast, the runs performed with 40 and 50 wt% HEA had a significantly increased concentration during the initial transient phase of the reaction, a surprising result given the increase in k_p^{cop} that occurs with increased f_{HEA}.[29] To further understand this unusual behaviour, the relative monomer composition, f_{HEA}, is calculated from the GC data, with the corresponding values of copolymer composition, F_{HEA}, calculated by mass balances. For the runs performed with low HEA content, the HEA monomer fraction is level at values significantly below the molar feed composition, which are denoted by the respective dotted lines, while the HEA fraction in the copolymer quickly attains the target (feed) value.

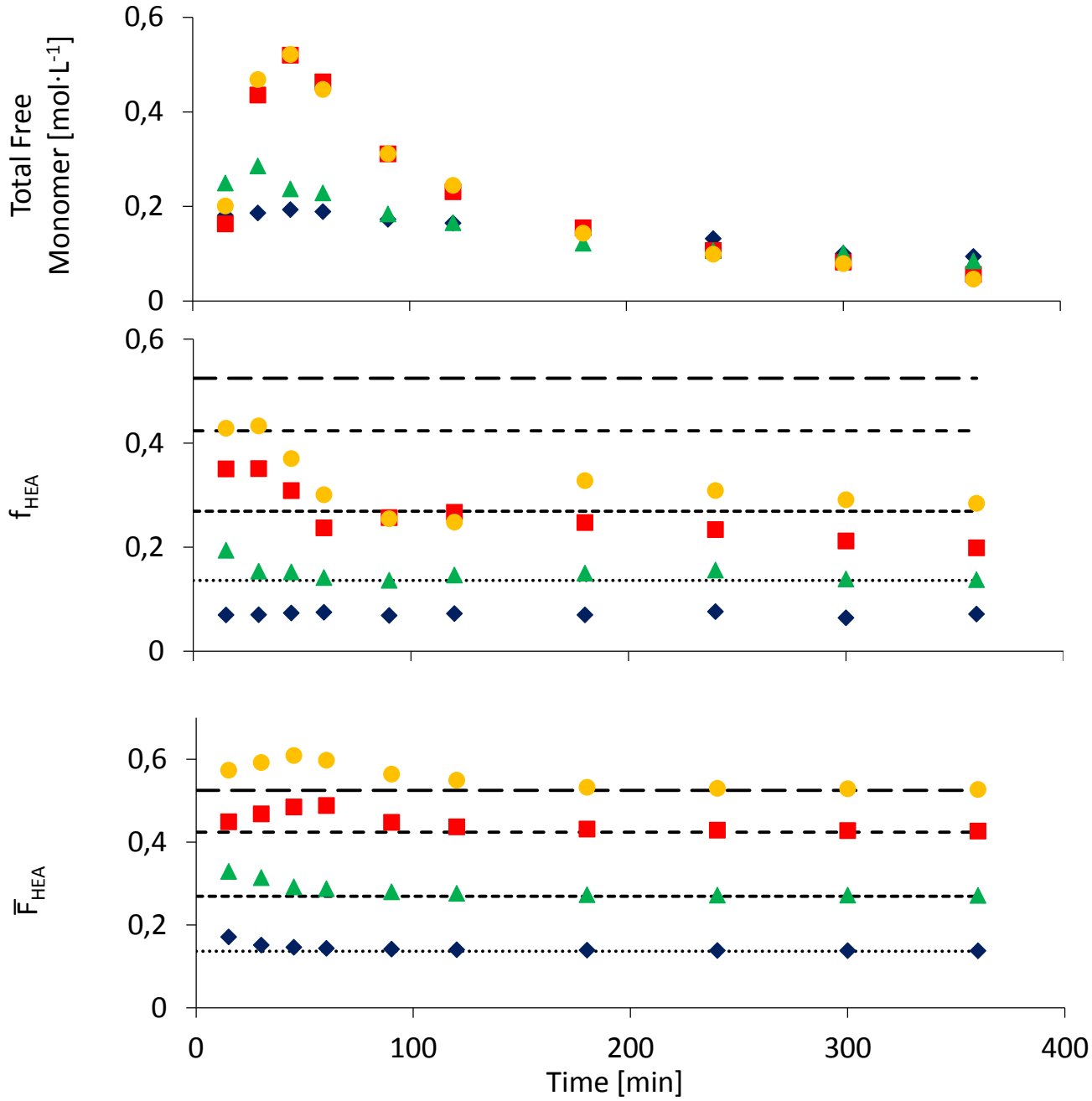

Figure 4.2: Total free monomer concentration, monomer composition and copolymer composition (from top to bottom) for BA/HEA semi-batch copolymerizations at 138 °C in BPi with HEA levels of 12.5 wt% (♦), 25 wt% (▲), 40 wt% (■) and 50 wt% (●). As discussed in the text, evidence suggests that the effective initiator loading for the high HEA runs were lower than expected

This behaviour (f_{HEA}<F_{HEA}) is expected from the low conversion PLP-SEC experiments, as there is an increased relative reactivity of HEA due to H-bonding. The same general finding holds for the two

experiments conducted with higher HEA content, but constant compositions are only achieved in the final 3 h of reaction. In the initial stages of the reaction (corresponding to the increased total monomer concentration), the HEA content in the copolymer is above the target value, and the HEA fraction in the monomer mixture is also high. This behaviour is also linked with the polymer molar mass averages summarized in Table 4.3.

Table 4.3: Molar mass averages for BA/HEA copolymer produced by radical polymerization in BPi under semi-batch conditions at 138 °C

Monomer Ratio as a function of HEA [w%]	M_n/M_w [g·mol^{-1}]	$Đ_M$
0	4000/8600	2.15
12.5	4200/8900	2.70
25	4400/11400	2.59
40	5400/22700	4.20
50	5900/33400	5.66

Whereas copolymerizations up to 25 wt% HEA show similar MM-averages as formed in BA homopolymerization, the weight-average and dispersity values for the copolymers formed with higher HEA content consecutive runs are significantly increased, with M_w values a factor of 2 and 3 higher for 40 and 50 % HEA, respectively. The concern with these results was that the increased MMs were a result of ethylene glycol diacrylate (EGDA) impurity in the HEA monomer, as was previously proposed to explain high MMs obtained during copolymerization of HEMA.[11] Thus, the full set of MMDs, including their evolution with reaction time, are included in Figure B.2 and Figure B.3. The higher M_w and $Đ_M$ values are associated with broad and tri-modal MMDs that exhibit both low and high molar mass shoulders. The entire distribution shifts higher with time from 30 to 180 min, which generally refutes incorporation of EGDA as the cause; based on previous experience, these crosslinkers would increase

molar masses through distinct high MM tails formed late in the reaction. For these runs, the MMD actually decreased from 180 to 360 min as the free monomer concentration decreased and in contrast to the behaviour observed for the standard BA homopolymerization.

Based on this analysis, the experiments with high HEA content were repeated using a new batch of initiator, with the monomer concentrations and HEA fractions plotted in Figure 4.3, and the evolution of MM averages in Figure 4.4. As discussed in detail below, the results for these repeats indicated that there was some unknown source of inhibition for the first experiments conducted at high HEA content. Although the exact cause is uncertain, we conjecture that the amount of effective initiator added during the reaction was significantly reduced, either by contamination (and increased inhibitor levels present in HEA) or by measurement error, and that the reduced rate of radical generation led to the buildup of free monomer in the system and the higher MMs. For the new set of experiments, total free monomer concentrations were found to be almost independent of the comonomer composition, with perhaps a slight decrease seen for the run performed with 40 wt% HEA, in agreement with the higher reactivity of this system. Furthermore, the compositions of free monomer do not fluctuate, which, due to the high conversions, result in stable copolymer compositions.

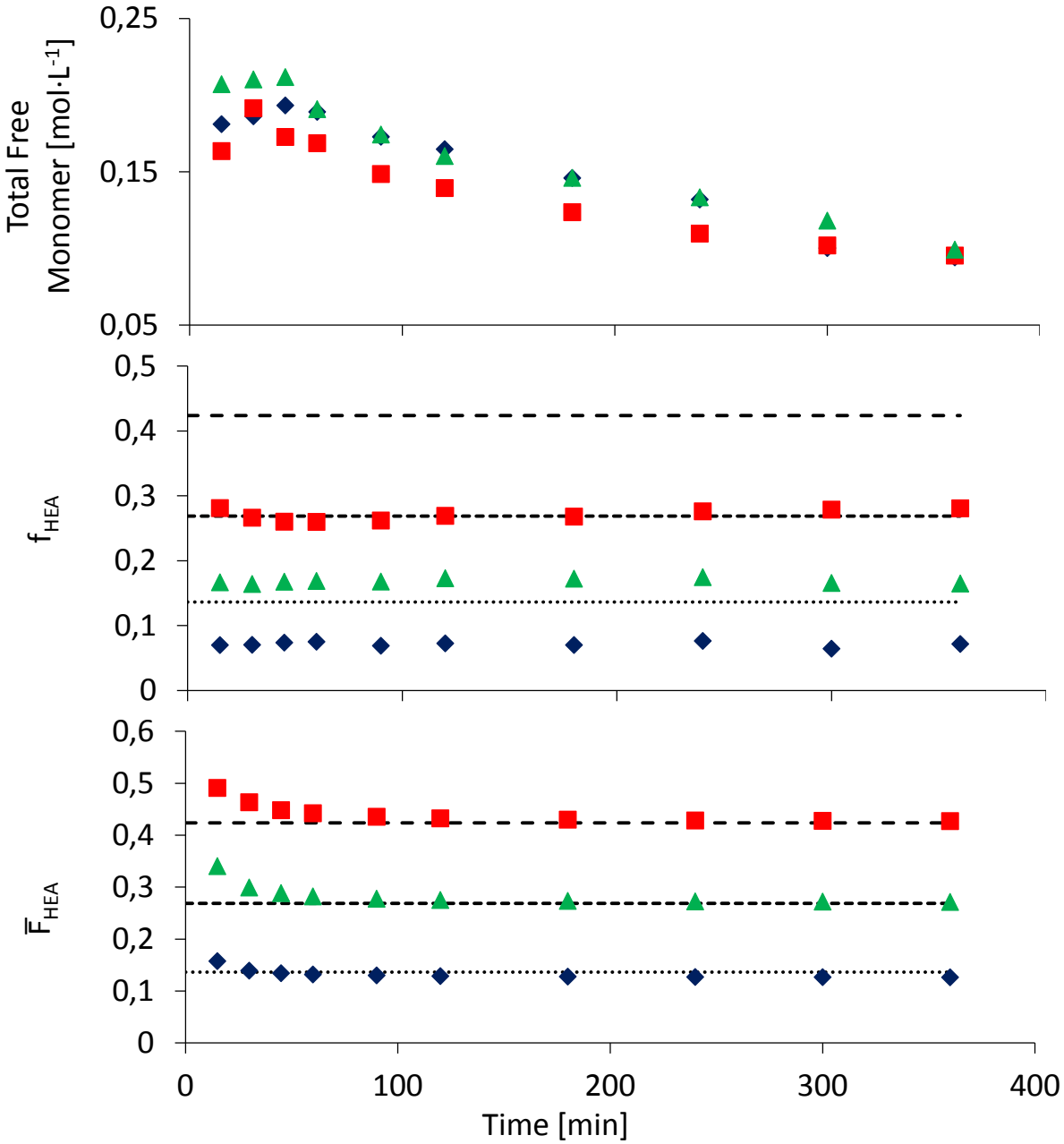

Figure 4.3: Total free monomer concentration, monomer composition and copolymer composition (from top to bottom) for BA/HEA copolymerizations in BPi with exact initiator concentration at HEA levels of 12.5 wt% (♦), 25 wt% (▲), 40 wt% (■)

With HEA level having only a minor effect on free monomer concentrations, the same is found for polymer MMs; as shown in Figure 4.4, the evolution of number and weight MM averages over time are similar with 12.5, 25 and 40 wt% HEA in the acrylate mixture, with the final values very similar to

those measured for BA homopolymerization (M_n = 4000 and M_w = 8600 g·mol^{-1}). The slightly lower M_n values observed for the experiment with 40 % HEA may be a result of the slightly lower monomer concentrations or an indication of increased transfer to BPi solvent at increased HEA content, an issue that will be explored in the following chapter.

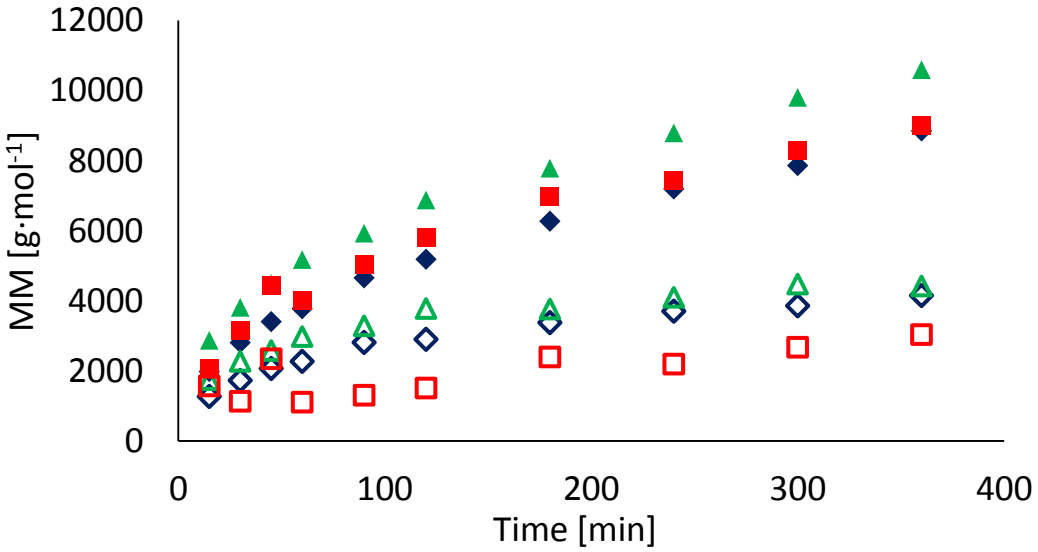

Figure 4.4: Evolution of number (hollow symbols) and weight (filled symbols) averages for BA/HEA copolymerizations in BPi with, 12.5 (♦), 25 (▲) and 40 wt% (■) HEA

In summary, the lack of initiator led to higher free monomer early in the reaction and thus a huge increase in polymer MMs. The question is whether there is additional information available based on a comparison of the 'failed' and successful runs, which are directly compared in Figure 4.5.

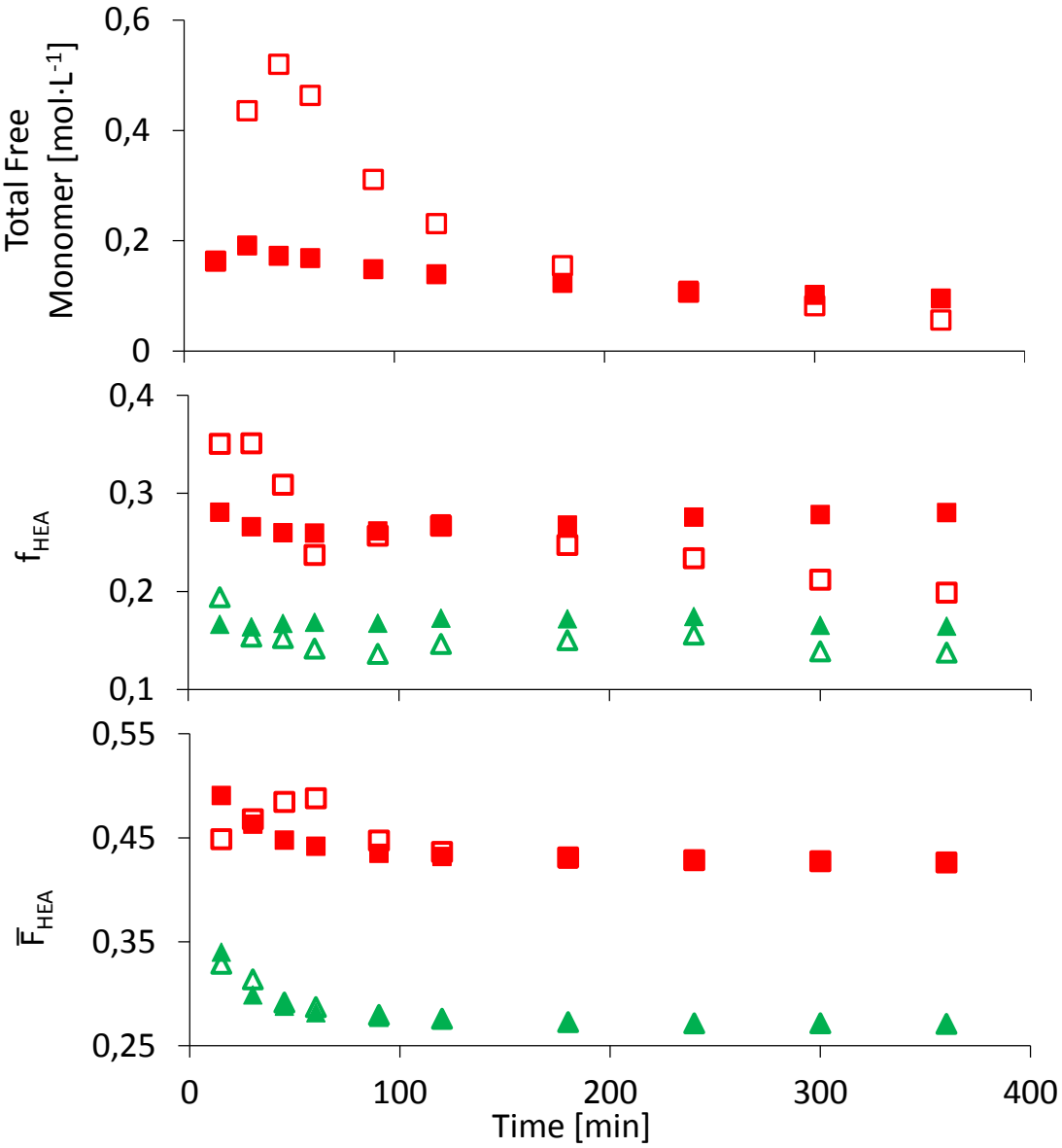

Figure 4.5: Comparison of total free monomer concentration, monomer composition and copolymer composition (from top to bottom) for BA/HEA copolymerizations in BPi with 25 wt% (▌) and 40 wt% (▌) HEA between initial (□, △) and updated (■, ▲)results

Despite the higher initial monomer concentrations, the final concentrations in the failed runs are lower than the repeat experiments. This behaviour may result from the increased viscosity of the high MM material formed, that may lower k_t and thus increase the rate of reaction. However, there is also a small difference in the comonomer compositions close to completion of the reaction. A possible explanation is that the formation or strength of H-bonds is different in the two experiments, based on the

formed polymer material (and the respective chemical environment), which may affect reactivity ratios. A direct comparison of the final composition data of each run with the PLP derived Mayo-Lewis plot for BA/HEA is given in Figure 4.6.

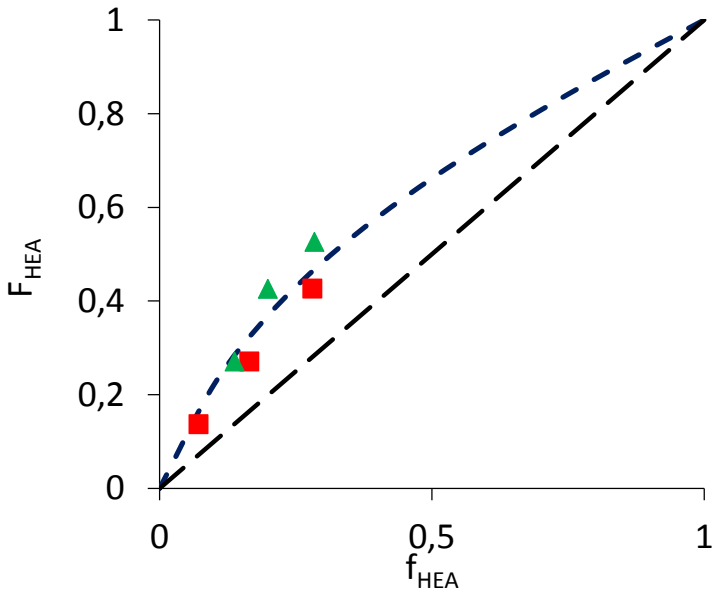

Figure 4.6: Mayo-Lewis Plot of BA/HEA in bulk[29] (derived by PLP, ---) and terminal semi-batch composition data for runs with high (▲) and low molar mass polymer (■)

The comparison with the terminal model fit for BA/HEA in bulk shows that both cases are close to the PLP-derived reactivity ratios, with data points for all semi-batch runs close to the fit. The best fit with reactivity ratios in ketones[29] would be below this line. Therefore, the chemical environment during the semi-batch process changes to conditions, which are best described by the bulk values. However, due to the dynamics of the process, semi-batch data points contain a degree of uncertainty.

From this set of HEA/BA copolymerizations in BPi it can be concluded that, although the HEA is preferentially incorporated into the polymer, its addition to the recipe has little effect on overall reaction rates (free monomer levels) and the molar masses of the polymer product. The major issue with adding HEA to the recipe is to ensure that the solvent has sufficient polarity to prevent polymer precipitation; in BPi, 40 wt% HEA in the copolymer could be tolerated at 138 °C, but 50 wt% HEA was too high. Semi-batch experiments with 25 wt% HEA in MIAK and xylenes have also been run, with results contained in

Figure B.4. As found in BPi, the addition of HEA to the recipe did not greatly impact the polymer molar masses compared to BA homopolymerization. Free monomer concentrations and comonomer compositions were of a similar magnitude as found for BPi, showing a significant promotion of HEA through H-bonding. Small differences found in the MMDs are most likely based on differences in transfer to solvent reactions.

4.3.2.2. Acrylate-only copolymerizations of BA and HEA in DMF and pentanol

To reveal more insights about H-bonding effects under semi-batch conditions further copolymerizations of BA and HEA were carried out in DMF and PeOH. Two viable comparisons should be possible based on the findings from previously published kinetic data.[29] PeOH was used instead of BuOH to keep isothermal conditions at 138 °C for a better comparison with previous results.

The same semi-batch operating conditions were used for these reactions, with monomer concentration and composition data shown in Figure 4.7. The copolymerization results in PeOH can be compared to a BA homopolymerization experiment conducted under the same conditions. For this reference experiment, the free monomer concentration was found to be quite low and stable, with no build-up in concentration observed during the transient state.

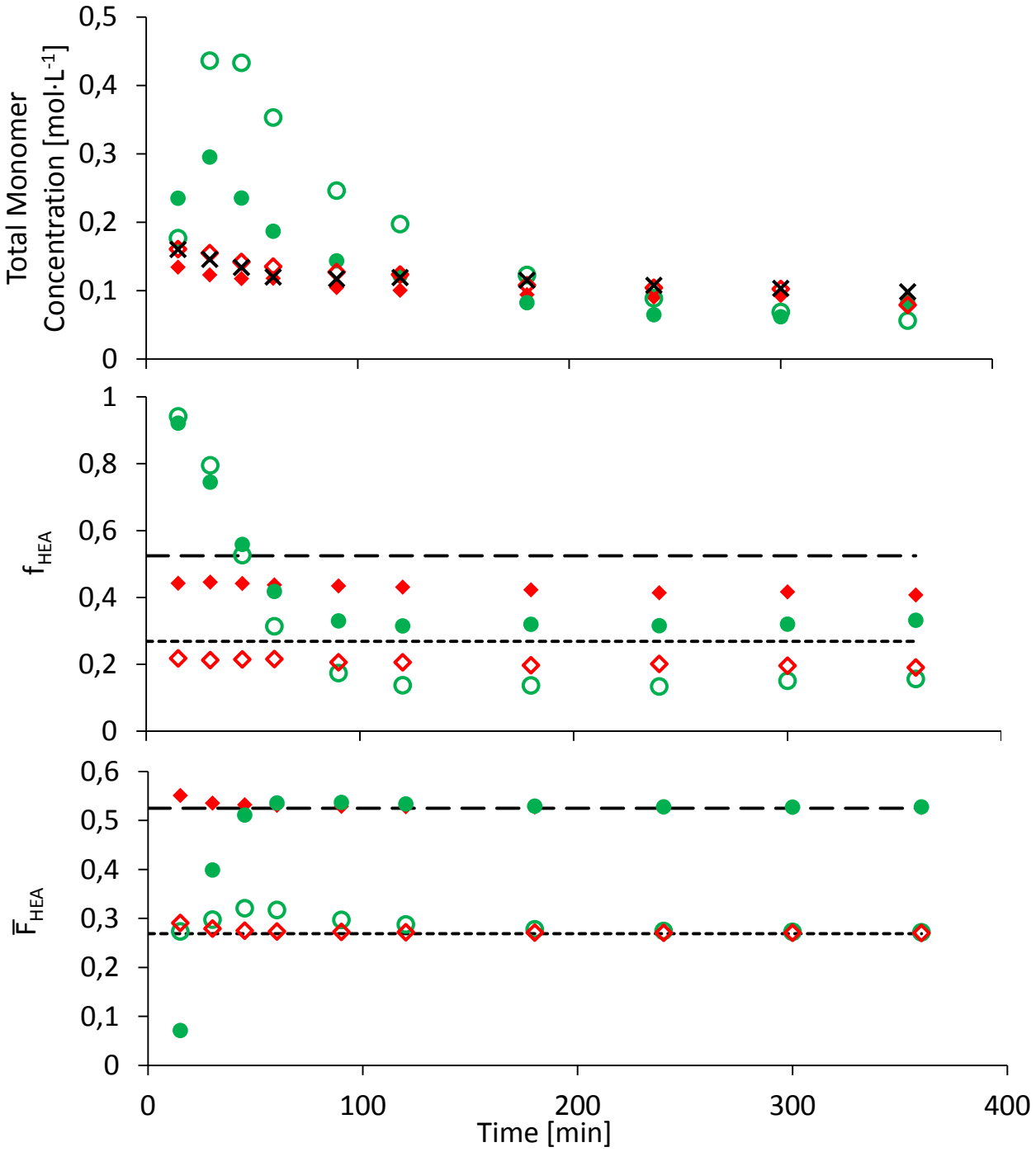

Figure 4.7: Total free monomer concentration, monomer composition and copolymer composition (from top to bottom) for BA/HEA semi-batch copolymerizations at 138 °C in PeOH (▌) and DMF (▌) with 25 wt% (○, ◊) and50 wt% (●, ♦) HEA. Monomer concentration profile also shown for BA homopolymerization in PeOH (x)

Some significant differences can be seen when the same reaction conditions were used for BA/HEA copolymerizations in PeOH, with total monomer concentration increasing to 0.3 and even 0.5 $mol \cdot L^{-1}$ during the first hour of reaction with 25 and 50 wt% HEA, respectively, before rapidly decreasing down to levels similar to (but slightly below) the homopolymerization basecase. In DMF, on the other hand, the total monomer concentration profiles pretty well match that of the homopolymerization in PeOH. As a result of this different transient behaviour for copolymerization in PeOH, the fraction of HEA in the monomer phase starts at a very high value (even close to unity) and the fraction of HEA in the copolymer phase starts at a very low value, before levelling out to constant compositions after the first hour.

In light of the notable difference in k_p^{cop} from PLP-SEC experiments,[29] with higher reactivity of the system in PeOH than DMF, these results are initially perplexing. Whereas BA in PeOH and all DMF runs share an efficient initiation process, the PeOH copolymerizations only catch up, starting from 2 h to reach similar low monomer concentrations. The answer for this phenomenon lies in the analysis of the relative consumption of comonomers. While f_{HEA} values in DMF are constant over the complete experiment, the values in PeOH suggest that HEA initially is not participating in the polymerization at all. At the beginning of the reaction, the concentration of PeOH is much higher than that of HEA in the system, so it may be that complexation occurs to remove its reactivity, while allowing BA to continue to polymerize. With continued feeding, the monomer to PeOH ratio continues to grow so that it reaches a molar ratio of ~1:1 after 3 h (counting both free and reacted monomer in this total). It is this condition, roughly a 1:1 monomer to solvent ratio that was examined in the PLP-SEC studies. This suggests that there is a drastic change in reactivity ratios for the copolymerization of BA/HEA in alcohols under very dilute conditions. Concentration dependent H-bonding effects are known from aqueous systems,[157,158] but usually related to an increase in reactivity or k_p of the functional monomer. Support for this argument of a threshold concentration can be made by comparing the two HEA copolymerization runs. The initial increase in total monomer concentration can be almost fully related to the non-reacting HEA monomer. However, the 50 wt% run returns back to a more 'normal' behaviour sooner than the 25 wt% run. This

suggests that the inhibition between PeOH and HEA only occurs until a certain HEA concentration is reached. As the described process is rapidly changing, only a rough estimate can be given for this critical concentration which is in the regime of 0.3 $mol \cdot L^{-1}$ HEA in PeOH. In terms of available H-bonds this represents a ratio of 1:24 in favour of the solvent.

Now considering the full set of experiments, there is a slight difference between runs in PeOH and DMF, with a higher value of f_{HEA} for reactions in DMF to produce the same copolymer composition. This difference indicates that the disruptive nature of DMF is slightly stronger than the capability of PeOH to create similar H-bonding effects with BA. Recall that in the PLP-SEC studies of this system (see Figure 3.8), the copolymer composition data was close to the diagonal, indicating very similar BA and HEA relative reactivities in these two solvents. Under the semi-batch conditions, however, HEA is preferentially incorporated ($F_{HEA} > f_{HEA}$ in Figure 4.7). This observation suggests that care must be taken when applying low-conversion reactivity ratios to semi-batch operating conditions when H-bonding influences the reactivity, as the ratios of monomer to solvent to polymer are very different. Solvent effects are definitely observed in the semi-batch system, but most likely vary in their importance as polymer content builds and solvent content decreases throughout the run. The question next to be addressed is focusing on the impact this complexity has on the development of polymer MMD in these systems compared to what was discussed in the previous section for reactions in BPi.

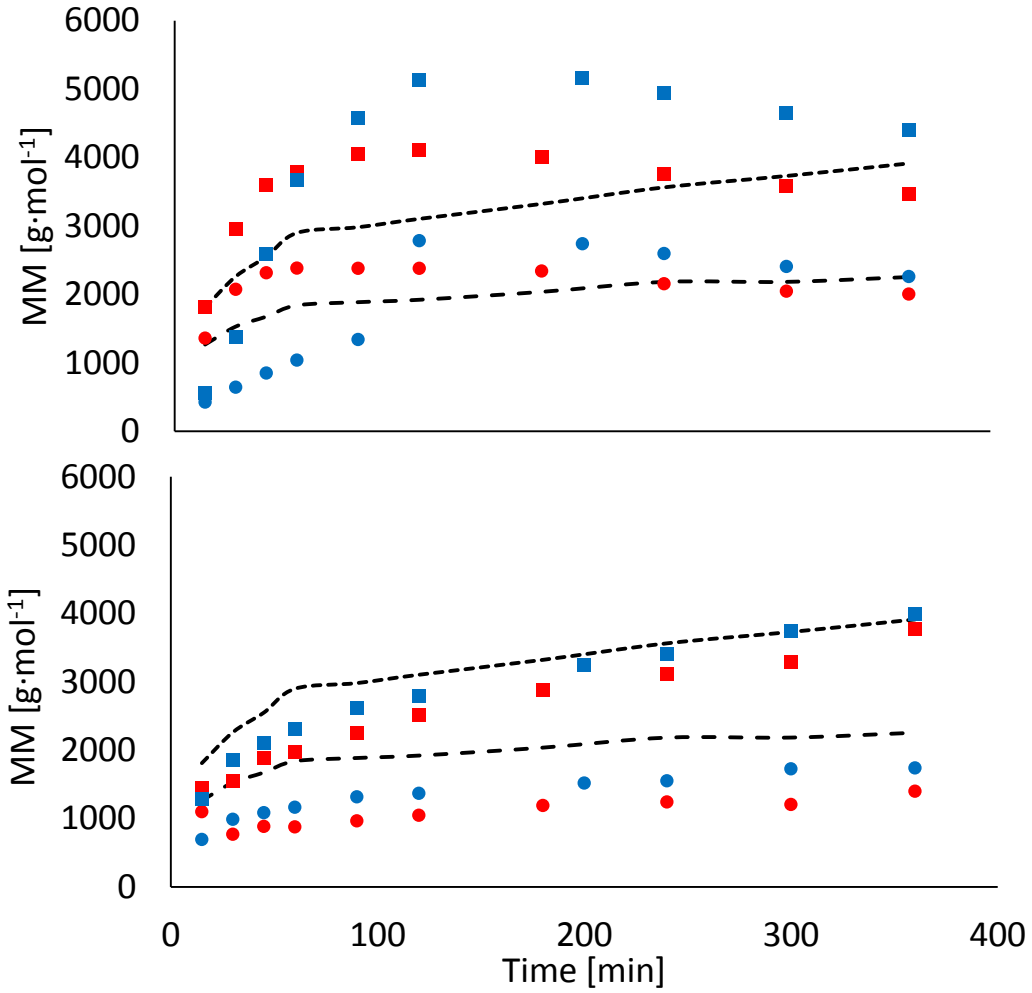

Figure 4.8: M_n (●) and M_w (■) for BA/HEA copolymerizations in PeOH (top) and DMF (bottom) at 25 wt% (▌)and 50 wt% (▌) HEA in comparison to BA homopolymerization in PeOH (M_n = ···, M_w = ---)

As shown in Figure 4.8 (top), it was found that the copolymerization reactions in PeOH that exhibited the high initial monomer concentrations also produced the highest MM polymer. However, the averages are highest for the 25 wt% HEA experiment, while the higher monomer concentrations were reached for the 50 wt% experiment. In addition, the maximum in MMs is reached later (at ~3 h) in comparison to the maximum found for monomer concentrations. Finally, the highest values reacted are M_w of about 5000 g·mol^{-1}, much lower than the values measured for the "bad" reactions in BPi (see Figure 4.3; note that a preliminary study shown in Figure B.5 and Figure B.6 showed similar trends). It is

clear, however, that the low initial HEA reactivity in PeOH also affects the development of the MMD, as the shapes of the curves differ significantly from those for BA homopolymerization in PeOH and the copolymerizations in DMF. It is difficult to comment further on these results, as differences in chain transfer to solvent and backbiting rates both affect polyacrylate MMDs and average molar masses.[142,159,160] For now, this behaviour cannot be fully explained, as other kinetic effects, like termination may play a role as well.

4.3.3. Acrylate backbiting under semi-batch conditions

Transfer to polymer reactions result in either short- (SCB) or long-chain branching (LCB) points, with the slow addition to midchain radicals (MCR) also decreasing polymer chain growth rates, and the scission of MCR also decreasing polymer molar masses. Although LCBs influence rheological performance, their level in poly(acrylate) systems is low, with the majority of branching occurring by backbiting to form SCBs, as has been shown in literature.[138,143,161] Branching levels (BLs, see Eqn 4.2) have been determined for the final samples from the set of semi-batch reactions discussed previously via quantitative ^{13}C-NMR. BL is calculated by measuring the amount of quaternary carbons (peak position at 48 ppm) relative to the total acrylate units in the polymer chain, as described in the example spectrum in Figure B.7 and as based on previous literature studies.[20,82,143]

One important question examined in this study is, how an increased HEA feed would influence the level of branching (and hence k_{bb}), as previous work has shown that H-bonding induced by alcohols tremendously reduces k_{bb} during semi-batch homopolymerization of BA.[17] Figure 4.9 presents the BLs measured for semi-batch BA/HEA copolymerizations in BPi with HEA levels up to 50 wt% based. Between 7-11% of the acrylate units in the polymer are quaternary, much higher than measured for the solution batch reactions (see Table 4.2); the difference is due to the higher temperature and the lower free monomer levels in semi-batch operation. These levels are similar to those reported for investigations of semi-batch BA systems in xylene,[11] indicating that BPi as a solvent does not greatly influence the rate of

backbiting. Remarkably, there is no real decrease in the measured BL with increasing HEA levels incorporated into the copolymer.

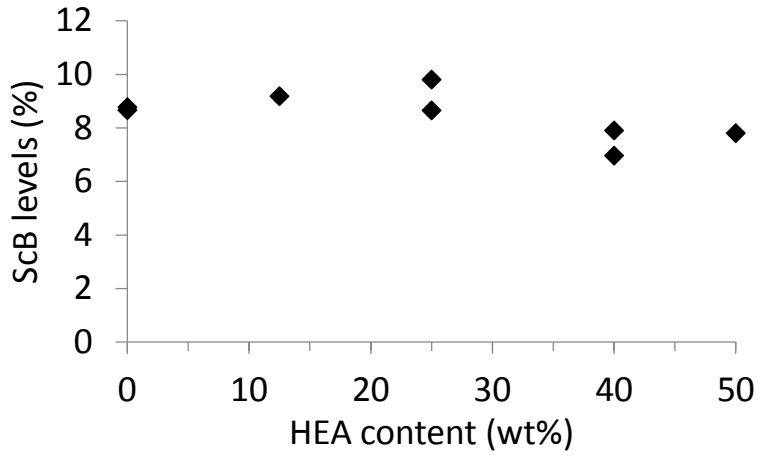

Figure 4.9: ScB levels for acrylate only semi-batch copolymerizations as a function of HEA content

The finding that HEA reduces acrylate BLs in batch (see Table 4.2) but not semi-batch (Figure 4.9) can be explained by considering the differences in reaction environment between the two systems. Under batch conditions, the level of unreacted HEA is much higher throughout much of the reaction compared to the semi-batch system, in which HEA concentrations are below 0.1 $mol \cdot L^{-1}$ (Figure 4.3). Thus, these results suggest that a minimum or threshold H-bonding concentration is required to have a significant effect on the backbiting mechanism. This interpretation also explains the major difference between this HEA/BA semi-batch system and the previous reduced BLs found with poly(BA) produced by semi-batch in an alcohol solvent: in the latter system, the H-bonding is provided by the solvent, which remains abundant over the entire course of the reaction. This finding is in contrast to propagation kinetics, where k_p values continuously increase with the introduction of even lower amounts of HEA.

The results shown in Figure 4.9 imply that the formed copolymer backbone of HEA and BA units must remain as flexible as the BA homopolymer within a BPi solution with low HEA content, allowing for the necessary H-abstraction from the 1:5 position and in contrast to the presumed rigidity for example in alcohol solutions. Therefore, a comparison to BLs measured for the semi-batch copolymerizations in

PeOH and DMF was completed, with experimental measurements summarized in Table 4.4. The branching levels measured in PeOH were in the range of 6-7%, consistently lower than the 8-9% levels measured in DMF and in BPi. For all solvents, the level of branching did not vary significantly with copolymer composition (as plotted for BPi in Figure 4.9).

A simple comparison of BLs between the systems, however, can be misleading, as the quantity is a function of monomer concentration and propagation kinetics, as well as the rate of backbiting. Thus, the data have been processed to provide an estimate of k_{bb} using Eqn 4.2. As total monomer concentration and composition do not vary greatly over the course of the semi-batch reactions, the value of [M] is taken as an average over the whole reaction time. The value of f_{HEA} was also combined with the reactivity ratios and the Arrhenius equations for the homopolymers determined in the low-conversion PLP-SEC studies to calculate k_p^{cop} at 138 °C using the terminal model. These estimates were then used in the following rearrangement of Eqn. 4.2 to calculate k_{bb} (more precisely, k_{bb}^{cop}) according to:

$$k_{bb} = \frac{BL \cdot k_p[M]}{(1-BL)} \tag{4.3.}$$

A summary of necessary parameters and the final results are given in Table 4.4. The normalization provides a better means of comparison between the systems. For example, while the BL measured in xylenes is lower than that in MIAK and BPi (0.07 compared with 0.08-0.09), the final estimates for k_{bb} were found to be in the same 2000-2800 s^{-1} range, independent of HEA content and solvent choice; this invariance with composition supports the hypothesis for a threshold H-bonding concentration. These values are lower in comparison to predictions from the literature[138] Arrhenius expression with $A = 7.41 \cdot 10^7$ and E_a = 32.7 kJ·mol^{-1} which results in k_{bb} = 5193 s^{-1}. However, Eqn 4.3 (and Eqn 4.2) assumes that all backbiting events lead to formation of a MCR, neglecting the consumption of MCRs by competing scission and termination reactions as well as the fact that growing chains of length less than 4 cannot undergo backbiting. Despite these simplifications, the analysis provides a good relative measure of backbiting rates in the system.

Table 4.4: Set of parameters and results for the calculation of k_{bb} at 138 °C

Run [w%]	BL	k_p [L· mol^{-1}]	∫[M] [mol·L^{-1}]	k_{bb} [s^{-1}]
BA BPi	0.088	127000	0.203	2472
BA/HEA (87.5/12.5) BPi	0.092	143400	0.141	2046
BA/HEA (75/25) BPi	0.087	159900	0.146	2212
BA/HEA (60/40) BPi	0.092	188000	0.125	2380
BA/HEA (75/25) MIAK	0.098	159900	0.151	2620
BA/HEA (75/25) Xyl	0.072	159900	0.193	2394
BA PeOH	0.064	164600	0.113	1280
BA/HEA (75/25) PeOH	0.067	175900	0.152	1914
BA/HEA (50/50) PeOH	0.071	193000	0.110	1630
BA/HEA (75/25) DMF	0.095	140200	0.111	1639
BA/HEA (50/50) DMF	0.093	158400	0.099	1603

For the simulations described in the following chapters and in agreement with previous semi-batch investigations,[142] the backbiting preexponential factor has been lowered to $A = 4.3 \cdot 10^7$ based on this analysis. Using this expression and the copolymerization model (described fully in Chapter 5) leads to a good description of BA homopolymerization under semi-batch conditions, as shown in Figure 4.10. Predicted branching levels were found to be in reasonable agreement with the experimental data. Most importantly, as the data in Table 4.4 indicate that backbiting kinetics for HEA and BA are the same the under semi-batch conditions with no detectable influence of changing HEA contents in ketone, xylenes,

or ester solvents, kinetic findings should be valid for a wide range of (non-)functional comonomer compositions. The copolymerization with methacrylates has a significant influence by reducing the rate of backbiting, as will be discussed later.

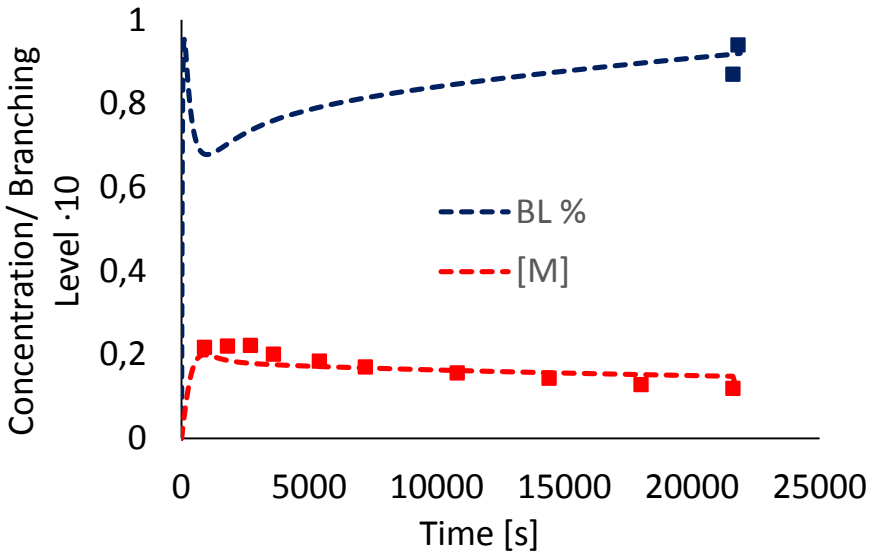

Figure 4.10: Modeled free monomer profile (– –) and branching level – –) as a function of time, for BA polymerized in BPi at 138 °C under semi-batch conditions, in comparison to experimentally determined monomer levels (■) and final branching content (■)

The influence of PeOH is to reduce k_{bb} to 1280 s^{-1} for BA homopolymerization, roughly a factor of 2 lower than found in the other solvents at 138 °C. This is quite significant, but lower than the factor of 4-5 reduction reported in a previous investigation at 110 °C by Liang et al.[17] Liang also compared branching levels for BA in xylene and pentanol at 138 C in his PhD thesis,[154] for which he found that branching levels decreased roughly by the same factor of two as found here. Thus, the influence of H-bonding diminishes with increased temperature, a result in agreement with the hypothesis that it the chain stiffness is induced by the interaction of the solvent with reacting chain ends. According to the results in Table 4.4, the introduction of HEA to the semi-batch polymerizations in PeOH leads to a slight increase in k_{bb}. However, in light of the unexpected free monomer profiles (see Figure 4.7) these estimates are uncertain, as the validity of assuming a constant value for [M] is questionable.

Finally, the results obtained in DMF warrant discussion. Although the branching levels are in the same 9% range as observed in other solvents, the reduced free monomer levels and estimated k_p^{cop} values lead lower estimates of k_{bb}, 1600 rather than 2000-2800 s^{-1}. Whereas in PeOH the effects are clearly derived from H-bonding, the reasoning for DMF is complicated, due to multiple possibilities of the polar or mesomerically charged DMF to affect the reactivity during the semi-batch copolymerization process. However, the trends agree with the findings from small-scale batch experiments, which showed reduced branching levels for both BA and HEA in DMF (Table 4.2).

As shown in previous investigations, the BL is closely associated with the rate of chain scission in the system due to the competition between monomer addition (leading to the formation of a quaternary carbon) and scission (resulting in the formation of a chain with an unsaturated double bond, or macromonomer) of the MCR formed by backbiting. Figure 4.11 shows the evolution of macromonomer levels over the course of a semi-batch reaction determined by measuring the presence of vinyl peaks in ^{1}H-NMR spectra, as detailed in Figure B.8. The general shape of the curve, with decreasing macromonomer levels with increasing time, is controlled not only by the generation rate of macromonomers through scission, but also by their consumption rate by reaction, as detailed in a previous study by Wang et al.[162] While the macromonomer levels shown in Figure 4.11 for BA are in good agreement with that previous work, the presence of HEA reduces the level of unsaturated double bonds. This reduction is independent of the HEA content, and occurs even though the M_n values of the HEA-containing polymers are lower than poly(BA) (see Figure 4.4). The question remains whether this is due to a reduced scission rate during HEA copolymerization, or a potential increase in reactivity of a hydroxyl-functional macromonomer. The MMD after 30 min reaction time also indicate, as shown in Figure B.2 and Figure B.3, that the initial increase in MM is due to a complete shift of the distribution for HEA containing systems, instead of forming a bimodal shoulder as seen in the BA case. In agreement with NMR results a higher population of low molar mass macromonomers is present in the BA samples, as seen by the peaks in SEC-traces at log 2.7-2.9. Whereas an exact mechanistic explanation cannot be given for the suppression of scission or increased reactivity of macromonomers through H-bonding, it

may be that the presence of HEA in the backbone allows for interactions with free monomer or solvent that provides some stabilization and inhibits the potential break-up of a MCR.

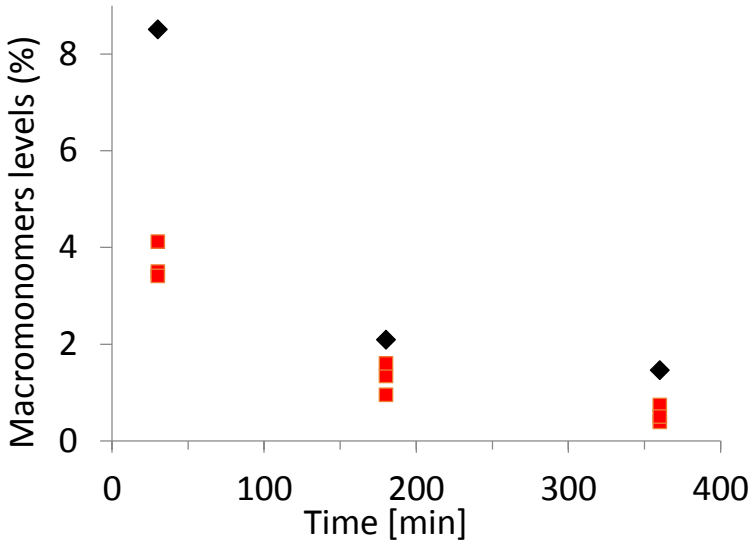

Figure 4.11: Amount of macromonomers, determined by ^{1}H-NMR, present in BA (♦) and multiple BA/HEA (■) semi-batch polymerizations in BPi at 138 °C

4.3.3.1. Remarks pertaining to branching in acrylate methacrylate copolymerizations

In contrast to acrylate-only copolymerizations, the backbiting process becomes limited in copolymerizations with methacrylates. It has been reasoned (and supported by quantum computations[163] and experimental evidence[164]) that backbiting can only occur through attack of an acrylate unit in the penpenultimate position by an acrylate radical; in other words, backbiting can only occur with an ~~AXA· radical structure, with A indicating an acrylate unit and X being an acrylate or methacrylate unit. It has also been proposed that the identity of the "X" unit affects the backbiting rate, as a methacrylate unit present in the penultimate position would inhibit the reaction; in previous modeling efforts due to the less flexible polymer backbone structure it was assumed that the backbiting rate of an acrylate-

methacrylate-acrylate chain end is reduced by the factor of 0.6.[28,165] The latter study specifically investigated the BA/MMA system, which already showed an increasing complexity of the resulting ^{13}C-NMR spectra. In this work, it was found that the BMA/HEA spectra are complicated by overlapping signals. Specifically, as shown in Figure B.9, the signal at 47-48 ppm, formerly attributed to the quaternary carbon resulting from branching, is increased by such proportion that is must be another chemical signal. To further study this complication, HSQC spectra were collected to assign the coupling of the surrounding peaks and identify the residual quaternary carbon at 47-48 ppm, as shown in Figure 4.12.

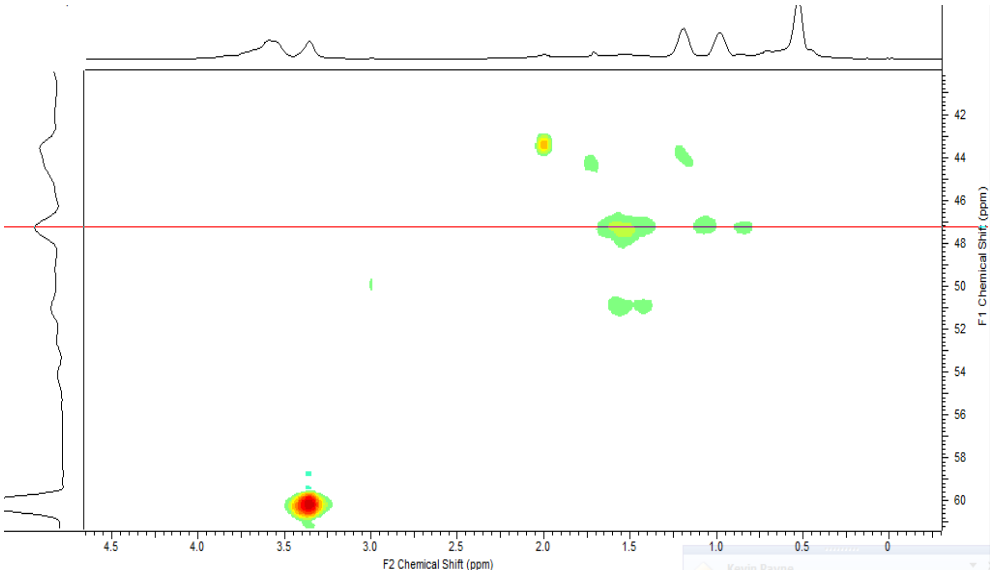

Figure 4.12: HSQC spectrum for BMA/HEA (75/25 wt%) copolymer synthesized in semi-batch

A distinct coupling was detected by HSQC in the region of 47-48 ppm, showing protons connected to the polymer backbone. Unfortunately, the shape of the signal is apparent for a direct chemical CH bond and does not allow the alternative of shadow coupling over 2 chemical bonds, which can occur even under HSQC pulsing conditions, depending on the chemical nature of the compound. To check for the additional presence of the quaternary carbon, another method is necessary to indirectly quantify their total amount. For this reason, a DEPT 135 experiment was conducted. Although these spectra are limited in their evaluation, their pulse sequence permits a quantitative comparison of carbons

of the same chemical nature.[166] An example spectrum is given in Figure B.10. If all carbons at 47-48 ppm are a quaternary nature, no signal would be observed in a DEPT spectrum. For BMA/HEA copolymer, however, the spectrum clearly shows an intense negative peak in this area, indicating a CH_2 group. After calibration of the relative intensities with a homopolymer sample of BA, the signal is compared to the CH_2s in the BMA and HEA ester side-chains, resulting in a signal integration of 12-14 %. A reasonable explanation for this peak is the alternating configuration of acrylate and methacrylate in the backbone, which can also be seen in case of BA/MMA, however without a notable overlay.[165] In this case the produced copolymer disturbs the homogenous structure as seen for acrylates, shifting backbone signals towards the area of interest. To correct for this interference and estimate the true branching level of acrylate/methacrylate copolymers, it is necessary to subtract this contribution of CH_2 units from the total quantitative signal. A few DEPT spectra of BA/HEA copolymers were taken to verify that this issue is only of importance for BMA/HEA systems, as no CH_2 peaks were present in the area of 47-48 ppm for BA/HEA.

To find a general solution for this dilemma a catalogue for BA/BMA with different copolymer compositions was created and analyzed via DEPT 135. Through direct comparison of BA/BMA and HEA/BMA spectra it was found that there is not a notable difference between peaks in the backbone for these two systems. The aim is to develop an equation to estimate the relative proportions of the different carbons and their influence even at low methacrylate contents. The analysis revealed an increasing CH_2 peak with increasing methacrylate content incorporated into the copolymer as shown in Figure 4.13. A reasonable detection limit was detected for the sample containing 5 wt% BMA. The signal then increases to an intermediate intensity of 2.2 % at 28 wt% BMA, before diverging towards the results derived from semi-batch runs. Clearly, there is no linear correlation, but more of a quadratic function as a function of the BMA content. Therefore, a significant contribution of CH_2 signals was identified and quantified, which further complicates the analysis of the backbiting mechanisms in copolymerizations. It is suggested to take special care with such acrylate/ methacrylate systems. More reliable results are found for the acrylate rich systems, and should be used to develop more insights on branching mechanisms.

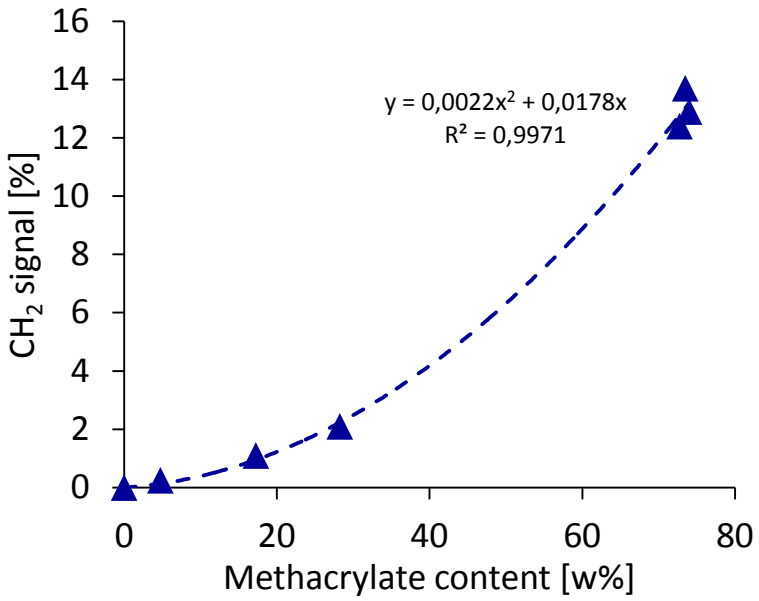

Figure 4.13: Intensity of CH_2 signals (per monomer unit) at 47-48 ppm determined by a DEPT 135 technique, based on the copolymer composition

4.4. Conclusions and outlook

The investigation of acrylate-only copolymerization of BA and HEA through small-scale and semi-batch experiments shone light into the special effect of H-bonding on copolymerization kinetics. A separation can be made based on effects induced by hydroxyl functional monomers themselves or alcohols as a solvent. Therefore, it was found that the hypothesis for an increased relative reactivity of HEA through H-bonding in copolymerization, derived by PLP experiments, withstands operational changes towards batch and semi-batch reactions up to temperatures of 138 °C. Though present in the high solids content semi-batch system, the solvent effects were found to be not as pronounced as in PLP low conversion experiments, as copolymer compositions were found to be closer to those expected for a bulk system.

Special concentration dependent behaviour was found for the semi-batch copolymerizations conducted in PeOH, with HEA incorporation inhibited early in the reaction. To further understand this

phenomenon, additional PLP copolymerization experiments are recommended with higher solvent contents to investigate the threshold concentration for such effects on composition. If accessible, it would be also interesting to investigate potential effects of solvent concentration on k_p for HEA homo- and copolymerization systems, especially at high dilution.

The influence of H-bonding on the acrylate side reactions of backbiting and scission were also investigated. Results suggest that H-bonding reduces k_{bb} in acrylate semi-batch polymerization in alcohols. While H-bonding introduced by HEA causes a similar reduction in branching levels during batch polymerization, the concentration of HEA is too low to affect the reaction under semi-batch conditions, as the HEA content within the copolymer had no notable effect on the k_{bb} values estimated in BPi, xylenes and MIBK. However, interactions affecting the polymer structure in solution are most likely not limited to H-bonding, as seen by the reduction in k_{bb} in DMF systems. In contrast, scission was found to be comonomer dependent with reduced macromonomer levels present in HEA copolymers. While further work is required to explore these phenomena, the experimental study shows clearly that adding HEA to an acrylate-only copolymerization system does not greatly impact the rates and polymer properties (molar masses and branching levels) under typical semi-batch operating conditions, provided that a suitable solvent for the polar copolymer system is chosen.

Chapter 5 Model development and validation for BMA/HEA semi-batch copolymerizations in industrially relevant solvents

5.1. Introduction

Comprehensive models for radical copolymerization of monomers of the acrylate, methacrylate and styrenic families have been successfully developed for application at industrially relevant conditions such as higher temperatures (> 100 °C) and semi-batch conditions.[28,35,167,168] However, the development and application of these models has focused on non-functional monomers, for which specific monomer solvent interactions do not significantly affect rate or polymer properties. As hydrogen bonding can greatly affect polymerization behaviour of hydroxyfunctional monomers, and since HEA and HEMA are frequently used as reactive components in automotive coatings resins, it is necessary to test whether the modeling framework can be applied to these important systems. With the introduction of these more polar copolymers, more polar solvents like ketones and esters become more feasible to use (in comparison to previously used xylenes). This change in VOC from formerly xylenes, should maintain relatively low viscosities. However, in a direct comparison, ketones in solution with (meth)acrylic resins maintain lower viscosities than ester equivalents.[169–171]

In the particular case of BMA/HEA copolymerization all relevant propagation kinetic coefficients are known from small-scale PLP experiments for bulk and a sufficient set of solvents.[19] To model methacrylate/acrylate copolymerization under elevated temperatures, however, methacrylate depropagation[116,172] and acrylate backbiting events (with associated midchain radical reactions such as monomer addition and scission)[84,173] to form branching points[20,86] must also be considered, as the importance of these reactions in copolymerization is dependent on the comonomer composition.

The challenge, then, is to validate whether generalized knowledge of these side reactions under industrially relevant conditions can be applied to represent BMA/HEA copolymerization, especially in light of the known H-bonding effects. A special focus will be made on the comparison with previously published studies of the BA/BMA system,[142,174] in terms of monomer reaction profiles and final molar mass distributions. The information gathered can then be used to aid process (i.e., rate of polymerization

and correlated reaction heats) and product (final polymer properties such as molecular weights and T_g[175,176]) design. As observed in the related HEMA systems,[11] the introduction of the functional comonomer not only affects the kinetics, but also adds a level of complexity in terms of solubility to maintain a single phase solution due to the polarity of the hydroxyfunctional monomer/polymer. HEA homopolymers are usually gel-like polymers[177–179] not generally soluble in solvents like xylenes or ketones used in this study. Therefore, in addition to development and verification of the model, experimental limitations should be exposed and described.

5.2. Experimental

5.2.1. Materials

Butyl methacrylate (99 %, Sigma), 2-hydroxyethyl acrylate (96 %, Sigma), deuterated dimethyl sulfoxide, deuterated toluene, 2,2-azobis(2-methylbutyronitrile) (Vazo-67, +99%, DuPont), *tert*-butyl peracetate (50 wt% in mineral spirits, Sigma), xylenes (>99%. Fisher Scientific), 5-methyl-2-hexanone (99 %, Sigma), 2-heptanone (99 %, Sigma) and butyl propionate (99 %, Sigma) were used as received without further purification.

5.2.2. Semi-batch reactions

Reactions were conducted in either a 0.6 or 1.0 L LabMax reactor with automatic stirring, heat control, reflux system and reagent flow control through gravimetric feed. Reactions were conducted at 138 °C, the boiling point of xylenes. Solvents also include ketones and esters. The reactor was charged with 129 g (or 220 g in case of the larger reactor) of solvent and then heated to reaction temperature under nitrogen inert gas atmosphere. The feed reservoir was charged with 239 g (or 408 g in case of the larger reactor) of monomer solution (with controlled composition in case of comonomer systems) before adding 2 mol% of TBPO relative to the monomer content, as reported elsewhere.[142] The reaction mixture was

then fed over 6 h into the reactor to achieve a final polymer content of 65 wt%, assuming 100 % monomer conversion. To monitor the dynamic behaviour, 10 samples of 2-3 mL were taken over the course of the reaction. Final samples usually contained more than 10 mL solution to allow for further sample analysis. All samples were immediately quenched through the addition of MEHQ inhibitor (2 $g \cdot L^{-1}$) and stored in the freezer. A small fraction was then taken to be analyzed via GC before residual solvent was removed through air stripping and evaporation under vacuum at 60 °C to isolate the polymer for characterization.

5.2.3. In-situ NMR batch reactions

In-situ batch experiments were performed inside the NMR tube with online recording of the reactions ^{1}H-NMR spectrum.[139,180] Reaction solutions were prepared at different BMA/HEA comonomer ratios at 20-40 wt% total monomer content relative to the deuterated solvents DMSO-d6 and toluene-d8; 2 wt% Vazo-67 based on the total reaction mass (monomers and solvent) was used to assure continuous radical generation throughout the whole reaction. The NMR-tube was charged with roughly 0.5 mL of the reaction mixture and carefully purged with nitrogen for a minimum of 15 min to remove oxygen. Reaction temperatures (usually 80 °C with some exceptions at 60 °C) were controlled through the air inlet stream of the Bruker-Avance 500 and assumed to be equal inside the reaction tube due to the small diameter. The tube was then inserted into the instrument as the controlled temperature approached its setpoint ($\Delta T \leq 5$ °C), allowing sufficient time to lock the NMR solvent and perform the manual shimming process during the final increase to reaction temperature. Using standard ^{1}H-NMR settings, recording of spectra was then started in a multi acquisition setup with 24 scans per acquisition. The number and time intervals between acquisitions was controlled by dummy scans to allow for collection of data every 2 min; for BMA rich recipes this time was increased to 4 min.

5.2.4. Sample Characterization via SEC and GC

Samples created within this work were analyzed and characterized via SEC or GC accordingly to the experimental procedure described in Chapter 4.2, to obtain MMD and residual monomer concentrations. For GC analysis, an additional external calibration was created for BMA, to determine monomer contents.

5.3. Results and discussion

5.3.1. In-situ NMR studies of BMA/HEA batch copolymerization

The PLP technique is used to measure copolymerization propagation kinetics at low conversion, representative of reaction conditions at the beginning of a batch polymerization. For most systems this is sufficient, as k_p^{cop} and reactivity ratios are independent of solvent choice and monomer concentration. However, potential monomer conversion dependencies arise in the case of H-bonding effects, as apparent reactivity ratios can vary not only with solvent choice but also with monomer concentration.[157,181] In addition, H-bonding between free monomer (decreasing in concentration as conversion increases) and the increasing polymer content over the course of a batch polymerization may also influence the relative reactivity of the H-bonding monomer. Thus, a limited set of in-situ NMR experiments was performed to examine the ability of PLP-derived reactivity ratios to predict composition drift in the BMA/HEA system over the course of a batch reaction. The reactions were performed at 80 °C in both DMSO-d6 and toluene-d8, with initiator concentration selected to achieve high conversions in less than 2 h.

The choice of DMSO-d6 was based on its chemical similarity to DMF (used in the PLP studies); both solvents have similar polarity (dipole moments of 3.86 D vs 3.96 D) with H-bonding acceptor capabilities, the sulfoxide group for DMSO and the aldehyde functionality for DMF. Hence, it is assumed that the relevant interactions with HEA are of similar magnitude, with no interactions expected with BMA. Similar assumptions were made for the replacement of xylenes with toluene-d8 in the second set of reactions. The in-situ NMR technique was chosen as a reliable method to track monomer and copolymer

composition[157,180,182] as a function of conversion for small scale batch reactions under isothermal conditions, as long as there is one set of distinctly identifiable peaks correlating with monomer and polymer signals. Figure 5.1 shows example spectra collected at two times in the course of a batch BMA/HEA experiment in 80 v% toluene-d8 with an initial monomer composition of 40 v% HEA.

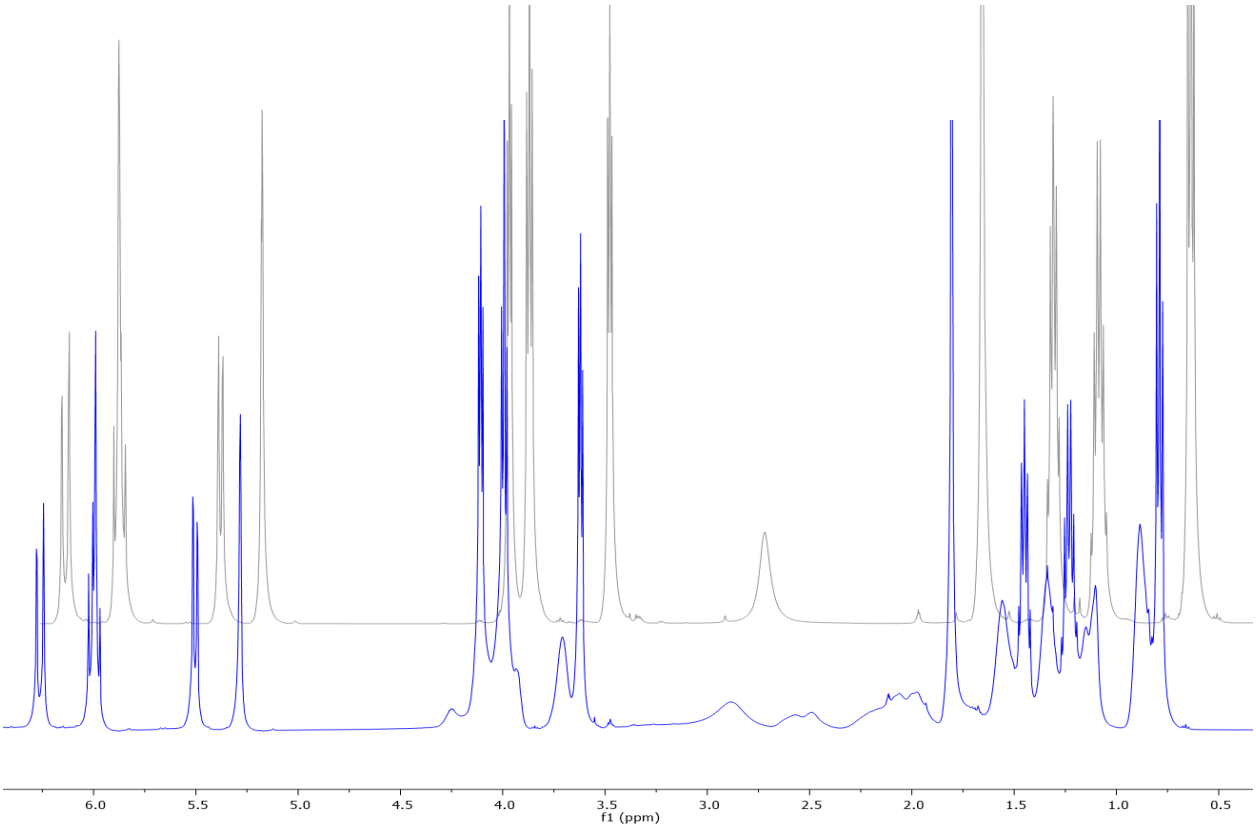

Figure 5.1: ^{1}H-NMR spectrum for BMA/HEA (60/40) copolymerization in Toluene-d8 at roughly 30% conversion (front) and the beginning of the reaction (back); formation of polymer is visible due to the presence of broader low field shadowing peaks next to respective monomer peaks

The relative amounts of BMA and HEA monomer present is identified by their aliphatic double bond signals in the region of 5.5 – 6.5 ppm. (Note that peak positions may shift about 0.1 ppm with increasing conversion.) Due to the influence of the adjacent methyl group of the methacrylate, the two BMA protons with chemical shifts of 5.50 ppm and 5.90 ppm are distinguishable from the three HEA

protons at 5.75 ppm, 6.00 ppm and 6.20 ppm. This allows for the calculation of HEA mole fraction in the monomer as follows, using all the available monomer peaks:

$$f_{HEA} = \frac{\int CH^{=}\,(5.75\ ppm) + \int CH^{=}\,(6.00\ ppm) + \int CH^{=}\,(6.20\ ppm)}{\left\{\begin{array}{c}[\int CH^{=}\,(5.75\ ppm) + \int CH^{=}\,(6.00\ ppm) + \int CH^{=}\,(6.20\ ppm)] \\ +\frac{3}{2}[\int CH^{=}\,(5.50\ ppm) + \int CH^{=}\,(5.90\ ppm)]\end{array}\right\}} \quad (5.1.)$$

$$f_{BMA} = 1 - f_{HEA}$$

Overall conversion is calculated by comparing the combined areas of the olefinic protons to identified monomer and polymer peaks that are invariant with conversion (thus representing 100% of the available material), as peaks from the copolymer backbone have too much interference. Based on previous work,[19] the combination of HEA and BMA CH_2 groups in the side-chain adjacent to the (meth-) acrylate ester at 3.80-4.20 ppm were used, resulting in the following expression for the overall monomer conversion:

$$X = 1 - \frac{2\left\{\int CH^{=HEA}\,(6.20\ ppm) + CH^{=BMA}\,(5.50\ ppm)\right\}}{\int 2\ CH_2\,(3.80-4.20)} \quad (5.2.)$$

To cover the complete range of composition, the first set of experiments was performed at HEA levels of 20, 50 and 70 wt% in the comonomer mixture, with no phase separation observed for any of the final samples (conversions higher than 90 %). Comonomer and copolymer compositions are plotted as a function of overall monomer conversion in Figure 5.2.

Consistent with expectations, BMA is preferentially incorporated into the copolymer, leading to an increase of the HEA fraction in the comonomer mixture with increasing conversion; the largest drift is observed for the BMA rich recipe, an obvious effect as r_{BMA} is larger than r_{HEA}. To check the validity of the reactivity ratios measured at low conversion, the expected monomer composition drift is calculated using the integrated version of the terminal model:[183]

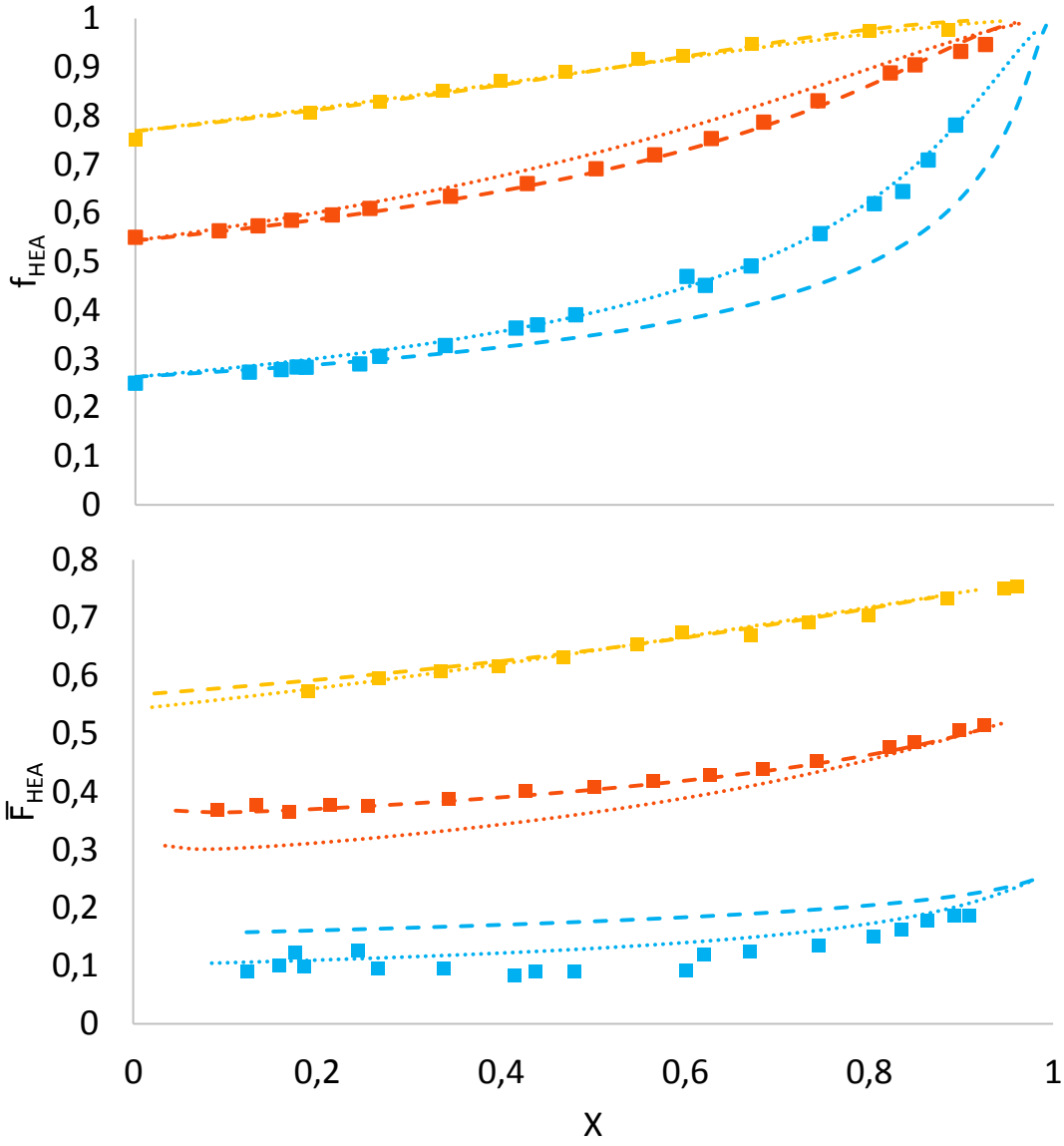

Figure 5.2: Mole fraction of BMA in comonomer (top) and copolymer (bottom) vs. overall monomer conversion, as measured for BMA/HEA batch copolymerizations at 80 °C in DMSO-d6 at 20 (■), 50 (■) and 70 wt% (■) initial HEA contents. Lines represent terminal model predictions with reactivity ratios taken from small scale PLP experiments (r_1 = 1.83, r_2 = 0.31, ——) and optimized values fit to this set of in-situ NMR data (r_1 = 3.29 ± 0.33, r_2 = 0.41 ± 0.08 ···)

$$X = 1 - \left[\frac{f_1}{f_{1,inital}}\right]^{\alpha} \cdot \left[\frac{1-f_1}{1-f_{1,initial}}\right]^{\beta} \cdot \left(\frac{[f_{1,initial} - \delta]}{[f_1 - \delta]}\right)^{\gamma} \quad (5.3.)$$

$$\text{with } \alpha = \frac{r_2}{(1-r_2)}, \beta = \frac{r_1}{(1-r_1)}, \gamma = \frac{(1-r_1 r_2)}{(1-r_1)\cdot(1-r_2)}, \delta = \frac{(1-r_2)}{(2-r_1-r_2)}$$

Corresponding copolymer compositions are calculated based on material balances.

$$\bar{F}_1 = \frac{f_{1,initial} - (1-X)\cdot f_1}{X} \quad (5.4.)$$

As shown in Figure 5.2, the composition drifts calculated using r_{BMA} = 1.83 and r_{HEA} = 0.31 (as determined by low conversion experiments in DMF)[19] provide a reasonable description of the experimental data for batch reactions containing initial HEA contents of 50 and 70 wt% in the monomer. However, some discrepancies were observed for the experiment with the lowest initial HEA level (20 wt%) at higher conversions, with HEA accumulation predicted to occur more slowly than measured experimentally. This result is a bit surprising, as DMF disrupts H-bonding influences on reactivity such that the BMA/HEA reactivity ratios in the solvent were close to those known from the classic BMA/BA system.[119] A small adjustment to reduce the HEA-incorporation at low HEA concentrations is required, although the possibility that differences occur between DMF and DMSO-d6 cannot be ruled out. Using PREDICI® parameter estimation tools applied to the composition drift in a batch reaction system[157] the new parameters were found to be r_{BMA} = 3.29 ± 0.33 and r_{HEA} = 0.41 ± 0.08. The resulting fits are also illustrated in Figure 5.2. While there is not much change to the r_{HEA} value, r_{BMA} is significantly increased to match the result obtained for the BMA-rich experiment; however, the equimolar copolymerization is not well-represented with these best-fit values. The reason for this discrepancy is not clear. The goal of the parameter estimation tool is to find a unique solution that describes the complete data set, while minimizing the total error. As the increased monomer drift also creates an increased error in comparison to the original data set, PREDICI® needs to weigh these data points at a higher fraction, while tolerating a slightly increased error for the two other cases. This mathematical issue complicates the exact

interpretation. In an attempt to simplify this dilemma, the Mayo-Lewis plot for both solutions are given in Figure 5.3.

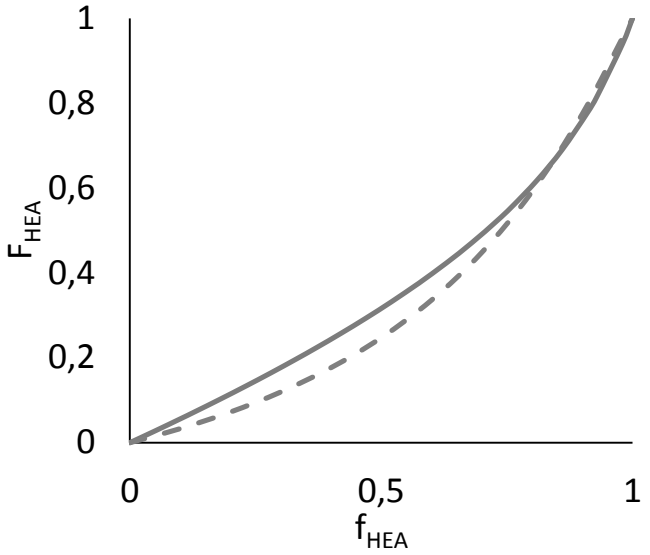

Figure 5.3: Mayo-Lewis plot for BMA/HEA in DMF based on terminal model predictions with reactivity ratios taken from small scale PLP experiments (r_1 = 1.83, r_2 = 0.31, ──) and optimized values based on the in-situ NMR data in DMSO-d6 (r_1 = 3.29 ± 0.33, r_2 = 0.41 ± 0.08, ─ ─)

It can be seen that the actual differences in copolymer vs comonomer composition between the two sets of parameters is larger at low HEA fractions because of the difference in the two r_{BMA} estimates. Keeping in mind that the comonomer composition drifts are not perfectly described by either set of *r*-values, it is likely that the truth is probably found as a combination of both fitted lines. Small-scale PLP derived *r*-values remain valid, but concentration dependent effects are most likely present as well.

Whereas DMF (DMSO) disrupts HEA H-bonding, its influence on kinetics is enhanced in non-polar solvents; the HEA/BMA copolymer produced in xylenes was even found to be enriched in HEA relative to the monomer composition from the PLP-SEC low conversion study.[19] Thus, it is quite interesting to compare copolymer composition drift under the changing conditions of a batch reaction to predictions made using the reactivity ratios estimated from low-conversion experiments. As mentioned previously, toluene-d8 was used for the in-situ NMR work, a solvent quite similar to the xylenes used in

the PLP-SEC study. Experiments were performed at 20, 30, 40 and 50 wt% HEA content; at higher HEA levels, it was observed that the polar copolymer began to precipitate from the mixture at higher conversions. The comonomer and copolymer composition drifts as a function of conversion are shown in Figure 5.4.

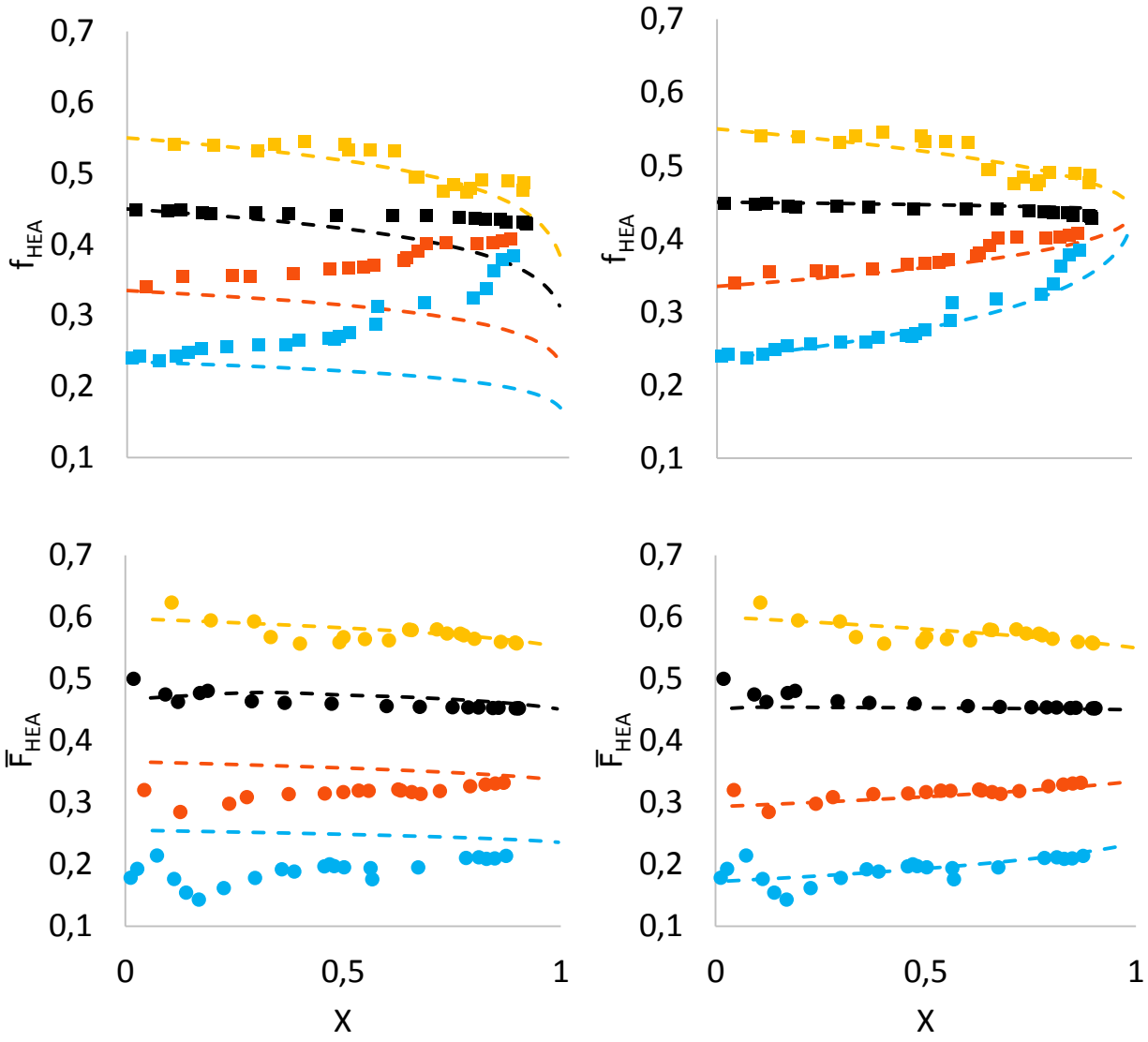

Figure 5.4: Comonomer composition (top) and copolymer composition (bottom) for BMA/HEA copolymerizations in toluene-d8 at 20, 30, 40 and 50 wt% HEA content as a function of conversion. Lines represent terminal model predictions with reactivity ratios taken from small scale PLP experiments (r_1 = 0.96, r_2 = 1.35, — —, left) and optimized values based on the in-situ NMR data (r_1 = 2.50 ± 0.33, r_2 = 2.93 ± 0.42 — —, right)

It is quite interesting to observe that the monomer compositions are converging to a final value of f_{BMA} of 0.6, despite the differing initial comonomer compositions. This behaviour suggest an azeotropic point, not expected from the previously reported reactivity ratios[19] that predict that comonomer composition should continuously become enriched in BMA. There is not a significant drift in copolymer composition with conversion, as the Mayo-Lewis plot of copolymer vs comonomer composition does not deviate far from the diagonal (Figure 5.5). As shown in Figure 5.4 (left hand plots), experimental and predicted monomer compositions clearly differ for the experiments with initial HEA level at 40 wt% and lower, with increasing discrepancy at increased initial BMA contents. Therefore, a new set of r-values has been fit to the monomer composition drift using the PREDICI® parameter estimation tools to provide a much-improved representation of the complete set of data, as shown at the right-hand side plots of Figure 5.4. However, the best fit r-values are both greater than unity, $r_1 = 2.50 \pm 0.33$ and $r_2 = 2.93 \pm 0.42$, a situation, to the best of our knowledge, not before reported in radical copolymerization. When directly comparing the Mayo-Lewis plots constructed using the reactivity ratios determined for xylenes (low conversion PLP-SEC experiments) and toluene-d8 (in situ NMR experiments limited to initial $f_{HEA} < 0.6$), as shown in Figure 5.5, it can be seen that both curves are close to the diagonal.

Thus, while the estimated reactivity ratios differ quite significantly between these two solvent systems, the predictions in copolymer composition are similar. The differences are not likely due to subtle differences in xylene vs toluene, but instead arise from the change in relative HEA incorporation rates that occurs with conversion during the batch polymerization as a result of the changing environment that influences H-bonding. It is likely that neither set of reactivity ratios can be considered as true kinetic values, as potential concentration dependent effects are present as well. Minor influences through the deuterated NMR-solvent are possible as well,[184,185] but are assumed to be negligible. In contrast to the previous DMF vs DMSO-d6 case, differences seem to be more drastic as the Mayo-Lewis equation crosses the diagonal, while creating an azeotropic point which significantly affects the shape and direction of comonomer drifts as seen in the direct comparison in Figure 5.4. Summarized, this again shows the special nature of H-bonding copolymerization systems and undermines the necessity for further

experimentation under industrially relevant conditions (at elevated temperatures and specific feeding profiles).

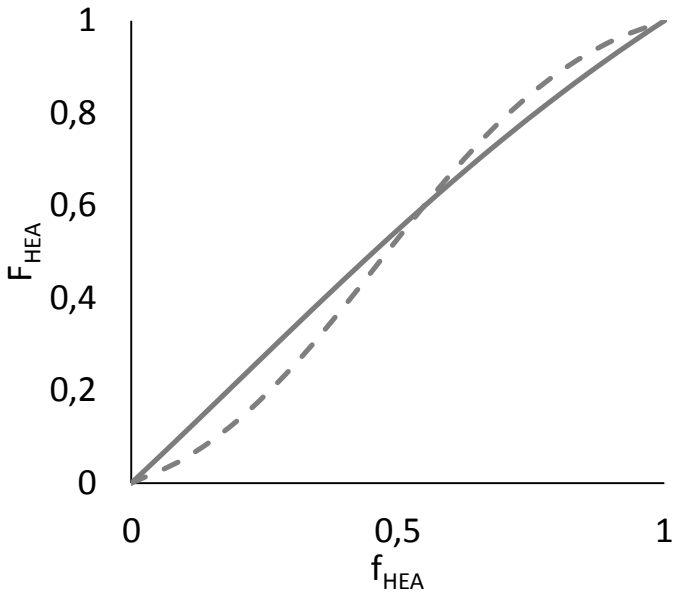

Figure 5.5: Mayo-Lewis plot for BMA/HEA in xylenes based on terminal model predictions with reactivity ratios estimated from small scale low-conversion PLP experiments ($r_1 = 0.96 \pm 0.05$, $r_2 = 1.35 \pm 0.14$, ──) in xylene and from in-situ NMR batch copolymerizations in toluene-d8 ($r_1 = 2.50 \pm 0.33$, $r_2 = 2.93 \pm 0.42$, ─ ─)

5.3.2. Status quo and steps from BMA/BA to BMA/HEA copolymerizations

The copolymerization of BMA and BA has been both studied experimentally and extensively modeled[28,116,142] under the starved-feed semi-batch reaction conditions used in this study. As such, it provides an excellent basis of comparison for the BMA/HEA system of interest to this work. An experiment with monomer feed of 25/75 wt% BA/BMA was performed at 138 °C in xylenes, with a final solids content of 65% (assuming full conversion) reached after a six-hour feeding time, with TBPA initiator feed of 2 mol% based on monomer content. As well as to compare to previous results, the experiment was also chosen to gain experience with the new PREDICI® 11 platform. All rate coefficients

and model parameters were taken from the publication describing the terpolymerization of BA and BMA with ST,[28] except for k_{bb}, which was reduced according to the results presented in Chapter 4. The results of the isothermal reaction of BA and BMA, with 25 wt% acrylate are compared with model predictions in Figure 5.6.

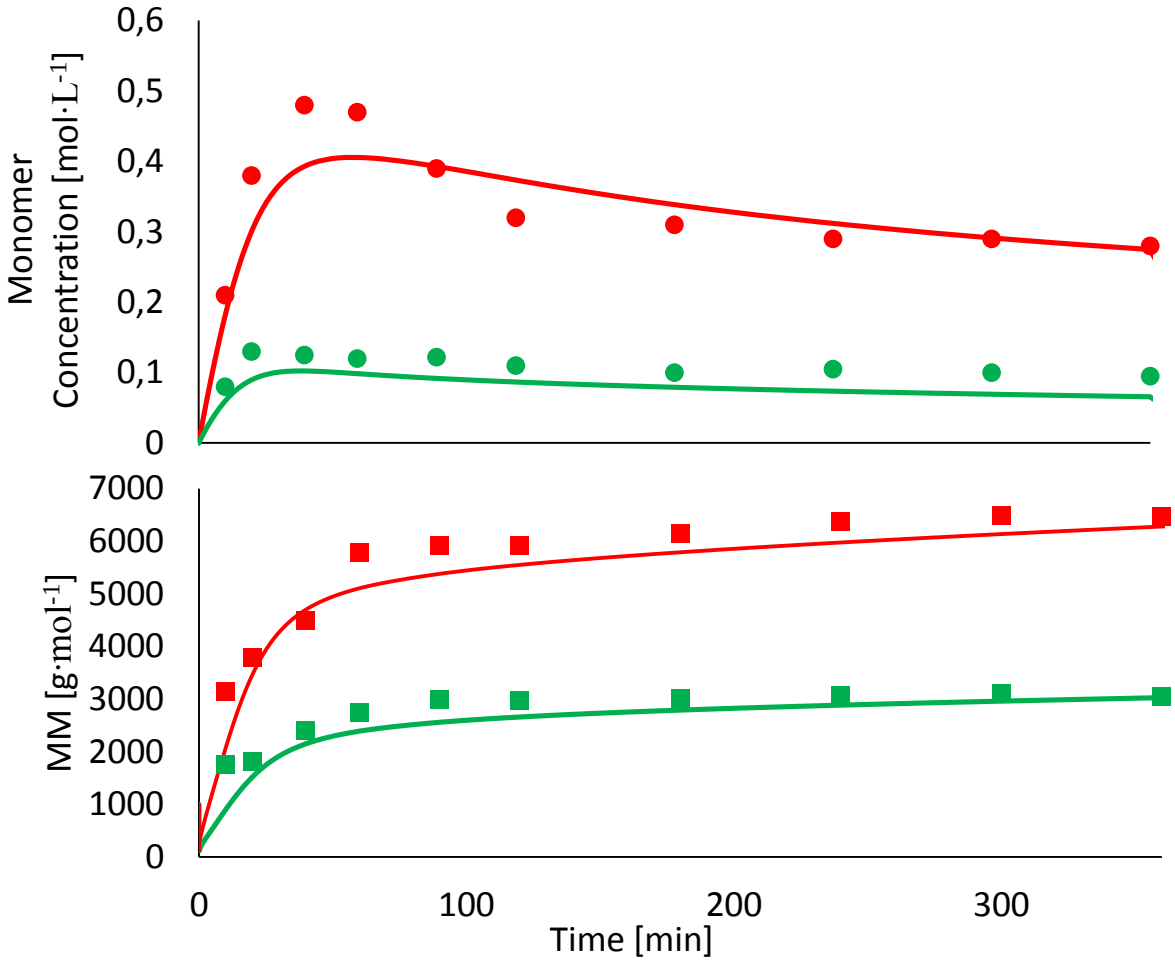

Figure 5.6: Free monomer concentrations (top) for BMA (●) and BA (●) and MM averages (bottom) presented as M_n (■) and M_w (■). Reactions were performed in xylenes at 138°C at a weight ratio of 75/25 wt% for BMA/BA, with modeled results given as lines in the respective color.

Typical semi-batch behaviour is achieved with constantly low and stable monomer concentrations attained after an initial transient state attributed to the time necessary for initiator levels to reach a relatively constant level (initiator feed rate balanced with decomposition rate based on the half-life time).

Consequentially, number and weight average polymer molar masses also stabilize after the initial transient period to produce polymer with constant properties throughout the whole semi-batch experiment. The comparison with model predictions is quite good; as the same model and parameter set successfully described a set of experiments run in 2012 with a slightly different recipe (initiator level), the agreement provides confidence both in the experimental and polymer analyses procedures as well as in the execution of the model in the upgraded PREDICI® version. Therefore, the next step was to replace BA with HEA, to investigate whether the H-bonding influences on copolymerization kinetics found in the small scale low conversion PLP experiments, also manifested itself in the semi-batch process. With the rest of the recipe kept constant, the evolution of polymer MM averages is compared to the BMA/BA base case in Figure 5.7.

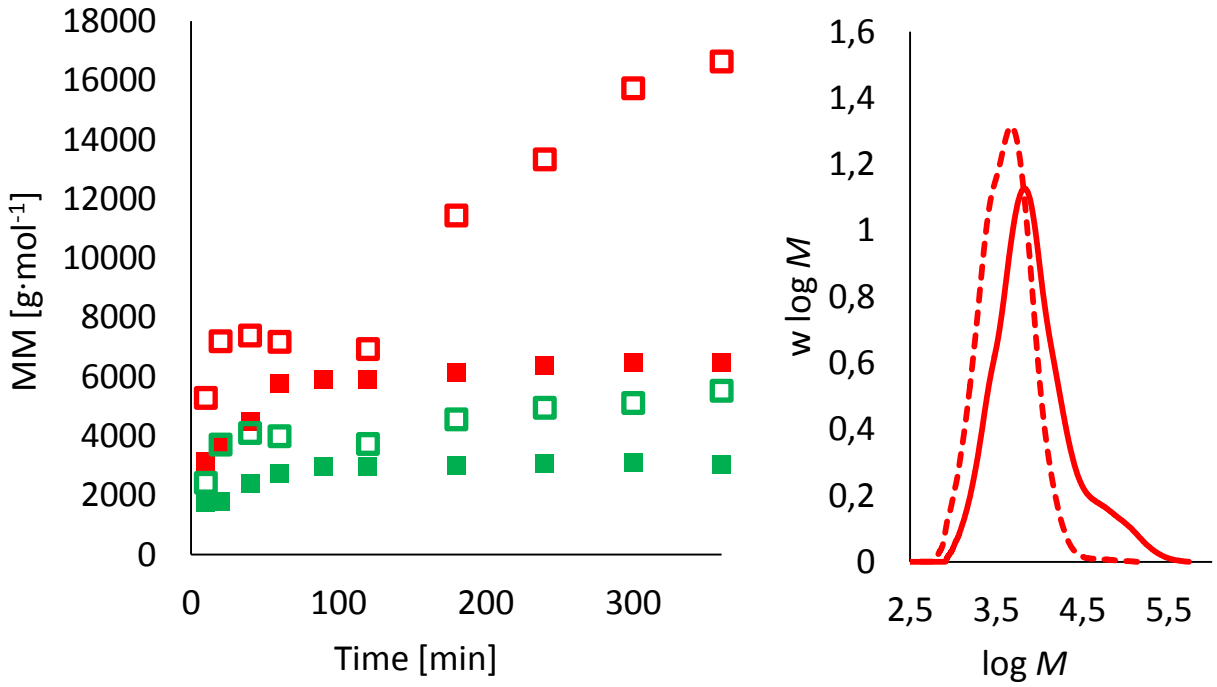

Figure 5.7: Evolution of MM averages and final polymer MMD for the copolymerization of BMA/acrylate in xylenes. The left graph presents M_n (▌) and M_w (▌) for BMA/HEA (□) and BMA/BA (■), whereas the right graph presents the measured MMD for BMA/HEA copolymer samples taken at 90 (- -) and 360 (—) min

A clear disparity between the systems is observed, with a huge increase in both M_n and M_w, values observed for the BMA/HEA copolymerization starting after 100 minutes. At the end of reaction, the M_w for the HEA copolymer is tripled (16600 $g \cdot mol^{-1}$) over the final value for the BA copolymer. Whereas some changes in kinetic behaviour were expected due to the differences in reactivity ratios in favor of HEA incorporation and the increase in k_p^{cop},[29] this very large change in polymer molar masses was surprising. Insight into the result can be obtained by examining the complete MMD of the poly(BMA/HEA) produced in xylenes, also shown in Figure 5.7. From as early as 90 min the development of a high MM tail can be observed that is quite significant in relative size by the end of reaction at 360 min. As the tail stretches to MM values greater than an order of magnitude larger than the main peak of the MMD, it greatly influences the MM averages, and is likely to have a profound effect on the use of these resins in coatings formulations. Formation of similar high MM material was found in the semi-batch copolymerization of HEMA with both styrene and with BMA in xylenes in a previous investigation.[11] At that time it was hypothesized that this high MM fraction was caused by the incorporation and subsequent crosslinking of difunctional impurities – ethylene glycol dimethacrylate (EGDMA) in HEMA and ethylene glycol diacrylate (EGDA) in HEA – present at ppm levels in hydroxyfunctional monomers. (Please refer to Chapter 6 for a detailed analysis of this phenomenon.) In the previous investigations with HEMA the importance of the high MM tail was found to be solvent dependent,[11] but modelling approaches were unable to represent these findings based on standard kinetic behaviour of difunctional monomers.[168] Following the idea of solvent dependency, further experiments were performed in ketones such as MIAK, which serve as a better solvent for HEA containing copolymers due to their polar carbonyl function.[156] As shown in Figure 5.8, no high MM material was formed, even with HEA levels in the copolymer increased to 40 wt%.

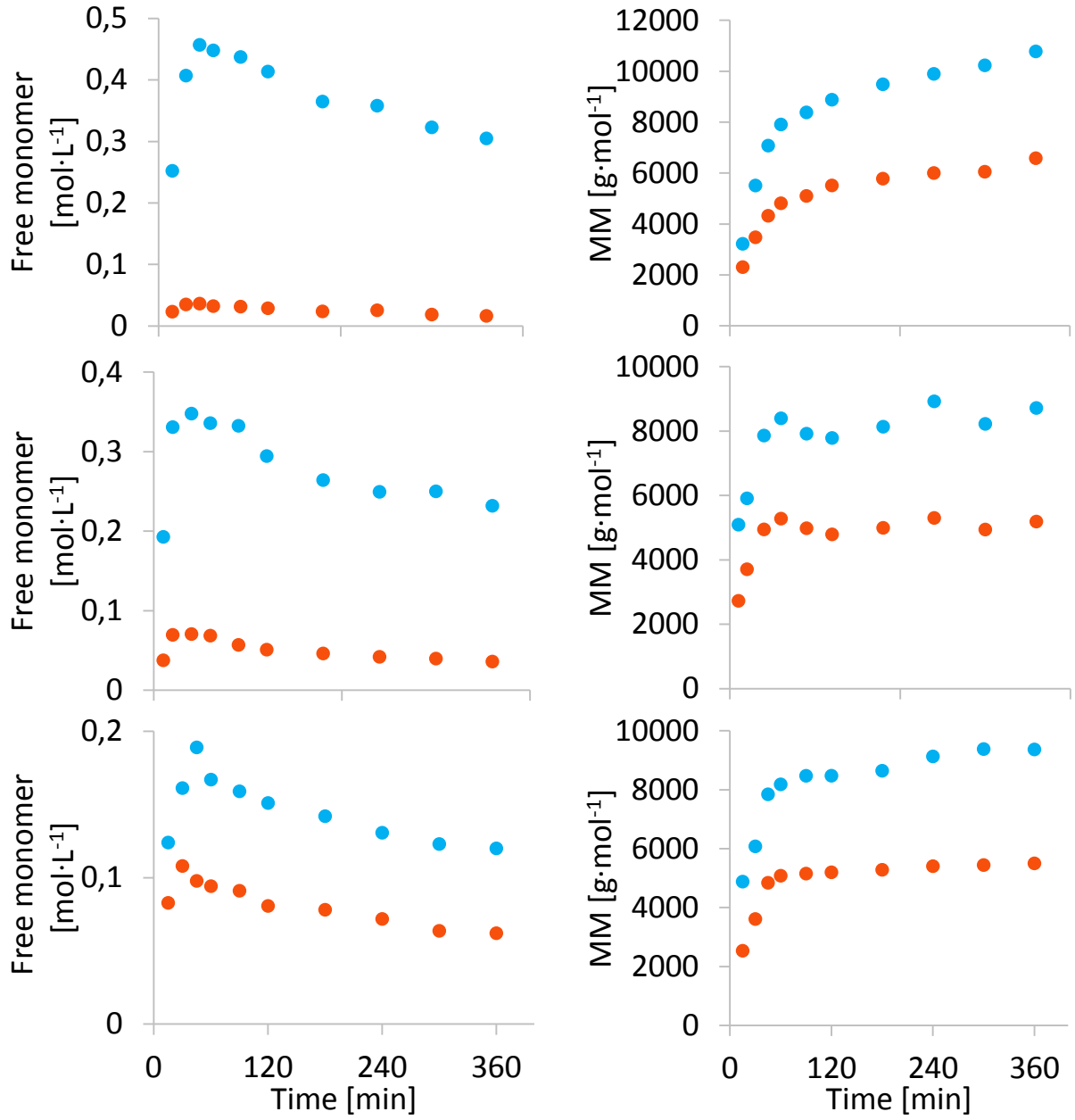

Figure 5.8: Free monomer concentrations for BMA (●) and HEA (●) on the left, and copolymer molar mass averages M_n (●) and M_w (●) on the right for BMA/HEA semi-batch copolymerizations (12.5, 25 and 40 wt% HEA, from top to bottom) in MIAK at 138 °C.

Starting with the more pressing analysis of M_n and M_w, all three copolymerizations with 12.5-40 wt% HEA show typical semi-batch behaviour, with an initial increase during the first 60 min, followed by a quite constant and stable evolution with M_n = 5000-6000 and M_w = 8000-10000 g·mol^{-1} for

all three compositions. In other words, the behaviour is quite similar to that observed for BA/BMA copolymerization in xylenes, with slightly higher MM averages. The differences between the three compositions are small, and there is no evidence of the formation of a high MM tail in the distributions, as was observed in xylenes (see Figure 5.14). Thus, it can be concluded that it is not abnormal polymerization kinetics (or EGDA crosslinking) that causes problems when HEA is selected as a comonomer, rather it is the poor solvency of the copolymer in xylene.

As no issues or dependencies for BMA/HEA copolymerizations in MIAK based on the HEA content are detected, it is possible to fully analyze the trends seen when HEA level is varied in the set of runs, starting with the monomer concentrations. With the increase in k_p^{cop} with increasing acrylate content,[19] total monomer levels ([BMA]+[HEA]) during the stable final semi-batch period were found to decrease from roughly 0.32 to 0.18 mol·L^{-1} as HEA fraction in the feed was increased from 12.5 to 40 wt%.

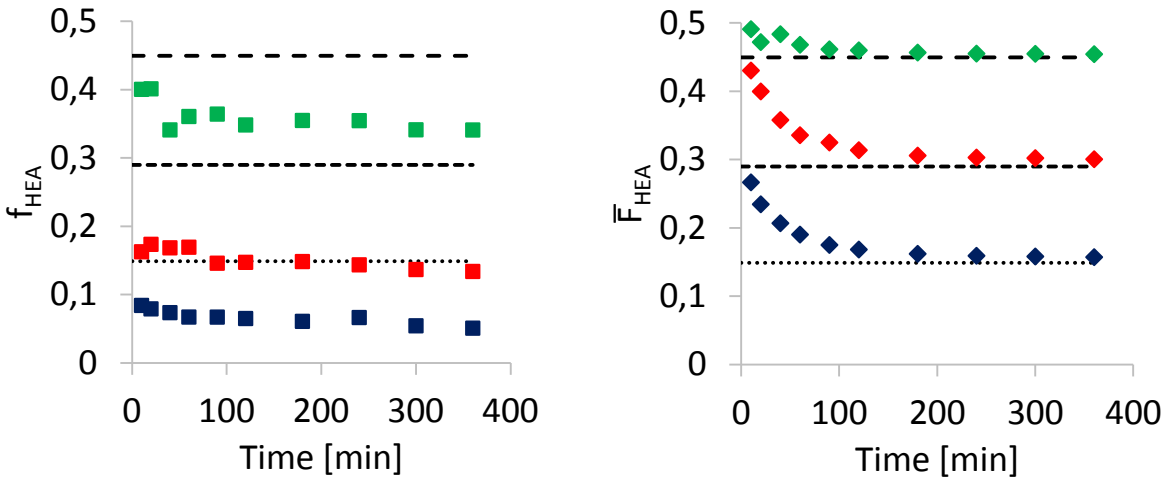

Figure 5.9: Relative molar monomer composition f_{HEA} (■) and copolymer composition F_{HEA} (♦) for BMA/HEA copolymerizations in MIAK with 12.5 ( ), 25 ( ) and 40 wt% HEA ( ), with feed compositions given as lines.

The measured free monomer concentrations are used to calculate values of f_{HEA} (directly from GC measurements of free monomer) and $\bar{F}_{HEA}$ (calculated from monomer mass balances) over the course of

the three reactions, which are compared to the fraction of HEA in the monomer feed (horizontal lines) in Figure 5.9. While the copolymer composition achieves the feed composition after the transient period, as expected under starved-feed operation, the HEA levels in the unreacted comonomer mixture are significantly decreased from the feed composition. This result can be related to two phenomena; depropagation of methacrylate radicals[142,172] and promotion of HEA incorporation through H-bonding.[19,186] Based on the difference between experimental levels with their respective feed composition, it can be concluded that the influence of depropagation plays a larger role under these reaction conditions, as the highest relative discrepancy between feed and reactor monomer composition is obtained for the experiment with 12.5 wt% HEA. Remember, small-scale PLP reactivity ratios suggest that $f_{HEA} \sim F_{HEA}$ for low HEA content comonomer mixtures in ketones (see Figure 3.2), such that the experimental data should be overlapping with the feed composition. (The influence of H-bonding will be further discussed in the direct comparison of BA/BMA with HEA/BMA copolymerizations below.)

Finally, it is interesting to observe from Figure 5.8 that the polymer chains formed during the initial (~90 min) transient period are of lower MM, but contain higher HEA fraction than the bulk of the polymer produced. Simulations have previously shown that it is the lower MM chains that lack functionality due to the stochastic nature of radical copolymerization.[187] However, during the semi-batch reactions, it is also seen that this low MM materials has a higher than average HEA content, therefore reducing the fraction of non-functional low MM material, and improving the uniformity (lowered non-functionalized fraction) of the final product.

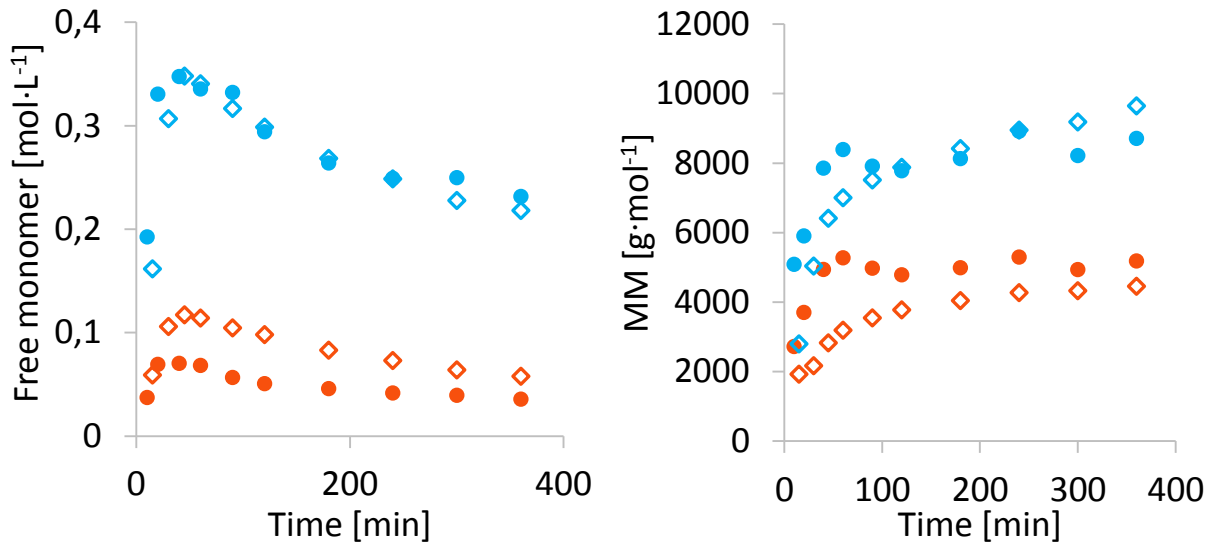

Figure 5.10: Free monomer concentrations for BMA (●)/ HEA (●) and BMA (◊)/ BA(◊) systems on the left, and respective polymer molar mass averages M_n (▌) and M_w (▌) for HEA (●) and BA (◊) semi-batch copolymerizations with BMA (with 25 wt% acrylate) on the right, in MIAK at 138 °C.

The direct comparison between HEA and BA copolymerizations with BMA shown in Figure 5.10 highlights similarities and differences between the systems, both with 25 wt% acrylate. While the BMA/BA run was conducted in xylene and the BMA/HEA in MIAK, the comparison is still useful, as solvent choice has no influence on BMA/BA copolymerization kinetics. As BMA is used in both cases, depropagation kinetics are assumed to be similar such that the differences between BA and HEA free monomer concentrations can be attributed to the enhanced reactivity of HEA influenced by H-bonding. As seen in Figure 5.10, the HEA concentration in the reactor is significantly lower than that of BA due to its higher relative reactivity, even though the BMA concentrations in the two systems are practically identical. Thus, the value of f_{HEA} required to achieve the desired copolymer composition is lower than f_{BA}, in good agreement with the results found in the small-scale PLP experiments,[19] despite the differences in operating temperature, monomer concentrations and conversion levels between the semi-batch and PLP systems. Although these changes are small, they are necessary and important based on a possible industrial mode of operation. Whereas monomer is fed constantly over the 6-hour period, the ratio of inlet

flow to total reaction volume decreases. Therefore, it may be possible for some applications to adjust feed ratios with time to keep monomer concentrations as constant as possible throughout the entire reaction.

A comparison of the evolutions for MM averages indicates that the lowered HEA free monomer (relative to the BA case) has no significant effect on polymer MM. Whereas M_n seems to be slightly lower for the BA copolymerization, there is no difference in the M_w curves. Obviously, the end-use properties of functional BMA/HEA are significantly different than those of BMA/BA; however, the change from BA to HEA does not create a significant difference in target MM, as might be expected from a methacrylate-rich system. These differences in dispersity suggest some minor H-bonding or solvent dependent effects on the relative importance of chain-ending termination or transfer to solvent events (possibly also scission events that follow backbiting), as will be further discussed in the modelling section.

Additional BMA/HEA copolymerizations were performed in 2-heptanone at 138 °C and in MIBK at 120 °C (due to the solvent's reduced boiling point). As the extended set of data (presented in Figure C.1 and Figure C.2) showed similar trends, it can be concluded that the ketones can be categorized alongside with esters like BPi, as one class of solvent, in agreement with the findings from the kinetic PLP-analysis.[19]

5.3.3. BMA/HEA copolymerization model in industrially relevant solvents

With the experimental work performed, the goal is now to verify a modelling framework that captures the described HEA copolymerizations, using the new kinetic parameters determined in Chapters 3 and 4.

5.3.3.1. Model development

The model was developed and modified based on the previously published terpolymerization model for BA/BMA/ST,[28] with ST mole fraction set to zero to represent the acrylate methacrylate

copolymerization systems. The side reactions such as depropagation, backbiting, β-scission and MCR-propagation, are included in the representation, as described in Table 5.1. In addition to the principal reactions shown, both long-chain branching in the reaction of macromonomers (created by chain scission and denoted by U) are also included, as described in the previous work.[28]

Table 5.1: Kinetic mechanisms used to model methacrylate/ acrylate copolymerization, with M representing the methacrylate monomer and A the acrylate

Initiation	$I \xrightarrow{k_d} 2 f_{ini} I^*$	
	$I^* + M \xrightarrow{k_p^M} P_1^M$	$I^* + A \xrightarrow{k_p^A} P_1^A$
Chain propagation and depropagation	$P_n^{MM} + M \underset{p_{MM} k_{dp}^M}{\overset{k_p^M}{\rightleftarrows}} P_{n+1}^{MM}$	$P_n^{AA} + A \xrightarrow{k_p^A} P_{n+1}^{AA}$
	$P_n^{MM} + A \xrightarrow{k_p^{MM-A}} P_{n+1}^{MA}$	$P_n^{AA} + M \xrightarrow{k_p^{AA-M}} P_{n+1}^{AM}$
	$P_n^{AM} + M \underset{p_{MM} k_{dp}^M}{\overset{k_p^{AM-M}}{\rightleftarrows}} P_{n+1}^{MM}$	$P_n^{MA} + M \xrightarrow{k_p^{MA-M}} P_{n+1}^{AM}$
	$P_n^{AM} + A \xrightarrow{k_p^{AM-A}} P_{n+1}^{MA}$	
		$P_n^{MA} + A \xrightarrow{k_p^{MA-A}} P_{n+1}^{AA}$
Transfer to solvent	$P_n^M + Sol \xrightarrow{k_{tr}^{MSol}} D_n^{BMA} + Sol^*$	$P_n^A + Sol \xrightarrow{k_{tr}^{ASol}} D_n^A + Sol^*$
SPR Termination	$P_n^M + P_m^{BMA} \xrightarrow{k_{td}^M} D_n + D_m \quad \vee \xrightarrow{k_{tc}^M} D_{n+m}$	
	$P_n^A + P_m^A \xrightarrow{k_{td}^A} D_n + D_m \quad \vee \xrightarrow{k_{tc}^A} D_{n+m}$	
	$P_n^{MM} + P_m^{AM} \xrightarrow{k_{td}^{MM-AM}} D_n + D_m \quad \vee \xrightarrow{k_{tc}^{MM-AM}} D_{n+m}$	
	$P_n^{MM} + P_m^{AA} \xrightarrow{k_{td}^{MM-AA}} D_n + D_m \quad \vee \xrightarrow{k_{tc}^{MM-AA}} D_{n+m}$	
	$P_n^{MM} + P_m^{MA} \xrightarrow{k_{td}^{MM-MA}} D_n + D_m \quad \vee \xrightarrow{k_{tc}^{MM-MA}} D_{n+m}$	

	$P_n^{AA} + P_m^{AM} \xrightarrow{k_{td}^{AA-AM}} D_n + D_m \quad \vee \xrightarrow{k_{tc}^{AA-AM}} D_{n+m}$
	$P_n^{AA} + P_m^{MA} \xrightarrow{k_{td}^{AA-MA}} D_n + D_m \quad \vee \xrightarrow{k_{tc}^{AA-MA}} D_{n+m}$
	$P_n^{AM} + P_m^{AM} \xrightarrow{k_{td}^{AM-AM}} D_n + D_m \quad \vee \xrightarrow{k_{tc}^{AM-AM}} D_{n+m}$
	$P_n^{AM} + P_m^{MA} \xrightarrow{k_{td}^{AM-MA}} D_n + D_m \quad \vee \xrightarrow{k_{tc}^{AM-MA}} D_{n+m}$
	$P_n^{MA} + P_m^{MA} \xrightarrow{k_{td}^{MA-MA}} D_n + D_m \quad \vee \xrightarrow{k_{tc}^{MA-MA}} D_{n+m}$
Backbiting	$P_n^A \xrightarrow{p_{aa}p_{aa}k_{bb}} Q_n^A \qquad P_n^{AMA} \xrightarrow{0.6 \times p_{am}p_{ma}k_{bb}} Q_n^{AMA}$
Scission	$Q_n^A \xrightarrow{k_s} U_{n-2} + P_2^A \quad \vee \xrightarrow{p_{AA}k_s} P_{n-3}^A + U_3 \quad \vee \xrightarrow{p_{MA}f_M k_s} P_{n-3}^M + U_3$
	$Q_n^{AMA} \xrightarrow{f_M k_s} U_{n-2} + P_2^M \vee \xrightarrow{p_{AA}k_s} P_{n-3}^A + U_3 \vee \xrightarrow{p_{AA}f_M k_s} P_{n-3}^M + U_3$
MCR Termination	$Q_n + Q_m \xrightarrow{k_{td}^{qq}} D_n + D_m \quad \vee \xrightarrow{k_{tc}^{qq}} D_{n+m}$
	$Q_n + P_m \xrightarrow{k_{td}^{pq}} D_n + D_m \quad \vee \xrightarrow{k_{tc}^{pq}} D_{n+m}$
MCR Propagation	$Q_n + A \xrightarrow{k_p^{tert}} P_{n+1}^A \qquad {k_p^{tert}}/{r_{AM}}$
	$Q_n + M \longrightarrow P_{n+1}^M$

* With fractions $p_{aa} = \frac{P^{AA}}{P^{AA} + P^{MA}}$, $p_{mm} = \frac{P^{MM}}{P^{MM} + P^{AM}}$, $p_{am} = \frac{P^{AM}}{P^{MM} + P^{AM}}$

The model uses literature parameters for BMA/BA (Table 5.2) with the following modifications: k_{bb} has been reduced based on measurements described in the previous chapter while k_{tr}^{sol} has been reduced for BPi (and following ketones) compared with published values for xylenes, as the measured MM averages were found to be significantly increased. Activation energies are assumed to be the same for the transfer to solvent reaction, with pre-exponential factors reduced by roughly 40%. Penultimate kinetics are considered by tracking the diad fractions at the chain ends, and termination in the copolymerization system is also modeled by a penultimate treatment, as described in the previous work.[28] Of course, physical properties of solvent such as density and MM also changed.

Table 5.2: Rate coefficients and parameters for BMA/BA copolymerization model in BPi

	Rate Expression	Value at 138°C	Ref
Initiation	$k_d^{TBPA}\ (s^{-1}) = 6.78 \times 10^{15} \exp\left(-\frac{17714}{T/K}\right)\ with\ f = 0.5$	1.32×10^{-3}	[28]
Chain propagation	$k_p^{BMA}\ (L \cdot mol^{-1} \cdot s^{-1}) = 3.80 \times 10^{6} \exp\left(-\frac{2750}{T/K}\right)$	4.69×10^{3}	[28]
	$k_p^{BA}(L \cdot mol^{-1} \cdot s^{-1}) = 1.80 \times 10^{7} \exp\left(-\frac{2074}{T/K}\right)$	1.16×10^{5}	[28]
	$r_{BA} = 0.40;\ r_{BMA} = 1.64$		[28]
	$s_{BA} = 0.43;\ s_{BMA} = 1.98$		[28]
Transfer to solvent	$C_{tr}^{BMA} = 14\ \exp\left(-\frac{4000}{T/K}\right)$	8.3×10^{-4}	This work
	$C_{tr}^{HEA} = 55\ \exp\left(-\frac{4444}{T/K}\right)$	1.11×10^{-3}	
SPR Termination	$k_t^{BMA}\ (L \cdot mol^{-1} \cdot s^{-1}) = 1.10 \times 10^{9} \exp\left(-\frac{1241}{T/K}\right)$	4.89×10^{7}	[28]
	$k_t^{BA}\ (L \cdot mol^{-1} \cdot s^{-1}) = 3.89 \times 10^{9} \exp\left(-\frac{1010}{T/K}\right)$	3.34×10^{8}	
Backbiting	$k_{bb}\ (s^{-1}) = 4.35 \times 10^{7} \exp\left(-\frac{3933}{T/K}\right)$	3.05×10^{3}	This work
Scission	$k_s\ (s^{-1}) = 3.30 \times 10^{9} \exp\left(-\frac{7989}{T/K}\right)$	1.20×10^{1}	[28]
MCR Termination	$k_t^{qq}\ (L \cdot mol^{-1} \cdot s^{-1}) = 5.30 \times 10^{9} \exp\left(-\frac{2357}{T/K}\right)$	1.72×10^{7}	[28]
	$k_t^{pq}\ (L \cdot mol^{-1} \cdot s^{-1}) = \sqrt{\left(k_t^{qq} \times k_t^{cop}\right)}$		
MCR Propagation	$k_p^{tert}\ (L \cdot mol^{-1} \cdot s^{-1}) = 1.2 \times 10^{6} \exp\left(-\frac{3440}{T/K}\right)$	2.79×10^{2}	[28]

Depropagation	$[M]_{eq} = \frac{k_{dp}}{k_p^{BMA}} =$ $\left(1.76 \times 10^6 - 1.37 \times 10^6 \, x_{wp}\right) \exp\left(-\frac{6240}{T/K}\right)$		[28]
Density	$\rho_{BPi}(g \cdot mL^{-1}) = 0.90244 - 1.1126 \times 10^{-3} \, T \, (°C^{-1})$	7.47×10^{-1}	[188]
	$\rho_{BMA}(g \cdot mL^{-1}) = 0.91454 - 9.6400 \times 10^{-4} \, T \, (°C^{-1})$	7.82×10^{-1}	[28]
	$\rho_{BA}(g \cdot mL^{-1}) = 0.91900 - 8.35 \times 10^{-4} \, T \, (°C^{-1})$	9.87×10^{-1}	[28]
	$\rho_{Polymer}(g \cdot mL^{-1}) = 1.19 - 8.07 \times 10^{-4} \, T \, (°C^{-1})$	1.08×10^{0}	[28]

Using respective recipe files in PREDICI®, model predictions for the BMA/BA copolymerizations with 25, 60 and 75 wt% acrylate content are compared to experimental data, both free monomer concentrations and MM averages, in Figure 5.11.

The model does a reasonable performance representing the experimental trends with varying monomer feed compositions. Both acrylate and methacrylate content are represented within experimental error. Trends are even in good agreement for high acrylate contents, with a minor, but typical discrepancy during the initial (and not always experimentally reproducible) transient state. However, the model still captures the methacrylate portion and delivers accurate final monomer concentrations. The same can be said for evolutions of M_n and M_w, with very good conformance for both averages between experimental data and modeled fits.

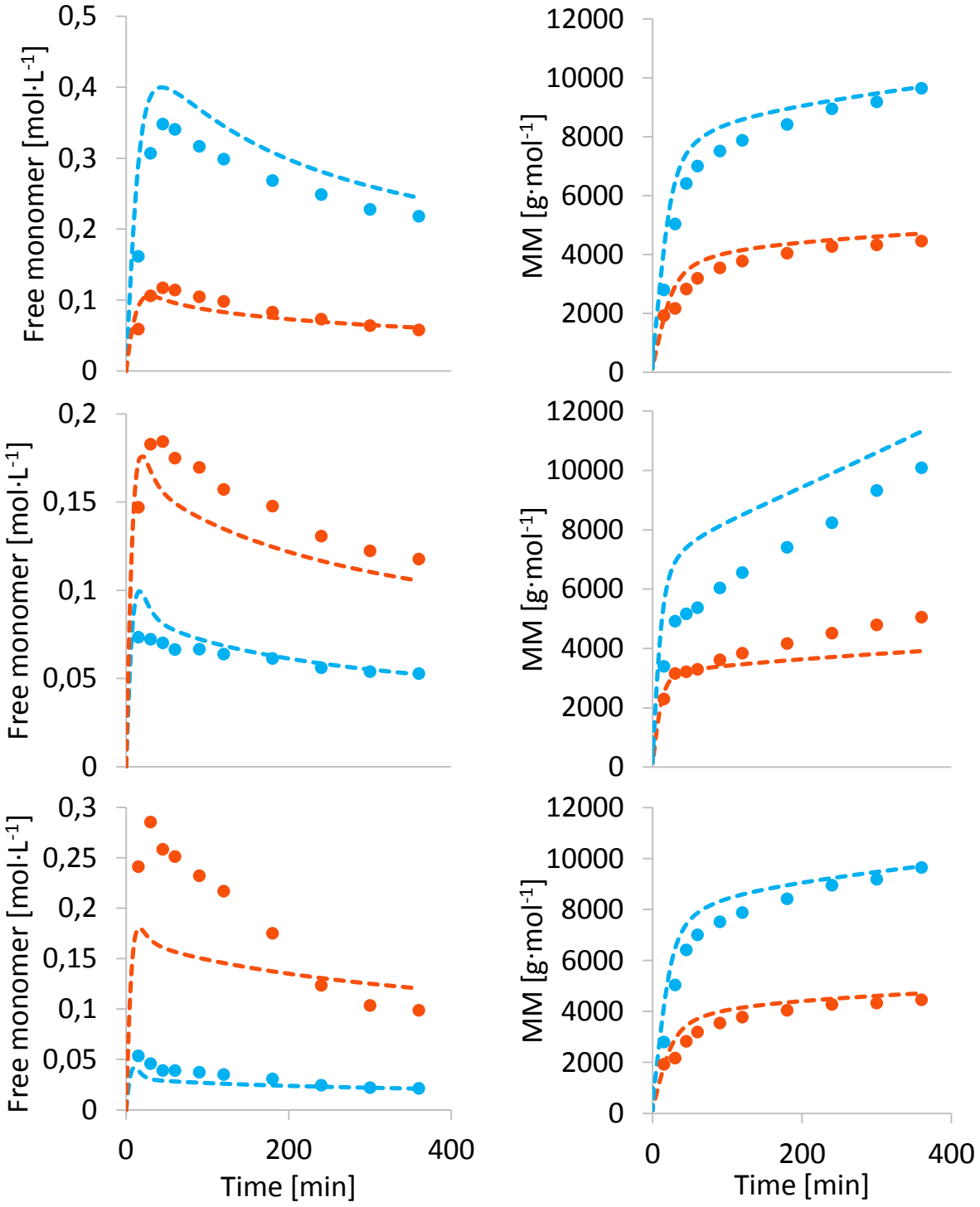

Figure 5.11: Comparison of free monomer concentrations (left) and polymer molar mass averages (right) for experimental data (●) and modelled trends (— —) for BMA/BA semi-batch copolymerizations (25, 60 and 75 wt% BA, from top to bottom) in BPi at 138 °C. Concentrations are shown for BA (▌) and BMA (▌) and MM averages as M_n (▌) and M_w (▌), respectively.

Based on this initial verification of solvent specific parameters (like transfer), model parameters were adjusted for the BMA/HEA copolymerization in MIAK. Transfer coefficients are assumed to be of a similar extent in ketones and esters, which is further supported by the following experiments. Additional changes of physical properties include the adjustment of densities and MM for the new solvent and monomer, MIAK and HEA respectively, as summarized in Table 5.3. Further changes only include propagation reactions involving HEA, as other mechanisms such as termination were assumed to be adequately described by the BA coefficients. The changes to propagation kinetics due to H-bonding and solvent effects present in HEA (co)polymerizations, were set as determined by PLP-SEC studies,[19,27] with HEA homopropagation kinetics taken from the previous investigation[36] that resulted in a 20% increase in k_p at 138 °C over the BA value. In copolymerization with BMA, reactivity ratios were determined to be solvent dependent, leading to the two sets a) and b) shown for in ketones and bulk, respectively. As determined by the kinetic studies,[19] the evolution of k_p^{cop} in all ketones was identical and well-represented by terminal model predictions. Only for bulk values, an IPUE approach was necessary to represent k_p^{cop} adequately.[19] Both cases (bulk and in ketones) will be discussed, as the semi-batch process starts in a solvent rich environment, while final compositions are bulk-like with copolymer rich fractions (of 70 wt%). Rate coefficients are assumed to be independent of monomer concentration, which is important for the initial transient state, as shown in a small preliminary evaluation of PLP samples at higher solvent contents (see Figure C.3). These changes were found to be necessary, to properly represent the influence of H-bonding for such semi-batch reactions.

Table 5.3: List of rate coefficients and parameters changed for BMA/HEA copolymerization model(s) in MIAK

	Rate Expression	Value at 138°C	Ref
Chain propagation	$k_p^{HEA}(L \cdot mol^{-1} \cdot s^{-1}) = 1.72 \times 10^7 \exp\left(-\frac{2018}{T/K}\right)$	1.27×10^5	27
	a) $r_{HEA} = 0.49$; $r_{BMA} = 0.72$ $s_{HEA} = s_{BMA} = 1$		19
	b) $r_{HEA} = 0.37$; $r_{BMA} = 0.98$ $s_{HEA} = 1$; $s_{BMA} = 3.03$		19
Density	$\rho_{MIAK}(g \cdot mL^{-1}) = 0.84070 - 1.0700 \times 10^{-3}\ T\ (°C^{-1})$	6.93×10^{-1}	
	$\rho_{BMA}(g \cdot mL^{-1}) = 0.91454 - 9.6400 \times 10^{-4}\ T\ (°C^{-1})$	7.82×10^{-1}	28
	$\rho_{HEA}(g \cdot mL^{-1}) = 1.1249 - 1.0000 \times 10^{-3}\ T\ (°C^{-1})$	9.87×10^{-1}	
	$\rho_{Polymer}(g \cdot mL^{-1}) = 1.19 - 8.07 \times 10^{-4}\ T\ (°C^{-1})$	1.08×10^0	28

5.3.3.2. Model verification

Summarizing modelling and experimental efforts, agreement between the software based copolymerization model and experimental semi-batch data needs to be found. Based on the designed system, a multitude of properties and data can be modelled in PREDICI®, as shown in Figure 5.12, with a major focus on monomer concentrations, molar mass distributions, copolymer composition, and levels of macromonomer and branching points.

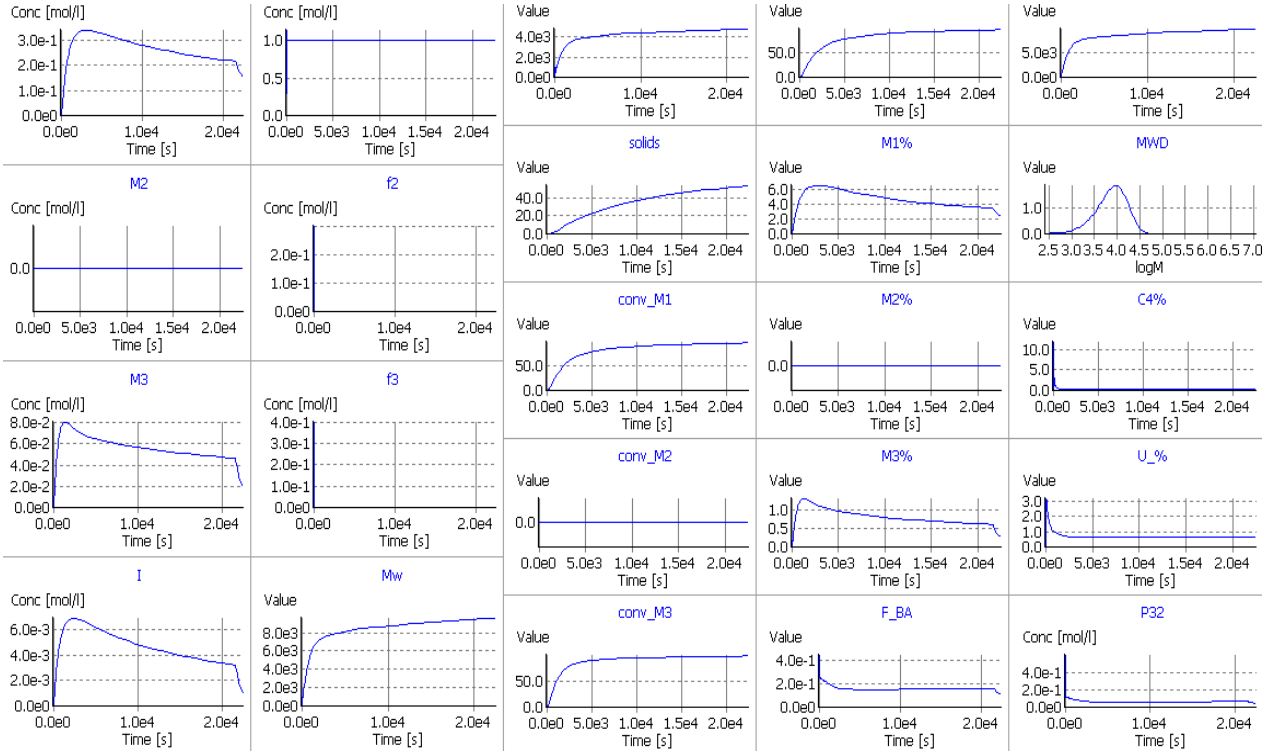

Figure 5.12: Data output of PREDICI® 11 for the described copolymerization model, with information related to concentrations of monomers and initiator, MMD (here MWD), MM averages and fractions of branching points and unsaturated macromonomers

Starting with a summary for three different BMA/HEA copolymerizations in MIAK with 12.5, 25 and 40 wt% HEA, results are given in Figure 5.13, overlaying measured data points and best fit lines, using only terminal model predictions and the reactivity ratios determined for BMA/HEA in ketones.

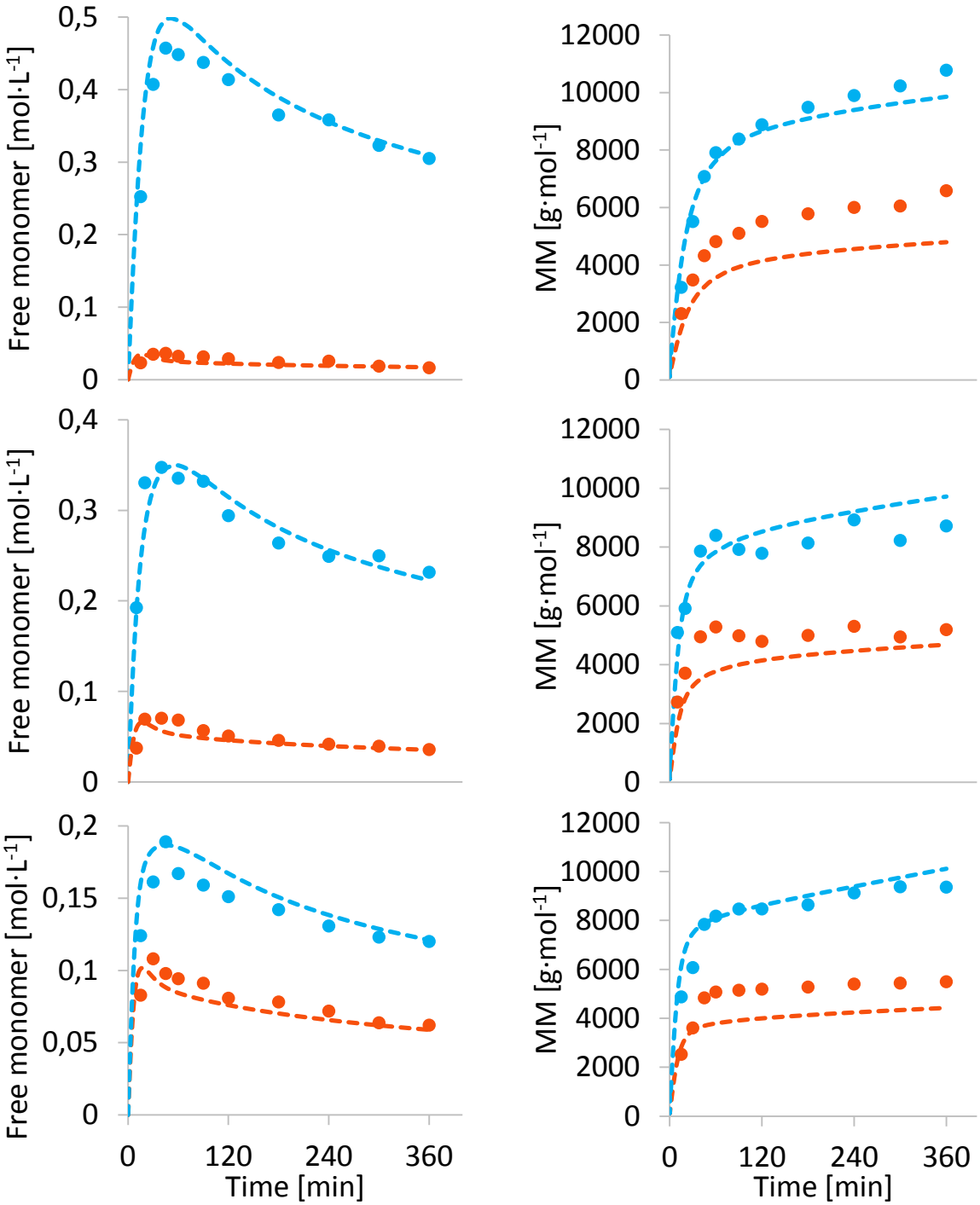

Figure 5.13: Comparison of free monomer concentrations and molar mass averages for experimental data (●) and modelled trends using kinetic parameters determined in ketones (and the terminal model) (— —) for BMA/HEA semi-batch copolymerizations (12.5, 25 and 40 wt% HEA, from top to bottom) in MIAK at 138 °C. Monomer levels are given for the monomers BMA (▮) and HEA (▮)on the left, vs the evolution of M_n (▮) and M_w (▮) on the right

The results show very good agreement between model and experimental data. In terms of free monomer concentrations, only marginal differences are observed during the initial transient state. For the continuing reaction time, each comonomer concentration is effectively represented by the prediction, allowing good estimates for both the total monomer concentration but also the relative monomer fractions in solution. Hence, both previously determined reactivity ratios and k_p^{cop} representations measured at low conversions provide a good description of copolymerization under semi-batch conditions at high temperatures. The same can be said for the evolution of MM averages: M_w is very well represented for all compositions, while M_n is underpredicted by the model. The reduced dispersity possibly suggests an increased importance of termination by combination. For industrial application M_w is one of the target parameters to meet projected coating properties and applications. The lower dispersity, not fully captured by the model, is beneficial from a product perspective; the more uniform distribution reduces the fraction of low molar mass chains, which are more likely to contain reduced or no functionality,[187] which is more crucial for recipes with low HEA contents. As PREDICI® not only calculates molar mass averages using the method of moments procedure,[41] but also approximates the entire distribution, it is possible to directly compare predicted and experimental polymer MMDs, as shown in Figure 5.14.

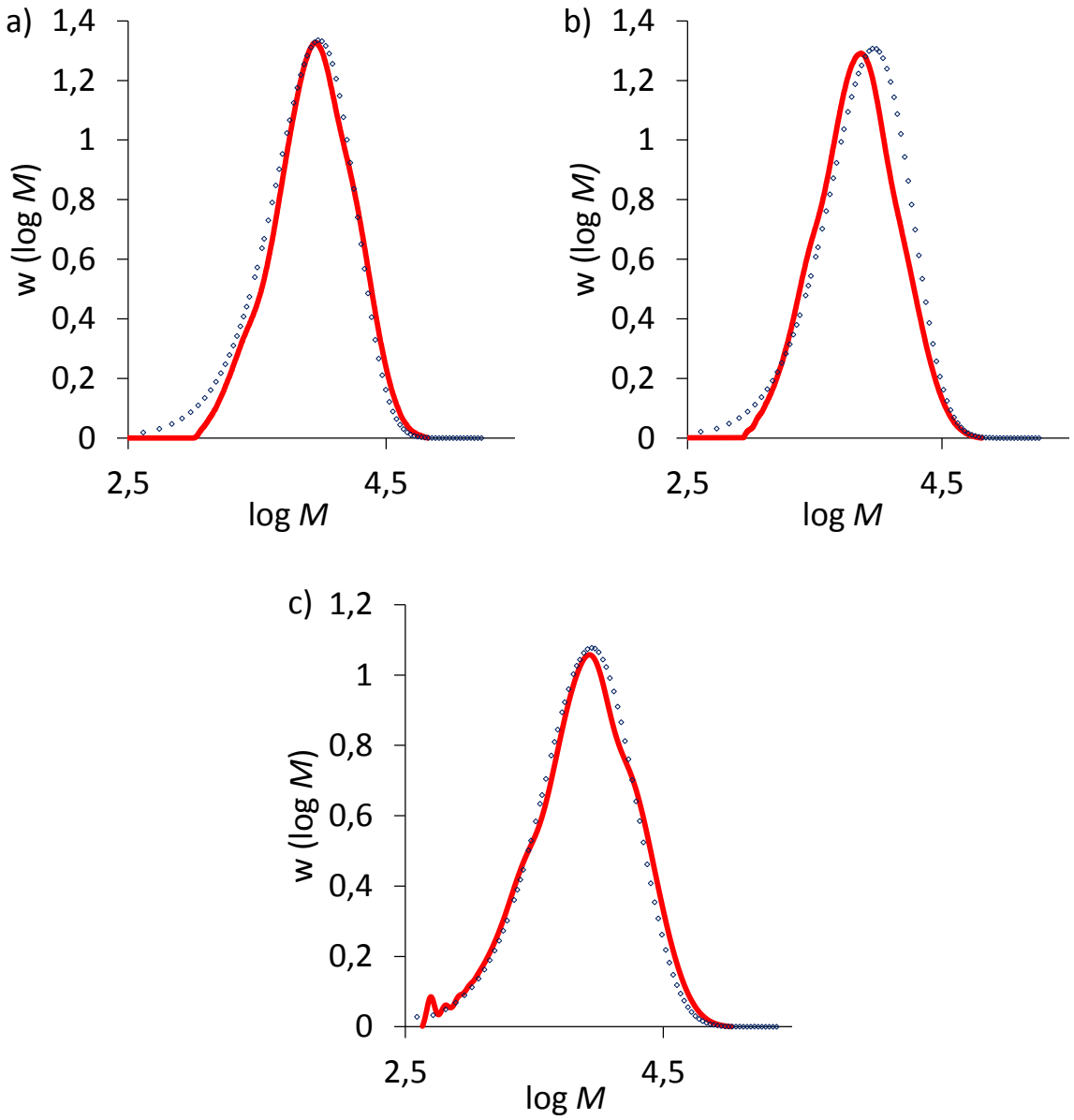

Figure 5.14: MMD of final copolymer produced from BMA/HEA (with 12.5, 25 and 40 wt% HEA, plots a), b) and c) respectively) semi-batch copolymerizations in MIAK; results are given for experimental (—) and modelled (●●) data

The overlay of experimentally determined distributions and their respective predictions show very good agreement, with minimal mismatch at the low and high MM portions of the distribution; the mismatch at the low end explains the minor differences in predicted M_n values. The excellent representation of the entire MMD as well as the good agreement between M_n and M_w values validates the

model in terms of the usage and interpretation of side reactions, including backbiting followed by scission or the formation of a branching point. Both side reactions significantly affect the shape of MMD: backbiting inhibits chain growth through the formation of MCRs that react at a reduced rate[49,163] (thus reducing the polymer MM averages) to form a branchpoint, while further reaction of macromonomers produced by MCR scission contributes to an increased high MM shoulder.[162] Both phenomena also add a small factor of uncertainty to interpretation of the experimental SEC traces including the use of KMH parameters to obtain absolute MMDs. Such parameters are generally valid for linear polymer chains while losing accuracy for highly branched and brushed copolymer. However, as shown in Figure 5.15, final branching levels in these methacrylate rich recipes are particularly low (as well as scission byproducts, as shown in Figure C.4). The predicted branching level around 0.5 % is particularly low and was found to be within the detection limits of the quantitative ^{13}C-NMR technique. The additional presence of overlapping peaks, as described in chapter 4, made an experimental verification for these samples impossible.

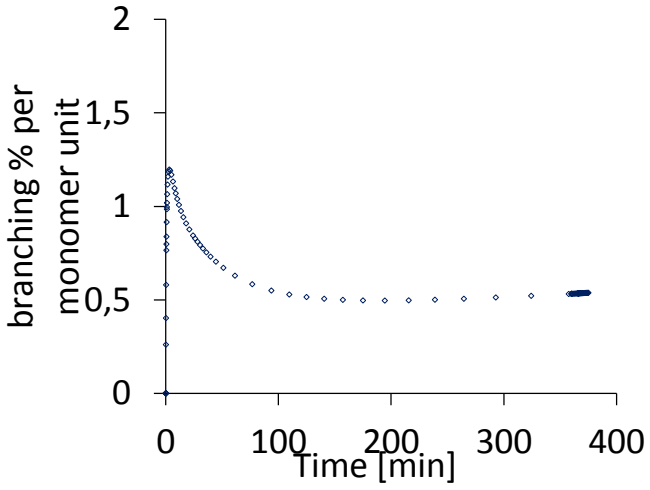

Figure 5.15: Predicted data (●●) for branching points present in the copolymer, for BMA/HEA (25 wt% HEA) copolymerizations in MIAK

Summarized, the existing model structure, combined with HEA-BMA propagation kinetics determined by PLP-SEC under low-conversion conditions, adequately represents H-bonding effects under semi-batch conditions. However, as discussed earlier, the final reaction conditions in the semi-batch systems are shifted towards a polymer rich environment. Based on the PLP investigations of BMA/HEA

in bulk, combined with the analysis of the in situ NMR batch data, it is likely that relative reactivity ratios are changing over the course of the reaction and perhaps require IPUE treatment to represent k_p^{cop}.[19] Therefore, additional simulations were conducted using the published r- and s-values for BMA/HEA in bulk (parameter set b) in Table 5.3). Whereas the effect of this change on simulated polymer MM averages was found to be negligible, the effect on predicted monomer concentrations was more notable, as shown in Figure 5.16, with slightly higher residual HEA concentrations predicted using the kinetic coefficients measured in bulk. The simpler terminal model approach is more than sufficient, and perhaps even slightly superior, in representing the experimental data.

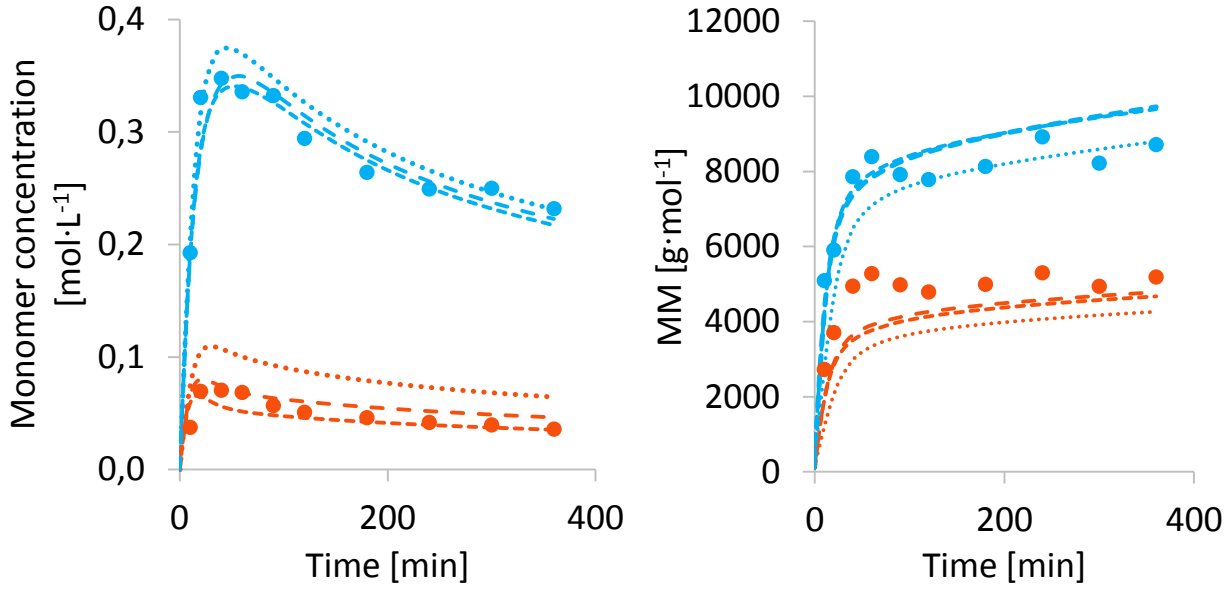

Figure 5.16: Free monomer concentrations (left) and polymer MM averages (right) comparing experimental data (●) to modelled trends (lines) for the BMA/HEA semi-batch copolymerization (25 wt% HEA) in MIAK at 138 °C. Monomer levels are given for the monomers BMA (▌) and HEA (▌) with three parameter sets to describe chain-growth kinetics: terminal model kinetics for BMA/HEA (--) in ketones, IPUE kinetics from BMA/HEA in bulk (- -) and IPUE kinetics for BA/BMA in bulk (···)

Subsequently, a final comparison was performed by comparing the experimental data with predictions using the reactivity ratios and s-values for BMA/BA (rather than BMA/HEA) copolymerizations,[127] as previously used in the terpolymerization model.[28] As also shown in Figure 5.16,

monomer concentrations were not as well represented, with predicted levels higher than measured experimentally, especially for HEA. The effect on MM averages was not as pronounced; however, both M_n and M_w are underestimated in comparison to the functional modeling approaches. These differences indicate that the new kinetic parameters for hydroxyl functional monomers can be used in the generalized modelling framework to describe an excellent representation of HEA/BMA copolymerizations.

5.4. Conclusions and future work

The goal of this work was to validate the application of small-scale PLP derived kinetic coefficients in a comprehensive kinetic copolymerization model to describe the semi-batch reaction of BMA and HEA in industrially relevant solvents. Experimental and modelled data were found to be in very good agreement for HEA contents up to 40 wt%, proving the correctness of inserting the HEA/BMA rate coefficients (as influenced by H-bonding) into the previous terpolymerization model,[28] at least for methacrylate rich recipes. The rate coefficient for acrylate backbiting was updated, although its influence is minor due to the higher fraction of methacrylate radicals under the range of HEA fractions that could be studied, limited by the solubility of the polar copolymer at higher HEA contents in these solvents. Future work includes the verification of model predictions in HEA terpolymerizations, as the current model retains the structure required to include ST as a third monomer. The propagation kinetics for ST/HEA in bulk has been studied,[27] such that the only effort required is to conduct the semi-batch terpolymerizations at selected conditions to compare to model predictions. As many industrial recipes include even more than three components to tune desired coating performance parameters such as glass transition temperature, extensions to a BA/BMA/HEA/HEMA model are also possible to meet the need for a flexible prediction tool, for both non- and functional (meth-)acrylates.

It would also be interesting to take advantage of the Monte-Carlo hybrid modelling capabilities of PREDICI® 11 to study structure-property related effects. Examples include tracking the population of branchpoints (related to polymer rheological properties) or non-functional chains (important for

postmodification reactions) as a function of chain lengths. While functional group distribution has been investigated in PREDICI® 11 using a simple scheme to describe BMA copolymerization with glycidyl methacrylate,[187] extension to the complex kinetic scheme (with multiple radical and polymer distributions) required to represent conditions of industrial interest, must be developed.

6. Perils and optimization approaches for hydroxyl functional monomers in industrial scale operations

6.1. Introduction

There have been significant efforts in our research group to develop an improved understanding and to develop models to represent the production of functional acrylic copolymers used in automotive coatings formulations dating back over a decade.[11,28,142] As cross-linkable functional groups used in industry include both epoxide and hydroxyl functionalities, we have studied first GMA and then HEMA and HEA.[11,19,51,75] As discussed throughout this thesis, there are significant kinetic complications that arise from the introduction of H-bonding.[19,29,153,186] Whereas the required catalogue of kinetic data and rate coefficients continues to expand, including methoxy and amine functionalities,[53,129,29] there are issues that remain in synthesis and processing due to the increased importance of polar interactions, for example between copolymer and solvent during the changing conditions of semi-batch polymer production. Feedstock quality also emerged as a potential issue, due to the presence of difunctional impurities that act as crosslinkers, such as EGDA or EGDMA: abnormal and unexpected high molar mass tails were found when producing HEA- or HEMA- containing copolymers under well controlled semi-batch operation,[11] a source for high viscosity and deteriorated viscoelastic properties of the acrylic resin product. As the difunctional impurities were present at very low (ppm) levels, modelling approaches combined with reasonable kinetic coefficients were unable to represent the huge increases in MM.[154] To complicate the matter further, experimental results suggested that the unexplained behaviour is solvent dependent.[11] Due to its industrial importance, the topic is revisited in this chapter, systematically studying this issue based on monomer choice and solvent influences by conducting a series of small scale batch and semi-batch experiments. Furthermore, with the help of previously published kinetic data,[11] the results are interpreted using a simplified modelling approach.

6.2. Experimental

6.2.1. Materials

Butyl methacrylate (99 %, Sigma), butyl acrylate (≥99 %, Sigma), 2-hydroxylethyl methacrylate (97 %, Sigma), 2-hydroxyethyl acrylate (96 %, Sigma), ethylene glycol dimethacrylate (98 %, Sigma), ethylene glycol diacrylate (90 % Sigma), 2,2-azobis(2-methylbutyronitrile) (Vazo-67, +99%, DuPont), *tert*-butyl peracetate (50 wt% in mineral spirits, Sigma), xylenes (>99%. Fisher Scientific), methyl isobutyl ketone (≥98.5 %, Sigma), 5-methyl-2-hexanone (99 %, Sigma), 2-heptanone (99 %, Sigma) and butyl propionate (99 %, Sigma) were used as received without further purification.

6.2.2. Experimental and analytical procedures

Experimental procedures were as described previously. Small scale batch experiments follow the same procedure as described in Chapter 4, and semi-batch reactions as described in Chapters 4 and 5, with specific reaction conditions and recipe details provided with the figures summarizing the experimental results. Post-reaction analyses using GC and SEC also followed the procedures described in the previous chapters.

6.3. Results and discussion

6.3.1. The influence of difunctional impurities on HEA and HEMA copolymerizations

With previous results in mind,[11] a series of small-scale batch experiments for BA and BMA polymerizations were performed with purposely spiked amounts of diacrylate and dimethacrylate monomers, EGDA and EGDMA, respectively, to represent the impurities present in both HEA and HEMA. Initial experiments were performed at levels of 100 ppm, based on the total reaction mass including the solvent, as this level is slightly higher than the concentrations in commercial hydroxyfunctional monomers, reported by the supplier Sigma-Aldrich. Xylenes were chosen as the first

solvent studied, due to the increases in MM found during the semi-batch reactions in xylenes presented in Chapter 5. Reaction times were kept constant at 30 minutes to allow for a good comparison of trials using the same monomer. Monomer conversions were found to be constantly around 80 % for acrylate and 30 % for methacrylate polymerizations, irrespective of the amount of di(meth)acrylate added. A bigger focus was made on the polymer MMDs, as shown in Figure 6.1 (and respective averages given in Table D.1 and following), to investigate for any observable high molar mass tails of the distribution.

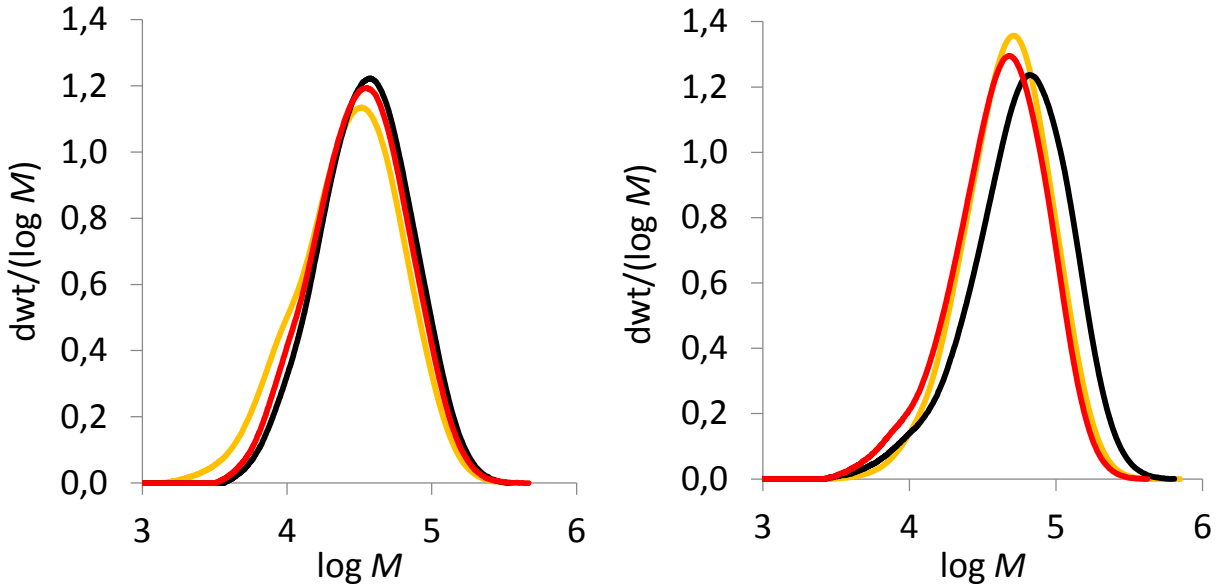

Figure 6.1: Polymer MMDs after 30 min batch reactions of BA (left) and BMA (right) (—) in 75 v% xylenes compared to runs performed with 100 ppm of added EGDMA (—) and EGDA (—).

It was found that neither the addition of EGDA nor EGDMA had an influence on either BA and BMA homopolymerizations, as the shape and position of all distributions are more or less overlapping, with perhaps a slight shift to the right for the BMA experiment with added EGDMA. However, it is seen that the whole distribution shifts, with no observable tails at higher MM, and hence no significant change in dispersity. For the BA homopolymerizations, this result is in agreement with what was previously reported,[11] i.e, that the presence of low concentrations of crosslinker does not influence polymer MMDs. However, the new results for BMA contradict what was reported in the earlier study. In an extensive set

of additional experiments (shown in Table D.1-Table D.3) conducted in MIBK as well as xylenes with up to 500 ppm impurity levels, it was verified that the addition of difunctional monomer did not influence the final MMD produced in this batch system.

As there were no effects seen in these classic systems, the possibility remains that the combination of impurities and H-bonding effects causes an increased incorporation of the crosslinker leading to a high MM tail in the distribution. Thus, batch BA/HEA and BMA/HEMA copolymerization reactions were also performed with up to 40 v% hydroxyfunctional monomer (as limited by phase separation). An example for MMDs in MIBK is given Figure 6.2 with a complete list of results presented in Table D.1-Table D.3.

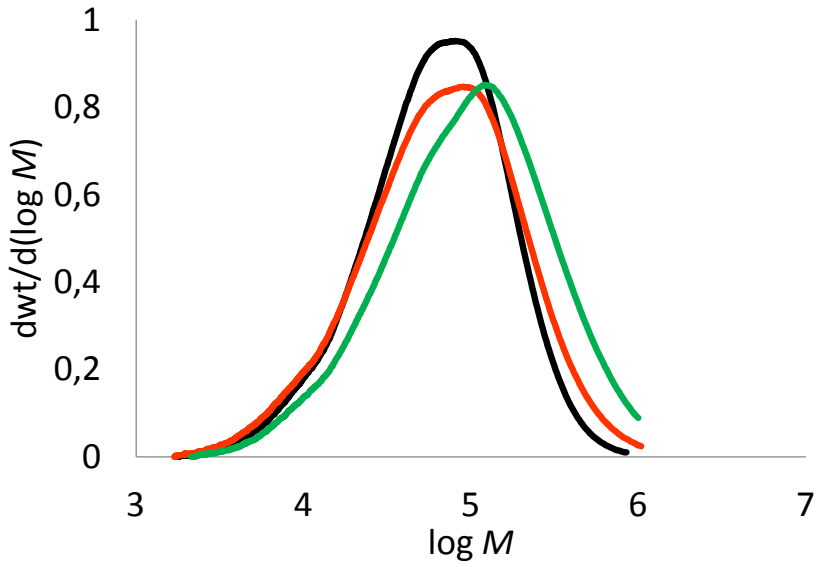

Figure 6.2: Polymer MMDs for small-scale batch polymerization experiments of BA (▌) and BA/HEA (with 25 (▌) and 40 (▌) v% HEA) in MIBK, synthesized at 80 °C with 10 mmol·L^{-1} Vazo-67 as the initiator

No significant broadening of the distribution or tailing was observed in any of the solvents studied, with stable ratios of M_w and M_n. Therefore, it can be concluded that the incorporation of impurities and H-bonding effects are not responsible for the formation of high MM material in a batch reaction system. Thus, the phenomenon may be specific to semi-batch operation, as the significantly

decreased free monomer levels in such systems are known to have significant effects on side reactions, such as backbiting,[28,143] that lead to the formation of the high MM material. Thus, a series of difunctional spiked semi-batch reactions were also performed. To simplify the investigation only EGDMA was investigated from now on, as its influence was found to be more significant previously,[3] and as the methacrylate double-bonds are more reactive during copolymerization in comparison to the acrylate analogue. However, even with 1000 ppm of EGDMA relative to added BMA, no difference in the evolutions of MM averages or the final product MMD for the final product was seen compared to a standard BMA homopolymerization, as shown in Figure 6.3.

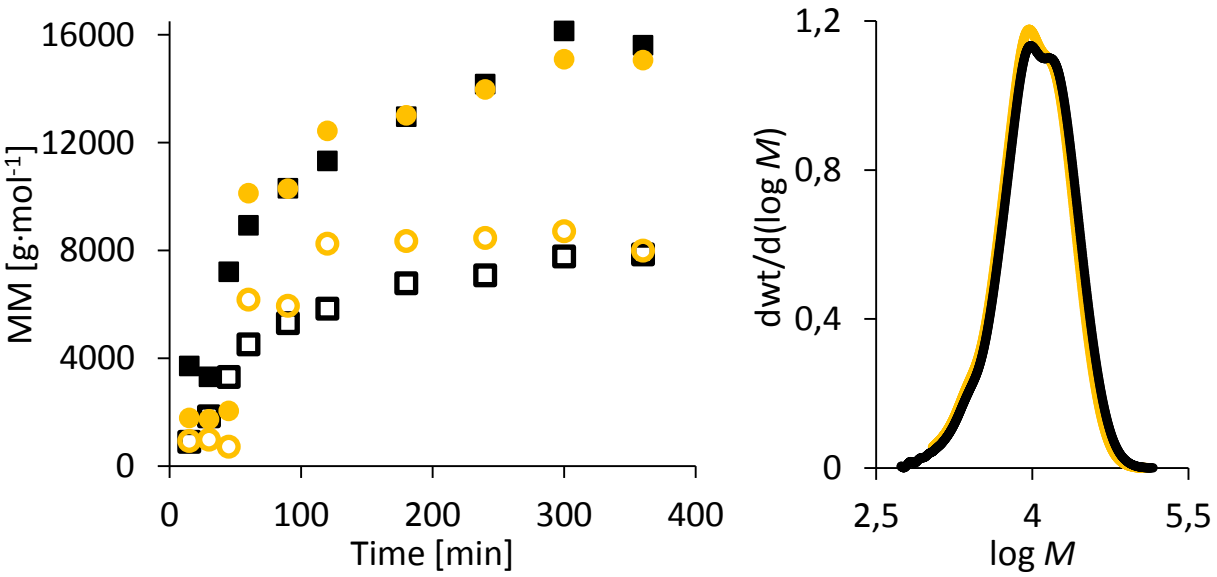

Figure 6.3: Evolution of M_n (○, □) and M_w (●, ■) (left) and the final MMD at 360 min for non-spiked ( )and spiked (, 1000 ppm EGDMA) BMA semi-batch homopolymerizations at 138 °C in BPi

These results contradict those previously published, for which an addition of 100 ppm EGDMA caused a quite significant increase in polymer molar masses.[11] While the current results indicate that variable levels of di(meth)acrylate levels in monomer feedstocks should have no significant influence on product quality and properties, the question remains how to interpret the previously published results. Some direction for resolving the discrepancy is found by examining the results in Chapter 5 that compare BMA/HEA copolymerizations in xylenes and ketones. The initial experiments in xylene (Figure 5.7) also

showed the formation of high MM tails in the product MMD distribution that fully vanished when solvent was switched to various ketones or BPi. As it appears that the phenomenon is solvent dependent, further experiments were performed for the BMA/HEMA system (25 wt% HEMA) in MIAK, 2-heptanone, and xylenes. The evolutions of the MM averages are shown in Figure 6.4; all products had final M_w values around 14000 g·mol^{-1}, comparable to results (of 15000 g·mol^{-1}) shown in Figure 6.3 and clearly below the previously published value of 25500 g·mol^{-1} for BMA/HEMA in xylenes.[11]

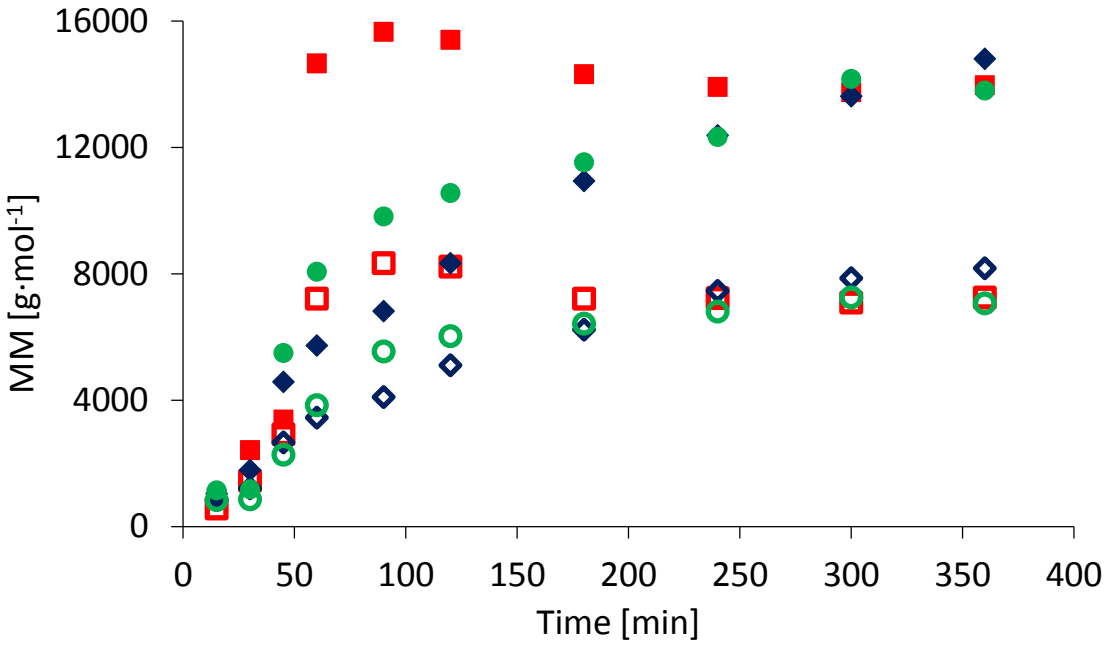

Figure 6.4: Evolution of M_n (○, ◊, □) and M_w (●, ♦, ■) for BMA/HEMA (25 w% HEMA) copolymers produced by semi-batch reactions in xylenes (▌), 2-heptanone (▌) and MIAK(▌) at 138 °C

Some differences are seen in the initial stages of the polymerizations, which may be related to the solubility of the polar copolymer in the solvents. It was observed for both xylenes and the linear ketone 2-heptanone that the solution became slightly opaque during the initial 90 min of reaction, indicating a reduced solubility of the formed copolymer in these solvents. Although, the solutions turned clear again with the increasing polymer content in the system, it may be that poor solvent/polymer compatibility is the reason behind the formation of high MM material under some (and not always reproducible)

conditions. In particular, the use of the less polar xylenes solvents is not recommended for the synthesis of copolymers containing hydroxyfunctional monomer (refer to Table D.4 for more details.)

Whereas many reactions pose no challenge in terms of homogeneity in a lab-scale assuming perfect mixing, industrial scale operations, especially for polymer production, must consider the issue of fouling.[189–191] Obviously, the solubility of a polar copolymer becomes a factor, as can be seen by comparing polymer Hansen solubility parameters to, for example, those of non-polar aromatics such as toluene or xylenes and solvents like ketones and esters.[156,192] For the latter, the polar and H-bonding contributions are significantly increased, facilitating the solubility of more polar copolymers containing HEA or HEMA. Therefore, it is not a real surprise that both esters and ketones provide better performance for the discussed copolymerizations. This fact becomes even more important because to the increased affinity of HEA and HEMA with polar surfaces, such as glass, as has been repeatedly observed in this investigation during small scale PLP experiments for monomer mixtures with high HEA contents: residual polymer often adhered to the cuvette walls. As pointed out in Table D.4, the only difference between the semi-batch runs in xylenes was the reactor vessel. Previous reactions,[11] including the BMA/HEA copolymerizations described in Chapter 5, were performed in a slightly larger reactor, such that the reaction volume was roughly 30 % higher, whereas the agitator and rotation speed remained constant. Although the vessel is still considered as "well-mixed" in terms of reaction kinetics, the slight change may have played a role in promoting some sort of formation of a polymer-rich phase, perhaps near the reactor wall, that led to the appearance of the observed high MM tails on the distributions when HEMA is copolymerized in a poorer solvent such as xylenes. In addition to ensuring adequate mixing and utilization of better solvents such as ketones, operation under reflux conditions, as commonly practiced in industry to aid with heat removal during the exothermic polymerization process, may also help prevent fouling: the evaporating solvent adds a second source of agitation to the system, while the condensed solvent continuously wets the reactor walls to reduce the probability of fouling.

6.3.2. Acrylate rich copolymerization of BA and HEMA: An experimental investigation and modelling approach

6.3.2.1. BA/HEMA semi-batch reactions in BPi

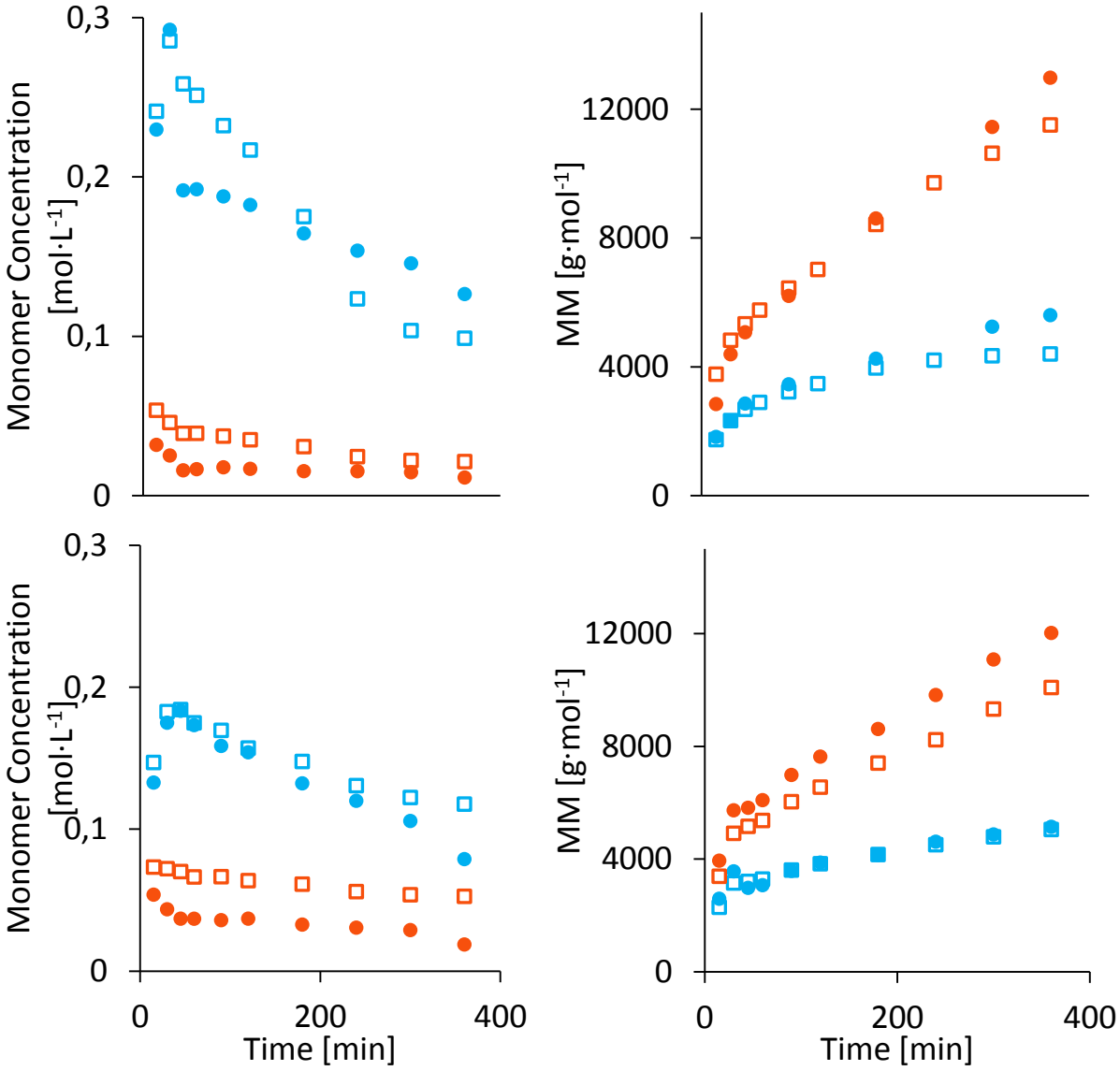

Figure 6.5: Free monomer concentration profiles for BA (□, ●), BMA (□) and HEMA (●) on the left and polymer molar mass averages M_n (▌) and M_w (▌) on the right, for BA/HEMA (●) and BA/BMA (□) semi-batch copolymerizations (25 and 40 wt% methacrylate, from top to bottom) in BPi at 138 °C

Ketones and esters have been shown to be more suitable solvents for hydroxyl functional copolymerizations due to their improved interactions of their more polar nature. To finalize the investigations of the copolymerizations of HEA and HEMA with BA and BMA, a small set of BA/HEMA copolymerizations was performed in BPi, to validate previously observed trends and results. With the hydroxyl functional group now connected to the methacrylate, a significantly increased relative incorporation of the functional monomer is expected due to H-bonding[11] and the methacrylate nature of HEMA in a copolymerization with BA. With this increased relative incorporation, the limiting HEMA fraction was found to be 40 wt%, based on the observation of a slightly turbid initial solution during the first 60 minutes of reaction. Experiments performed with both 25 and 40 wt% HEMA are compared to the respective BA/BMA reactions in Figure 6.5.

The replacement of BMA with HEMA results in a more reactive copolymerization system, which can be seen by the slightly lower concentrations of HEMA compared to BMA at both methacrylate levels, with BA concentration profiles remaining similar (within expected experimental variation, see Chapter 4). In agreement with the previous investigation,[11] the HEMA concentrations were as much as 50% lower in comparison to BMA with 40 wt% methacrylate content. Again, this result is in good agreement with the previously reported higher reactivity ratios of HEMA vs. BA in bulk (with $r_{HEMA} = 5.54$ and $r_{BA} = 0.18$)[11] in comparison to BMA vs. BA (with $r_{BMA} = 2.28$ and $r_{BA} = 0.40$).[119] Accordingly, the methacrylate fractions in the unreacted comonomer mixture are significantly decreased for HEMA vs. BMA (see Figure D.1), whereas both system exhibit reasonable evidence of depropagation influences[142] in comparison to terminal model predictions.

Taking a look at the polymer properties, similar evolutions were obtained for both M_n and M_w when comparing HEMA with BMA copolymerizations: runs containing 25 wt% methacrylate were almost indistinguishable, and the 40 wt% HEMA run may exhibit a small increase in M_w relative to the BMA experiment while M_n remains constant. As the evolutions of the polymer MM averages are similar, it can be assumed that the general kinetic mechanisms are comparable, causing the increases seen in the MM averages for BA/BMA and BA/HEMA to the same extent consistent with an acrylate-rich copolymer

system. Similar behaviour was observed in the acrylate only experiments in Chapter 4, when replacing or increasing the HEA content in copolymerization with BA. Thus, it will be interesting to determine what changes, if any, are required to apply the model previously developed for BA/BMA to represent the BA/HEMA system, as was done for BA/BMA vs HEA/BMA in the previous chapter.

6.3.2.2. Modelling approach for BA/HEMA copolymerizations

The copolymerization model for BMA/BA in BPi, as discussed in Chapter 5 was used as the starting point, followed with the replacement of BMA physical parameters being replaced by HEMA: ρ_{mon} ($kg \cdot L^{-1}$) was changed from $0.901 - 8.35 \times 10^{-4}$ T to $1.092 - 9.80 \times 10^{-4}$ T and MM_{mon} from 142.2 to 130.1 $g \cdot mol^{-1}$. Based on the similarities between the experimental data, the penultimate model used for BA/BMA was also applied to BA/HEMA. This hypothesis is also supported by PLP kinetic studies, as the terminal model combined with experimentally-determined reactivity ratios ($r_{HEMA} = 5.54$ and $r_{BA} = 0.18$) failed to represent the evolution of k_p^{cop}.[11] However, due to the limited data set, no attempt was made in the previous study to estimate the values of the radical reactivity ratios required for the model. Whereas these reactivity ratios were implemented into the model to represent copolymer composition, k_p^{cop} data was further investigated in order to fit s-parameters for the IPUE approach using the parameter estimation tool in PREDICI®. Due to the high preference of HEMA being incorporated into the copolymer, there was no unique solution found, representing the published data and the continuous increase in k_p^{cop} with increasing acrylate content. In an attempt to find a solution in the area of interest for f_{BA} = 0.5-0.9, the closest agreement was found for the s-values $s_{HEMA} = 2$ and $s_{BA} = 4$, which were implemented into the copolymerization model. An example for the experimental cross check is given in Figure 6.6.

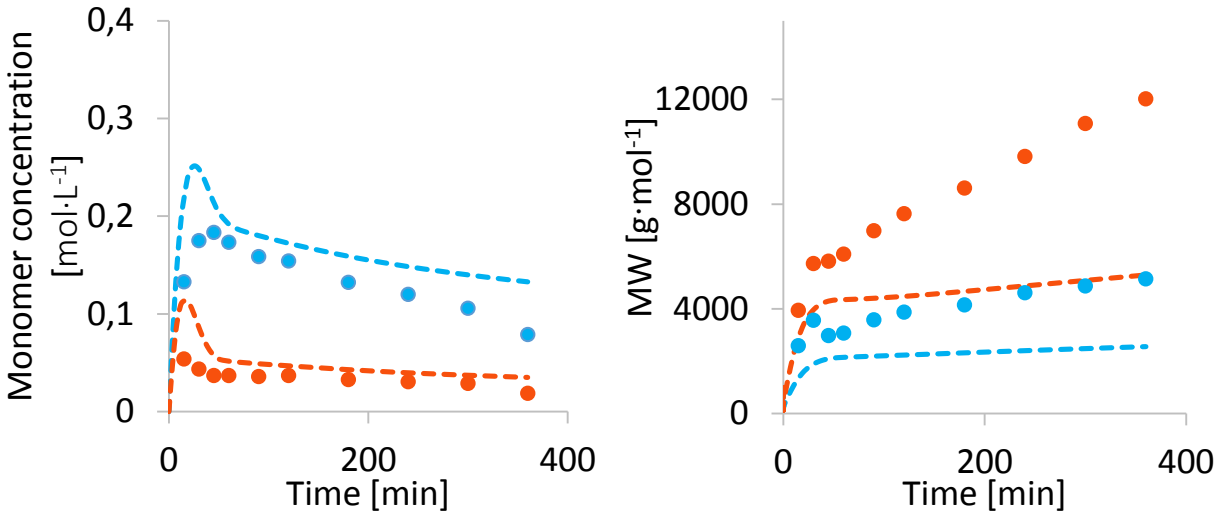

Figure 6.6: Comparison of simulated (lines) and experimental (points) free monomer concentrations and molar mass averages for a BA/HEMA semi-batch copolymerization (40 wt% HEMA) in BPi at 138 °C, using PLP-determined BA/HEMA kinetic parameters for propagation, with all other parameters according to the final model in Chapter 5. Monomer concentrations for BA (▮) and HEMA (▮) are shown on the left, and the evolution of M_n (▮) and M_w (▮) on the right.

While concentration trends were properly represented, the comparison for MMD is not in reasonable agreement, with the model underpredicting the evolution for both averages. Predictions for individual recipes (even with changed HEMA contents from 25 to 40 wt%) caused significant mathematical issues within the copolymerization model itself, due to the increased asymmetric reactivity ratios. A comment explaining this specific problem can be found in the last section of Appendix D. Whereas this result is undesirable, it shows the importance of H-bonding in HEMA systems, which is more influenced by solvent choice than in HEA systems. While copolymerization composition and evolutions for k_p^{cop} are accessible, the actual influence of H-bonding can be very solvent dependent[19,89,114,29] and hard to mechanistically understand. The idea is put forth to include an additional mechanism, like the coordination of monomer units along the formed copolymer backbone,[186] which could affect local concentrations or facilitate the incorporation of the functional monomer into the

copolymer. It may be that the level of free HEMA in the semi-batch system is too low to induce H-bonding effects.

While this idea still needs further verification, a successful modelling approach was performed by using the BA/BMA model in BPi, with the respective monomer density and MM values for HEMA. An overlay of experimental data and predicted reaction curves are given in Figure 6.7.

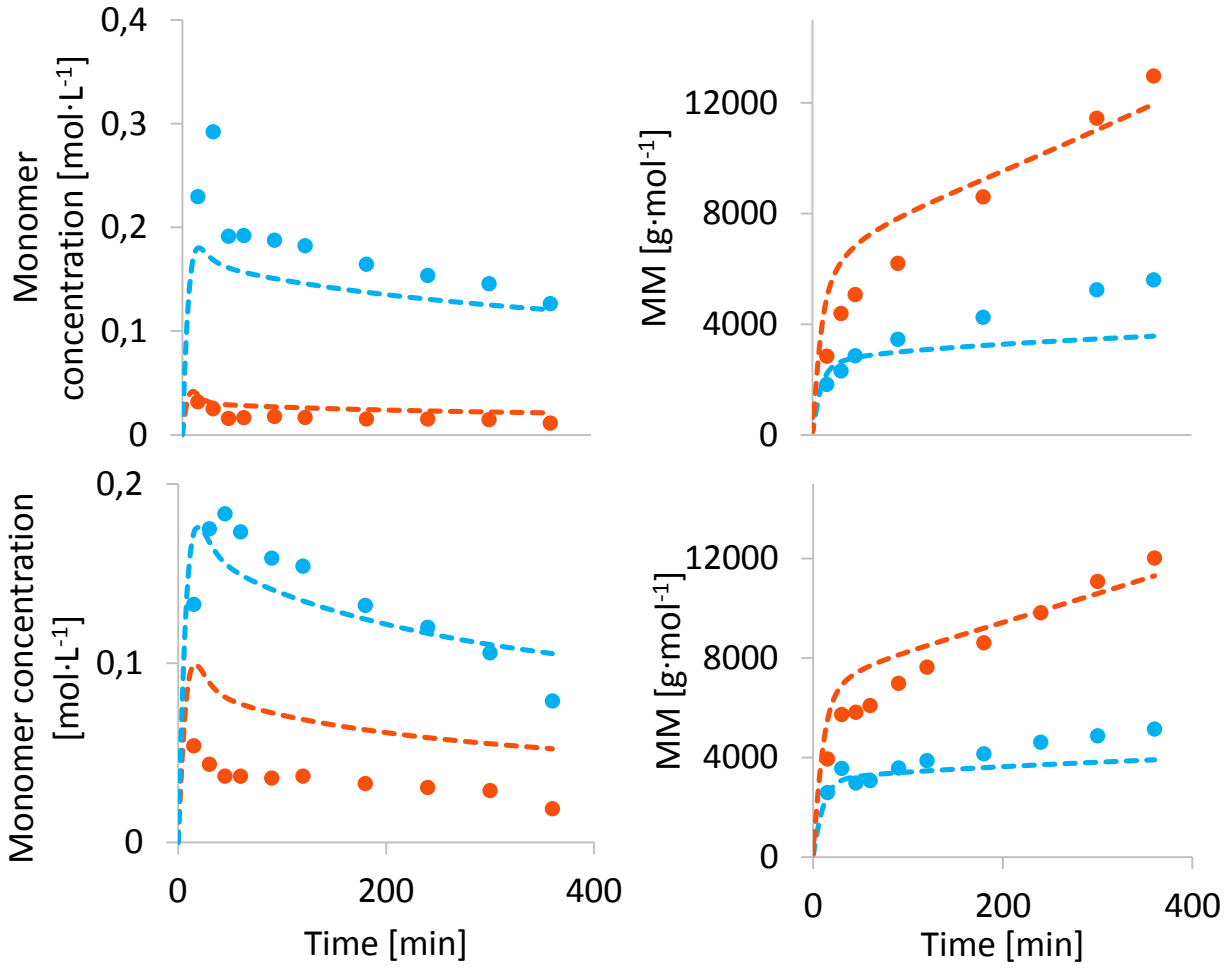

Figure 6.7: Comparison of simulated (lines) and experimental (points) free monomer concentrations and molar mass averages for a BA/HEMA semi-batch copolymerization (25 and 40 wt% HEMA, from top to bottom) in BPi at 138 °C, using the BA/BMA model in BPi as described in Chapter 5. Monomer concentrations for BA (▮) and HEMA (▮) are shown on the left, and the evolution of M_n (▮) and M_w (▮) on the right.

By simply replacing the HEMA/BA kinetic propagation rate parameters with those for BMA/BA, the evolution of MM averages is now almost perfectly represented. However, the increased reactivity of the HEMA monomer is not captured, as seen by comparing the predicted HEMA monomer concentration profiles. For the 25 wt% HEMA trial the difference in projected and actual HEMA concentrations is within a reasonable agreement. Once the methacrylate content is increased to 40 wt%, a real discrepancy is observed, with the prediction lying about 90 % above the actual experimental values, from 0.052 to 0.029 $mol \cdot L^{-1}$. Through the starved feed conditions, this difference is not really notable for the final copolymer composition. Only during the early transient state at lower conversions, the model does not adequately represent the increased HEMA incorporation, which is important for the analysis of functional groups present in the formed copolymer: as the fraction of non-functional copolymer-chains is a function of chain length,[187] more non-functional chains tend to be formed during the initial phase where lower MM chains are formed. Both, the methacrylate reactivity and the H-bonding boost in HEMA allow for an increased incorporation of the functional monomer during the transient state, hence reducing the formation of non-valuable coating material. With increasing conversions, this effect diminishes as copolymer composition equals monomer feed compositions, which shifts the focus towards MMD. As these evolutions are properly represented, properties of the final copolymer material are represented as well. Therefore, the use of the non-functional BA/BMA copolymerization model is largely sufficient to represent BA/HEMA copolymerization, provided that the solvent selected provides sufficient solubility for the polar copolymer.

6.4. Conclusion and future work

In this work, the source of high MM tails was isolated by purposely spiking batch and semi-batch reactions with ppm levels of difunctional crosslinker such as EGDA and EGDMA. In contrast to previous experiments, high MM tails did not occur in any of the experiments, including copolymerizations with HEMA. Therefore, the presence of ppm levels of crosslinker can be neglected in terms of its importance

for the copolymerization kinetics. A more reasonable explanation for the previously-reported problems was found to be the reduced solubility of hydroxyl functional copolymers in solvents such as xylenes, which allows for polymer fouling at the glass reactor walls due to the polymer affinity for such surfaces. Using more polar solvents such as esters and ketones were found to completely resolve this issue. Consequently, the problem was identified to be more a physical issue related to polymer/solvent compatibility, rather than a kinetic one. Similar conclusions were drawn from the copolymerization study of BA/HEMA in BPi, which demonstrated very similar trends during semi-batch operations as seen for BA/BMA systems. Surprisingly, use of the BA/BMA kinetic parameter set in the model provided a better description of the average polymer molar masses measured in the BA/HEMA experiment study than using the BA/HEMA propagation rate coefficients determined in a previous PLP-SEC study.[11] However, the prediction of the free HEMA level in the reactor was not satisfactory. In addition to further investigations on solvent dependency of kinetic parameters for the BA/HEMA system, the data presented can be used to test models under development to provide a better description of the influence of H-bonding under changing reaction conditions.[186]

Chapter 7 Conclusions and future recommendations

7.1. Conclusions and original contributions

Propagation chain-growth parameters were determined for multiple copolymerization involving the functional acrylates HEA[19] and MEA.[29] For the BMA/HEA system, copolymer compositions were found to be highly solvent dependent, with a general promotion of HEA incorporation in comparison to non-functional counterparts (like BA). These H-bonding effects could be substituted or disrupted by proper solvent choice. The k_p^{cop} behaviour, on the other hand, was found to be very similar in xylenes, ketones and esters solutions to that measured under bulk conditions. The terminal model was found to be sufficient to represent such solvent containing systems, while an IPUE approach was used to describe k_p^{cop} for the bulk case.

To better understand the influence and magnitude of H-bonding in organic media solution polymerization, a second investigation was performed for the acrylate-only BA/HEA system. The enhanced HEA incorporation into the copolymer relative to an alkyl acrylate was found to be of a similar magnitude in comparison to that found for BMA/HEA. However, notable differences were observed in the evolution of k_p^{cop} in different solvents, with xylenes promoting system reactivity and DMF disrupting reactivity relative to the bulk system. The increased reactivity in non-interacting solvents may be related to H-bonding between HEA monomer and polymer chains near the radical chain-end.

The copolymerization kinetics of MEA, the methoxylated version of HEA, was studied to explore the importance of the hetero-atom in the side-chain without the allocation of H-bonding through a hydroxyl group. In direct comparison to the HEA investigations it was found that, despite the increase in k_p^{MEA} relative to BA, the copolymerization kinetics (both composition and k_p^{cop}) remained comparable to a classic non-functional case for both acrylate/acrylate and acrylate/methacrylate systems, with no solvent dependencies. Results could be well-represented following an IPUE approach, using previously published universal acrylate/methacrylate s-parameters.[127] Thus, the effects of solvent choice found in the HEA copolymerizations can be attributed to the influence of H-bonding.

As these functional monomers are of particular importance for the coating industry, HEA copolymerization was studied under semi-batch operating conditions typical of those used in industry. Starting with the acrylate-only system, it was shown that BA/HEA polyacrylates can be produced with up to 50 wt% HEA content in ketones or esters. Furthermore, low-conversion derived reactivity ratios provided a good description of the residual monomer composition under these high temperature conditions. The effect of copolymer composition and solvent choice on the backbiting reaction was also investigated. Whereas H-bonding reduces branching if introduced by the solvent such as an alcohol, the influence derived from HEA was found to be negligible under starved-feed conditions. It is concluded that the backbiting reaction is more affected by the general solvation of the polymer chain in solution (i.e., chain flexibility), rather than directly to H-bonding.

BMA/HEA semi-batch copolymerizations in industrially relevant solvents were also investigated, with experimental results compared to predictions from a comprehensive copolymerization model. Using the kinetic chain-growth parameters determined by the PLP investigation, it was demonstrated that the existing acrylate/methacrylate modelling framework was able to represent both residual monomer concentrations as well as polymer properties such as MM averages and the full MMD. It was also demonstrated that, as HEA/BMA copolymerizations demonstrated similar behaviour to the BA/BMA system, that HEA/BMA starved-feed semi-batch conditions could be adequately represented using a BA/BMA parameter set.

In addition to providing data to help verify model development, the influence of introducing HEA and HEMA on reactor operation was explored. The importance of maintaining a single-phase solution was identified, as the increase in total polarity of the reaction environment (including the synthesized polymer chains) can lead to solubility issues in solvents like xylenes. The previously suspected cause– impurities of a difunctional nature in the hydroxyfunctional monomer – was shown not to be responsible for the reported anomalies in copolymer MMDs; rather, poor miscibility and the possibility of polymer fouling were found to be a more reasonable explanation. Therefore, HEMA copolymerizations were revisited and demonstrated to be manageable if more polar solvents like ketones or esters are used.

7.2. Outlook and recommendations for future work

7.2.1. Suggestions for direct follow-up investigations

This investigation demonstrates the importance and necessity of the determination of system-specific kinetic parameters to describe copolymerization chain growth for the H-bonding monomers HEA and HEMA. While the influence of a variety of solvents was systematically investigated in this work, more work can be done to develop a generalized understanding, and perhaps representation, of these effects. This also includes the considerations of other theories describing H-bonding interactions, such as Kamlet Taft solvatochromatic parameters. Experimentally it would be useful to perform PLP experiments for lower monomer concentrations in xylenes, as the particular promotion of HEA (HEMA) reactivity in this solvent is not fully understood yet. An earlier investigation[76] suggests that the coordination of H-bonding monomer units along the polymer backbone affects their relative incorporation into the polymer chain, an idea currently being pursued in our research group.[128] In addition to conducting additional small scale kinetic experiments, the ideas can be tested against the semi-batch behaviours observed in this work, such as the peculiar monomer concentration profiles found for BA/HEA copolymerizations in PeOH during the early stage of reaction that suggest that H-bonding with solvents can also inhibit the HEA incorporation. PLP experiments with increased alcohol content would help to clarify this behaviour. In general, the system reactivity ratios may change as a function of both monomer concentration and polymer concentrations in solution when H-bonding is a factor. Although the modeling work in this thesis suggests that these variations can largely be neglected, a systematic representation of these changing influences under semi-batch conditions could help eliminate the need to enter solvent-dependent kinetic parameters. Finally, a complete analysis of k_p^{HEA} in solvents (currently limited by THF-solubility of the homopolymer) should be completed to improve the analysis of the trends seen in HEA copolymerization systems.

As a related but separate model extension, the current model formulated in PREDICI® can be combined with the Monte-Carlo simulation tools now available in the package. This technique allows for the exact determination of features such as functional groups or branch points, within each chain as a

function of chain length.[187,193] This microscopic information can be related to end-use properties such as, for example, the cross-linkable fraction of the copolymer product, as non-functional chains will not participate in the post modification reaction.

7.2.2. Perspectives for kinetic investigations

As shown by this study, there is a shortage of copolymerization data available for functional comonomers, despite their increasing importance in the field of polymer chemistry and reaction engineering. Whereas there is a multitude of examples,[74] particular trends are determined by industry and regulations. The most obvious example is the shift of radical polymerizations to more sustainable solvents, such as under aqueous conditions. It is already known that water provides a unique H-bonding environment for polar (water soluble) monomers, with very specific and concentration dependent rate coefficients.[91,180,181] Whereas there are ongoing investigations of the radical polymerization kinetics of water-soluble polymers, the number of studies comparing their behaviour to polymerization in organic solvents are limited.[15,194] The aqueous-phase kinetics of (co)polymerization of standard monomers, such as MA, in water is also needed for better representation of heterogeneous polymerizations such as emulsion systems. Perhaps by systematically studying how copolymerization reactivity ratios and k_p^{cop} vary with solvent composition in, for example, a methanol/water mixture, it will be possible to extrapolate the behaviour to the pure aqueous system.

7.2.3. Perspectives in coating applications

Classically, many coating recipes are multi component systems, with more than two comonomers (and their relative amounts) selected to control polymer properties such as T_g, based on the target application. As well as deciding between methacrylate and acrylate structure, other modifications include substitutions within each class by selection of analogues with shorter or longer ester side-chains. With the development and need for improved coatings or other high performance products, more functional

monomers are also introduced. Examples include functional precursors which allow for manifold post modifications[97] or CO_2-switchable polymers for latex stabilization, including monomers the like of dimethylaminoethyl methacrylate or dimethylaminopropyl methacrylamide.[195] Although the catalogue of kinetic parameters is continuously growing, with homopropagation coefficients available for more of the aforementioned functional monomers,[97,196] there still is a lack of sophisticated knowledge of their copolymerization behaviour. Through the course of this thesis, it was shown that H-bonding alone is a very powerful mechanism, which is yet to be fully understood. The introduction of new functional groups can therefore significantly affect copolymerization kinetics, a great opportunity for future investigation also under industrially relevant conditions. With regards to global resources and the increasing role and accessibility of bio-renewable feedstocks as monomers, the kinetics of these new (and often functional) monomers become more important.[197–199]

More specifically for the family of acrylic coatings discussed in this thesis, another option (rather than crosslinking through hydroxyl groups) to allow for post modification is via the acidic opening of epoxides. Hence, recipes are extended to include GMA and/or acrylic acid/ methacrylic acid. Depending on reaction conditions, both functional groups can also react during the polymerization, which has been shown to be beneficial in non-aqueous dispersion polymerization.[200] In case of homogeneous solution polymerization this can be challenging for two reasons. In a direct comparison to HEA or HEMA, the acid group increases the polarity of the copolymer, which will limit the range of possible feed compositions in industrially relevant solvents. In addition, monomers of the AA/MAA family have been shown to undergo significant H-bonding effects,[76,91,139,158] which may be even more substantial then found for HEA/HEMA. Even though the latter were shown to be well manageable for relevant semi-batch operations, the same may not be true for the acid comonomers. Thus, models of these systems must be developed and tested against data collected under typical starved-feed operating conditions.

References

1 B. B. Noble and M. L. Coote, *Int. Rev. Phys. Chem.*, 2013, **32**, 467–513.

2 J. S. Wang and K. Matyjaszewski, *J. Am. Chem. Soc.*, 1995, **117**, 5614–5615.

3 J. Chiefari, Y. K. (Bill) Chong, F. Ercole, J. Krstina, J. Jeffery, T. P. T. Le, R. T. A. Mayadunne, G. F. Meijs, C. L. Moad, G. Moad, E. Rizzardo and S. H. Thang, *Macromolecules*, 1998, **31**, 5559–5562.

4 C. J. Hawker, G. G. Barclay, A. Orellana, J. Dao and W. Devonport, *Macromolecules*, 1996, **29**, 5245–5254.

5 M. Szwarc, *Nature*, 1956, **178**, 1168–1169.

6 R. Mülhaupt, *Macromol. Chem. Phys.*, 2003, **204**, 289–327.

7 A. Rudin and P. Choi, *The elements of polymer science and engineering*, Academic, 2013.

8 K. Matyjaszewski and T. P. Davis, Eds., *Handbook of Radical Polymerization*, John Wiley & Sons, Inc., Hoboken, NJ, USA, 2002.

9 A. N. F. Peck and R. A. Hutchinson, *Macromolecules*, 2004, **37**, 5944–5951.

10 J. Lebduška, J. Šnupárek, K. Kašpar and V. Čermák, *J. Polym. Sci. Part A Polym. Chem.*, 1986, **24**, 777–791.

11 K. Liang, T. R. Rooney and R. A. Hutchinson, *Ind. Eng. Chem. Res.*, 2014, **53**, 7296–7304.

12 Y.-M. Baek, N.-S. Kwak and T.-S. Hwang, *Polym. Korea*, 2011, **35**, 586–592.

13 B. Hanbeyoglu, B. Kiskan and Y. Yagci, *Macromolecules*, 2013, **46**, 8434–8440.

14 M. Kamachi, D. J. Liaw and S. Nozakura, *Polym. J.*, 1977, **9**, 307–316.

15 M. Stach, I. Lacík, D. Chorvát, M. Buback, P. Hesse, R. A. Hutchinson and L. Tang, *Macromolecules*, 2008, **41**, 5174–5185.

16 K. F. O'Driscoll, T. P. Davis, B. Klumperman and E. L. Madruga, *Macromol. Rapid Commun.*, 1995, **16**, 207–210.

17 K. Liang, R. A. Hutchinson, J. Barth, S. Samrock and M. Buback, *Macromolecules*, 2011, **44**, 5843–5845.

18 O. A. Kazantsev, D. M. Kamorin, A. P. Sivokhin, S. I. Samodurova, D. V. Orekhov and T. V. Korotkova, *J. Polym. Res.*, 2014, **21**, 1–6.

19 J. E. S. Schier and R. A. Hutchinson, *Polym. Chem.*, 2016, **7**, 4567–4574.

20 K. Liang and R. A. Hutchinson, *Macromol. Rapid Commun.*, 2011, **32**, 1090–1095.

21 S. Beuermann, M. Buback, P. Hesse and I. Lacík, *Macromolecules*, 2006, **39**, 184–193.

22 M. Buback, R. G. Gilbert, R. A. Hutchinson, B. Klumperman, F.-D. Kuchta, B. G. Manders, K. F.

O'Driscoll, G. T. Russell and J. Schweer, *Macromol. Chem. Phys.*, 1995, **196**, 3267–3280.

23 O. F. Olaj, I. Bitai and F. Hinkelmann, *Die Makromol. Chemie*, 1987, **188**, 1689–1702.

24 M. Lejars, A. Margaillan and C. Bressy, *Polym. Chem.*, 2014, **5**, 2109.

25 B. Lessard, C. Tervo, S. De Wahl, F. J. Clerveaux, K. K. Tang, S. Yasmine, S. Andjelić, A. D'Alessandro and M. Marić, *Macromolecules*, 2010, **43**, 868–878.

26 F. R. Mayo and F. M. Lewis, *J. Am. Chem. Soc.*, 1944, **66**, 1594–1601.

27 E. Mavroudakis, K. Liang, D. Moscatelli and R. A. Hutchinson, *Macromol. Chem. Phys.*, 2012, **213**, 1706–1716.

28 W. Wang and R. A. Hutchinson, *AIChE J.*, 2011, **57**, 227–238.

29 J. E. S. Schier, D. Cohen-Sacal and R. A. Hutchinson, *Polym. Chem.*, 2017.

30 K. E. Russell, *Prog. Polym. Sci.*, 2002, **27**, 1007–1038.

31 J.-L. Luna-Xavier, E. Bourgeat-Lami and A. Guyot, *Colloid Polym. Sci.*, 2001, **279**, 947–958.

32 H. Tobita and A. E. Hamielec, *Polymer (Guildf).*, 1991, **32**, 2641–2647.

33 C.-U. Schmidt, M. Busch, D. Lilge and M. Wulkow, *Macromol. Mater. Eng.*, 2005, **290**, 404–414.

34 I. Zapata-González, R. A. Hutchinson, K. A. Payne and E. Saldívar-Guerra, *AIChE J.*, 2016, **62**, 2762–2777.

35 K. A. Payne, J. Debling, P. Nesvadba, M. F. Cunningham and R. A. Hutchinson, *Eur. Polym. J.*, 2016, **80**, 186–199.

36 P. Krys, T. G. Ribelli, K. Matyjaszewski and A. Gennaro, *Macromolecules*, 2016, **49**, 2467–2476.

37 J. Brandrup, E. H. Immergut and E. A. Grulke, *Polymer handbook*, Wiley-Interscience, 1999.

38 C. Barner-Kowollik, S. Beuermann, M. Buback, P. Castignolles, B. Charleux, M. L. Coote, R. A. Hutchinson, T. Junkers, I. Lacík, G. T. Russell, M. Stach and A. M. van Herk, *Polym. Chem.*, 2014, **5**, 204–212.

39 M. Buback, L. H. Garcia-Rubio, R. G. Gilbert, D. H. Napper, J. Guillot, A. E. Hamielec, D. Hill, K. F. O'Driscoll, O. F. Olaj, J. Shen, D. Solomon, G. Moad, M. Stickler, M. Tirrell and M. A. Winnik, *J. Polym. Sci. Polym. Lett. Ed.*, 1988, **26**, 293–297.

40 S. Beuermann and M. Buback, *Prog. Polym. Sci.*, 2002, **27**, 191–254.

41 R. A. Hutchinson, in *Handbook of Polymer Reaction Engineering*, Wiley-VCH Verlag GmbH, Weinheim, Germany, pp. 153–212.

42 B. B. Noble, L. M. Smith and M. L. Coote, *Polym. Chem.*, 2014, **5**, 4974.

43 M. Buback, M. Busch and R. A. Lämmel, *Macromol. Theory Simulations*, 1996, **5**, 845–861.

44 A. N. Nikitin, R. A. Hutchinson and P. Hesse, *Macromol. Chem. Phys.*, 2013, **214**, 2670–2682.

45 R. Rotzoll and P. Vana, *Macromol. Rapid Commun.*, 2009, **30**, 1989–1994.

46 B. Dervaux, T. Junkers, M. Schneider-Baumann, F. E. Du Prez and C. Barner-Kowollik, *J. Polym. Sci. Part A Polym. Chem.*, 2009, **47**, 6641–6654.

47 C. Barner-Kowollik, F. Günzler and T. Junkers, *Macromolecules*, 2008, **41**, 8971–8973.

48 J. M. Asua, S. Beuermann, M. Buback, P. Castignolles, B. Charleux, R. G. Gilbert, R. A. Hutchinson, J. R. Leiza, A. N. Nikitin, J.-P. Vairon and A. M. van Herk, *Macromol. Chem. Phys.*, 2004, **205**, 2151–2160.

49 M. Buback, P. Hesse and I. Lacík, *Macromol. Rapid Commun.*, 2007, **28**, 2049–2054.

50 A. P. Haehnel, M. Schneider-Baumann, K. U. Hiltebrandt, A. M. Misske and C. Barner-Kowollik, *Macromolecules*, 2013, **46**, 15–28.

51 W. Wang and R. A. Hutchinson, *Macromolecules*, 2008, **41**, 9011–9018.

52 R. Ferrari, T. R. Rooney, M. Lupi, P. Ubezio, R. A. Hutchinson and D. Moscatelli, *Macromol. Biosci.*, 2013, **13**, 1347–1357.

53 A. P. Haehnel, M. Stach, A. Chovancová, J. M. Rueb, G. Delaittre, A. M. Misske, I. Lacík and C. Barner-Kowollik, *Polym. Chem.*, 2014, **5**, 862–873.

54 B. Wenn and T. Junkers, *Macromol. Rapid Commun.*, 2016, **37**, 781–787.

55 G. N., K. Kalli and K. Sugde, in *Frontiers in Guided Wave Optics and Optoelectronics*, InTech, 2010.

56 A. N. Nikitin, I. Lacík and R. A. Hutchinson, *Macromolecules*, 2016, **49**, 9320–9335.

57 M. Buback and T. Junkers, *Macromol. Chem. Phys.*, 2006, **207**, 1640–1650.

58 H. Kattner and M. Buback, *Macromolecules*, 2015, **48**, 309–315.

59 H. Kattner and M. Buback, *Macromolecules*, 2016, **49**, 3716–3722.

60 C. Barner-Kowollik, M. Buback, M. Egorov, T. Fukuda, A. Goto, O. F. Olaj, G. T. Russell, P. Vana, B. Yamada and P. B. Zetterlund, *Prog. Polym. Sci.*, 2005, **30**, 605–643.

61 C. Barner-Kowollik and G. T. Russell, *Prog. Polym. Sci.*, 2009, **34**, 1211–1259.

62 V. E. Trommsdorff, H. Köhle and P. Lagally, *Die Makromol. Chemie*, 1948, **1**, 169–198.

63 R. G. W. NORRISH and R. R. SMITH, *Nature*, 1942, **150**, 336–337.

64 W. Sutherland, *Philos. Mag. Ser. 6*, 1905, **9**, 781–785.

65 A. Einstein, *Ann. Phys.*, 1905, **322**, 549–560.

66 M. Buback, H. Schroeder and H. Kattner, *Macromolecules*, 2016, **49**, 3193–3213.

67 G. Johnston-Hall, A. Theis, M. J. Monteiro, T. P. Davis, M. H. Stenzel and C. Barner-Kowollik, *Macromol. Chem. Phys.*, 2005, **206**, 2047–2053.

68 H. Kattner and M. Buback, *Macromol. Chem. Phys.*, 2014, **215**, 1180–1191.

69 J. Barth, M. Buback, G. T. Russell and S. Smolne, *Macromol. Chem. Phys.*, 2011, **212**, 1366–

1378.

70 M. Buback, *Die Makromol. Chemie*, 1990, **191**, 1575–1587.

71 H. Bakhshi, M. J. Zohuriaan-Mehr, H. Bouhendi and K. Kabiri, *Iran. Polym. J.*, 2010, **19**.

72 C. Guerrero-Sanchez, S. Harrisson and D. J. Keddie, *Macromol. Symp.*, 2013, **325**–**326**, 38–46.

73 T. Kodaira, J.-Z. Yang and H. Aida, *Polym. J.*, 1988, **20**, 1021–1029.

74 F. Brandl, M. Drache, J. E. S. Schier, T. Nentwig, D. Contreras-Lopez, E. Saldivar-Guerra, R. A. Hutchinson and S. Beuermann, *Macromol. Rapid Commun.*, 2017.

75 K. Liang and R. A. Hutchinson, *Macromolecules*, 2010, **43**, 6311–6320.

76 A. Noguchi and M. Kuzuya, *Macromol. Chem. Phys.*, 2001, **202**, 1021–1030.

77 T. Fukuda, Y. D. Ma and H. Inagaki, *Macromolecules*, 1985, **18**, 17–26.

78 E. Merz, T. Alfrey and G. Goldfinger, *J. Polym. Sci.*, 1946, **1**, 75–82.

79 I. Rintoul and C. Wandrey, *Macromolecules*, 2005, **38**, 8108–8115.

80 D. Yamamoto and A. Matsumoto, *Macromol. Chem. Phys.*, 2012, **213**, 2479–2485.

81 N. M. Ahmad, F. Heatley and P. A. Lovell, *Macromolecules*, 1998, **31**, 2822–2827.

82 I. González, J. M. Asua and J. R. Leiza, *Polymer (Guildf).*, 2007, **48**, 2542–2547.

83 J. Mai and L. Wang, *Polym. Chem.*, 2014, **5**, 2118–2129.

84 W. Wang and R. A. Hutchinson, *Macromolecules*, 2009, **42**, 4910–4913.

85 C. Quan, M. Soroush, M. C. Grady, J. E. Hansen and W. J. Simonsick, *Macromolecules*, 2005, **38**, 7619–7628.

86 A. Agirre, J. I. Santos, A. Etxeberria, V. Sauerland and J. R. Leiza, *Polym. Chem.*, 2013, **4**, 2062.

87 J. Chiefari, J. Jeffery, R. T. A. Mayadunne, G. Moad, E. Rizzardo and S. H. Thang, *Macromolecules*, 1999, **32**, 7700–7702.

88 S. Beuermann, M. Buback, T. P. Davis, R. G. Gilbert, R. A. Hutchinson, A. Kajiwara, B. Klumperman and G. T. Russell, *Macromol. Chem. Phys.*, 2000, **201**, 1355–1364.

89 S. Beuermann, *Macromol. Rapid Commun.*, 2009, **30**, 1066–1088.

90 A. P. Haehnel, B. Wenn, K. Kockler, T. Bantle, A. M. Misske, F. Fleischhaker, T. Junkers and C. Barner-Kowollik, *Macromol. Rapid Commun.*, 2014, **35**, 2029–2037.

91 P. Drawe, M. Buback and I. Lacík, *Macromol. Chem. Phys.*, 2015, **216**, 1333–1340.

92 I. Lacík, P. Sobolčiak, M. Stach, D. Chorvát and P. Kasák, *Polymer (Guildf).*, 2016, **87**, 38–49.

93 L. Uhelská, D. Chorvát, R. A. Hutchinson, S. Santanakrishnan, M. Buback and I. Lacík, *Macromol. Chem. Phys.*, 2014, **215**, 2327–2336.

94 L. Pauling and R. B. Corey, *Arch. Biochem. Biophys.*, 1956, **65**, 164–181.

95 M.-O. Simon and C.-J. Li, *Chem. Soc. Rev.*, 2012, **41**, 1415–1427.

96 I. Chaduc, A. Crepet, O. Boyron, B. Charleux, F. D'Agosto and M. Lansalot, *Macromolecules*, 2013, **46**, 6013–6023.

97 A. Zoller, K. B. Kockler, M. Rollet, C. Lefay, D. Gigmes, C. Barner-Kowollik and Y. Guillaneuf, *Polym. Chem.*, 2016, **7**, 5518–5525.

98 D. Mertz, C. J. Ochs, Z. Zhu, L. Lee, S. N. Guntari, G. K. Such, T. K. Goh, L. A. Connal, A. Blencowe, G. G. Qiao and F. Caruso, *Chem. Commun.*, 2011, **47**, 12601.

99 Y. W. Marien, P. H. M. Van Steenberge, K. B. Kockler, C. Barner-Kowollik, M.-F. Reyniers, D. R. D'hooge and G. B. Marin, *Polym. Chem.*, 2016, **7**, 6521–6528.

100 A. N. Nikitin, R. A. Hutchinson, M. Buback and P. Hesse, *Macromolecules*, 2007, **40**, 8631–8641.

101 S. Beuermann and M. Buback, *Pure Appl. Chem.*, 1998, **70**, 1415–1418.

102 S. Beuermann, M. Buback, T. P. Davis, N. García, R. G. Gilbert, R. A. Hutchinson, A. Kajiwara, M. Kamachi, I. Lacík and G. T. Russell, *Macromol. Chem. Phys.*, 2003, **204**, 1338–1350.

103 A. Jeličič, F. Köhler, A. Winter and S. Beuermann, *J. Polym. Sci. Part A Polym. Chem.*, 2010, **48**, 3188–3199.

104 M. Buback and C. H. Kurz, *Macromol. Chem. Phys.*, 1998, **199**, 2301–2310.

105 M. Buback, *Macromol. Symp.*, 2009, **275**–**276**, 90–101.

106 S.-Y. Chang and H. Morawetz, *J. Phys. Chem.*, 1956, **60**, 782–786.

107 S. A. Dergunov, G. A. Mun, M. A. Dergunov, I. E. Suleimenov and E. Pinkhassik, *React. Funct. Polym.*, 2011, **71**, 1129–1136.

108 Z. Li, Y. Wang, N. Wu, Q. Chen and K. Wu, *Environ. Sci. Pollut. Res.*, 2013, **20**, 1511–1525.

109 W. Steinhauer, R. Hoogenboom, H. Keul and M. Moeller, *Macromolecules*, 2010, **43**, 7041–7047.

110 R. Hoogenboom, A.-M. Zorn, H. Keul, C. Barner-Kowollik and M. Moeller, *Polym. Chem.*, 2012, **3**, 335–342.

111 K. Nitta, A. Kimoto and J. Watanabe, *Polymer (Guildf).*, 2016, **96**, 45–53.

112 I. Javakhishvili, K. Jankova and S. Hvilsted, *Polym. Chem.*, 2013, **4**, 662–668.

113 L. Hou and P. Wu, *Phys. Chem. Chem. Phys.*, 2016, **18**, 15593–15601.

114 K. Liang, M. Dossi, D. Moscatelli and R. A. Hutchinson, *Macromolecules*, 2009, **42**, 7736–7744.

115 R. A. Hutchinson, S. Beuermann, D. A. Paquet and J. H. McMinn, *Macromolecules*, 1997, **30**, 3490–3493.

116 D. Li, N. Li and R. A. Hutchinson, *Macromolecules*, 2006, **39**, 4366–4373.

117 Michelle L. Coote, and Lloyd P. M. Johnston and T. P. Davis*, 1997.

118 D. J. . Hill, N. . Moss, P. . Pomery and A. . Whittaker, *Polymer (Guildf).*, 2000, **41**, 1287–1296.

119 A. M. Aerdts, A. L. German and G. P. M. van der Velden, *Magn. Reson. Chem.*, 1994, **32**, S80–S88.

120 J. M. Catala, A. Nonn, J. M. Pujol and J. Brossas, *Polym. Bull.*, 1986, **5**.

121 M. L. Coote, T. P. Davis, B. Klumperman and M. J. Monteiro, *J. Macromol. Sci. Part C Polym. Rev.*, 1998, **38**, 567–593.

122 M. Buback and E. Müller, *Macromol. Chem. Phys.*, 2007, **208**, 581–593.

123 S. Beuermann and N. García, *Macromolecules*, 2004, **37**, 3018–3025.

124 S. Beuermann, *Macromolecules*, 2004, **37**, 1037–1041.

125 J. Schrooten, I. Lacík, M. Stach, P. Hesse and M. Buback, *Macromol. Chem. Phys.*, 2013, **214**, 2283–2294.

126 M. Buback, A. Feldermann, C. Barner-Kowollik and I. Lacík, *Macromolecules*, 2001, **34**, 5439–5448.

127 R. A. Hutchinson, J. H. McMinn, D. A. Paquet, S. Beuermann and C. Jackson, *Ind. Eng. Chem. Res.*, 1997, **36**, 1103–1113.

128 T. R. Rooney, *PhD-Thesis*, Queen's University, Kingston, ON, 2017.

129 K. B. Kockler, F. Fleischhaker and C. Barner-Kowollik, *Polym. Chem.*, 2016, **7**, 4342–4351.

130 M. D. Zammit, T. P. Davis, G. D. Willett and K. F. O'Driscoll, *J. Polym. Sci. Part A Polym. Chem.*, 1997, **35**, 2311–2321.

131 X. Li, M. Drache, U. Gohs and S. Beuermann, *J. Memb. Sci.*, 2015, **495**, 20–28.

132 J. F. J. Coelho, J. Gois, A. C. Fonseca, R. A. Carvalho, A. V. Popov, V. Percec and M. H. Gil, *J. Polym. Sci. Part A Polym. Chem.*, 2009, **47**, 4454–4463.

133 R. Siegmann, A. Jeličić and S. Beuermann, *Macromol. Chem. Phys.*, 2010, **211**, 546–562.

134 R. A. Hutchinson, S. Beuermann, D. A. Paquet, J. H. McMinn and C. Jackson, *Macromolecules*, 1998, **31**, 1542–1547.

135 N. M. Ahmad, B. Charleux, C. Farcet, C. J. Ferguson, S. G. Gaynor, B. S. Hawkett, F. Heatley, B. Klumperman, D. Konkolewicz, P. A. Lovell, K. Matyjaszewski and R. Venkatesh, *Macromol. Rapid Commun.*, 2009, **30**, 2002–2021.

136 P. Derboven, P. H. M. Van Steenberge, J. Vandenbergh, M.-F. Reyniers, T. Junkers, D. R. D'hooge and G. B. Marin, *Macromol. Rapid Commun.*, 2015, **36**, 2149–2155.

137 N. Ballard, M. Salsamendi, J. I. Santos, F. Ruipérez, J. R. Leiza and J. M. Asua, *Macromolecules*, 2014, **47**, 964–972.

138 A. N. Nikitin, R. A. Hutchinson, G. A. Kalfas, J. R. Richards and C. Bruni, *Macromol. Theory Simulations*, 2009, **18**, 247–258.

139 C. Preusser and R. A. Hutchinson, *Can. J. Chem. Eng.*, 2016, **94**, 2045–2051.

140 J.-N. Ollagnier, T. Tassaing, S. Harrisson and M. Destarac, *React. Chem. Eng.*, 2016, **1**, 372–378.

141 X.-S. Chai, Q. . Hou and F. . Schork, *J. Chromatogr. A*, 2004, **1040**, 163–167.

142 D. Li, M. C. Grady and R. A. Hutchinson, *Ind. Eng. Chem. Res.*, 2005, **44**, 2506–2517.

143 S. Hamzehlou, N. Ballard, Y. Reyes, A. Aguirre, J. M. Asua and J. R. Leiza, *Polym. Chem.*, 2016, **7**, 2069–2077.

144 J. Barth, M. Buback, P. Hesse and T. Sergeeva, *Macromolecules*, 2010, **43**, 4023–4031.

145 P. Giraudeau and E. Baguet, *J. Magnetic Resonance*, 2006, **180**, 110-117.

146 D.-M. Kim, M. Busch, H. C. J. Hoefsloot and P. D. Iedema, *Chem. Eng. Sci.*, 2004, **59**, 699–718.

147 M. H. Wagner, *Macromol. Symp.*, 2006, **236**, 219–227.

148 M. Kontopoulou, *Applied Polymer Rheology: Polymeric Fluids with Industrial Applications*, John Wiley & Sons, Inc., 2011.

149 F. J. Stadler and T. Mahmoudi, *Korea-Australia Rheol. J.*, 2011, **23**, 185–193.

150 S. Beuermann, D. A. Paquet, J. H. McMinn and R. A. Hutchinson, *Macromolecules*, 1996, **29**, 4206–4215.

151 R. A. Hutchinson, D. A. Paquet, J. H. McMinn, S. Beuermann, R. E. Fuller and C. Jackson, *DECHEMA Monograms*, 1995, **131**, 467–492.

152 E. F. McCord, J. . and W. H. Shaw and R. A. Hutchinson*, 1997.

153 S. Beuermann, *Macromolecules*, 2004, **37**, 1037–1041.

154 K. Liang, *PhD-Thesis*, Queen's University, Kingston, ON, 2013.

155 R. A. Orwoll and P. A. Arnold, in *Physical Properties of Polymers Handbook*, Springer New York, New York, NY, 2007, pp. 233–257.

156 C. M. Hansen, *Hansen solubility parameters : a user's handbook*, CRC Press, 2007.

157 C. Preusser, I. H. Ezenwajiaku and R. A. Hutchinson, *Macromolecules*, 2016, **49**, 4746–4756.

158 S. Beuermann, M. Buback, P. Hesse, S. Kukucková and I. Lacík, *Radic. Polym. Kinet. Mech.*, 2007, 23–32.

159 D. Britton, F. Heatley and P. A. Lovell, *Macromolecules*, 2000, **33**, 5048–5052.

160 N. Ballard, S. Hamzehlou and J. M. Asua, *Macromolecules*, 2016, **49**, 5418–5426.

161 A. N. Nikitin, R. A. Hutchinson, W. Wang, G. A. Kalfas, J. R. Richards and C. Bruni, *Macromol. React. Eng.*, 2010, **4**, 691–706.

162 W. Wang, A. N. Nikitin and R. A. Hutchinson, *Macromol. Rapid Commun.*, 2009, **30**, 2022–2027.

163 D. Cuccato, E. Mavroudakis and D. Moscatelli, *J. Phys. Chem. A*, 2013, **117**, 4358–4366.

164 W. Wang and R. A. Hutchinson, *Macromol. React. Eng.*, 2008, **2**, 199–214.

165 I. González, J. M. Asua and J. R. Leiza, *Polymer (Guildf).*, 2007, **48**, 2542–2547.

166 M. Bardet, M.-F. Foray and D. Robert, *Die Makromol. Chemie*, 1985, **186**, 1495–1504.

167 R. Wang, Y. Luo, B. Li, X. Sun and S. Zhu, *Macromol. Theory Simulations*, 2006, **15**, 356–368.

168 L. G. Aguiar, *Polym. Int.*, 2016, **65**, 142–151.

169 Eastman TM, *Eastman methyl n-amyl ketone (MAK) and Estman methyl isoamyl ketone (MIAK). Solvents for high-solids coatings*, 2013.

170 G. M. Bristow and W. F. Watson, *Trans. Faraday Soc.*, 1958, **54**, 1742–1747.

171 M. V Rathnam, M. S. S. Kumar, R. T. Sayed and D. R. Ambavadekar, *Chem. Bull*, 2014, **3**, 166–172.

172 M. Izu and K. F. O'Driscoll, *J. Polym. Sci. Part A-1 Polym. Chem.*, 1970, **8**, 1687–1691.

173 S. Liu, S. Srinivasan, M. C. Grady, M. Soroush and A. M. Rappe, *Int. J. Quantum Chem.*, 2014, **114**, 345–360.

174 H. Bakhshi, H. Bouhendi, M. J. Zohuriaan-Mehr and K. Kabiri, *J. Appl. Polym. Sci.*, 2010, **117**, 2771–2780.

175 T. G. Fox and P. J. Flory, *J. Appl. Phys.*, 1950, **21**, 581–591.

176 C. S. J. Selvamalar, T. Krithiga, A. Penlidis and S. Nanjundan, *React. Funct. Polym.*, 2003, **56**, 89–101.

177 W. Steinhauer, R. Hoogenboom, H. Keul and M. Moeller, *Macromolecules*, 2013, **46**, 1447–1460.

178 J. C. R. Hernández, M. M. Pradas and J. L. G. Ribelles, *J. Non. Cryst. Solids*, 2008, **354**, 1900–1908.

179 E. Vargün, The Middle East Technical University, 2003.

180 C. Preusser and R. A. Hutchinson, *Macromol. Symp.*, 2013, **333**, 122–137.

181 M. Riahinezhad, N. McManus and A. Penlidis, *Macromol. React. Eng.*, 2015, **9**, 100–113.

182 T. R. Rooney, O. Monyatsi and R. A. Hutchinson, *Macromolecules*, 2017, acs.macromol.6b02297.

183 V. E. Meyer and G. G. Lowry, *J. Polym. Sci. Part A Gen. Pap.*, 1965, **3**, 2843–2851.

184 R. P. Sheridan, E. T. Knight and L. C. Allen, *Biopolymers*, 1984, **23**, 195–200.

185 C. N. R. Rao, *J. Chem. Soc. Faraday Trans. 1 Phys. Chem. Condens. Phases*, 1975, **71**, 980.

186 A. Noguchi and M. Kuzuya, *Macromol. Chem. Phys.*, 2001, **202**, 1021–1030.

187 M. Ali Parsa, I. Kozhan, M. Wulkow and R. A. Hutchinson, *Macromol. Theory Simulations*, 2014, **23**, 207–217.

188 M. V Rathnam, D. R. Ambavadekar and M. Nandini, *Eur. Chem. Bull.*, 2013, **2**, 642–650.

189 J. Zhang, A. J. Morris, E. B. Martin and C. Kiparissides, *Comput. Chem. Eng.*, 1999, **23**, 301–314.

190 M. N. Cardoso and A. G. Fisch, *Ind. Eng. Chem. Res.*, 2016, **55**, 9426–9432.

191 M.-C. Chevrel, S. Hoppe, D. Meimaroglou, L. Falk and A. Durand, *Macromol. React. Eng.*, 2016, **10**, 354–363.

192 DOW, *Hansen Solubility Parameters for custom processing esters and derivates compared to other conventional solvents used in the coatings, inks and cleaning industry*, 2012.

193 C. Schütte and M. Wulkow, *Macromol. React. Eng.*, 2010, **4**, 562–577.

194 S. Beuermann, *Macromol. Rapid Commun.*, 2009, **30**, 1066–1088.

195 A. Darabi, P. G. Jessop and M. F. Cunningham, *Chem. Soc. Rev. Chem. Soc. Rev*, 2016, **45**, 4391–4436.

196 K. B. Kockler, F. Fleischhaker and C. Barner-Kowollik, *Macromolecules*, 2016, **49**, 8572–8580.

197 S. Bednarz, A. Błaszczyk, D. Błażejewska and D. Bogdał, *Catal. Today*, 2015, **257**, 297–304.

198 US 8227560 B2, 2012.

199 J. Kollár, M. Mrlík, D. Moravčíková, Z. Kroneková, T. Liptaj, I. Lacík and J. Mosnáček, *Macromolecules*, 2016, **49**, 4047–4056.

200 W. Yang and R. A. Hutchinson, *React. Funct. Polym.*, 2017, **114**, 31–37.

201 K. Bian and M. F. Cunningham, *Macromolecules*, 2005, **38**, 695–701.

A. Appendix A: Supporting data for chapter 3

Tabulated NMR data for copolymer composition analysis of BMA/HEA systems

Table A.1: Copolymer composition for BMA/HEA samples produced by PLP in bulk, xylenes, MIBK and BPi

Bulk		**Xylenes**		**MIBK**		**BPi**	
$\mathbf{f_{HEA}}$	F_{HEA}	f_{HEA}	F_{HEA}	f_{HEA}	F_{HEA}	f_{HEA}	F_{HEA}
0.13	0.145	0.13	0.14	0.13	0.170	0.13	0.130
0.26	0.230	0.26	-	0.26	0.270	0.26	-
0.37	0.295	0.37	0.430	0.37	0.340	0.37	0.370
0.48	0.410	0.48	-	0.48	0.455	0.48	-
0.58	0.480	0.58	0.620	0.58	0.505	0.58	0.585
0.68	-	0.68	-	0.68	0.620	0.68	-
0.76	0.625	0.76	0.775	0.76	0.695	0.76	0.760
0.84	0.715	0.84	-	0.84	0.800	0.84	-
0.92	0.860	0.92	0.925	0.92	0.885	0.92	0.920

Table A.2: Copolymer composition for BMA/HEA samples produced by PLP in BuOH and DMF

BuOH		**DMF**	
$\mathbf{f_{HEA}}$	F_{HEA}	f_{HEA}	F_{HEA}
0.13	0.080	0.13	0.075
0.37	0.240	0.37	0.215
0.58	0.400	0.58	0.380
0.76	0.590	0.76	0.570
0.92	0.820	0.92	0.810

Tabulated PLP data for k_p^{cop} for BMA/HEA systems

Table A.3: k_p^{cop} values for BMA/HEA PLP copolymerizations in bulk; two values show duplicates

$\mathbf{f_{HEA}}$	υ **(Hz)**	**T (°C)**	k_p^{DRI} **(L·mol^{-1}·s^{-1})**	**L1/L2**	k_p^{LS} **(L·mol^{-1}·s^{-1})**
0	20	50	681	0.500	699
0	50	50	727	0.492	755
0	75	50	775	0.494	794
0.13	75	50	999	0.498	1116
0.13	150	50	1021	0.495	1189
0.26	75	50	1286	0.507	1305
0.26	150	50	1256	0.484	1304
0.37	75	50	1464	0.497	1598

0.37	150	50	1466	0.500	1607
0.48	75	50	1836	0.501	1900
0.48	150	50	2007	0.489	2194
0.48	300	50	2261	0.492	2422
0.58	300	50	2185	0.499	2336
0.58	400	50	2351	0.504	2409
0.58	500	50	2500	0.487	2744
0.68	300	50	2600	0.491	2781
0.68	400	50	2750	0.490	2860
0.68	500	50	2915	0.492	3095
0.76	300	50	3833/ 3743	0.497/0.494	4022/3943
0.76	400	50	4013	0.500	4301
0.76	500	50	3515/ 3971	0.492/0.493	3549/ 4287
0	100	80	1545	0.491	1597
0	200	80	1509	0.491	1525
0	300	80	1615	0.497	1672
0.13	100	80	2094/ 2394	0.499/0.494	2186/ 2517
0.13	200	80	2149/ 2324	0.497/0.491	2366/ 2401
0.26	100	80	2483/ 2461	0.500/0.502	2647/ 2680
0.26	200	80	2478/ 2610	0.507/0.497	2525/ 2799
0.26	300	80	2594/ 2719	0.490/0.499	2736/ 2844
0.37	100	80	3003/ 2992	0.506/0.490	3245/ 3117
0.37	200	80	3184/ 3209	0.496/0.488	3396/ 3485
0.37	300	80	3056/ 3302	0.499/0.499	3304/ 3754
0.48	100	80	3644	0.511	3802
0.48	200	80	3786	0.507	3947
0.48	300	80	3395	0.494	3412
0.58	300	80	4433	0.498	4566
0.58	400	80	4612	0.489	4968
0.58	500	80	4878	0.497	5148
0.68	300	80	5818	0.491	6223
0.68	400	80	6304	0.496	6684
0.68	500	80	6864	0.498	7004
0.76	300	80	7431	0.504	7651
0.76	400	80	7797	0.501	7997
0.76	500	80	8162	0.514	8450

Table A.4: k_p^{cop} values for BMA/HEA PLP copolymerizations in 50 v% MIBK; two values show duplicates

f_{HEA}	υ (Hz)	T (°C)	k_p^{DRI} (L·mol^{-1}·s^{-1})	L1/L2	k_p^{LS} (L·mol^{-1}·s^{-1})
0	50	50	807	0.495	914
0	100	50	841	0.479	927
0.13	25	50	970	0.502	1055
0.13	50	50	962	0.511	1030
0.13	100	50	1097	0.476	1174
0.26	50	50	1123	0.493	1199
0.26	100	50	1084	0.490	1207
0.26	150	50	1218	0.514	1376
0.37	50	50	1596	0.501	1680
0.37	100	50	1388	0.478	1492
0.37	150	50	1308	0.479	1439
0.48	125	50	1778	0.488	1921
0.48	175	50	1664	0.496	1785
0.48	225	50	1679	0.498	1794
0.58	125	50	2600	0.504	2749
0.58	175	50	2597	0.514	2671
0.58	225	50	3074	0.489	3218
0.68	300	50	2872	0.493	3026
0.68	400	50	3109	0.497	3543
0.68	500	50	3376	0.483	3616
0	100	80	1545	0.482	1597
0	200	80	1509	0.501	1525
0.13	100	80	2050	0.492	2186
0.13	200	80	2088	0.500	2215
0.13	100	80	2130	0.497	2364
0.26	200	80	2393	0.489	2476
0.26	300	80	2445	0.487	2596
0.26	100	80	2407	0.506	2540
0.37	200	80	3157	0.504	3366
0.37	300	80	2975	0.475	3147
0.37	100	80	2980	0.479	3186
0.48	200	80	3534	0.483	3704
0.48	300	80	3363	0.491	3596
0.48	300	80	3691	0.504	3829
0.58	400	80	4262	0.517	4492
0.58	500	80	4655	0.473	4801
0.68	500	80	6000	0.481	6402
0.68	300	80	5821	0.480	6008

Table A.5: k_p^{cop} values for BMA/HEA PLP copolymerizations in 50 v% BPi; two values show duplicates

f_{HEA}	υ (Hz)	T (°C)	k_p^{DRI} (L·mol^{-1}·s^{-1})	L1/L2	k_p^{LS} (L·mol^{-1}·s^{-1})
0	40	50	794	0.504	826
0	80	50	890	0.532	941
0.13	40	50	978	0.524	1006
0.13	80	50	984	0.501	1014
0.37	40	50	1411	0.507	1546
0.37	80	50	1337	0.487	1398
0.58	80	50	2170	0.485	2280
0.58	100	50	2248	0.501	2414
0	60	80	1633	0.524	1711
0	120	80	1696	0.513	1786
0.13	60	80	1950	0.522	2049
0.13	120	80	1974	0.490	2002
0.37	60	80	2751	0.510	2906
0.37	120	80	2758	0.497	2893
0.58	60	80	4076	0.495	4217
0.58	120	80	4465	0.495	4454

Table A.6: k_p^{cop} values for BMA/HEA PLP copolymerizations in 50 v% xylenes; two values show duplicates

f_{HEA}	υ (Hz)	T (°C)	k_p^{DRI} (L·mol^{-1}·s^{-1})	L1/L2	k_p^{LS} (L·mol^{-1}·s^{-1})
0	50	50	801	0.490	829
0	100	50	917	0.522	1001
0.13	50	50	925	0.484	1021
0.13	100	50	1042	0.507	1186
0.37	50	50	1428	0.475	1596
0.37	100	50	1509	0.461	1675
0.58	50	50	2333	0.464	2450
0.58	100	50	2235	0.459	2421
0.76	75	50	3751	0.460	3910
0.76	150	50	3999	0.467	4056
0	75	80	1596	0.479	1670
0	150	80	1851	0.527	1958
0.13	75	80	1913	0.483	2063
0.13	150	80	2075	0.478	2198
0.37	75	80	3024	0.473	3217
0.37	150	80	2862	0.474	3041
0.58	75	80	4623	0.466	4850
0.58	150	80	5203	0.462	5377
0.76	90	80	7870	0.470	8104
0.76	180	80	8291	0.472	8364

Table A.7: k_p^{cop} values for BMA/HEA PLP copolymerizations in 50 v% BuOH; two values show duplicates

f_{HEA}	υ (Hz)	T (°C)	k_p^{DRI} (L·mol^{-1}·s^{-1})	L1/L2	k_p^{LS} (L·mol^{-1}·s^{-1})
0	50	50	1190	0.500	1214
0	100	50	1175	0.511	1207
0.13	50	50	1122	0.484	1243
0.13	100	50	1179	0.501	1281
0.37	50	50	1445	0.495	1519
0.37	100	50	1548	0.462	1674
0.58	50	50	2548	0.501	2758
0.58	100	50	2014	0.478	2148
0.76	50	50	4717	0.471	4952
0.76	100	50	4225	0.484	4451
0.93	80	50	13329	0.469	13670
0.93	160	50	12794	0.475	12968
0	75	80	2154	0.504	2214
0	150	80	2116	0.497	2208
0.13	75	80	2153	0.507	2274
0.13	150	80	2268	0.484	2339
0.37	75	80	3053	0.519	3107
0.37	150	80	2900	0.480	3061
0.58	75	80	4005	0.496	4206
0.58	150	80	4273	0.489	4388
0.76	90	80	6011	0.472	6250
0.76	180	80	5745	0.481	5896

Table A.8: k_p^{cop} values for BMA/HEA PLP copolymerizations in 50 v% DMF; two values show duplicates

f_{HEA}	υ (Hz)	T (°C)	k_p^{DRI} (L·mol^{-1}·s^{-1})	L1/L2	k_p^{LS} (L·mol^{-1}·s^{-1})
0	50	50	851	0.479	874
0	100	50	972	0.519	1004
0.13	50	50	920	0.478	983
0.13	100	50	1039	0.501	1079
0.37	50	50	1131	0.461	1183
0.37	100	50	1276	0.496	1356
0.58	50	50	1714	0.478	1807
0.58	100	50	1657	0.463	1728
0.76	50	50	2563	0.464	2727
0.76	100	50	2894	0.478	3017
0.93	160	50	4734	0.457	4930
0	75	80	1657	0.480	1723
0	150	80	1843	0.507	1902
0.13	75	80	1854	0.473	1928

0.13	150	80	2071	0.490	2203
0.37	75	80	2574	0.494	2636
0.37	150	80	2510	0.467	2682
0.58	75	80	3537	0.479	3699
0.58	150	80	3479	0.468	3642
0.76	90	80	5362	0.469	5561
0.76	180	80	6254	0.484	6328

IR measurements

To further explore the effects of H-bonding on the system some supplementary infrared (IR) spectroscopy measurements were performed. All previously used solvents were investigated at different monomer compositions (50 vol% solvent), except esters, which had significant overlays with the (meth-) acrylates CO-swing at 1710 cm^{-1}, which was chosen as a reference peak. The presence of H-bonding, if present, leads to a second peak with a maximum around 1700 cm^{-1} due to the interaction of H-bonds with the CO-acceptors[103] Ketone signals could also not be completely separated from monomer signals, but showed sufficient information. Although these measurements were done at room temperature, examining the relative changes in peak intensities is useful.

As outlined above the importance and influence of hydrogen bonding also seems to be dependent on monomer composition. It was shown that effects are already strong at low concentration of the H-donating component. Figure A.1 shows the respective IR-spectra for varying HEA concentrations, already zoomed into the wavelength area of interest. Without any H-bonding present the CO-swing for BMA in absence of HEA remains very distinct at 1710 cm^{-1} without much broadening in bulk and most solvents (except BuOH). But, as shown in the bulk case, as soon as HEA is added into the solution a clear broadening of the peak is visible including the appearance of the second maxima. The differences seen with increasing HEA addition between 30% and pure HEA is not as large as the leap observed between pure BMA and 30% HEA mixtures. The first increase accounts for more than 50% of the total growth of intensity, as detected by relative area and height. This behaviour could be observed for all solvents other than BuOH and DMF. H-bonding is always observed in the presence of BuOH, as seen from the IR-

measurements. With increasing HEA content the CO-swing only increases minimally. In contrast, DMF clearly disrupts H-bonding with no visible peak developing at 1700 cm^{-1} for all mixtures. This again underlines the postulated disruption and promotion mechanism in highly interacting solvents. In good agreement, similar spectroscopy results have been obtained before for HEMA/ST systems in bulk, DMF, Xylenes and BuOH.[3] The xylenes results also reveal a very strong CO-swing once H-bonds are present, which are of a similar magnitude as seen in BuOH. This is an indication of the H-bonding introduced by the addition of HEA. The same trend is visible in MIBK but is less obvious in the spectra due to its quality. The "negative" peak seen in here unfortunately occurs due to the solvents carbonyl swing, which has been removed from the spectra based on previous solvent-only measurements. It may also be that the peaks are not as pronounced, as the ketone CO also can act as a weak H-acceptor. This also shows that the providing H-donor is of crucial relevance for the systems kinetics. Whereas BuOH and xylenes almost have the same swings present the kinetic parameters are very different. Whereas solvent donors promote the whole system as seen from composition and k_P^{cop} analysis, HEA as a donor tends to promote itself in non-interacting solvents. This behaviour seems to be most pronounced in xylenes, a solvent where HEA-rich polymers have limited solubility. Consecutively it can be assumed that HEA molecules interact stronger with each other and create local pockets with concentration gradients. These gradient areas may also be present around HEA rich polymer radicals, affecting the propagation.

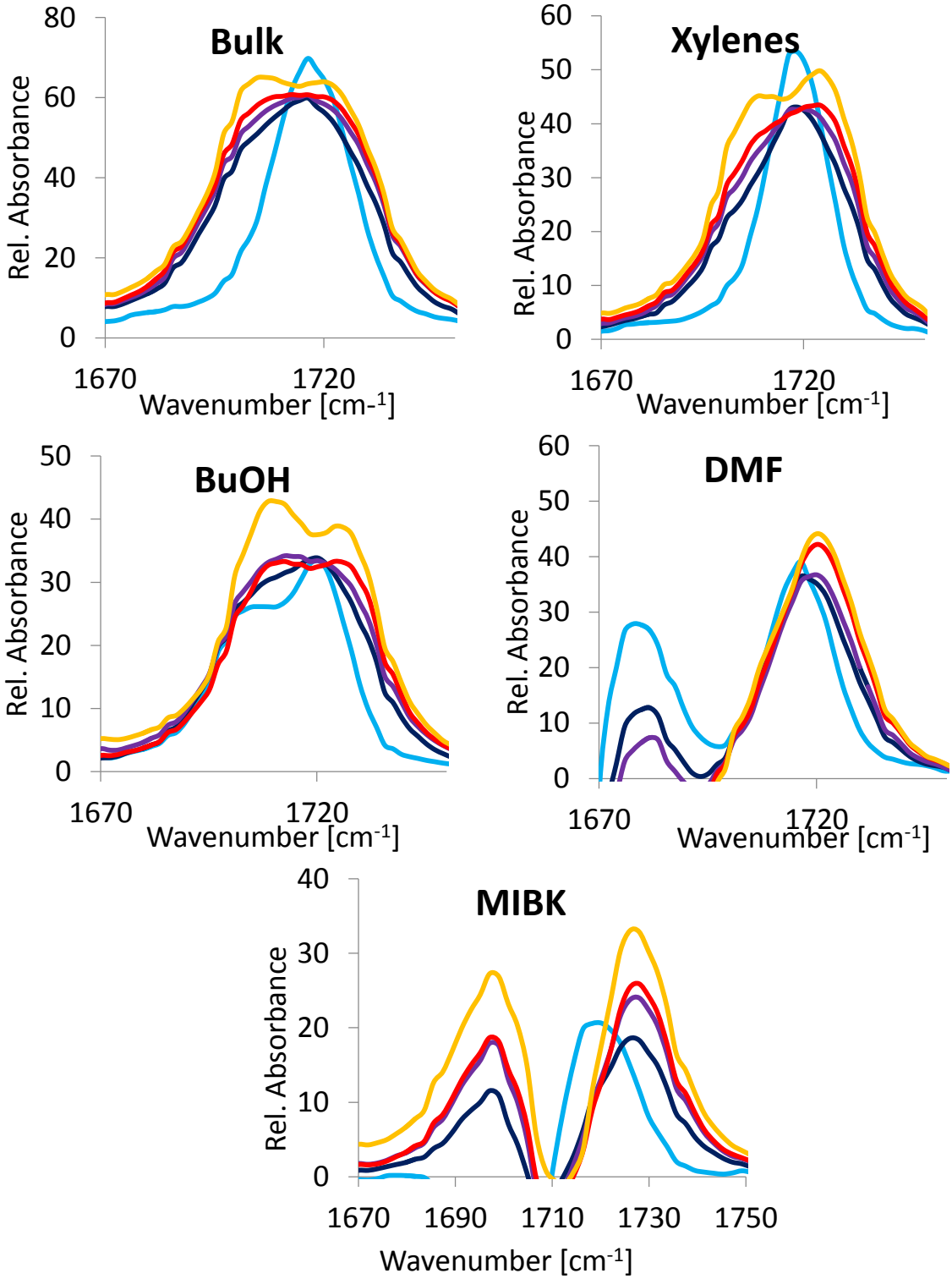

Figure A.1: IR-spectra of BMA/HEA samples in bulk and solution (50 v%) as a function of f_{HEA}; a) bulk, b) xylenes, c) BuOH, d) DMF, e) MIBK (lines represent absorbance of BMA (blue), BMA/HEA 70/30 v% (dark blue), 50 v% (purple), 70 v% (red) and HEA (yellow)

TM and IPUE models

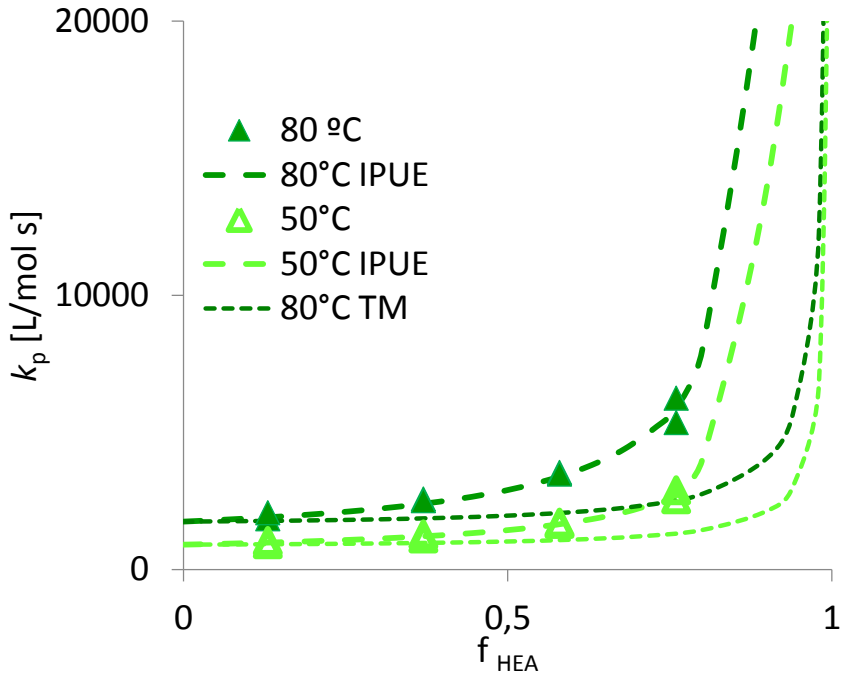

Figure A.2: TM and IPUE fits for k_p^{cop} data for BMA/HEA in DMF; s_{BMA} = 8.25, s_{HEA} = 1.10

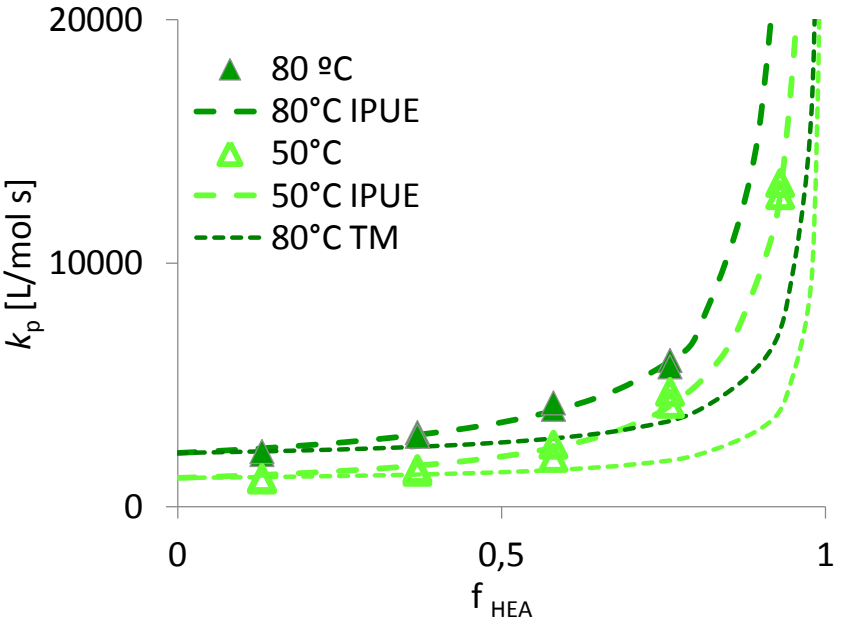

Figure A.3: TM and IPUE fits for k_p^{cop} data for BMA/HEA in BuOH; s_{BMA} = 4.30, s_{HEA} = 1.05

Tabulated NMR data for copolymer composition analysis for BA/HEA, BA/MEA and BMA/MEA systems

Table A.9: Copolymer composition for BA/HEA samples produced by PLP in bulk, xylenes, MIBK, BuOH and DMF

Bulk		**Xylenes**		**MIBK**		**BuOH**		**DMF**	
$\mathbf{f_{HEA}}$	F_{HEA}	f_{HEA}	F_{HEA}	f_{HEA}	F_{HEA}	f_{HEA}	F_{HEA}	f_{HEA}	F_{HEA}
0.13	0.27	0.13	0.16	0.13	0.17	0.13	0.14	0.13	0.11
0.25	0.44	0.25	0.34	0.25	0.281	-	-	0.25	0.22
0.36	0.52	0.36	0.50	0.36	0.484	0.36	0.40	0.36	0.35
0.47	0.65	-	-	-	-	-	-	0.47	0.47
0.57	0.69	0.57	0.75	0.57	0.681	0.57	0.62	0.57	0.58
0.66	0.82	0.66	0.82	0.66	0.77	-	-	0.66	0.65
-	-	0.75	0.86	-	-	0.75	0.79	0.75	0.73
0.84	0.91	-	-	0.84	0.883	-	-	-	
0.92	0.96	0.92	0.95	0.92	0.9517	0.92	0.95	-	

Table A.10: Copolymer composition for BA/MEA samples produced by PLP in bulk, BuOH and DMF

Bulk		**BuOH**		**DMF**	
$\mathbf{f_{MEA}}$	F_{MEA}	f_{MEA}	F_{MEA}	f_{MEA}	F_{MEA}
0.11	0.09	0.11	0.10	0.11	0.11
0.32	0.31	0.32	0.32	0.32	0.30
0.52	0.53	0.52	0.53	0.52	0.51
0.72	0.74	0.72	0.73	0.72	0.70
0.91	0.91	0.91	0.92	0.91	0.92

Table A.11: Copolymer composition for BMA/MEA samples produced by PLP in bulk, xylenes, MIBK, BuOH and DMF

Bulk		**BuOH**		DMF	
$\mathbf{f_{MEA}}$	F_{MEA}	f_{MEA}	F_{MEA}	f_{MEA}	F_{MEA}
0.12	0.09	0.12	0.06	0.12	0.05
0.35	0.21	0.35	0.19	0.35	0.18
0.55	0.35	0.55	0.35	0.55	0.33
0.74	0.55	0.74	0.53	0.74	0.52
0.92	0.81	0.92	0.82	0.92	0.79

Tabulated PLP data for k_p^{cop} and supplementary graphs for BA/HEA, BA/ MEA and BMA/MEA systems

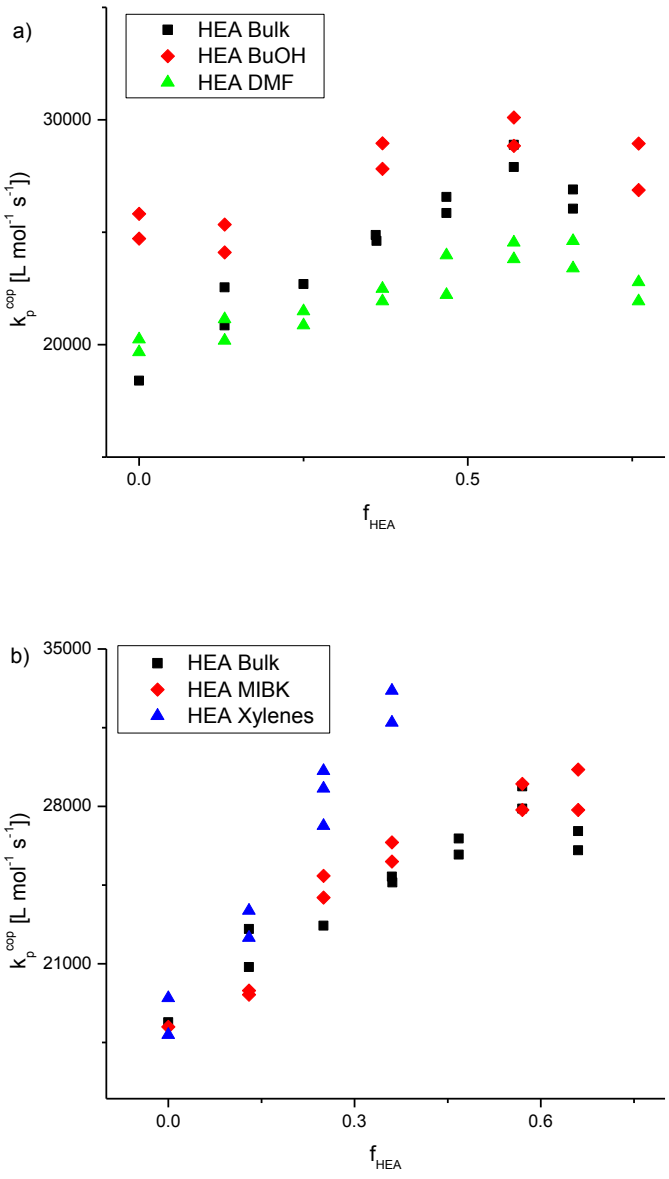

Figure A.4: a) Evolution of k_p^{cop} for BA/HEA as a function of HEA monomer mole fraction at 30 °C in (a) bulk (black), BuOH (red) and DMF (green), and (b) in bulk (black), MIBK (red) and xylenes (blue).

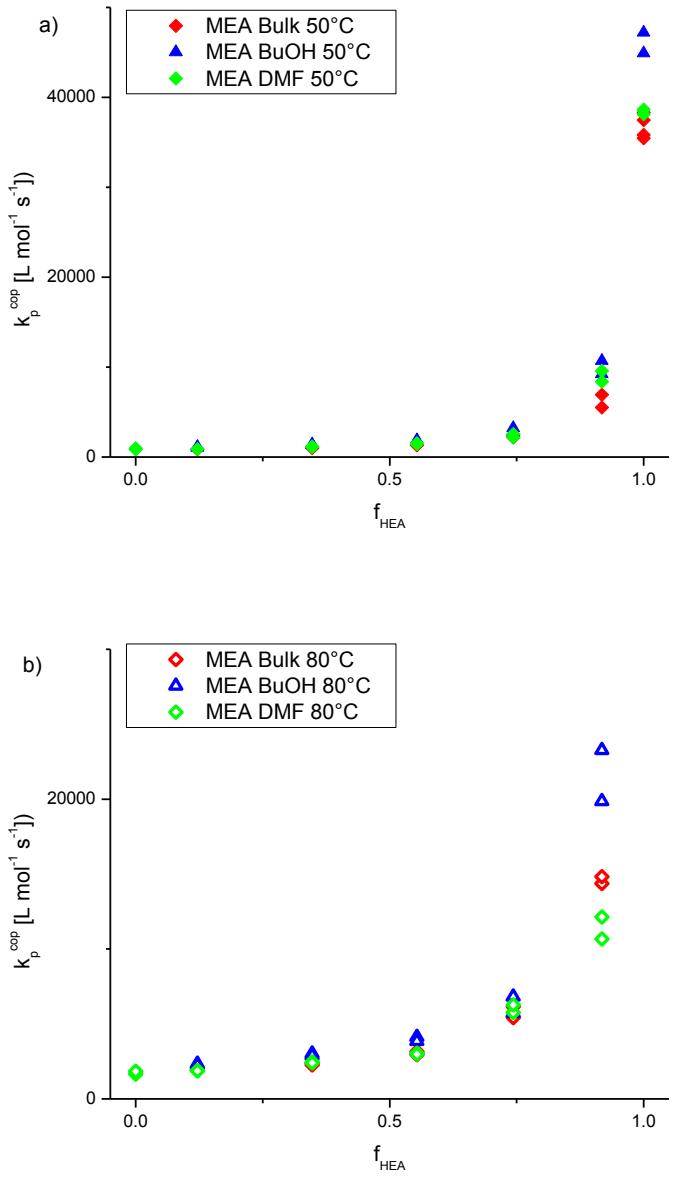

Figure A.5: a) Evolution of k_p^{cop} for BMA/MEA as a function of MEA monomer mole fraction at 50 °C in (a) bulk (red), BuOH (blue) and DMF (green), and (b) at 80 °C in the respective solvents.

Table A.12: k_p^{cop} values for BA/HEA PLP copolymerizations in bulk

f_{HEA}	υ (Hz)	T (°C)	k_p^{DRI} (L·mol^{-1}·s^{-1})	L1/L2	k_p^{LS} (L·mol^{-1}·s^{-1})
0	400	30	18400	0.514	19005
0.13	400	30	20847	0.571	21417
0.13	500	30	22549	0.524	25063
0.25	500	30	22694	0.529	22240
0.36	400	30	24871	0.495	26767
0.36	500	30	24617	0.567	27110
0.47	400	30	25854	0.555	26237
0.47	500	30	26568	0.492	28219
0.57	400	30	27895	0.559	27789
0.57	500	30	28884	0.527	28910
0.66	400	30	26050	0.503	29501
0.66	500	30	26903	0.559	27374
0	450	50	26246	0.522	25666
0	500	50	27620	0.553	28304
0.13	450	50	30836	0.515	32934
0.13	500	50	31943	0.497	34510
0.25	450	50	34699	0.511	36775
0.25	500	50	34215	0.512	35183
0.36	400	50	38229	0.544	41540
0.36	500	50	40221	0.517	40854
0.47	450	50	41346	0.495	41278
0.47	500	50	42446	0.550	46380
0.60	450	50	41971	0.530	44917
0.60	500	50	44090	0.499	43223

Table A.13: k_p^{cop} values for BA/HEA PLP copolymerizations in 50 v% BuOH

f_{HEA}	υ (Hz)	T (°C)	k_p^{DRI} (L·mol^{-1}·s^{-1})	L1/L2	k_p^{LS} (L·mol^{-1}·s^{-1})
0	300	30	25813	0.501	25715
0	400	30	24717	0.513	24189
0.13	300	30	24106	0.515	25521
0.13	400	30	25338	0.499	26179
0.36	300	30	27820	0.533	29698
0.36	400	30	28956	0.537	30515
0.57	300	30	28845	0.558	28388
0.57	400	30	30104	0.541	32744
0.76	300	30	26873	0.510	27268
0.76	400	30	28938	0.544	29821
0	420	50	33142	0.515	35506
0	500	50	35714	0.548	34909
0.13	420	50	33379	0.554	32868

0.13	500	50	36004	0.516	37282
0.37	420	50	37912	0.507	40157
0.37	500	50	40407	0.561	40180
0.58	420	50	41416	0.506	41954
0.58	500	50	44410	0.571	47102

Table A.14: k_p^{cop} values for BA/HEA PLP copolymerizations in 50 v% DMF

$\mathbf{f_{HEA}}$	υ **(Hz)**	**T (°C)**	$\boldsymbol{k_p^{DRI}}$ **(L·mol^{-1}·s^{-1})**	**L1/L2**	$\boldsymbol{k_p^{LS}}$ **(L·mol^{-1}·s^{-1})**
0	300	30	19672	0.567	19171
0	400	30	20241	0.535	21773
0.13	300	30	20179	0.554	20054
0.13	400	30	21139	0.528	22855
0.25	300	30	20860	0.518	22638
0.25	400	30	21484	0.501	22277
0.36	300	30	21926	0.559	23094
0.36	400	30	22484	0.575	23282
0.47	380	30	22217	0.521	22957
0.47	480	30	23977	0.564	24319
0.57	380	30	23812	0.545	24060
0.57	480	30	24549	0.570	23832
0.66	380	30	23395	0.551	25197
0.66	480	30	24617	0.570	24506
0.76	380	30	21933	0.509	23112
0.76	480	30	22782	0.500	22725
0	380	50	29221	0.503	30620
0	500	50	31204	0.530	31870
0.13	380	50	29797	0.499	29407
0.13	500	50	32439	0.530	33298
0.25	380	50	31794	0.532	33780
0.25	500	50	34244	0.564	37196
0.36	380	50	32751	0.514	32664
0.36	500	50	36234	0.553	37301
0.47	400	50	35246	0.518	36118
0.47	500	50	35349	0.530	37921
0.57	400	50	34916	0.494	36012
0.57	500	50	36593	0.538	35854
0.66	400	50	35453	0.550	37388
0.66	500	50	36248	0.498	39318
0.76	400	50	31621	0.556	32015
0.76	500	50	33180	0.540	35093

Table A.15: k_p^{cop} values for BA/HEA PLP copolymerizations in 50 v% MIBK

f_{HEA}	υ (Hz)	T (°C)	k_p^{DRI} (L·mol^{-1}·s^{-1})	L1/L2	k_p^{LS} (L·mol^{-1}·s^{-1})
0	420	30	18195	0.542	18805
0.13	320	30	19623	0.528	19194
0.13	420	30	19802	0.522	20327
0.25	320	30	24913	0.509	26128
0.25	420	30	23947	0.545	24157
0.36	320	30	25547	0.554	26283
0.36	420	30	26398	0.551	26184
0.57	320	30	27844	0.523	29850
0.57	420	30	29005	0.527	28826
0.66	320	30	27845	0.499	27577
0.66	420	30	29637	0.540	31513
0	400	50	29833	0.561	29989
0	500	50	30493	0.537	32525
0.13	400	50	28589	0.564	31097
0.13	500	50	29292	0.564	30149
0.25	400	50	30123	0.520	30799
0.25	500	50	32476	0.573	34135
0.36	400	50	37757	0.526	38059
0.36	500	50	38554	0.498	41707
0.57	400	50	37816	0.557	39040
0.57	500	50	41593	0.573	45252

Table A.16: k_p^{cop} values for BA/HEA PLP copolymerizations in 50 v% Xylenes

f_{HEA}	υ (Hz)	T (°C)	k_p^{DRI} (L·mol^{-1}·s^{-1})	L1/L2	k_p^{LS} (L·mol^{-1}·s^{-1})
0	320	30	17841	0.515	18414
0	420	30	19477	0.499	20528
0.13	330	30	22156	0.569	23248
0.13	430	30	23361	0.499	22748
0.25	400	30	28800	0.504	29051
0.25	500	30	27139	0.547	28571
0.25	500	30	29580	0.523	28966
0.36	340	30	31729	0.536	31667
0.36	440	30	33148	0.503	35816
0	400	50	28732	0.511	27986
0	500	50	30514	0.571	29643
0.13	400	50	33647	0.529	35846
0.13	500	50	35788	0.506	37776
0.25	400	50	41421	0.523	43241
0.25	500	50	42045	0.569	45606
0.37	400	50	46098	0.500	48455
0.37	500	50	49919	0.571	53319

Table A.17: k_p^{cop} values for BA/MEA PLP copolymerizations in bulk;[a] samples polymerized with 7 mM/L photoinitiator

f_{MEA}	υ (Hz)	T (°C)	k_p^{DRI} (L·mol^{-1}·s^{-1})	L1/L2	k_p^{LS} (L·mol^{-1}·s^{-1})
0	400	30	18400	0.514	19005
0.11	380	30	18165	0.535	19439
0.11	480	30	18900	0.534	19379
0.32	380	30	19212	0.564	20235
0.32	480	30	20137	0.562	20992
0.53	380	30	20228	0.503	20107
0.53	480	30	20902	0.497	21286
0.72	380	30	21251	0.495	21519
0.72	480	30	22784	0.560	22558
0.91	380	30	23095	0.536	24876
0.91	480	30	24362	0.534	24145
1	380	30	22819	0.563	22171
1	480	30	24459	0.516	26472
1	380 [a]	30	23525	0.502	22885
1	480 [a]	30	24459	0.570	23732
0	450	50	26246	0.522	27438
0.11	400	50	23927	0.549	24263
0.11	500	50	26391	0.567	28842
0.32	400	50	25903	0.562	26720
0.32	500	50	27681	0.567	28404
0.53	400	50	29765	0.518	32460
0.53	500	50	30273	0.568	31474
0.72	400	50	32807	0.567	33693
0.72	500	50	32532	0.502	32697
0.91	400	50	35147	0.512	37468
0.91	500	50	35384	0.527	36642
1	400	50	38285	0.548	40858
1	500	50	37479	0.509	39395
1	400[a]	50	35822	0.491	35285
1	500 [a]	50	35468	0.555	36308

Table A.18: k_p^{cop} values for BA/MEA PLP copolymerizations in 50 v% BuOH

f_{MEA}	υ (Hz)	T (°C)	k_p^{DRI} (L·mol^{-1}·s^{-1})	L1/L2	k_p^{LS} (L·mol^{-1}·s^{-1})
0	300	30	22396	0.526	22841
0	400	30	22867	0.544	23047
0.11	380	30	22938	0.522	22791
0.11	480	30	24072	0.560	25114
0.32	380	30	25022	0.504	25697
0.32	480	30	26261	0.566	27683
0.53	380	30	27302	0.523	27451

0.53	480	30	28453	0.494	30445
0.72	380	30	29310	0.496	31342
0.72	480	30	30963	0.512	30795
0.91	380	30	31184	0.560	33705
0.91	480	30	32726	0.543	31896
1	380	30	31921	0.573	33846
1	480	30	33284	0.557	36195
0	420	50	33295	0.542	36306
0	500	50	35689	0.516	34943
0.11	450	50	34580	0.519	34811
0.11	500	50	35007	0.515	34325
0.32	450	50	36120	0.556	36128
0.32	500	50	37639	0.493	37914
0.53	450	50	39417	0.523	42446
0.53	500	50	39919	0.530	40779
0.72	450	50	41703	0.521	43222
0.72	500	50	44391	0.507	46893
0.91	450	50	44673	0.555	47634
0.91	500	50	45890	0.520	48339
1	450	50	44907	0.544	46390
1	500	50	47226	0.512	48872

Table A.19: k_p^{cop} values for BMA/MEA PLP copolymerizations in bulk

$\mathbf{f_{MEA}}$	υ **(Hz)**	**T (°C)**	$\boldsymbol{k_p^{DRI}}$ **(L·mol^{-1}·s^{-1})**	**L1/L2**	$\boldsymbol{k_p^{LS}}$ **(L·mol^{-1}·s^{-1})**
0.12	20	50	803	0.539	833
0.12	40	50	886	0.548	875
0.35	23	50	993	0.525	1029
0.35	43	50	1107	0.543	1172
0.55	26	50	1313	0.492	1395
0.55	46	50	1449	0.480	1470
0.74	75	50	2196	0.507	2306
0.74	120	50	2481	0.540	2505
0.92	150	50	5521	0.546	5983
0.92	300	50	6932	0.537	7404
0.12	50	80	1734	0.515	1776
0.12	100	80	1927	0.535	2095
0.35	55	80	2264	0.492	2402
0.35	105	80	2392	0.549	2595
0.55	60	80	2946	0.501	3184
0.55	110	80	3161	0.498	3235
0.74	300	80	6156	0.527	6265
0.74	400	80	5419	0.539	5851
0.92	400	80	14366	0.520	15595
0.92	500	80	14833	0.538	16019

Table A.20: k_p^{cop} values for BMA/MEA PLP copolymerizations in 50 v% BuOH

f_{MEA}	υ (Hz)	T (°C)	k_p^{DRI} (L·mol^{-1}·s^{-1})	L1/L2	k_p^{LS} (L·mol^{-1}·s^{-1})
0.12	20	50	1048	0.540	1032
0.12	40	50	1139	0.536	1111
0.35	40	50	1434	0.517	1501
0.35	60	50	1338	0.505	1426
0.55	60	50	1859	0.550	1970
0.55	80	50	1865	0.550	1864
0.74	100	50	2721	0.507	2860
0.74	150	50	3243	0.495	3341
0.92	380	50	9227	0.531	9619
0.92	480	50	10702	0.492	11091
0.12	50	80	2332	0.493	2372
0.12	100	80	2249	0.512	2255
0.35	70	80	3016	0.527	3082
0.35	120	80	2872	0.503	3000
0.55	90	80	4118	0.510	4254
0.55	140	80	3847	0.533	3864
0.74	200	80	5727	0.532	5697
0.74	300	80	6823	0.501	6838
0.92	400	80	19850	0.490	20626
0.92	500	80	23262	0.512	23688

Table A.21: k_p^{cop} values for BMA/MEA PLP copolymerizations in 50 v% DMF

f_{MEA}	υ (Hz)	T (°C)	k_p^{DRI} (L·mol^{-1}·s^{-1})	L1/L2	k_p^{LS} (L·mol^{-1}·s^{-1})
0.12	20	50	869	0.510	880
0.12	40	50	891	0.513	891
0.35	40	50	1159	0.547	1131
0.35	60	50	1120	0.509	1170
0.55	60	50	1440	0.501	1458
0.55	80	50	1523	0.506	1497
0.74	150	50	2188	0.521	2384
0.74	200	50	2556	0.496	2727
0.92	400	50	8380.	0.518	8886
0.92	500	50	9562	0.548	10245
1	450	50	38638	0.554	38632
1	500	50	38133	0.538	38831
0.12	50	80	1899	0.506	1873
0.12	100	80	1879	0.496	2000
0.35	70	80	2464	0.534	2408
0.35	120	80	2404	0.540	2479
0.55	90	80	3051	0.507	3052

0.55	140	80	2985	0.515	3106
0.74	150	80	5764	0.546	5746
0.74	200	80	6277	0.507	6214
0.92	450	80	11664	0.492	12209
0.92	500	80	12143	0.554	12219

Comments and preliminary results on PLP-investigations for HEA homopolymers

To enhance the knowledge of H-bonding effects on reaction kinetics further PLP experimentation was performed with HEA homopolymerizations in bulk, DMF, BuOH, Xylenes and under aqueous conditions with solvent levels of 50 v%. Due to solubility issues in THF, samples were shipped to the University of Paderborn, Germany (at the group of Prof. Dirk Kuckling), to be analyzed via SEC, using dimethylacetamide (DMAc) as the eluent.

For the synthesis of these HEA homopolymers, but also HEA rich copolymers, special care needs to be taken for the following reasons. HEA being an acrylate is already assumed to be very reactive, with standard reaction times about 1-2 seconds in a PLP setup at 50 °C, as known form BA samples. However, the formation of polymer results in an instantaneous gel formation, if the manual control at the laser setup is being used, even at maximum frequencies of 500 Hz, where the formed polymer material should contain the lowest MM. It was found, that the formed polymer (despite being very low in conversion) coils up and forms regions of high viscosity or gel like regimes, especially close to the cuvette surface, where the laser beam initially hits the sample. With the accumulation of this material, it is assumed that viscosity increases, hence termination decreases resulting in the loss of PLP structure and the formation of high MM material. Again, the material was found to be very adhesive to glass surfaces, as formed material remained inside the cuvette, stuck to the surface. The solution for this problem was the use of the pulse sequence, implemented into the laser control software. Here, the exact number of pulses can be put in, which was found to be around 250-300 total shots. It is recommended to divide the total amount of shots into 3 separate bursts, which a ‘cool-down’ period of two seconds in between each burst (which can be all put into the software). The created polymer samples were then isolated through the precipitation in

diethyl ether, cooled through liquid nitrogen. The sticky homopolymer is easily separated, as supernatant liquids can be decanted before the samples are fully dried under vacuum at 60 °C. Multiple samples were then sent to Germany to be analyzed. Despite the efforts, prepared samples could not be analyzed using this setup, with a typical result shown in Figure A.6.

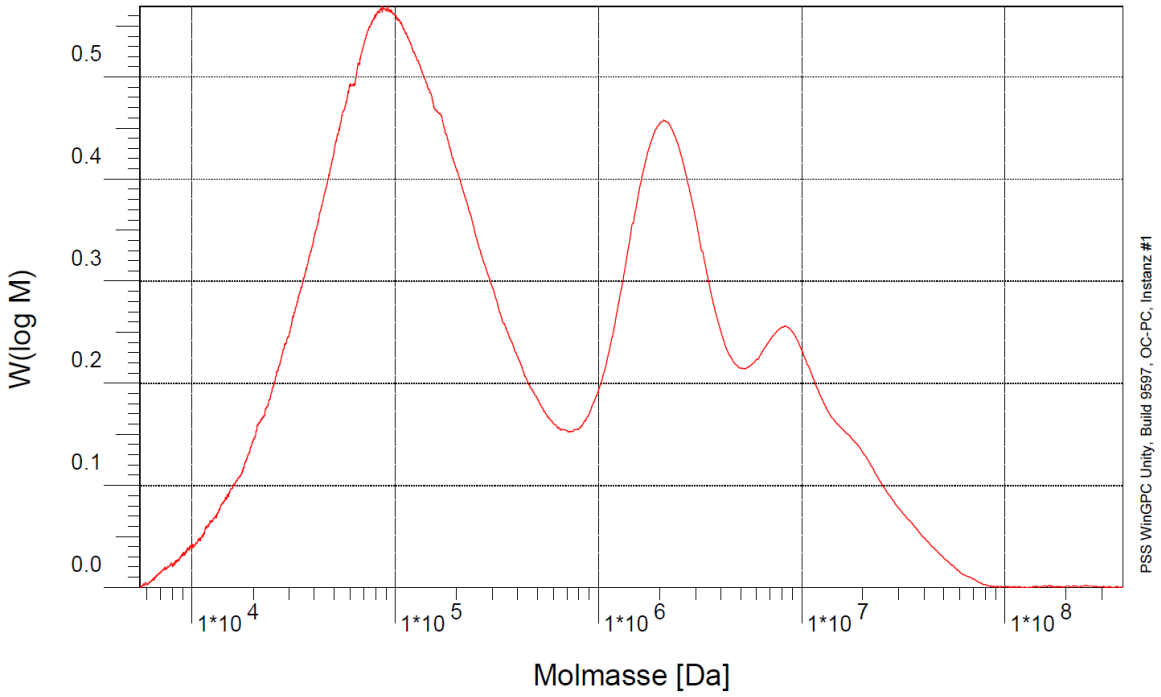

Figure A.6: MMD for HEA homopolymer analyzed in DMAc

All samples analyzed showed this typical bimodal distribution with maxima around 10^5 and 10^6 Da (usually $g \cdot mol^{-1}$). Whereas the first distribution does not show any kind of PLP structure, the one does look typical with several maxima. However, their respective positions are not in agreement with the consistency criterion, as values from first to second inflection point did not double. Whereas, there is no final explanation for these bizarre traces, H-bonding is suspected to play a role. Possible scenarios include multiple different HEA chains to coil up, appearing as one larger polymer chain in the SEC, as they could not be physically separated through the chromatography.

Other options to solve this remaining issue include to acetylate the hydroxyl functionality of HEA. However, with the increased MM of formed polymer, previously reported procedures are not as trivial,[201] due to solubility issues.

B. Appendix B: Supporting data for chapter 4

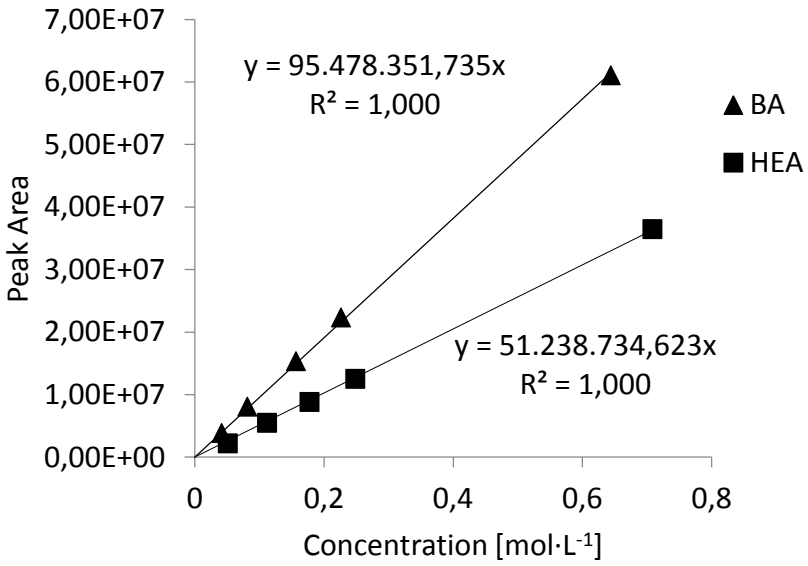

Figure B.1: External GC calibration curves for BA and HEA for the FID detector

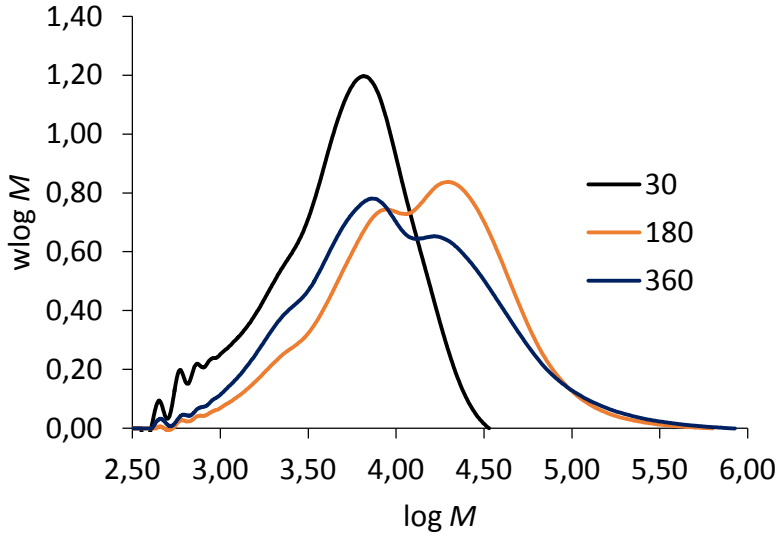

Figure B.2: MMD for BA/HEA copolymers (40 wt% HEA) prepared under semi-batch conditions in BPi at 138 °C. SEC traces are shown after 30 min, 180 min and 360 min

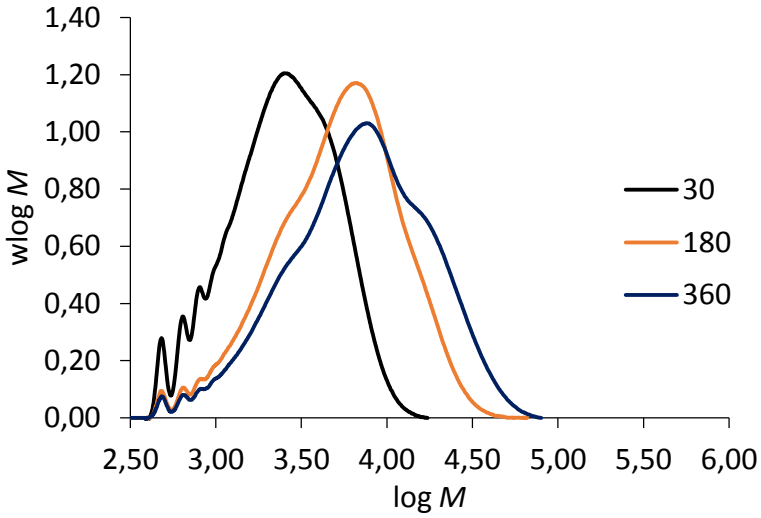

Figure B.3: MMD for BA homopolymers prepared under semi-batch conditions in BPi at 138 °C. SEC traces are shown after 30 min, 180 min and 360 min

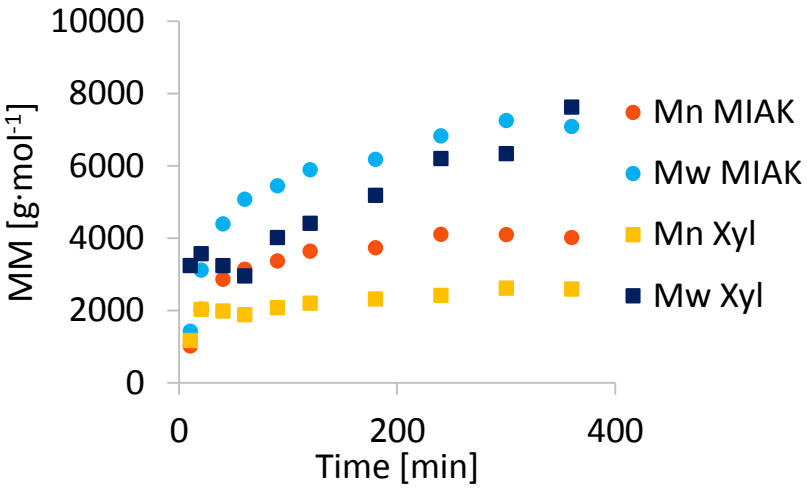

Figure B.4: Evolution of M_n and M_w for BA/HEA copolymerizations under semi-batch conditions at 138 °C in various solvents

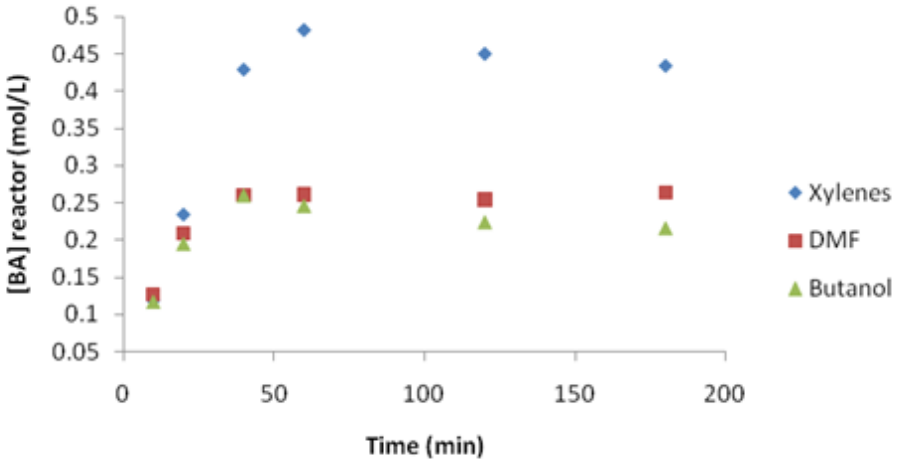

Figure B.5: Residual monomer concentration for BA homopolymerization prepared under semi-batch conditions in varying solvents at 138 °C.

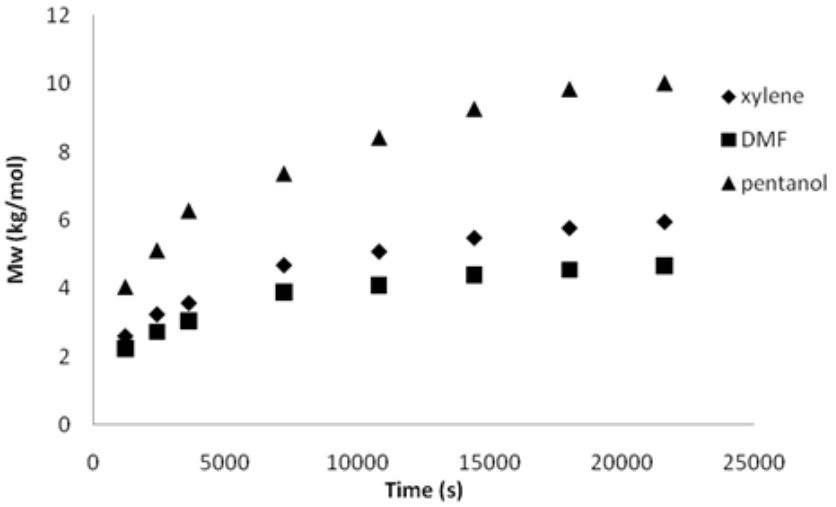

Figure B.6: Evolution of M_w averages for BA homopolymerization prepared under semi-batch conditions in varying solvents at 138 °C.

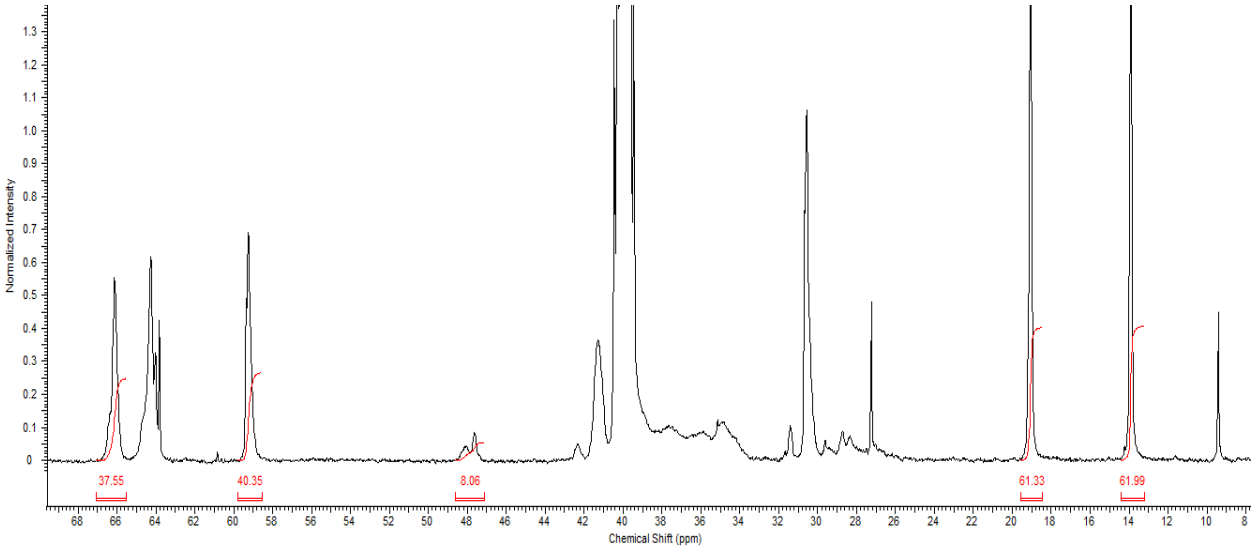

Figure B.7: Quantitative ^{13}C-NMR spectrum for BA/HEA copolymer prepared via semi-batch reaction in BPi at 138 °C, with the quaternary carbon at 48 ppm

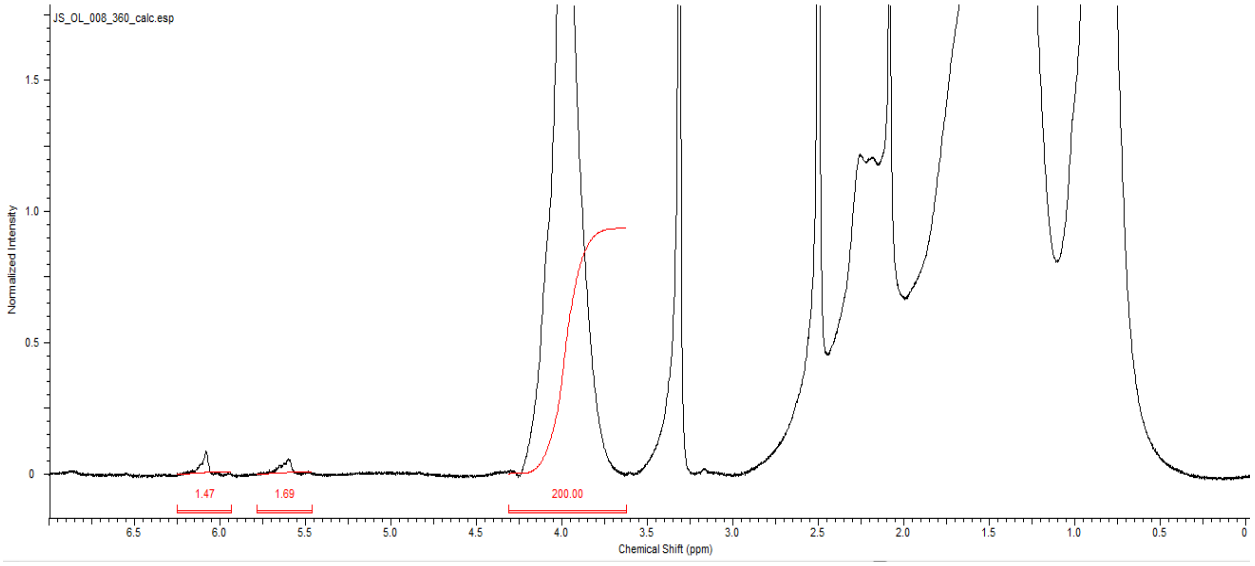

Figure B.8: ^{1}H-NMR spectrum for BA homopolymer prepared via semi-batch reaction in BPi at 138 °C, with residual macromer signals at 5.6 and 6.1 ppm

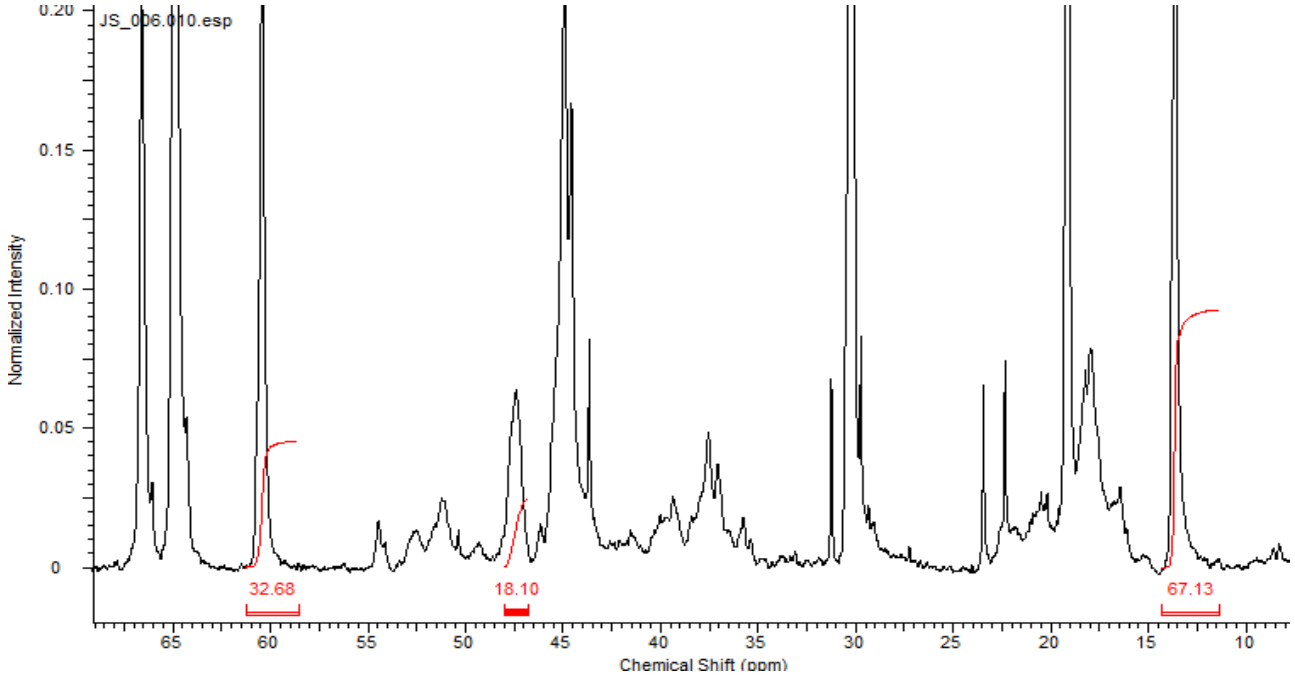

Figure B.9: Quantitative ^{13}C-NMR spectrum for BMA/HEA samples prepared via semi-batch reaction in MIAK at 138 °C

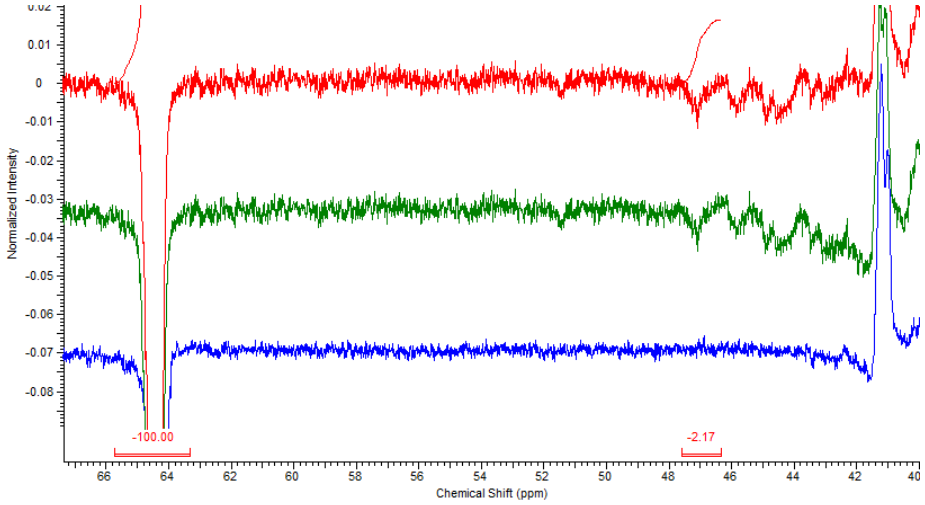

Figure B.10: Zoom into DEPT 135 spectra for BMA/BA copolymers with increasing acrylate content from top to bottom

C. Appendix C: Supporting data for chapter 5

Supplementary semi-batch reactions

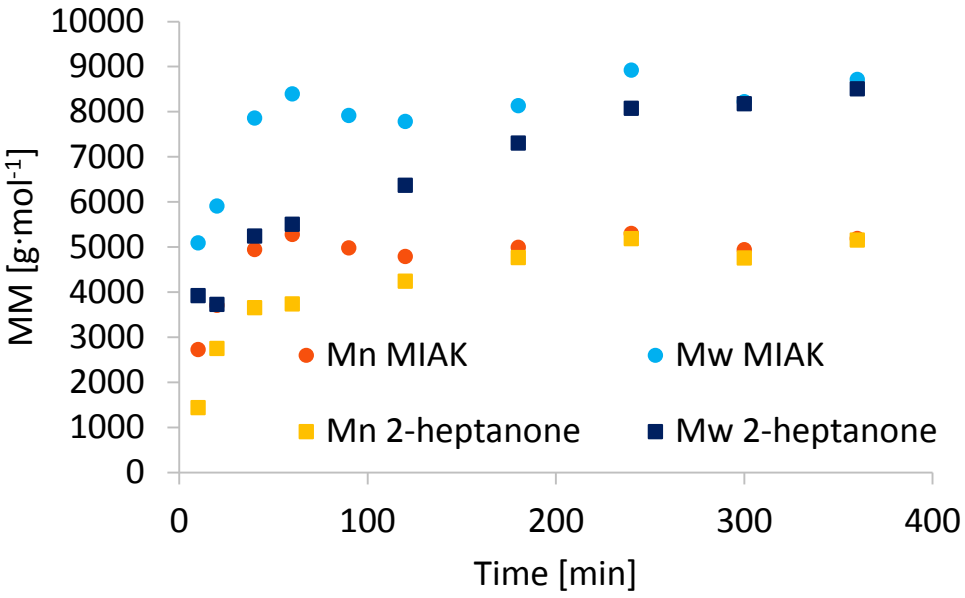

Figure C.1: Comparison of M_n and M_w between BMA/HEA semi-batch copolymerizations at 138 °C in different kinds of ketones

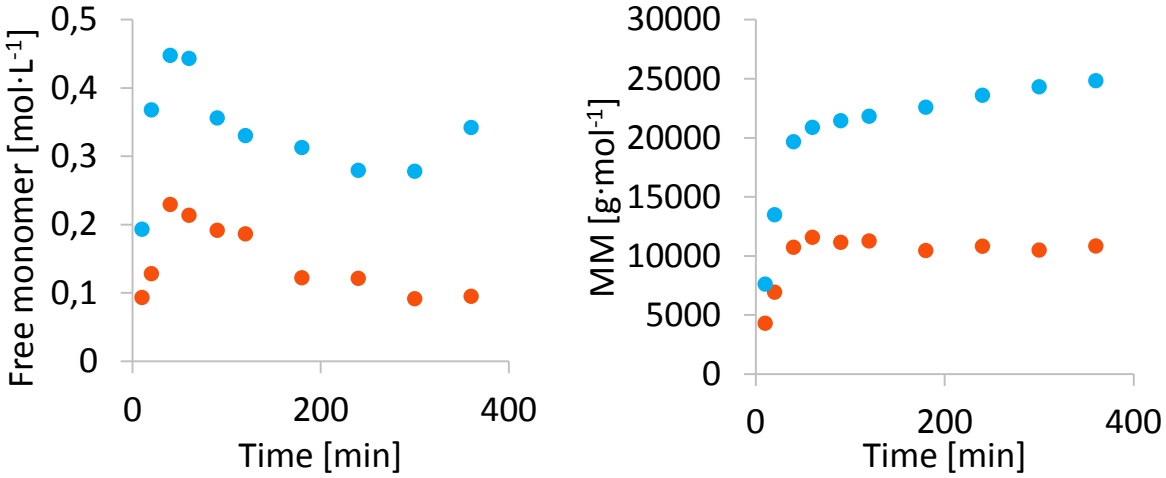

Figure C.2: Residual free monomer levels for BMA (●) and HEA (●, left) and evolutions of M_n (●) and M_w (●, right) for BMA/HEA semi-batch copolymerizations at 120 °C in MIBK

Small-scale PLP experiments with changing solvent contents

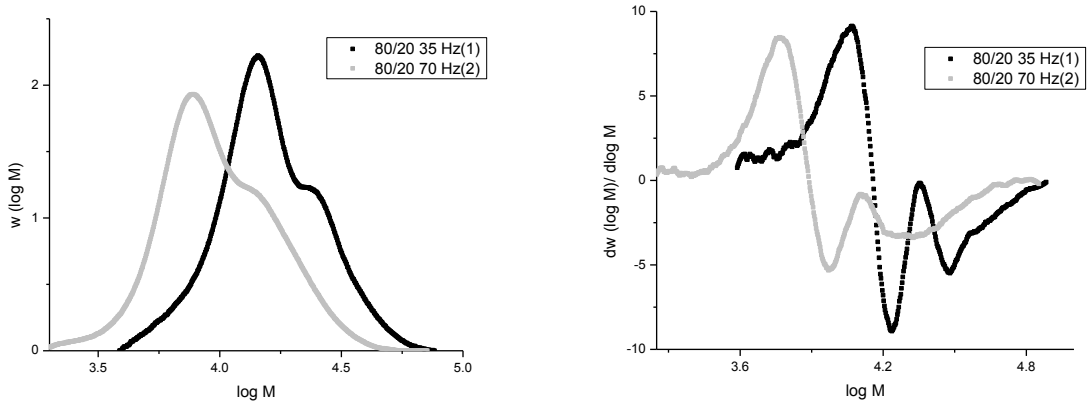

Figure C.3: SEC traces (left) and respective first derivative plots (right) for BMA/HEA copolymers (20 v% HEA) prepared via PLP polymerization in 60 v% xylenes

A limited amount of PLP experiments was performed and evaluated as reported elsewhere[19] with increased solvent contents of xylenes (60 & 80 v%) at 50 °C. All systems contained regular PLP structure with no further anomalies. However, a reduced amount of pulses was used due to the decreased monomer concentration. The results, documented in the following table, suggest no concentration dependency in comparison to the bulk and 50 v% xylenes case. The minimal increase by roughly 100 $L \cdot mol^{-1} \cdot s^{-1}$ determined at 80 v% is noted but too insignificant.

Table C.1: k_p^{cop} values at 50 °C for BMA/HEA PLP copolymerizations in xylenes with different solvent levels

f_{HEA}	$\boldsymbol{\nu}$ (Hz)	Sol. v %	k_p^{cop} ($L \cdot mol^{-1} \cdot s^{-1}$)
0.26	35	50	1261
0.26	70	50	1284
0.26	35	60	1310
0.26	70	60	1280
0.26	15	80	1356
0.26	30	80	1385

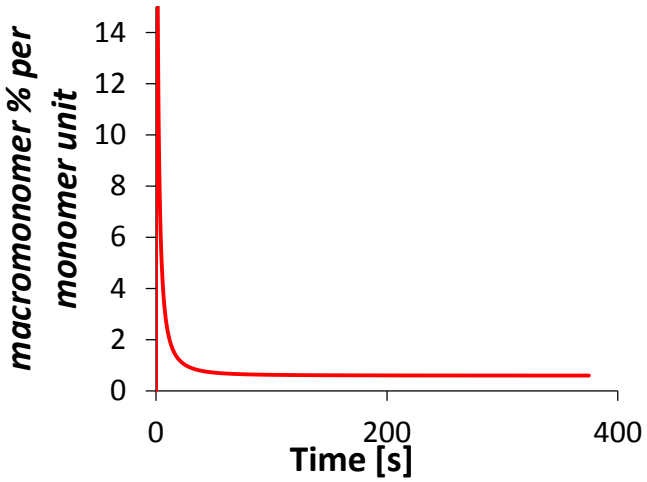

Figure C.4: Predicted macromonomer level in BMA/HEA semi-batch copolymerizations in MIAK at 138 °C

D. Appendix D: Supporting data for chapter 6

Supplementary data for impurity related investigations

Table D.1: Summary of SEC results for batch polymerizations of BA and BMA in xylenes with different levels of impurity

	BA MM Mn/Mw/PDI	**BMA MM Mn/Mw/PDI**
Xylene (run 1)	21000/38500/1.83	31100/47900/1.54
Xylene (run 2)	--	37000/69800/1.86
w/ EGDA (100 ppm)	23900/41400/1.73	30200/52500/1.74
w/ EGDA (500 ppm)	18700/42600/2.28	25300/53900/2.13
w/ EGDMA (100 ppm)	26500/44700/1.68	40000/74400/1.86
w/ EGDMA (500 ppm)	20000/45300/2.26	39900/74500/1.87

Table D.2: Summary SEC results for batch polymerizations of BA and BMA in MIBK with different levels of impurity

	BA MM Mn/Mw/PDI	**BMA MM Mn/Mw/PDI**
MIBK (run 1)	38800/99500/2.57	37000/62100/1.68
MIBK (run 2)	--	49100/75200/1.53
w/ EGDA (100 ppm)	43400/11600/2.57	45800/69100/1.51
w/ EGDA (500 ppm)	38000/107900/2.84	47000/76800/1.63
w/ EGDMA (100 ppm)	46100/113600/2.46	41400/62800/1.52
w/ EGDMA (500 ppm)	38100/102300/2.65	43700/67900/1.55

Table D.3: Summary of GC and SEC results for batch copolymerizations of BA/HEA and BMA/HEMA

	BA/HEA			**BMA/HEMA**		
	Mn/Mw/PDI	**Conversion**		**Mn/Mw/PDI**	**Conversion**	
(60:40 v%)		**BA**	**HEA**		**BMA**	**HEMA**
Xylene	181200/34200/1.88	54.30%	97.7%	36900/76500/2.02	28.30%	98.10%
MIBK	35600/110500/3.10	82.40%	100%	50100/96600/1.93	37.50%	70.70%
(75:25 v%)						
Xylene	41400/75700/1.83	75.20%	97.4%	56400/93300/1.66	40.50%	97.30%
MIBK	48600/156300/3.21	78.80%	100%	48600/156300/3.21	44.40%	54.20%

Table D.4: Summary of semi-batch results with different levels of impurity and hydroxy functional monomer contents. Note that initial 3 experiments were performed in a larger reactor setup

Monomer	Sovlent	Impurity Level EGDMA	Observation
BMA[11]	DMF	100 ppm	Significantly increased M_w in comparison to BMA homopolymerizaton
BMA[11]	Xylenes	100 ppm	
BMA/HEMA (75/25 wt%)[11]	Xylenes	Unknown through HEMA	
BMA	Xylenes	100 ppm	No significant increase in M_w observed for any of the reactions in comparison to BMA homopolymerizations
BMA	Xylenes	500 ppm	
BMA	Butyl propionate	100 ppm	
BMA	Butyl propionate	500 ppm	
BMA	Butyl propionate	1000 ppm	
BMA/HEMA (75/25 wt%)	Xylenes	Unknown through HEMA	
BMA/HEMA (75/25 wt%)	MIAK	Unknown through HEMA	
BMA/HEMA (75/25 wt%)	2-heptanone	Unknown through HEMA	

Supporting information for BA/HEMA results

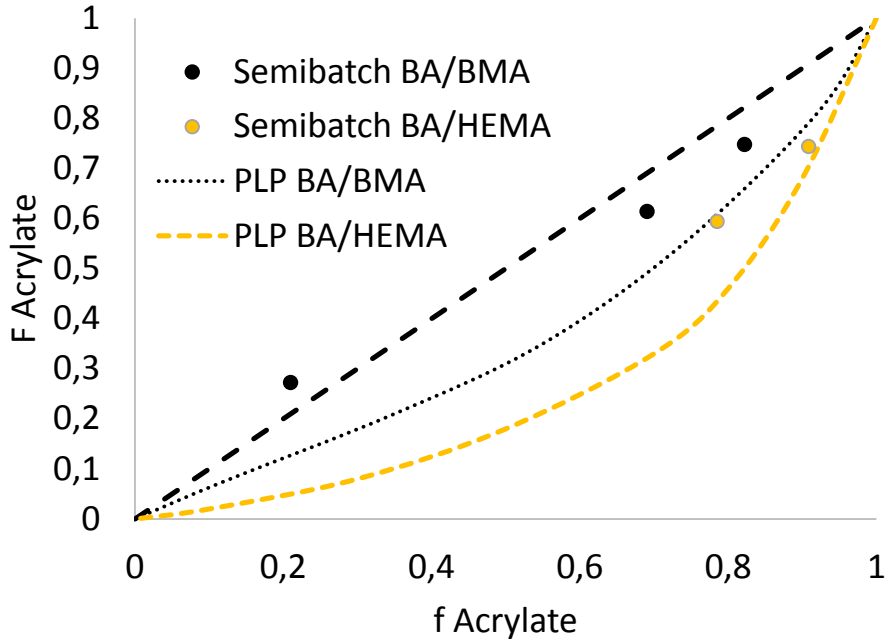

Figure D.1: Terminal model predictions and semi-batch results in a direct comparison

Comments on the peculiarities of the BA/HEMA modelling approach

The previously discussed terpolymerization model,[28] which is used as the base model for this investigation is using a fictional mathematical second reactor, R2 in the model. This trick is necessary to calculate and count populations in terms of the IPUE approach, defining polymer radicals P^{xy} and corresponding monomer fractions f_x and f_y. With each modelling step, the change in populations in R2 is solved by a corresponding matrix. To start R2, initial conditions need to be defined. These values are relatively arbitrarily chosen, as they adjust within the initial seconds of the model towards the actual concentrations present in the real reactor and reaction. The chosen values were also found to be quite robust, as there were no changes necessary for the BA/BMA system over the whole range of possible initial conditions, including BMA/HEA copolymerizations shown in chapter 5. Hence, changes in the matrix continuously resolved.

With the change to BA/HEMA, and the respective (more extreme) reactivity ratios, this statement was found to be not valid anymore. In here, changes in the initial composition, hence the recipe file,

caused the model to crash as the matrix could not be solved. Adjustments of the initial conditions of R2 were necessary for each individual composition. It was found that these changes were quite specific, including further abnormal behaviour, like spikes in the representation of monomer concentrations and MMD in the representation of R1 in case of improper conditions. This reduces the feasibility of such a model for a routine application in industry as such limitations were found to be hard to generalize and may appear random and unpredictable.